NASA CR-134892

SINGLE STAGE, LOW NOISE, ADVANCED TECHNOLOGY FAN

VOLUME IV FAN AERODYNAMICS

Section 1: Results and Analysis

BY: T.J. SULLIVAN, I. SILVERMAN AND D.R. LITTLE

ADVANCED ENGINEERING AND TECHNOLOGY
PROGRAMS DEPARTMENT
GENERAL ELECTRIC COMPANY
CINCINNATI, OHIO

PREPARED FOR

NATIONAL AERONAUTICS AND SPACE ADMINISTRATION

NASA LEWIS RESEARCH CENTER
CONTRACT NAS 3-16813

1. Report No.	2. Government Accession No.	3. Recipient's Catalog No.
NASA-CR-134892		

4. Title and Subtitle	5. Report Date
Single Stage, Low Noise, Advanced Technology Fan, Volume IV - Fan Aerodynamics Section 1, Results and Analysis	February 1977
	6. Performing Organization Code
7. Author(s)	8. Performing Organization Report No.
T.J. Sullivan, I. Silverman, and D.R. Little	R76AEG565
	10. Work Unit No.
9. Performing Organization Name and Address General Electric Company Aircraft Engine Group Advanced Engineering and Technology Programs Department Cincinnati, Ohio 45215	11. Contract or Grant No. NAS3-16813
	13. Type of Report and Period Covered Contractor Report
12. Sponsoring Agency Name and Address National Aeronautics and Space Administration Washington, D.C. 20546	14. Sponsoring Agency Code

15. Supplementary Notes

Fan Aerodynamics Results and Analysis Report. Project Manager, T.F. Gelder, Fluid System Components Division. Technical Advisor, M.F. Heidmann, V/STOL and Noise Division, NASA-Lewis Research Center, Cleveland, Ohio 44135.

16. Abstract

Aerodynamic test results and analysis for a scale-model fan vehicle, applicable on an advanced transport aircraft, are described. The single-stage advanced technology fan was designed to a 1.8 pressure ratio at 503 m/sec (1650 ft/sec) tip speed.

Fan components were designed and fabricated in a scale-model flow size to fit existing facility and vehicle hardware. Design-corrected flow per unit fan face annulus area was 215 kg/sec m^2 (44.0 lbm/sec ft^2) with a hub-tip ratio of 0.38 at the rotor leading edge. This results in an inlet corrected airflow of 117.9 kg/sec (259.9 lbm/sec) for the selected rotor tip diameter of 90.37 cm (35.58 in.).

The fan was tested on a ground static facility in a rear-shaft drive mode for fan and inlet performance and front-quadrant noise. A front-shaft drive mode was tested for fan bypass duct aerodynamic performance and aft-propagating noise. Three inlet configurations were tested to fully determine the aerodynamic and acoustic performance of the fan, the "hybrid" acoustic inlet, and the acoustically designed bypass duct.

Test results at design speed show fan total pressure ratio, weight flow, and adiabatic efficiency to be 2.2, 2.9, and 1.8% lower than design goal values. The "hybrid" acoustic inlet (which utilizes a high throat Mach number and acoustic wall treatment for noise suppression) demonstrated total pressure recoveries of 98.9 and 98.2% at takeoff and approach. Exhaust duct pressure losses differed between the hardwall duct and treated duct with splitter by about 0.6% to 2.0% in terms of fan exit average total pressure (depending on operating condition). When the measured results were used to estimate pressure losses, a cruise sfc penalty of 0.68%, due to the acoustically treated duct, was projected.

This along with "Section 2 - Overall and Blade Element Performance Data Tabulations," (bound in separate cover) is one of two final analysis reports. The other is "Volume V - Fan Acoustics". Three design reports precede this series. They are: "Volume I - Aerodynamic Design," "Volume II - Structural Design" and "Volume III - Acoustic Design".

17. Key Words (Suggested by Author(s))	18. Distribution Statement
Engine acoustics High speed fan Aerodynamic design Hybrid inlet	Unclassified - Unlimited

19. Security Classif. (of this report)	20. Security Classif. (of this page)	21. No. of Pages	22. Price*
Unclassified	Unclassified	148	

* For sale by the National Technical Information Service, Springfield, Virginia 22151

TABLE OF CONTENTS

LIST OF ILLUSTRATIONS

LIST OF ILLUSTRATIONS (Continued)

LIST OF ILLUSTRATIONS (Continued)

LIST OF ILLUSTRATIONS (Continued)

LIST OF ILLUSTRATIONS (Concluded)

LIST OF TABLES

SECTION I

SUMMARY

A high speed, low noise, high bypass ratio single-stage research fan with a variable-geometry inlet has been designed, fabricated, and tested by the General Electric Company under the sponsorship of NASA (Contract No. NAS3-16813). This report entitled "Volume IV, Fan Aerodynamics," is one of two in a series of final analysis reports. Three design reports precede the series of final analysis reports. They are: Volume I - Aerodynamic Design, Volume II - Structural Design, and Volume III - Acoustic Design, which are References 1, 2, and 3 respectively. The other final analysis report in the series, Volume V - Fan Acoustics, is Reference 4. The present volume is bound in two separate covers:

Section 1: Results and Analysis

Section 2: Overall and Blade Element Performance Data Tabulations

The 90.37 cm (35.58 in.) diameter tip-shrouded fan was designed to a bypass pressure ratio of 1.8, and a corrected airflow of 117.9 kg/sec (259.9 lbm/sec) at a tip speed of 503 m/sec (1650 ft/sec). The fan was designed to a stall margin goal at constant speed of 13% and an objective adiabatic efficiency of 84.0%, with a peak efficiency objective of 85%. Several low fan-source-noise features were included in the design, such as a vane/blade ratio of 2.05, a rotor/stator spacing of 2.06 (rotor tip chords), and a fan blade airfoil shape designed for a swallowed shock at takeoff.

Two separate series of tests were conducted at General Electric's Peebles, Ohio, Site IV-B outdoor facility. The rear-shaft drive test series provided fan and inlet aerodynamic performance as well as the evaluation of front-quadrant acoustic performance. The inlet configurations tested are shown in the schematics on page 2, Fan Inlet Configurations for Rear-Drive Tests. The major portion of the fan and inlet aerodynamic performance tests were conducted with a long (L/D_F = 2.3) bellmouth inlet (not shown) which contained an instrumentation section ahead of the fan. This was followed by a brief test with a shorter (L/D_F = 1.4) bellmouth inlet. The inlet noise suppression system employed a hybrid inlet (L/D_F = 1.5), which combined an adjustable-geometry cowl, capable of generating high throat Mach numbers (design throat Mach number = 0.79) at all critical noise operating points, with acoustic wall treatment. The acoustically treated wall panels were replaceable with hardwall panels so that the effects of the treatment on inlet aerodynamic performance and noise suppression could be isolated.

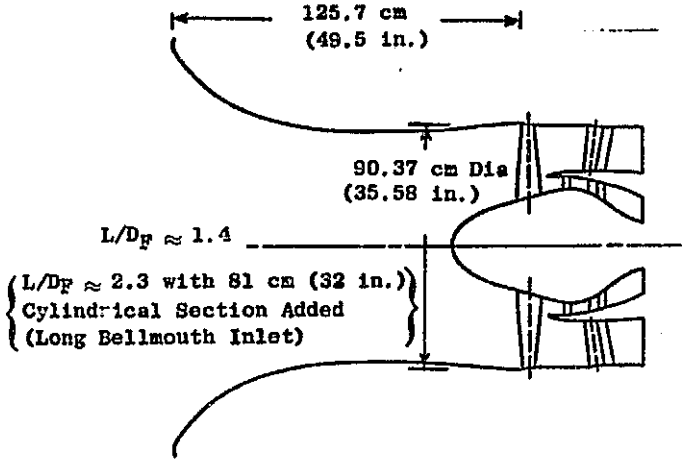

Short Bellmouth Inlet (Acoustic Baseline)

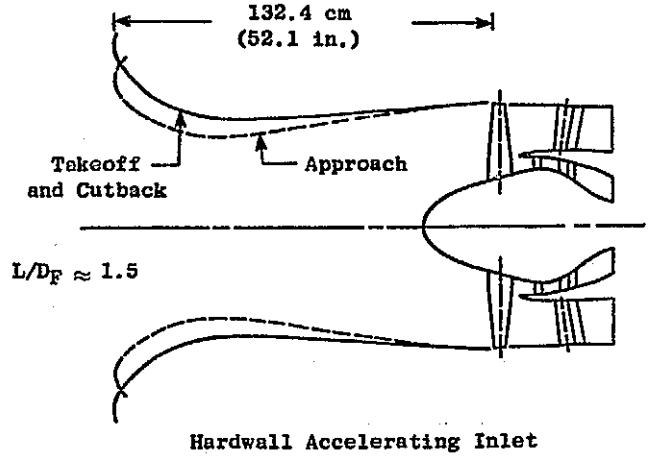

Hardwall Accelerating Inlet

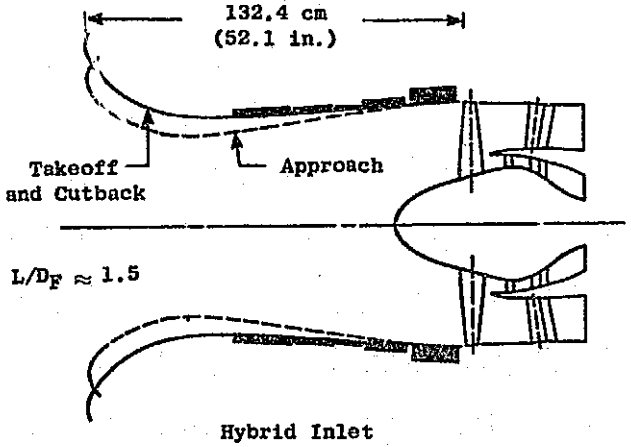

Hybrid Inlet
(Accelerating Inlet + Acoustic Wall Treatment)

Fan Inlet Configurations for Rear-Drive Tests.

The second series of tests involved driving the fan vehicle from a front shaft for the evaluation of bypass duct aerodynamic performance and aft-propagating fan noise. The configurations tested included a hardwall bypass duct without splitter and a fully treated duct with a midstream acoustic splitter. They are shown schematically on page 4, Fan Duct Configurations for Front-Drive Tests.

A. Fan Aerodynamic Performance

A summary of fan performance results, including comparisons with design values, is given in Table I.

Table I. Fan Aerodynamic Performance Summary.

(100% Speed - Operating Line)

Parameter	Design Objective	Long Inlet	Short Inlet	Hybrid Inlet*
Bypass Pressure Ratio	1.80	1.74	1.76	1.67
Corrected Flow (kg/sec)	117.9	113.8	114.5	114.1
Adiabatic Efficiency, %	84.0	80.6	82.2	80.1
Stall Margin, %	13.0	7.8	10.8	9.3

* Data point is below operating line.

The measured flow at design speed with the long bellmouth inlet was 3.5% lower than the design intent. Experimental evidence indicates that the flow was limited by inadequate rotor design incidence angle rather than inadequate rotor throat area. The large throat-to-capture area ratio that resulted is believed to have been a contributing factor to the larger than design-intended rotor total pressure loss coefficients.

The rotor work input was close to design intent in the outer 65% of the blade span. The larger than design-intended losses in the tip appear to have been the main contributor to the lower than design-intended pressure ratio of this portion of the blade.

The stall margin at 100% speed with the long bellmouth inlet was 7.8%, or 5.2% below the stall margin goal. At part speed, the demonstrated stall line was within 1.5% of the goal. Some additional testing was performed to investigate the effects of off-design bypass ratios with the long bellmouth inlet installed. Overall performance comparisons showed a distinct difference in the speed line shape, but no significant performance penalties were associated with the off-design bypass ratios.

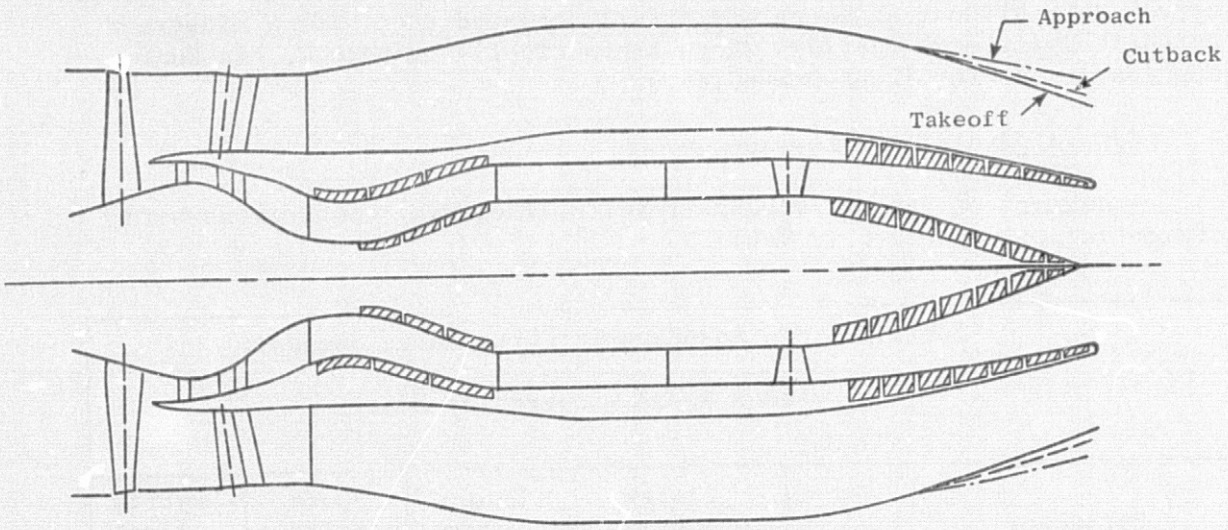

• Hardwall Duct without Splitter

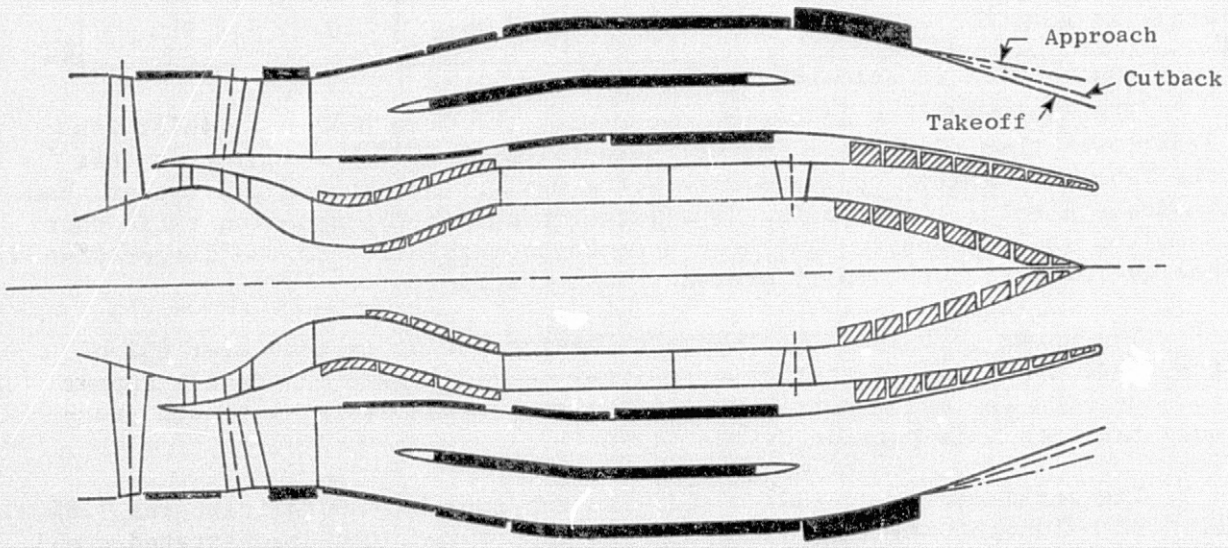

• Acoustically Treated Duct with Splitter

Fan Duct Configurations for Front-Drive Tests

Testing with the short bellmouth inlet showed a distinct improvement in the fan performance. The measured airflow at design speed was slightly larger (0.6%) with the short bellmouth inlet and the efficiency increased 1.6% to a level of 82.2%. Three intentional stalls were made at 100% speed. The initial stall showed a 3% improvement in stall pressure ratio, and the subsequent stalls showed somewhat lesser stall pressure ratios, but still greater than the stall pressure ratio measured with the long bellmouth inlet. It should be noted that prior to the short bellmouth inlet test, the tip-shroud seal teeth clearances were set smaller than they had been during the long bellmouth inlet test. The intent was to set the clearances such that operation at 100% speed would produce zero clearance. During the initial stall at 100% speed, a rub was encountered and the clearances grew with each additional stall, leading to a deterioration in the stall pressure ratio limit.

With the hybrid inlet installed in its takeoff position, the stall line depression from that measured with the long bellmouth inlet was minimal, about 2 to 3%. The measured flow at any given speed line along a constant throttle area (operating line) showed little or no loss, and the adiabatic efficiency was down approximately 0.5%. With the hybrid inlet at its approach setting, the stall margin losses were greater, ranging from 3.6% at 50% speed to 6.5% at 70% speed. This was attributed to the more severe diffusion that had to take place in the inlet (see Fan Inlet Configurations schematic on page 2) which degraded the boundary layer characteristics of the inlet in the approach mode. Even with the additional stall margin loss, the margin remaining above the low operating line approach point was sizeable (approximately 35%). Again, the measured flow at any given speed and throttle setting showed no appreciable difference from the long bellmouth inlet test. Overall, the hybrid inlet was verified as a viable fan noise suppression device from a fan aerodynamic performance standpoint, at least under static conditions.

B. Inlet Aerodynamic Performance

The hybrid inlet used as the suppression device for forward-quadrant noise demonstrated the ability to operate at the design throat Mach number of 0.79 at takeoff and approach conditions. The hybrid inlet tended to retard separation relative to the hardwall accelerating inlet, which was attributed to the greater surface roughness of the acoustic treatment, producing greater shear stresses at the wall.

Inlet total pressure recoveries were 98.9% at takeoff and 98.2% at approach for the hybrid inlet at the design points. In view of the long inlet length, high area ratios, high throat Mach number, and the amount of acoustic treatment material in the inlet, these were encouragingly high levels. The acoustic treatment of the wall of the hybrid inlet resulted in only a 0.3% loss in total pressure recovery at the 0.79 design throat Mach number point, for both takeoff and approach inlet configurations. The hybrid inlet in either configuration gave less than 10% distortion over the entire operating range for static conditions. Even with throat Mach numbers

of 0.81 at approach and 0.84 at takeoff, this level of distortion was not exceeded.

C. Bypass Duct Aerodynamic Performance

Exhaust duct aerodynamic performance data were taken during the fan acoustic tests on the two configurations shown in the schematics on page 4. Measured fan duct Mach numbers were slightly higher than originally predicted, due principally to differences in fan duct entrance conditions. Total pressure losses of the acoustically treated splitter duct were in general agreement with the original predictions. A comparison of these losses with those of the hardwall duct is provided in Table II.

Table II. Duct Pressure Losses.

	Takeoff	Cutback	Approach	Cruise*
Treated Duct with Splitter ($\Delta P_T/P_T$), %	1.35	3.24	2.05	1.41
Hardwall Duct ($\Delta P_T/P_T$), %	0.79	1.28	0	0.79
$\Delta(\Delta P_T/P_T)$, %	0.56	1.96	2.05	0.62

*Estimated, based on measured results

In high bypass ratio engines, the change in specific fuel consumption (sfc) associated with a change in duct pressure loss can be translated through an influence coefficient of about 1.1 at cruise conditions. Thus, the acoustically treated duct results in a penalty of about 0.68% in cruise sfc.

SECTION II

INTRODUCTION

Low noise and exhaust emissions and economical operation are the primary requirements for advanced transport aircraft. The successful development and acceptance of a subsonic, long-range transport for the next generation are greatly dependent upon technological improvements in the areas of fan aerodynamics and acoustic suppression. To help provide this fan technology, the General Electric Company was contracted to design, build, and test a high-speed, low-noise, single-stage research fan (hereafter referred to as an advanced technology fan), a variable geometry inlet with high throat Mach number capability and an acoustically treated fan exit duct, all applicable for an advanced high-bypass, low-noise engine. To utilize existing hardware and facilities, the subject fan was designed to be half-scale.

Under a separate and earlier contract with NASA (Contract NAS3-15544, References 5 and 6), parametric studies were performed to optimize the engine cycle for a typical advanced transport aircraft. Based on these studies, plus the current contract Statement of Work, an engine cycle was selected for an advanced transport designed to cruise between 0.85 and 0.90 Mach number. A fan pressure ratio of 1.8 to 1.9 and a bypass ratio of approximately 6:1 are desirable. Furthermore, it is desirable to raise the pressure ratio of the flow entering the core compressor to about 2.5 to 3.0 by the addition of booster stages. This then provides an overall cycle pressure ratio of 30:1 or greater and still uses only a single-stage turbine to drive the high pressure compressor. Fan tip speeds of 488 to 518 m/sec (1600 to 1700 ft/sec) are required to achieve the desired pressure ratio in a single, low radius-ratio stage with adequate stall margin. A high specific flow rate of 215 kg/sec m^2 (44.0 lbm/sec ft^2) was chosen to maintain a high inlet Mach number just ahead of the fan to help reduce the inlet noise without suffering severe aerodynamic performance penalties.

The aerodynamic and acoustic performance of the fan vehicle was evaluated in two separate series of tests conducted at General Electric's Peebles, Ohio outdoor sound-field facility. In the first series of tests, the fan was driven by a rear shaft. Detailed fan and inlet aerodynamic performance information was obtained. A long bellmouth inlet ($L/D_F = 2.3$) was used for the majority of the fan aerodynamic performance tests, because it contained an instrumentation section ahead of the fan. Unsuppressed and suppressed forward-propagating fan noise was evaluated with the shorter bellmouth inlet and with aft-propagating noise virtually eliminated from the system by a massive exhaust suppressor. In the second series of tests, the fan was shaft-driven from the front and the inlet system was enclosed in a large silencer box to eliminate forward-propagating fan noise. This test program was used to evaluate bypass duct aerodynamic performance and aft-

radiating fan noise, both suppressed and unsuppressed. An abbreviated description of the complete test program is provided in Table III.

The advanced technology fan, in combination with the inlet and bypass duct system, was designed to the very challenging noise goal of 20 EPNdB below FAR 36. As a result, the fan design incorporated many low noise features such as a vane/blade ratio of 2.05, a rotor/stator spacing of 2.06 (rotor tip chords) and a blade designed for a swallowed shock at takeoff. The inlet noise suppression system employed a "hybrid" inlet with an adjustable-geometry cowl (two position) capable of generating high throat Mach numbers (design $M_{TH} = 0.79$) at all critical noise conditions [takeoff (sideline), cutback, and approach]. The high Mach number, variable-geometry inlet concept was designed to operate in conjunction with a variable-area fan exhaust nozzle, which was already determined to be necessary for reducing exhaust velocity at the cutback position. This combination reduces the range of area change required of the inlet. At takeoff the exhaust area was assumed to be at the nominal value (necessary to reach takeoff rated thrust), and the inlet throat was adjusted to obtain $M_{TH} = 0.79$. Throat area at cutback (0.457 m^2) was maintained at the takeoff setting for operational simplicity, and the cycle was matched to the proper weight flow by selecting the appropriate combination of throttle setting and exhaust nozzle area. The nozzle was opened during the cutback setting tests 25% above nominal, compared to pretest design estimates of 15%. The difference was due to variation in vehicle performance relative to design. At approach the exhaust nozzle was opened to an area 35% greater than nominal (design estimate was 40%) and the inlet throat was reduced to 0.339 m^2 in order to achieve $M_{TH} = 0.79$ at the low thrust level required at approach. During rear-drive tests, these nozzle positions were simulated with core and bypass stream discharge valves; during the front-drive tests, three separate nozzles were employed and trimmed to duplicate the appropriate operating lines.

Four segments of acoustic-treatment panels, which were tuned to the predicted dominant noise frequencies, were combined with airflow acceleration to form the hybrid inlet. The acoustic-treatment panels were replaceable with hardwall panels so that suppression due to flow acceleration and suppression due to treatment could be isolated, and the effect of acoustic treatment on inlet aerodynamic performance could be evaluated. The exhaust duct suppression system consisted of a full complement of acoustic treatment of walls and a mid-duct splitter. The hardwall duct without splitter served as the acoustic baseline and as the reference in determining the aerodynamic performance penalty associated with the suppressed configuration.

The present volume first describes the test vehicle design and the test specifications and procedures, followed by aerodynamic performance results and discussion for the fan, inlet, and exhaust duct, respectively. Section 2 of this Volume (under separate cover) contains overall and blade-element performance data tabulations. Other reports of work performed under this contract include: Volume I - Aerodynamic Design, Volume II - Structural Design, Volume III - Acoustic Design, and Volume V - Fan Acoustics, which are References 1, 2, 3, and 4, respectively.

Table III. Advanced Technology Fan Test Program Outline.

Rear-Drive Tests

Fan Aerodynamic Performance Tests

Long Bellmouth Inlet
- Inlet L/D_F = 2.3
- Full instrumentation
- Bypass Ratio Migration

Short Bellmouth Inlet
- Inlet L/D_F = 1.4
- Tip Clearance Tightened Initially
- Limited Aerodynamic Instrumentation

Hybrid Inlet
- Inlet L/D_F = 1.5
- Limited Aerodynamic Instrumentation
- Takeoff/Cutback and Approach Configurations

Inlet Aerodynamic Performance Tests

Hybrid Inlet
- Inlet L/D_F = 1.5
- Takeoff/Cutback and Approach Configurations

Accelerating Inlet
- Inlet L/D_F = 1.5%
- Hybrid Inlet without Wall Treatment
- Takeoff/Cutback and Approach Configurations

Inlet Acoustics Tests

Short Bellmouth Inlet (Baseline)
- Takeoff, Cutback, and Approach Operating Lines

Hybrid Inlet
- Takeoff, Cutback, and Approach Operating Lines

Accelerating Inlet
- Takeoff, Cutback, and Approach Operating Lines

Front-Drive Tests

Bypass Duct Aerodynamic Performance Tests

Fully Treated Duct with Splitter
- Takeoff, Cutback, and Approach Nozzles

Hardwall Duct without Splitter
- Takeoff, Cutback, and Approach Nozzles

Aft-Noise Acoustic Tests

Fully Treated Duct with Splitter
- Takeoff, Cutback, and Approach Nozzles

Hardwall Duct without Splitter (Baseline)
- Takeoff, Cutback, and Approach Nozzles

A visual representation of the overall program and report organization is shown on page 11, Description of Advanced Technology Fan Reports.

Description of Advanced Technology Fan Reports

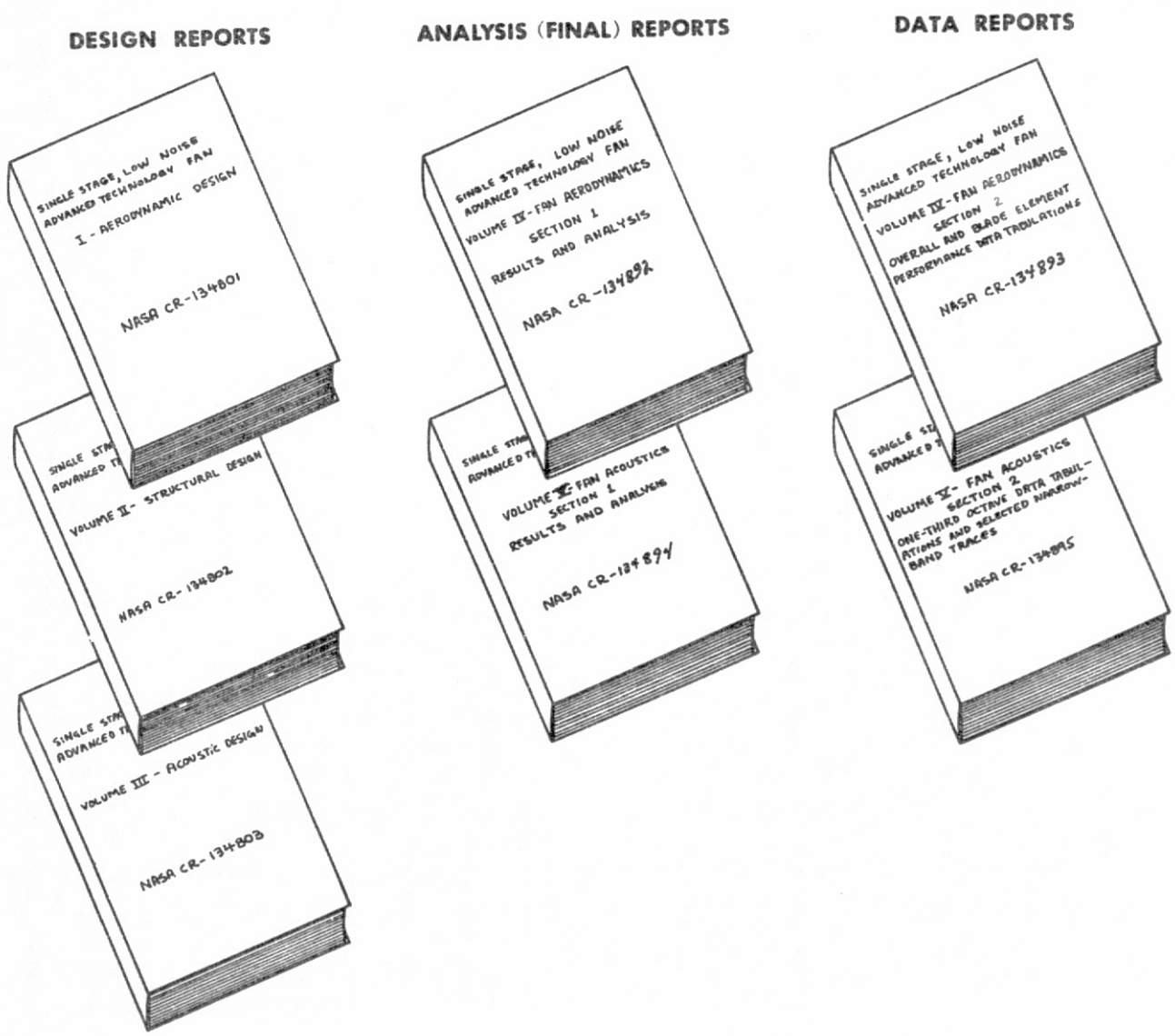

SECTION III

FAN VEHICLE DESCRIPTION

A. Fan Design

Parametric studies were performed under a separate, earlier contract with NASA (Contract NAS 3-15544) to optimize the engine cycle characteristics for a typical advanced transport aircraft. These studies indicated that a fan pressure ratio of 1.8 to 1.9 and a bypass ratio of approximately 6:1 are desirable for a cruise Mach number between 0.85 and 0.90. Furthermore, it is desirable to raise the pressure ratio of the flow entering the core compressor to about 2.5 to 3.0 by the addition of booster stages. This then provides an overall cycle pressure ratio of 30:1 or greater while permitting the use of a single-stage turbine to drive the high pressure compressor. Fan tip speeds of 488 to 518 m/sec (1600 to 1700 ft/sec) are required to achieve the desired pressure ratio in a single, low radius-ratio stage with adequate stall margin. The present fan and boosters were designed to fulfill the above requirements. The booster stages were not subsequently fabricated or tested, however.

The fan and booster flowpaths are shown in Figure 1. The inlet hub/tip radius ratio of 0.38 and the high specific flow rate of 215 kg/sec m^2 (44.0 lbm/sec ft^2) of inlet-annulus area were selected to minimize the required fan size and nacelle diameter, and to help minimize forward noise radiation. The 0.38 inlet radius ratio approaches the practical structural limit for tip-shrouded rotor blades at the design tip speed of 503 m/sec (1650 ft/sec) using current titanium alloys. The integral tip shroud was chosen in preference to a part-span shroud because of its lower aerodynamic loss penalty and possible benefits from an acoustic standpoint. A shroud is necessary to provide satisfactory aeromechanical operation for blading aspect ratios compatible with low weight. The design had 44 rotor blades with an aspect ratio of 3.34. The blades were designed to have a swallowed shock at takeoff (92.1% equivalent design speed) to reduce multiple pure tone noise at this critical operating condition.

The fan rotor inlet tip diameter of 90.37 cm (35.58 in.) was selected to permit the use of existing inlet and frame hardware for testing. The selected diameter results in a design point corrected airflow of 117.9 kg/sec (259.9 lbm/sec). The flow is split immediately downstream of the rotor, dividing the bypass flow and the booster/core flow by the design bypass ratio of 6:1.

A large axial spacing between the fan rotor and the bypass outlet stator vanes (approximately two rotor tip chords) was provided to minimize fan noise generation. The axial spacing between the rotor hub and the booster inlet stator is 0.9 rotor hub chord lengths.

A summary of the significant aerodynamic parameters associated with the fan and booster design are presented in Table IV. A photograph of the fan is provided in Figure 2. Details of the fan vehicle aerodynamic design, including that for the inlet, exhaust duct, and nozzles are given in Reference 1. A description of the structural design for the vehicle is given in Reference 2.

Table IV. Aerodynamic Design Parameters.

Corrected Tip Speed	503 m/sec (1650 ft/sec)
Corrected Airflow	117.9 kg/sec (259.9 lbm/sec)
Inlet Specific Flow Rate	215 kg/sec m^2 (44.0 lbm/sec ft^2)
Predicted Stall Margin (Constant Speed)	13%
Objective Adiabatic Efficiency (Bypass)	84%
Bypass Pressure Ratio	1.80
Core Pressure Ratio	1.69
Bypass Ratio	6.0
Inlet Hub/Tip Ratio	0.38
Tip Diameter	90.37 cm (35.58 in.)
Rotor Aspect Ratio	3.34
OGV Aspect Ratio	3.94
Rotor Tip/Hub Solidity	1.50/2.74
OGV Tip/Hip Solidity	1.37/2.05

B. Inlet Design

The flight-type, variable-geometry inlet was designed to utilize a combination of airflow acceleration suppression and diffuser acoustic treatment (hybrid inlet) in order to meet a goal of FAR 36 minus 20 EPNdB for fan-only noise. A conceptually variable fan exhaust nozzle was also utilized in conjunction with the variable-inlet throat to limit the required throat-area change at approach-power conditions, and hence limit the overall

diffusion and inlet length. The inlet selected from the design studies for construction and testing had a length of 1.5 fan diameters. Overall inlet length was determined based on that length which was required for diffusing between the throat and fan face or acoustic treatment length requirements, whichever was the larger length, plus the inlet lip length between the leading edge and throat, and finally, any additional length that was required to accommodate the inlet variable-geometry features and produce a smooth flowpath contour. A bellmouth lip was designed to simulate flight inflow conditions for takeoff and approach operation during the static testing. A flight inlet forebody was also designed (not tested) which would be compatible with a cruise Mach number of 0.90 and consistent with an advanced transport operational envelope. The flight inlet is shorter than the test version with its bellmouth, having a length of 1.4 fan diameters. A sketch of the aerodynamic lines is shown on Figure 3.

In order to generate a throat Mach number of 0.79 at all three important noise conditions (takeoff, cutback, and approach) the actual test hardware was designed to have adjustable panels which rotated around a pivot point, as shown on Figure 4.

For the approach condition, the panels were dropped to the minimum throat radius to reduce throat area, plus the nozzle (discharge valve for the rear-drive tests) was opened an additional 40% from the nominal (takeoff) setting in order to high-flow the fan. The panels were separated by wedges so that a smooth contour and seal would result for the retracted position (takeoff and cutback). The wedges can be seen exposed for the takeoff and cutback configuration on Figure 5. The bellmouth lip included fairings for the adjustable panels when in the approach position. These were removed for testing in the takeoff and cutback configuration, and in practice would be remotely variable on the same mechanical system which controlled the diffuser panels.

The inlet acoustic-treatment panels were designed to be removable and replaceable with hardwall panels. Inlet performance was measured with the hardwall panels, as well as with the treatment, in order to determine the performance penalty associated with the treatment. Also, fan aerodynamic performance was measured with a long (L/D_F = 2.3), hardwall bellmouth inlet. This inlet was fitted with more fan performance instrumentation than was possible on the hybrid inlet during acoustic tests. Fan aerodynamic performance tests were also performed on a shorter (L/D_F = 1.4) bellmouth inlet with the cylindrical instrumentation section removed. This also served as the acoustic baseline inlet. During front-drive tests, to obtain fan bypass-duct aerodynamic performance and aft-directed noise, the shorter bellmouth inlet was used inside a large inlet noise muffler. The test inlets are illustrated in Figure 6.

C. Exhaust Duct Design

The design of the fan bypass duct was dictated primarily by the acoustic design objective, which was to meet a goal of FAR 36 minus 20 EPNdB (for fan noise only). (Details of the acoustic design for the vehicle are given in Reference 3.) Illustrations of the fan exhaust systems tested in this program during the front-shaft drive tests are shown on Figure 7. The splitter was located in the middle of the duct with its leading edge at approximately one channel-height downstream of the fan frame struts. The total duct length aft of the struts was about 3.5-fan diameters. The duct was designed with the objective of limiting the wall and splitter surface Mach number to 0.35.

The system was also tested in a hardwall configuration with the splitter removed, to determine the aerodynamic performance penalty and acoustic benefit of all the treatment. The outer duct wall of this configuration was slightly different in that its radius was reduced to maintain the same duct area and average Mach number distribution as when the splitter was present. Three nozzles were fabricated and trimmed to put the fan on the three important operating lines, as follows:

Condition	Nozzle Flow Area cm^2 ($in.^2$)
Takeoff	2948 (457)
Cutback	3677 (570)
Approach	3980 (617)

These nozzle areas differ somewhat from the design values due to variations in vehicle performance relative to the design intent. A photograph of the exhaust duct with the nozzles removed is provided in Figure 8. The photograph shows the core-stream discharge valves which were used to regulate core airflow and bypass ratio during testing.

SECTION IV

TEST DESCRIPTION AND PROCEDURES

A. Test Facility

All testing was conducted at General Electric's test facility near Peebles, Ohio, with the test vehicle located at outdoor Site IV-B. The fan component was shaft-driven by a General Electric LM1500 gas turbine with a rating of 15,000 horsepower. The fan component was driven from the rear for all fan aerodynamic and hybrid inlet performance tests, and from the front for the series of hardwall and suppressed fan exit duct tests.

The fan exhaust total airflow was measured by a set of four standard-ASME venturis located downstream of the fan discharge valves and then ducted into a large sound-suppression plenum before being exhausted vertically to the atmosphere. In addition, a core-measuring section downstream of the fan component was used to measure core flow and determine bypass ratio. A top-view schematic of the rear-drive setup is shown on Figure 9.

The front-drive setup is shown in Figure 10. During the front-drive portion of the tests, the flow-measuring venturis and most of the fan total pressure instrumentation were necessarily deleted from the system. Correlations of static pressures with flow and bypass-pressure ratio were used to define the proper fan-map operating points. The correlations were developed from rear-drive fan performance data. During the mechanical check-out run in front-drive, inlet-distortion rakes were used to define the pressure recovery of the inlet operating inside the silencer box.

B. Instrumentation

A listing of the major fixed and traversing instruments employed for the different phases of fan and inlet aerodynamic testing is given in Table V. The location of these instruments and the hub, casing, and flow-splitter static pressure taps are shown on Figure 11.

Overall fan aerodynamic performance data with the long bellmouth inlet section were calculated from fluid properties measured by fixed instrumentation at inlet and exit measuring stations. Measurements of total pressure and total temperature were obtained by four 6-element radial rakes at the fan inlet plane (Station 12 on Figure 11), located 0.7 diameters ahead of the rotor, seven 11-element arc rakes at seven radial immersions at the bypass outlet vane plane (Station 13 on Figure 11) and five 9-element arc rakes at five radial immersions at the core stator exit plane (Station 2.1 on Figure 11). The immersion measurements were made at centers of equal flow at each station. In addition to the main performance-measuring instruments mentioned above, total pressure radial rakes were located behind the rotor in the bypass and core-inlet ducts.

Table V. Major Instrumentation List for Advanced Technology Fan Vehicle Testing.

Location (See Figure 11)	Checkout Tests and Long Bellmouth Inlet Tests	Short Bellmouth Inlet Tests	Hybrid Inlet Tests
Station 12.0 Vehicle Inlet	Four 6-element P_T, T_T Radial Rakes	No Inlet Rakes	No Inlet Rakes
Station 0.9 Rotor Inlet	One 7-element Boundary Layer Rake	One 7-element Boundary Layer Rake	One 7-element Boundary Layer Rake
Station 1.0 Rotor Inlet	One p, β Wedge Probe, and One P_T, T_T, β Cobra Probe for Radial Traverses	No Traverses	One p, β Wedge Probe, and One P_T, T_T, β Cobra Probe for Radial Traverses
Station 1.5 Rotor Exit	One p, β Wedge Probe, and One P_T, T_T, β Cobra Probe for Radial Traverses	No Traverses	No Traverses
Station 2.0 Core Inlet	Three 5-element P_T Radial Rakes	Three 5-element P_T Radial Rakes	Three 5-element P_T Radial Rakes
Station 2.1 Core Exit	Five 9-element P_T, T_T Wake Rakes	Five 9-element P_T, T_T Wake Rakes	Five 9-element P_T, T_T Wake Rakes
Station 2.9 Core Measuring Section	Two 3-element P_T Radial Rakes	Two 3-element P_T Radial Rakes	Two 3-element P_T Radial Rakes
Station 12.5 Bypass Inlet	Two 7-element P_T Radial Rakes One 7-element P_T Boundary Layer Rake (OD) One 7-element P_T Boundary Layer Rake (ID)	One 7-element P_T Boundary Layer Rake (OD) One 7-element P_T Boundary Layer Rake (ID)	One 7-element P_T Boundary Layer Rake (OD) One 7-element P_T Boundary Layer Rake (ID)
Station 13.0	Seven 11-element P_T, T_T Wake Rakes	Seven 11-element P_T, T_T Wake Rakes	No Discharge Rakes
Station 13.0	One P_T element (Pitchline)	One P_T element (Pitchline)	One P_T element (Pitchline)

Note: See Appendix A for nomenclature.

Radial traverses at the fan rotor inlet and exit were made at selected map data points during the aerodynamic performance test with the long bellmouth inlet. Two traverse probes, a cobra and a wedge probe, were immersed at each station. The cobra probe (see Figure 12) was used primarily to measure total temperature and total pressure. In addition, it also measured the absolute flow angle. The wedge probe (see Figure 13) measured static pressure and absolute flow angle. Radial traverses were also taken at the fan rotor inlet during the hybrid inlet aerodynamic performance test to determine the inlet recovery.

Blade-element data were obtained from the fixed arc-rake probes, each rake in the bypass flow portion spanning four vane passages and in the core flow portion spanning 2.5 vane passages. The fan rotor exit total pressure used to calculate rotor blade-element data was assumed to be equivalent to the average of the three highest arc-rake measurements at the OGV or stator 1 exit at each radial immersion. An interpolation routine was used to determine the blade-element data at the standard immersions of 5, 10, 15, 30, 50, 70, 85, 90, and 95% for the fan rotor; 10, 15, 30, 50, 70, 85, and 90% for the bypass outlet guide vane; and 15, 30, 50, 70, and 85% for the core stator vane.

For the test configuration with the inlet instrumentation section removed (short bellmouth), the ambient pressure and temperature were recorded in the environment of the test vehicle before each test reading and used for the inlet total pressure and temperature. During the hybrid inlet performance test, traverses of total pressure and temperature were made at the fan rotor inlet, and the inlet recovery was determined as a function of airflow and applied to the recorded data.

The total physical airflow for all tests was measured at the discharge of the vehicle using the venturi flow-measuring system described in Section IV-A.

The hybrid inlet aerodynamic performance instrumentation (Figure 14) consisted of two traverse probes (wedge and cobra), a boundary layer total pressure rake of seven elements and 38 wall static pressure taps. The wedge probe was used to determine yaw angle and static pressure depression (from inlet total pressure). The cobra probe gave readouts for the same yaw angle, total temperature, and total pressure. Readouts were made on a chart recorder. Both traverses were located radially between the wedges and at an axial location approximately 5 cm (2 in.) forward of the rotor face (Station 1.0), see Figure 14. Supplementing the traverse total pressure data was a boundary layer rake situated behind a wedge, 6.9 cm (2.7 in.) forward of the rotor leading edge. Having total pressure surveys between and behind the wedges allowed consideration of circumferential total pressure variations at the rotor face, due to the wedges, and permitted a more realistic evaluation of inlet recovery levels.

A total of 38 static pressure taps were located in the inlet at 30 axial locations, to define Mach number variation along the inlet wall. Distances between the taps ranged from 1.8 cm (0.7 in.) in the high velocity gradient region near the throat, to 5 cm (2 in.) well into the diffuser. There are also two rings of four taps each in the inlet to assess circumferential flow uniformity. Readouts of the static taps and the boundary layer rake were in the form of Aerodynamic Data Handling (ADH) digital data.

Two wall Kulites were installed in the inlet ahead of the fan and two behind it. This enabled determination of the magnitude and frequency of total pressure fluctuations, and the direction in which the disturbances travelled when unsteady rotor blade stress levels appeared on strain gages at certain operating conditions beyond the $M_{TH} = 0.79$ design point. The two forward Kulites were placed 2.8 cm (1.1 in.) and 13.0 cm (5.1 in.) ahead of the fan and the other two were placed like distances behind it. Kulite readings were recorded on tape.

The evaluation of exhaust duct aerodynamic performance was conducted during the front-drive tests. A schematic of the instrumentation utilized is provided in Figure 15. The traversing total pressure and temperature probes behind the fan frame struts (Station 14.2) and at the entrance to the nozzles (Station 14.3) were used to define the pressure drop through the duct and to measure flow velocity. These probes were all removed for subsequent acoustic testing. The static pressure distribution over the duct walls and splitter surface was used to define surface Mach number and possible areas of flow separation. Comparisons of these data between the hardwall duct without splitter and the treated duct with splitter were made to define the effects and penalty of treating the duct for fan aft-propagating noise suppression. It should be noted that the outer flowpath of the hardwall duct without splitter was designed and built to a lower radius through that portion which contained the splitter in the suppressed configuration. The intent was to duplicate duct Mach number distribution between the two configurations for the same fan operating conditions. In this way, duct Mach number differences were not a factor in the performance difference of the two configurations.

C. Test Program

1. Check-out Tests and Long Bellmouth Inlet Tests (Rear-Drive)

A check-out test was conducted in the initial phase of testing with the long bellmouth inlet to assure safe mechanical operation over the range of speeds and pressure ratios to be investigated during the aerodynamic performance testing. Blade and vane stresses were monitored continuously as the vehicle was accelerated to maximum design speed along the nominal operating line (defined by a constant throttle area setting required to pass through the design point). The facility systems were checked out and all instrumentation readings were checked for consistency and accuracy.

The vehicle was intentionally stalled by closing the bypass discharge valve (DV) after selecting a core DV setting such that the stalling valve-settings would produce a bypass ratio approximating the design value of 6:1. Stalls were recorded at 50, 65, 70, 80, 85, 90, 95, 100, 105, and 110% corrected speeds.

Fan overall and blade-element performance data were obtained at speeds from 50 to 110% of design for the long bellmouth inlet flow test. The range of speeds covered the important engine and system design operating points of takeoff (92.1% speed), cutback (89.6% speed), and approach (64.7% speed). At each speed, data points were taken between the maximum flow attainable and the near-stall, low-flow limit. For all performance map points the bypass and core DV settings were chosen to maintain approximately the design bypass ratio. Additional testing was performed with off-design bypass ratios ranging from 5.0 to 12.0, to investigate performance effects, if any.

An additional test was then conducted with the 81 cm (32 in.) cylindrical instrumentation section removed, reducing the inlet L/D_F from 2.3 to 1.4 (short bellmouth inlet configuration). This run was made after data from the boundary layer rake in front of the rotor suggested that the long inlet was generating a boundary layer larger than expected for a normal subsonic inlet. Just prior to this test, the grooves in the abradable stationary shroud adjacent to the rotor tip shroud were partially refilled. These grooves had previously been widened artificially after the original check-out test in order to avoid hard rubs during stalls. An examination of the rub material showed a lack of witness marks after the test stalls at high speed, suggesting that one of the shroud seal teeth might not have been sealing. During an abbreviated aerodynamic performance test with the short bellmouth inlet, data were recorded at 70, 80, 90, 95, and 100% corrected speeds along the nominal operating line. At 95% speed, two points were taken slightly above the nominal operating line to the stall point. At 100% speed, six points define the speed line from below the operating line to stall. There, three successive stalls were recorded. The second and third stalls happened while trying to set a near-stall condition for a data reading. These stalls indicated a deterioration in the limit pressure ratio as the shroud seal teeth rubs increased the tip clearances. The stall line remained slightly higher than that established during the long inlet tests, however. The primary objective of the high speed testing was to determine the effect of the inlet length and tip clearances on the aerodynamic performance.

2. Bypass Ratio Migration Test (Rear-Drive)

Off-design bypass ratio effects on the fan aerodynamic performance were investigated at 80 and 95% of design speed with the long bellmouth inlet installation. Nominal and high operating-line bypass discharge valve (DV) settings were selected and the core DV was throttled to stall for each of the bypass DV settings. Overall performance data were obtained at various core DV settings from wide-open (low bypass ratio) to a near-fully closed setting (high bypass ratio) for each of the two bypass DV settings.

3. Hybrid Inlet Tests (Rear-Drive)

Fan aerodynamic performance was measured with the hybrid inlet (L/D_F = 1.5) installed in place of the long bellmouth inlet. Two positions of the hybrid inlet throat were investigated: (1) the approach position, designed to produce a throat Mach number of 0.79 at 64.7% speed (low operating line), and (2) the takeoff/cutback position, designed for a 0.79 throat Mach number at takeoff and cutback power settings, corresponding to 92.1% and 89.6% design speeds (nominal and low operating-line).

Overall and blade-element performance were measured at three speed lines (50, 65, and 70% speeds) for the approach position and five speed lines (70, 80, 90, 95, and 100% speeds) for the takeoff position. Data were obtained along each speed line from the maximum flow point to the near stall point. The fan was stalled at each speed line to determine the effect of the inlet on stall margin.

Inlet aerodynamic performance was measured for both the hybrid inlet and the hardwall accelerating inlet, in order to determine the effect of the hybrid inlet wall's acoustic treatment on inlet performance. Total pressure traverses were taken at four operating points over a range of flows which gave a variation in average inlet throat Mach number of 0.72 to 0.94 for the accelerating hardwall inlet in the takeoff/cutback configuration. Traverse data at two points (M_{TH} = 0.73 and 0.88) for this same configuration were taken on the hybrid (treated) inlet. In the approach configuration, three traverses were taken for each of the accelerating hardwall and hybrid inlets, covering a range of throat Mach numbers from 0.71 and 0.81. Boundary layer rakes located behind the wedges, which separated the radial translating panels in the inlet, were also used in the determination of inlet recovery because the translating probe was located between wedges and missed the wedge-wake effect on the recovery factor. The boundary layer rake data were obtained during the fan performance test with the hybrid inlet as described above. Inlet wall static pressures were recorded continuously throughout the entire aerodynamic and acoustic test program on the accelerating and hybrid inlets.

4. Bypass Duct Performance Test (Front-Drive)

The first configuration tested was the acoustically treated splitter duct. A mechanical check-out with the takeoff nozzle installed preceded actual testing. In this check-out the vehicle was operated from 52 to 105% corrected fan speed. At each speed setting, data were taken at two additional core discharge valve settings to establish the bypass ratio relationships. Aerodynamic, stress, and vibration data were recorded.

When the mechanical check-out was complete, testing was initiated with the takeoff nozzle installed at the settings of core discharge valve determined from the check-out data. In the takeoff mode the vehicle was operated at speeds from 53.3 to 106.5% corrected fan speed with each of the six speed points being run twice. Recorded were: fixed aerodynamic data

once for each speed point, traverse aerodynamic data for three points at and near the design takeoff speed, acoustic traverse data once at the design takeoff speed, and far-field acoustic and Kulite data at all points.

Upon completion of the takeoff-mode testing, a shutdown was made and the approach-point nozzle installed, testing then resumed in a similar manner. The speeds for the approach-point operation were between 58.5 and 65.2% corrected fan speed inclusive. The data were recorded in the same pattern as the takeoff mode. When complete, the power-cutback nozzle was installed and the procedure repeated for corrected fan speeds between 69.5 and 99.5% inclusive. Following the completion of the power-cutback mode the test vehicle underwent a configuration change in which the duct wall's acoustic treatment was replaced by hardwall panels and the duct splitter was removed. This configuration was then tested using the same procedure as described for the acoustically treated splitter duct.

D. Data Reduction Calculation Procedures

The fan aerodynamic test data were handled by three phases of data reduction. Each phase used a separate computer program to calculate the overall and blade-element performance for each of the aerodynamic tests. The overall airflow, bypass ratio, bypass, and core portion pressure ratios and efficiencies were calculated on-line using the Phase I data reduction program. This program obtained mass-weighted radial averages of flow conditions at the inlet and exit stations of the fan using the fixed probe instrumentation. The Phase II program circumferentially mass-weighted the output from Phase I to calculate overall performance, rotor, and stator performance parameters such as blade-element efficiencies and loss coefficients at the immersions of the fixed instrumentation. The Phase III program is an axisymmetric streamline flow calculation procedure where the output is interpolated along streamlines to obtain the detailed rotor and stator blade-element performance parameters at the standard percent immersions.

The methods used in calculating inlet total pressure recovery and distortion from the test instrumentation are described in Section VI. Also included in Section VI is a description of the procedure used to analyze the inlet wall Kulite data. Kulites were installed in the inlet just forward and aft of the fan rotor after unsteady rotor blade stresses appeared while testing the approach inlet.

The total pressure loss in the bypass duct was determined from the average total pressures calculated from the profile data supplied by each of the two radial traversing probes. These profile data were in analog form via X-Y plots giving total pressure, total temperature, and probe yaw angle as a function of percent annular height at both locations. The calculation of average total pressure and temperature was performed by digitizing the data and integrating by an area-weighted averaging technique across the annulus. Calculations were corrected for yaw angle, annulus blockage area (due to structural pylons), and estimated pitch misalignment in the diffuser section. This same procedure was used for both duct configurations.

Bypass duct Mach number distributions were based on both the upstream and downstream measured total pressures. This resulted in the definition of an upper and lower duct Mach number boundary. This procedure was utilized to express the variation of total pressure with respect to axial length between the two probes.

The nozzle discharge coefficients were calculated for the three nozzles tested (i.e., takeoff, cutback, and approach) using the measured aft-probe average total pressure and estimated total pressure loss factors for the nozzles at the given conditions. The loss factors used at each condition are given in Section VII.

SECTION V

FAN PERFORMANCE RESULTS AND DISCUSSION

A. Check-Out and Bellmouth Inlet Tests

Aerodynamic testing of the high speed, single-stage fan was conducted with a bypass ratio set at approximately 6:1 for all data points. For the initial testing the inlet configuration consisted of a long bellmouth inlet with instrumentation section, as shown in the top half of Figure 16, with a length-to-fan diameter ratio of 2.3. Following the initial test run, it was discovered that the casing boundary layer measurements from a 6-element total pressure rake and a static pressure on the wall just forward of the fan rotor indicated a rather large boundary layer buildup inhibiting the fan tip performance. To investigate the effect of the long inlet, the cylindrical instrumentation section [81 cm (32 in.) of length] was removed, reducing the length-to-diameter ratio to a more representative value of 1.4. This inlet configuration is compared with the longer inlet in Figure 16. In addition to the removal of the instrumentation section, the rub material above the rotor tip shroud was built up to reduce the seal teeth clearances opened up during the stall testing.

Overall performance and blade-element data were recorded for both test configurations.

1. Overall Performance

The overall fan-stage performance map is presented in Figure 17, showing data points taken during the check-out and bellmouth inlet tests. The fan-rotor performance map is shown in Figure 18. The open symbols on the maps represent data with the long bellmouth inlet and the shaded symbols show data from the short bellmouth inlet.

The measured overall aerodynamic performance parameters for all fan aerodynamic tests are given in Table VI. The pressure ratios and efficiencies are mass-averaged values from the Phase II data reduction program. This phase of the data reduction program uses the actual test measurements with the proper circumferential and radial averaging routine and hence, represents the most accurate overall performance values. Section II of this volume tabulates the overall and blade-element performance data from the Phase III data reduction program. The Phase III program calculates slightly different overall performance data because of a difference in the method that the radial average of pressures and temperatures are calculated.

Table VI(a) presents the data taken during the check-out tests. The objective of these tests was to determine the proper discharge valve (DV) setting to approximate a 6:1 bypass ratio and to establish the baseline stress levels and safe operating regions. Table VI(b) lists data points

Table VI. Single Stage Fan Overall Aerodynamic Performance Data.

(a). Checkout Tests with Long Bellmouth Inlet.

Rdg	% Design Speed	Throttle Setting		Bypass Ratio	Inlet Corrected Weight Flow		Bypass Stage		Core Stage	
		Bypass	Core		kg/sec	lbm/sec	P/P	η_{ad}	P/P	η_{ad}
17	50.2	52	52	5.43	58.71	129.42	1.116	.799	1.164	.947
18	50.2	55	52	5.74	59.98	132.23	1.105	.755	1.161	.864
19	50.2	55	52	5.52	59.93	132.13	1.106	.761	1.161	.873
20	50.1	38	30	5.75	47.36	104.40	1.142	.724	1.158	.821
21	50.1	56	50	5.81	59.11	130.31	1.102	.730	1.154	.876
22	65.3	56	40	6.51	74.97	165.28	1.191	.755	1.269	.906
23	65.2	38	30	5.98	61.37	135.31	1.262	.713	1.265	.805
24	70.3	54	50	5.88	82.70	182.32	1.239	.779	1.317	.884
25	80.0	56	50	6.20	95.32	210.14	1.327	.766	1.411	.905
26	84.9	54	52	6.05	101.25	223.21	1.418	.798	1.471	.901
27	90.1	54	54	5.96	107.53	237.07	1.498	.808	1.514	.857
28	94.6	54	56	5.92	112.09	247.11	1.558	.832	1.559	.850
29	100.1	54	52	5.99	114.90	253.31	1.608	.781	1.614	.814
30	100.1	48	43	6.34	113.46	250.15	1.763	.799	1.633	.818
36	90.1	45	40	6.18	97.48	214.91	1.596	.789	1.531	.847
37	95.1	46	40	6.29	104.54	230.47	1.682	.797	1.579	.837
38	100.1	47	42	6.33	112.25	247.47	1.789	.815	1.637	.822
39	100.1	51	48	6.11	114.22	251.81	1.673	.795	1.613	.818
44	70.2	45	36	6.23	74.01	163.17	1.289	.761	1.315	.861
45	70.2	40	30	6.28	67.53	148.87	1.309	.733	1.304	.818
46	70.2	54	50	6.03	82.49	181.86	1.243	.778	1.319	.916
47	80.1	41	35	5.95	79.38	175.01	1.432	.732	1.406	.822
48	85.0	43	35	6.22	87.41	192.71	1.508	.759	1.456	.832
49	95.0	47	40	6.22	105.82	233.29	1.686	.802	1.573	.831
50	95.1	60	60	5.84	112.42	247.84	1.479	.736	1.559	.843
51	95.1	52	52	6.10	111.70	246.25	1.604	.830	1.560	.846
52	95.0	49	47	6.00	109.72	241.89	1.667	.830	1.578	.856
53	95.1	50.5	50	6.19	111.27	245.30	1.631	.817	1.571	.845
54	89.7	60	60	5.88	108.52	239.25	1.425	.761	1.502	.857

Table VI. Single-Stage Fan Overall Aerodynamic Performance Data (Continued).

(b). Long Bellmouth Inlet Tests.

Rdg	% Design Speed	Throttle Setting		Bypass Ratio	Inlet Corrected Weight Flow		Bypass Stage		Core Stage	
		Bypass	Core		kg/sec	lbm/sec	P/P	η_{ad}	P/P	η_{ad}
55	89.9	50	50	6.05	105.16	231.84	1.552	.831	1.524	.873
56	89.9	47	45	6.12	101.40	223.55	1.586	.811	1.535	.869
57	50.0	70	70	5.17	63.83	140.73	1.077	.694	1.144	.901
58	50.1	45	45	5.64	54.46	120.06	1.128	.784	1.158	.890
59	50.1	41	40	5.74	51.16	112.79	1.138	.776	1.161	.899
60	65.2	45	40	6.02	69.97	154.25	1.238	.780	1.277	.889
61	85.3	60	60	5.86	103.85	228.96	1.365	.737	1.469	.889
62	85.2	49	45	5.71	97.55	215.07	1.477	.807	1.473	.882
63	85.2	45	43	5.95	93.41	205.94	1.511	.795	1.478	.861
64	80.1	60	60	5.85	97.77	215.55	1.300	.754	1.409	.898
65	80.1	47	45	6.02	90.21	198.88	1.409	.813	1.423	.880
66	80.0	44	40	5.92	85.60	188.71	1.422	.772	1.416	.849
67	70.0	60	60	5.67	85.84	189.24	1.206	.755	1.309	.913
68	70.1	49	45	6.04	79.62	175.52	1.267	.790	1.320	.906
69	93.1	50	50	5.98	108.85	239.98	1.609	.829	1.556	.865
70	97.1	50	50	6.02	112.51	248.04	1.669	.824	1.591	.842
72	99.9	49	47	6.00	113.84	250.97	1.742	.806	1.625	.829
73	99.9	60	60	5.79	115.20	253.98	1.518	.715	1.612	.830
74	104.9	55	50	5.99	116.84	257.59	1.637	.741	1.679	.816
75	105.0	48	40	6.41	115.86	255.43	1.850	.782	1.678	.782
76	105.0	51	45	6.20	116.51	256.87	1.747	.770	1.657	.787
77	105.0	60	55	5.64	117.08	258.11	1.566	.704	1.684	.841
78	110.1	55	50	5.86	118.36	260.94	1.671	.715	1.724	.780
87	109.7	48	40	6.27	117.49	259.02	1.873	.740	1.738	.775
88	109.9	51	50	5.92	117.82	259.74	1.760	.725	1.734	.789
107	95.3	65	65	5.70	112.47	247.95	1.448	.706	1.561	.854
117	100.0	49	47	6.34	112.93	248.96	1.754	.820	1.628	.791
118	100.1	50	50	6.08	113.40	250.00	1.718	.802	1.628	.817
121	95.1	50	48	6.30	109.38	241.14	1.648	.810	1.562	.843
124	95.1	52	52	5.88	110.83	244.35	1.602	.829	1.571	.813
127	90.0	50	50	5.94	102.83	226.71	1.556	.806	1.523	.865

Table VI. Single-Stage Fan Overall Aerodynamic Performance Data (Continued).

(c). Bypass Migration Tests with Long Bellmouth Inlet.

Rdg	% Design Speed	Throttle Setting		Bypass Ratio	Inlet Corrected Weight Flow		Bypass Stage		Core Stage	
		Bypass	Core		kg/sec	lbm/sec	P/P	η_{ad}	P/P	η_{ad}
79	80.0	47	22	9.06	83.00	182.90	1.396	.762	1.363	.764
80	80.0	47	98	5.10	92.76	204.51	1.407	.811	1.404	.863
81	80.1	47	60	5.29	91.81	202.40	1.408	.810	1.433	.900
82	80.1	47	35	6.40	87.06	191.93	1.404	.777	1.407	.848
83	80.3	44	15	10.94	78.10	172.10	1.403	.723	1.364	.730
84	80.2	44	98	4.87	90.79	200.14	1.431	.808	1.413	.854
85	80.2	44	50	5.47	87.97	193.93	1.429	.799	1.440	.877
86	80.1	44	25	7.66	81.16	178.94	1.410	.742	1.373	.769
89	95.0	50	15	11.94	100.90	222.20	1.622	.752	1.522	.715
90	94.9	50	98	5.77	111.50	245.80	1.616	.831	1.569	.823
91	95.0	50	60	5.57	111.30	245.30	1.624	.826	1.580	.857
92	94.8	50	30	7.60	106.40	234.50	1.646	.803	1.522	.767
93	94.9	48	20	10.24	100.00	220.40	1.642	.756	1.541	.745
94	95.0	48	99	5.63	110.96	244.62	1.662	.836	1.597	.849
95	94.9	48	60	5.42	110.51	243.63	1.663	.823	1.606	.871
96	95.0	48	35	6.87	104.86	231.17	1.664	.788	1.546	.786

(d). Traverse Test Points with Long Bellmouth Inlet.

Rdg	% Design Speed	Throttle Setting		Bypass Ratio	Inlet Corrected Weight Flow		Bypass Stage		Core Stage	
		Bypass	Core		kg/sec	lbm/sec	P/P	η_{ad}	P/P	η_{ad}
102	100.2	54	100	5.85	114.36	252.12	1.567	.771	1.600	.826
105	100.2	47	100	5.97	113.71	250.69	1.721	.796	1.649	.831
106	100.3	50	100	6.75	114.29	251.97	1.641	.786	1.619	.822
113	100.0	54	70	5.56	114.65	252.76	1.597	.782	1.618	.878
114	100.1	50	70	5.43	114.06	251.46	1.693	.800	1.649	.832
116	100.1	47	70	6.07	112.68	248.42	1.763	.810	1.642	.828
111	79.3	47	30	7.51	81.86	180.47	1.388	.760	1.375	.786
119	100.1	52	50	6.24	114.00	251.32	1.674	.790	1.621	.815
122	95.0	49	48	5.92	108.28	238.72	1.658	.813	1.593	.885
125	95.4	52	52	5.78	110.93	244.55	1.625	.829	1.578	.863
129	89.8	52	50	6.62	104.17	229.67	1.529	.827	1.514	.884
133	95.1	49	30	7.82	102.12	225.13	1.664	.782	1.528	.731

Table VI. Single-Stage Fan Overall Aerodynamic Performance Data (Continued).

(e). Short Bellmouth Inlet Tests.

Rdg	% Design Speed	Throttle Setting		Bypass Ratio	Inlet Corrected Weight Flow		Bypass Stage		Core Stage	
		Bypass	Core		kg/sec	lbm/sec	P/P	η_{ad}	P/P	η_{ad}
140	69.8	49	45	5.94	76.98	169.72	1.275	.779	1.322	.892
141	70.0	49	45	5.91	77.05	169.86	1.277	.782	1.321	.864
142	79.8	48	45	6.05	88.55	195.21	1.419	.803	1.428	.891
143	89.7	51	50	6.06	104.82	231.09	1.581	.829	1.543	.880
144	90.3	51	50	5.95	104.81	231.07	1.577	.826	1.549	.867
145	94.6	52	52	6.04	110.87	244.43	1.645	.839	1.581	.859
146	95.1	51	52	5.89	110.66	243.97	1.677	.831	1.592	.868
147	95.1	53	53	6.11	112.04	247.00	1.657	.858	1.593	.865
149	100.0	51	48	5.88	114.50	252.53	1.756	.822	1.665	.823
150	99.9	50	48	5.93	114.03	251.40	1.779	.817	1.645	.823
152	99.9	49	47	6.49	113.79	250.85	1.808	.813	1.634	.841
154	99.9	48	45	5.80	112.23	247.43	1.817	.816	1.648	.826
155	99.9	54	52	6.07	115.34	254.29	1.675	.819	1.629	.823

(f). Hybrid Inlet Tests, Takeoff Mode.

Rdg	% Design Speed	Throttle Setting		Bypass Ratio	Inlet Corrected Weight Flow		Bypass Stage		Core Stage	
		Bypass	Core		kg/sec	lbm/sec	P/P	η_{ad}	P/P	η_{ad}
170	69.9	53	53	5.34	82.91	182.79	1.259	.769	1.322	.910
171	80.0	53	53	5.92	93.64	206.45	1.382	.785	1.436	.950
172	90.0	53	53	6.28	105.62	232.85	1.553	.807	1.546	.883
173	93.0	53	53	6.98	109.00	240.31	1.608	.850	1.577	.923
174	94.9	53	53	6.27	110.83	244.35	1.616	.820	1.570	.869
176	69.9	51	49	5.99	79.24	174.69	1.275	.779	1.326	.933
177	69.9	42	30	6.41	67.37	148.52	1.310	.743	1.303	.856
178	80.0	51	49	6.47	88.86	195.90	1.400	.798	1.431	.921
179	80.0	46	40	6.22	80.92	178.39	1.437	.782	1.415	.848
181	90.0	51	49	6.36	103.62	228.44	1.562	.812	1.543	.919
182	90.1	60	60	6.02	107.81	237.68	1.461	.780	1.511	.886
183	90.1	48	40	7.06	99.41	219.17	1.586	.781	1.526	.838
184	95.0	51	49	6.15	109.33	241.03	1.666	.827	1.597	.896
185	95.0	51	40	6.83	108.69	239.62	1.679	.814	1.580	.844
191	100.1	97	97	5.92	114.69	252.85	1.465	.670	1.569	.809
192	100.1	53	53	6.38	114.08	251.49	1.666	.801	1.625	.865
194	100.5	51	49	6.58	113.18	249.51	1.720	.773	1.633	.810
195	100.5	51	45	6.50	112.93	248.96	1.753	.790	1.653	.839
196	93.1	52	49	6.35	108.20	238.55	1.624	.820	1.580	.890
197	91.2	70	70	5.75	111.33	245.44	1.427	.716	1.534	.898
198	90.2	60	60	6.03	108.67	239.57	1.476	.763	1.519	.861
199	89.0	65	65	5.90	108.14	238.40	1.416	.721	1.503	.864

Table VI. Single-Stage Fan Overall Aerodynamic Performance Data (Concluded).

(g). Hybrid Inlet Tests, Approach Mode.

Rdg	% Design Speed	Throttle Setting		Bypass Ratio	Inlet Corrected Weight Flow		Bypass Stage		Core Stage	
		Bypass	Core		kg/sec	lbm/sec	P/P	η_{ad}	P/P	η_{ad}
202	65.0	54	50	5.90	74.61	164.48	1.214	.801	1.277	.959
203	50.0	54	50	5.18	56.91	125.35	1.113	.870	1.157	.970
204	66.6	56	50	5.41	77.47	170.80	1.216	.772	1.289	.935
206	50.0	100	100	4.88	64.40	141.99	1.074	.743	1.140	.983
207	49.9	43	30	5.99	48.86	107.72	1.139	.797	1.152	.960
208	62.6	100	100	5.13	79.17	174.54	1.120	.706	1.222	.946
210	64.7	70	70	5.39	79.64	175.58	1.152	.696	1.253	.919
211	64.7	76	70	5.49	80.21	176.83	1.142	.696	1.250	.926
212	64.7	45	30	6.33	65.20	143.72	1.243	.793	1.255	.908
213	66.5	50	40	6.46	72.66	160.19	1.239	.829	1.281	.963
214	70.0	50	40	6.57	76.44	168.51	1.273	.798	1.313	.944
215	69.9	52	50	5.84	79.23	174.66	1.261	.787	1.322	.959
216	69.9	47	30	6.71	72.26	159.31	1.287	.777	1.294	.844
217	62.6	100	100	5.18	79.13	174.44	1.122	.646	1.219	.858

recorded during the major portion of the aerodynamic performance test with the long bellmouth inlet. Table VI(c) shows the test points taken during the bypass ratio investigation where the major objective was to determine whether throttling the fan with the core valve at a fixed bypass valve setting had any effect on the aerodynamic performance. This investigation was carried out at 80% and 95% corrected speeds. Table VI(d) indicates the points which were associated with traverse measurements at the inlet and exit stations of the fan rotor. Table VI(e) lists the overall performance results from the run with the short bellmouth inlet. The major objective here was to determine the effect of the inlet length and rotor tip clearances on the fan aerodynamic performance. Tables VI(f) and (g) show the data points taken during the aerodynamic performance test of the hybrid inlet in the takeoff and approach modes. This testing was conducted to evaluate the effect of the hybrid inlet on fan aerodynamic performance.

At 100% speed with the long bellmouth inlet (Figure 17), the test point closest to the operating line passing through the design point has a total pressure ratio of 1.74 at 113.8 kg/sec (251.0 lbm/sec) airflow and an adiabatic efficiency of 80.6%. This test point [Rdg 72, Table VI(b)] is 3.4% low in flow and 3.4 points low in efficiency relative to objectives. The design specific flow rate was 215 kg/sec m^2 (44.0 lbm/sec ft^2) of inlet annulus area with the actual test data indicating a value of 208 kg/sec m^2 (42.5 lbm/sec ft^2) at the operating-line throttle setting. The maximum flow attained at design speed was 115.2 kg/sec (254.0 lbm/sec), 2.2% lower than the design objective.

The overall performance with the short bellmouth inlet showed a significant improvement in efficiency at the higher corrected speeds. For a point near the operating line at 100% corrected speed [Rdg 149, Table VI(e)], the measured airflow was 114.5 kg/sec (252.2 lbm/sec) at a bypass pressure ratio of 1.76 and a bypass portion adiabatic efficiency of 82.2%. This represents an improvement of 1.6% in efficiency and 0.6% in flow. A comparison of the stage exit efficiency radial profile indicated that the efficiency did not improve in the tip region, as would be expected, but improved over the lower half of the bypass portion. A comparison of the radial distributions of total pressure and efficiency for the long and short bellmouth inlet configurations for the nominal operating line at 100% speed is shown in Figure 19. The corresponding profiles of rotor diffusion factor, total temperature ratio, and rotor loss coefficient are shown in Figure 20.

The bellmouth inlet was shortened by removing the cylindrical instrumentation section which contained the fan inlet total pressure and total temperature rakes. The drag of these rakes was calculated (using a typical drag coefficient) to have a total pressure loss of about 0.3% near the operating line at 100% speed. This would account for more than half of the measured flow increase and approximately 0.5% efficiency gain. At the same time the inlet instrumentation section was removed, the two radial total pressure rakes in the bypass stream between the rotor and outlet guide vanes were also removed.

There is a possibility that the wakes from the inlet rakes were causing local high temperature and low pressure regions at the fan exit which were being measured by the fan discharge rakes at the inner three immersions,

though a simplified calculation indicated that the wakes should miss the discharge rakes.

Inspection of the individual pressure and temperature elements of the three innermost fan discharge arc-rakes shows a higher average total pressure and lower total temperature for the short bellmouth inlet test with a more consistent pattern across a vane pitch. Review of these data suggests that the apparent improvement in efficiency for the short bellmouth inlet test cannot be fully explained.

Another possibility for part of the difference in performance between the long and the short bellmouth inlet tests is that the bypass ratios were slightly lower during the short inlet test. A lower bypass ratio would allow for better flow conditions in the inner portion of the outer duct, which is the region where the efficiency improvement is most noticeable.

Several items of data were examined in order to explain the flow deficiency relative to design. Inspection of the rotor incidence angles for the most unthrottled point at each speed indicates that the incidence angle stayed essentially constant from 90 to 100% corrected speed. This suggests that the flow limit was set by the flow induction surface angle rather than by too small a blade passage throat area. This is not surprising since the blade passage area distribution was designed so that it could operate with a swallowed shock at the takeoff condition (92.1% corrected speed), and it can only do this if the throat is not limiting the flow. If the flow were being limited by the rotor throat area, the incidence angle would tend to decrease with increasing speed because the inlet relative Mach number is above unity over the outer 70% of the span at 90% speed. It was previously mentioned that the maximum flow measured at the design speed was 2.2% lower than design. It would require opening (making more axial) the flow induction portion of the blade by about one degree to increase the flow to the design value.

A correlation, based on past General Electric experience, was used in the design procedure to determine the amount that the flow induction surface must be displaced from a "free-flow" streamline to account for the finite leading edge thickness, bow wave loss, and surface boundary-layer growth. However, there were several differences in the design procedure for this fan relative to the designs included in the correlation, such that an adjustment should have been made to the correlation, but was not. First, a rotor inlet annulus boundary layer allowance of 1.1% was used in the design of this fan, while most of the designs included in the correlation had used a 2% boundary layer allowance. This accounts for 0.9% of the flow deficiency. Second, the rotor blade coordinates for the other designs had been specified on cylindrical surfaces, but manufactured as if the coordinates were for plane surfaces. The rotor blade coordinates for this fan were generated on plane surfaces. The net effect of the older practice was that the leading and trailing edges of the blade, as manufactured, were actually somewhat more open than design intent. This was not accounted for in the correlation. In addition, the suction surface incidence angle was selected to be toward the low side of the correlation because of concern about adverse effects on part speed performance with a blade designed for a larger incidence angle.

The 100% corrected speed line, Figure 17, is less vertical at throttle settings below the operating line than one would expect for this relatively high Mach number fan. The measured flow at the operating line is about 1% less than the flow at the most unthrottled setting at this speed. Most stages of this design Mach number level operate on a rotor cascade flow limit (either set by throat area or by the flow induction surface) at the lower back pressure operating points. Under these conditions, the leading edge shock is either attached, or remains at a fixed standoff distance. The flow will remain constant until the back pressure is increased sufficiently to cause the leading edge shock to move out in front of the cascade passage. Additional throttling beyond this point will cause the flow to decrease and the shock standoff distance to increase. It is believed that somewhat greater effective camber in the trailing edge region would probably cause the speed line to be more vertical, increasing flow at the operating line, and possibly improving the operating line efficiency. The reasoning behind this belief is as follows: The static pressure rise coefficient produced by a cascade is related to the ratio of the cascade passage exit area to the inlet (capture) area, the inlet Mach number, and the cascade losses. Increasing the cascade exit area by increasing the camber in the rear of the blade permits a larger static pressure rise for given inlet conditions, provided the losses do not significantly increase. This permits a higher pressure ratio to be achieved before the flow begins to decrease and the shock moves out ahead of the leading edge. However, since the speed line is not completely vertical, even at 110% speed where the relative Mach numbers are significantly higher, there is speculation that the increased leakage through the rotor tip shroud seals as the fan is throttled may also be at least a partial explanation for the speed line's shape.

The rotor work input was close to design intent over the outer 65% of the blade span as shown by the plot of stage temperature ratio on Figure 20. The rotor loss coefficients (also shown on Figure 20) were larger than design intent and appear to be the main contributor to the lower-than-design-intent pressure ratio of this portion of the blade (Figure 19). The measured temperature rise was below design intent for the inner 35% of the rotor blade and the calculated rotor deviation angle (Figure 21) was larger than design intent. This discrepancy in deviation angle was greatest in the vicinity of the flow splitter, but the reasons for this are not apparent.

For the short bellmouth inlet tests, the calculated rotor total pressure loss coefficient (Figure 20) was larger than design intent over the outer 50% flow and locally in the hub region. Preliminary test results of the lower aerodynamically loaded 488 m/sec (1600 ft/sec) tip speed stage of Reference 7 became available during the early design phase of this fan. These very encouraging test results led to the selection of lower loss coefficients for the outer 50% span than would have otherwise been used. Furthermore, it is believed that the lower-than-design flow of the fan reported here contributed to the higher-than-design rotor losses. The lower-than-design flow reduced the blade capture area, which increased both the mouth-to-capture and throat-to-capture area ratios. This caused the Mach number ahead of the leading edge shock to be higher than design intent, leading to increased shock losses. The design rotor throat-to-capture area ratio was set to give approximately

6% margin above the critical area ratio after allowances for losses equal to those of a normal shock at the upstream Mach number. The reduced capture area resulting from the low flow increased the "throat margin" from the 6% design value to about 15% near the tip and to about 8% at 50% design flow (at the 100% speed operating line point). It is believed that this "excess" throat area increased the degree of separation in the blade passage, contributing to the higher-than-design losses.

The effects of bypass-stream throttling on the radial profiles of stage pressure ratio and efficiency are shown in Figure 22. Three test points are shown, representing low, nominal, and high operating-line test points. The pressure profiles shift with throttling in the normal manner. The lack of a substantial decrease in efficiency in the tip region when the back pressure is significantly reduced from design is attributed to the fact that the rotor blade has very little camber in the outer 25% of the span. At the reduced back pressures, the flow will remain supersonic behind the leading edge shock and reaccelerate to the cascade exit in the diverging passage downstream of the throat. The flow then undergoes a shock at the cascade exit. If the rotor blades had more camber (greater area increase from the throat to the cascade exit), the flow would accelerate to a higher Mach number ahead of the trailing edge shock, resulting in larger shock losses and poorer efficiency at back pressures significantly below design. Increased camber in the outer portion of the blade would lower the efficiencies at the low back pressure, but would probably result in higher efficiencies at the more throttled conditions.

The stall limits for each speed line shown on the performance map in Figure 17 are within 1.5% of the stall-line goal at speeds up to 85% of design. Above 85% speed, the measured stall line is 3 to 5% below the goal for the long bellmouth inlet test. The first time the fan was stalled, with the short bellmouth inlet installed and with the rotor tip-shroud seal clearances reduced to zero at 100% speed, the stall margin was only 1.6% below the goal. Each successive stall, after the initial rub-in of the tip clearance, produced less stall margin, but still above the value measured with the long bellmouth inlet. The third stall is shown approximately 4% below the stall-line goal. The second stall (not shown on the map) occurred approximately halfway between the two stall symbols shown on the performance map at 100% speed. The tighter rotor tip-shroud seal clearance probably accounted for most of the stall-line improvement, with some possible gain due to the thinner boundary layer entering the fan with the short bellmouth inlet. The tighter tip-shroud seal clearances may have also contributed to the improved efficiency, though it isn't evident from the measured radial profiles.

A map of the fan hub performance determined from core duct arc-rake measurements of pressure and temperature is shown in Figure 23. The speed line shapes representing the hub pumping characteristics are extremely flat, as is expected for a low radius ratio stage fan where throttling occurs primarily in the tip region. The 100% speed-line pressure ratio is about 1.62 compared to the design intent of 1.69. The hub efficiency is about 2% below the design objective. The half-shaded symbols represent data taken

during the short inlet test run and show that the pressure-ratio capability of the blade has improved somewhat in the hub region too. The efficiency level, however, is not significantly different. The fully shaded symbols on this map show the test points taken with off-design bypass ratios at 80 and 95% corrected speed. The data points at the very low flow levels were taken with extremely high bypass ratios. Although no surge was encountered as the core flow was throttled, a large degree of flow separation from the core stator, as determined by stator strain gage instrumentation, did occur, and caused a significant performance penalty. On the other hand, the test data taken [Readings 90, 91, 94, and 95 in Table VI(c)] at lower-than-design bypass ratios (in the range of 5.4 to 5.8) showed a slight improvement in the hub efficiency at 95% speed. Inspection of the static pressures on the surface of the flow splitter suggests that a bypass ratio setting slightly below the design value of 6.0 shows a better flow condition in the ducts downstream of the rotor. This indicates that the flow splitter was positioned at just slightly too high an angle of attack relative to the actual flow conditions.

2. Blade-Element Performance

Blade-element performance data for the rotor, bypass OGV, and core stator are shown in Figures 24 through 42. For the standard immersions, deviation angle, diffusion factor, and loss coefficient are plotted versus the mcanline incidence angle. The open symbols represent data points listed in Table VI(a) and (b) and taken during the long bellmouth inlet tests. The shaded symbols represent data points listed in Table VI(e) taken with the short bellmouth inlet. Blade-element data were calculated using the Phase III data reduction program for nearly all the test points listed in Table VI(a) through (g).

The listings of blade-element performance quantities for the rotor, bypass OGV, and core stator are contained in Section 2 of this volume, under a separate cover.

Figures 24 through 32 present the rotor blade-element data at the standard percent immersions from tip to hub. The loss coefficients, diffusion factors, incidence angles, and deviation angles are calculated from the input quantities of total pressure and total temperature at the blade row inlet and exit and the total corrected airflow and speed. The total pressures used at the rotor exit station are the three highest values from each of the seven bypass OGV exit arc-rakes and the five core stator exit arc-rakes. The average total temperature at each arc-rake is also transposed to the rotor exit station. The Phase III data reduction program then interpolates the data to the standard percent immersions.

The open-symbol data points show that, at the tip immersions, the rotor incidence angle at 100% speed is 1 to 2 degrees higher than design intent. Data from the short bellmouth inlet test also do not show a lower incidence angle at the 5% immersion, where the 0.6% flow increase would have been expected. Instead, the incidence in the 30 to 70% immersion range appears

slightly lower for the short inlet test, suggesting the flow increase in this region (see also Figure 21). The loss coefficients are higher than design intent in the tip region (Figure 24) for both inlet tests and any gain in performance from the short inlet appears most noticeably at the 70% immersion. At the other immersions, no significant difference in performance from the open to the shaded symbols is evident. The diffusion factors are the highest in the region of 50 to 85% immersion, which is consistent with the design values and influenced by the flow splitter just aft of the rotor at approximately 72% immersion. There is a lack of concrete evidence that the overall performance gains with the short inlet are attributable to a cleaner boundary layer in the tip region. This further suggests the possibility of the inlet and bypass stream rakes influencing the performance measurements.

The bypass OGV blade element data are shown in Figures 33 through 37 at five radial immersions. Design deviation angles were used to calculate blade element parameters, since OGV exit flow angles were not measured. The total pressure loss coefficients were calculated by assuming that the OGV inlet pressure is the average of the three highest elements of the total pressure arc-rake and the downstream value is the mass averaged value at each rake immersion. The difference in the OGV losses between the operating line and an unthrottled point increases rapidly with speed when the vane operates in a region where the incidence is a large negative value. This is particularly evident in the 30 to 70% immersion region where the open symbols on the choke side of the loss bucket represent data points taken with the bypass throttle area nearly wide open. On the stage performance map (see Figure 17) these are the lowest throttle points at each speed. As the speed increases from 70 to 80%, the loss coefficient begins to climb rapidly as the throttle valve is opened to its maximum area. At the lower speeds (50 to 85%), the loss bucket is relatively flat over the incidence angle swing from choke to stall.

The core stator blade element data is shown on Figures 38 through 42 at 15, 30, 50, 70, and 85% immersion, respectively. Again, design deviation angles are employed. The losses appear highest in the hub region but do not vary much as the fan is throttled from the lowest pressure ratio on each speed-line to the near-stall point. This is due to the fact that the core region is not as sensitive to throttling as the bypass in this high bypass ratio fan.

B. Bypass Ratio Migration Tests

Additional testing was performed to investigate the effect of off-design bypass ratios on fan performance. Test readings were taken at 80 and 95% of design speed with the bypass throttle valve set at nominal operating-line and high operating-line settings. The core valve was then throttled from each of these points until a surge (heavy rotating stall) was encountered. The point of rotating stall was determined by the onset of a modulating stress signal from the rotor strain gages. Four data points were taken along each speed-line with the bypass valve set at both the high and nominal operating-line settings and the core valve settings from wide-open to nearly fully closed.

In the case at 80% speed, where the bypass valve was set at an operating-line position, throttling the core valve did not produce a fan surge but rather a rotating stall getting progressively worse with the throttling. In the other three excursions, two at 95% speed and one at 80% speed from the high operating line, fan rotor stresses took a noticeable jump in level at core DV settings very near the fully closed point.

The fan overall performance map with the off-design bypass ratio test points is shown in Figure 43. The shaded symbols represent test points taken with the bypass DV at a high operating-line setting and the throttling done with the core valve only. The lowest flow test point at each speed was taken with the core valve almost fully closed. The open symbols represent the data for a nominal operating line bypass valve setting with different core valve settings from fully open to almost fully closed.

The most noticeable results from this test indicate that off-design bypass ratios have little effect on the overall stage performance. The speed-line characteristic is flatter and unique for each bypass DV setting. The flow and efficiency levels, however, are not much different from the nominal bypass ratio data.

These off-design bypass ratio points were also shown on the fan hub performance map in Figure 23 (shaded symbols). Here, the amount of hub throttling capability is quite evident as the speed lines become very flat and the amount of flow rollback exceeds 50% of the flow at the nominal throttle setting.

C. Hybrid Inlet Tests

Aerodynamic performance test measurements were taken with the flight-type hybrid inlet installed ahead of the fan vehicle. The main objective of this test was to determine the effect of the inlet on fan aerodynamic performance by comparing overall and blade-element data with that taken from the long bellmouth inlet testing. Test readings were taken with the inlet positioned in both the approach and takeoff modes. The sketch in Figure 44 shows the inlet flow lines for both the takeoff and approach positions. In the takeoff mode, with the inlet throat area designed for a Mach number of 0.79 at approximately 92% speed, performance data were taken at 70, 80, 90, 95, and 100% speed lines, mapping each speed line from below the nominal operating line to stall. The adjustable inlet, when positioned in the approach mode, also was designed for a 0.79 Mach number at approximately 65% speed. With the inlet in this position, performance data were taken at 50, 65, and 70% speeds and compared with the long bellmouth inlet testing at these same speeds. These three speed lines were mapped to stall from low operating-line points. The overall fan aerodynamic performance data for both the approach and takeoff positions are shown on Figure 45. The blade-element data are listed in Section 2 of this volume (under separate cover). The acoustic test results of the hybrid inlet are presented in Reference 4 and the inlet aerodynamic test results are presented in Section VI of this volume.

The fan aerodynamic performance was measured with the same downstream instrumentation as in the long bellmouth inlet testing, but there was no fixed instrumentation upstream of the fan. Inlet thermodynamic properties were determined for some of the data points from radial traverses of total pressure and total temperature. The inlet recovery was calculated from the traverse total pressure and the barometric pressure recorded at the time of each reading. The dry bulb temperature, measured in the vicinity of the test vehicle for every reading, was the main source for an inlet temperature. This is not considered a highly accurate measurement and can greatly influence the efficiency calculated for each data point. This is particularly true at the flow speeds where a one-degree error in inlet temperature can cause a 6% error in the calculated efficiency. Static pressures were aligned axially along the inlet from the throat to the fan face. A seven-element, total-pressure boundary-layer rake mounted just upstream of the fan rotor was also present.

The open data symbols on Figure 45 show the fan performance with the inlet in the takeoff mode. At speeds from 70 to 95%, the data show that the stall pressure ratio of the long bellmouth inlet test was achieved, and the loss in stall margin is primarily a loss in flow rollback at constant speed in the order of magnitude of 1.5 to 4%. At 100% speed, beyond the design throat Mach number of 0.79, the loss in stall pressure ratio is 3.7% from the stall line measured with the long bellmouth inlet at a constant airflow of 112.4 kg/sec.

The speed/flow relationship of the fan with the inlet in the takeoff position matches the long bellmouth inlet testing quite well. At 95 and 100% speeds, the flow along the nominal operating-line is about 1% low relative to the short bellmouth inlet test results.

The overall fan efficiency as measured by rakes in the bypass duct is approximately 1.5 to 2.0 points low relative to the long bellmouth inlet testing at 70, 80, and 90% speeds. At 95 and 100%, the efficiency is quite similar to the long bellmouth inlet results but 1.5 to 2.0 points lower than the short bellmouth inlet test data. Although these efficiency calculations are not considered the most accurate because of the uncertainties in the measurements, the differences from the long bellmouth inlet performance results are considered fairly realistic.

The fan overall aerodynamic performance with the inlet in the approach mode is also shown in Figure 45, as indicated by the shaded data symbols. In this speed range (50-70%), the flow again matches the long bellmouth inlet data quite well. The loss in stall margin, calculated at a constant flow, is greater for this inlet position ranging from 3.8% at 50% speed to 6.4% at 70% speed. The amount of stall margin remaining from the approach condition on the map is sizeable however, being approximately 35%. The calculated efficiencies shown on the performance map in Figure 45 are suspect because of the inaccurate inlet measurements described earlier in this section.

Blade-element data for all the test points taken with the hybrid inlet are listed in Section 2 of this volume. Figures 46, 47, and 48 show the fan rotor deviation angle, diffusion factor, and loss coefficient variations with incidence, for three different immersions. Figures 49 through 54 show the same blade-element type data for the bypass OGV and the core stator. The open symbols represent the data points taken with the hybrid inlet in the takeoff position and the shaded symbols the approach position data.

The rotor blade-element data (Figures 46 through 48) show slightly higher loss coefficients in the tip region (10% immersion) relative to the standard bellmouth inlet data (Figures 24 through 32). The loss increases are only very minimal considering the added boundary layer associated with the hybrid inlet. At the pitchline immersion, the losses are about the same, while at the hub they are somewhat lower than the long bellmouth configuration test results. The negative loss coefficients shown in Figures 47 and 48 occur mostly at the very low corrected speeds and in the extreme hub region. It was pointed out previously that the hybrid inlet performance data were taken without fixed inlet instrumentation. The uncertainty of the actual inlet total pressure and temperature, and of the radial distributions, is believed to be the cause of the negative loss coefficients and the unusually high efficiencies calculated for the core flow region.

The rotor diffusion factors and deviation angles show the same trends and levels as demonstrated with the bellmouth tests. The highest D-factors appear in the hub region at high speed and vary with throttling from 0.42 to 0.54. The tip has less aerodynamic loading and throttles at nearly a constant incidence angle without much flow rollback.

The bypass OGV and core stator blade element data shown in Figures 49 through 54 indicate little or no difference when compared to the bellmouth inlet data. This is to be expected since the method of calculation is the same and dependent only on the vane exit wake profiles, i.e., the three highest total pressures from the wake rake are used as the vane inlet average total pressure.

SECTION VI

INLET PERFORMANCE RESULTS AND DISCUSSION

A. Inlet Recovery and Distortion

Because of the complex system of wedges in the hybrid inlet, it was impossible to determine an exact value of inlet recovery with the available amount of circumferential total pressure instrumentation. However, it was possible to determine a value of inlet recovery within a fairly narrow band.

By normalizing and then integrating the total pressure profiles determined by the cobra probe, a value of η'_T was determined as if there were no wedge blockage in the inlet. Because the total pressure is noticeably reduced in the wake behind a wedge, the value determined by the cobra probe represents the highest level in the inlet recovery band. Integrating the pressure profile determined by the boundary layer rake located in the wake behind a wedge gives a considerably lower value for recovery, which is labeled η'_ω. The recovery bandwidth was determined by area weighting these recovery values based on area blockage at the throat. The method follows:

For each recovery value, assign a corresponding recovery "defect" D_η. In the traverse zone (with the cobra probe),

$$D_{\eta'_T} = 1 - \eta'_T$$

and behind the wedges (with the boundary layer rake),

$$D_{\eta'_\omega} = 1 - \eta'_\omega$$

If R_o is the inlet wall radius and R_i is the radius where the total pressure reaches ambient, compute the area of the so called defect region.

$$A_{Def} = \pi[R_o^2 - R_i^2]$$

Now define A_ω as the area occupied by the 12 wedges* and call A_T the area not under the influence of wedge blockage.

$$A_T = A_{Def} - A_\omega$$

*A_ω is measured at the throat to give a better indication of the wedges' influence on pressure recovery. Everything else is measured at the rake or traverse plane. A_T is therefore not a true physical area.

An area weighted total pressure defect can now be determined.

$$D\eta'_R = \frac{A_\omega D\eta'_\omega + A_T D\eta'_T}{A_{Def}}$$

Finally, evaluate the area-weighted inlet total pressure recovery:

$$\eta'_R = 1 - D\eta'_R$$

which is the recovery value determined by the filled-in symbol in Figures 55 and 56. As was previously noted, the upper bound of the recovery band is the value determined by considering no wedge blockage. For the lower bound, double area weighting was given to the wedge blockage. Since the shape and size of the wakes developing around the wedges is not well known, doubling the effective area of the wedges should compensate for unknowns and serve as a guideline in bounding the probable recovery level.

The effect of this area weighting is immediately obvious upon examining Figures 55 and 56. In the takeoff position, where most of the wedge is exposed to the airstream, recovery can be determined to within a 1/2% band. In the approach mode, where very little of the wedge is exposed, recovery can be more accurately pinpointed, this time to within 1/20%.

Figure 55 shows the area-averaged inlet total pressure recovery for the inlet in the takeoff mode. As can be seen, the accelerating inlet just meets the pretest estimate on its upper band, but still is operating at 99% efficiency at the design throat Mach number of 0.79. It is to be expected that actual recovery levels are lower than estimates, since no wedge wake or mixing losses were accounted for in those estimates. Similarly, the hybrid inlet is slightly lower in pressure recovery than the accelerating inlet due to the additional scrubbing losses of the wall treatment, but is still at 98.9% recovery at the design point. Both inlets exhibit a sharp dropoff in operating efficiency above a nominal throat Mach number of 0.84, due in part to the development of a shock system at the throat.

For the approach inlet, recovery levels (Figure 56) are somewhat lower than for the takeoff modes but follow a similar pattern. The design recovery factor was overestimated, this time by 1% at the 0.79 design Mach number. This is probably due to much greater mixing losses in the approach inlet as compared to the takeoff inlet, resulting from the greater contraction ratio demanded by the approach inlet. The absolute level of recovery is still high, 98.4% for the accelerating and 98.2% for the hybrid inlet at Mach 0.79. Again there is a sharp dropoff above the 0.79 design Mach number.

Inlet total pressure distortion was defined as the ratio of the maximum pressure loss from ambient to the mean total pressure, neglecting the 10% of the area nearest the wall (in this case, 2 centimeters) for boundary layer.

$$\text{Distortion} = \frac{P_{T_{amb}} - P_{T_{min}}}{\bar{P}_T}$$

Distortion measurements should be made behind a wedge since that is where the pressure defect will potentially be the largest. Because no boundary layer rake was positioned behind the wedge in the hybrid takeoff inlet, the distortions discussed here will all be for the accelerating inlets. However, because the 2 centimeters nearest the wall were neglected, results should be very nearly identical to the hybrid inlets.

As shown in Figure 57 at the design Mach number, pressure distortions fall below 10% and don't actually reach that value until well past the design point. Below the design point, the approach inlet is more distortion free than the takeoff inlet because the wedge blockage is less pronounced at approach.

The practical throat Mach number limit of an inlet can be indicated on a distortion or recovery curve by the point where a small Mach number increase produces a large increase in distortion or decrease in recovery. Using the distortion parameter and the approach inlet, this occurs near M_{TH} = 0.81 to 0.82. With the takeoff inlet this doesn't occur until M_{TH} = 0.95+. The difference in limiting Mach number is to be expected because the area ratio at approach is greater than at takeoff.

B. Boundary Layer Pressure Profiles

The cobra traverse probe data were used to give a detailed total pressure distribution between the wedges at a distance corresponding to 0.06 fan diameters ahead of the fan face. This traverse profile was transferred to graph paper, and, in the process, sharp pressure fluctuations were smoothed. These new traverse profiles were then compared to a pressure profile corresponding to $u/u_\infty = (y/\delta')^{1/7}$ as shown in Figures 58 and 59. This comparison was made because the 1/7 power relationship represents the classical flat plate turbulent boundary layer profile for moderate Reynolds numbers. The relative similarity a given boundary layer has to a 1/7 power profile is therefore useful in assessing the impact of the inlet's adverse pressure gradient and determining the relative stability of the boundary layer. Instability, or flow separation, is characterized by an inflection point in the profile and a zero-velocity gradient normal to the surface, denoting zero wall shear. With the usual assumption of constant static pressure in the boundary layer at a given station, changes in total pressure are proportional to velocity changes and may be used to infer boundary layer stability. Additionally for each configuration tested, the hybrid inlet was compared to its corresponding accelerating inlet as shown in Figures 60 and 61.

In the case of the hybrid takeoff inlet (Figure 58), very good agreement is demonstrated between the traverse profile and the equivalent 1/7-power profile. The comparison of the same inlet with its corresponding accelerating inlet shows fair agreement, but the accelerating inlet has a greater slope than the hybrid inlet in most of the defect region, and is less like the power profile. Since the pressure slope at the wall is nonzero in each case, neither inlet indicates diffuser separation. However, the accelerating inlet appears closer to separation than the hybrid inlet, in view of its less full profile and incipient inflection point. The greater surface roughness of the hybrid inlet, and its correspondingly greater shear stress, is acting to keep the flow attached.

With the inlet configured for approach, the hybrid inlet does approximate a 1/7-power law (Figure 59) although not quite as well as the same inlet tested in takeoff mode (Figure 58). The shape of the hybrid inlet boundary layer pressure profile, specifically the developing inflection point, indicates the emergence of flow retardation that precedes separation. In the case of the accelerating inlet (Figure 61), separation is apparent from the constant pressure region near the wall. This particular case of impending separation (during testing in the approach mode the inlet seems to separate and reattach randomly) is not considered critical to fan operation, but higher than expected unsteady stress levels were measured on the fan blades at throat Mach numbers in excess of the design value. Wall Kulites were installed in the inlet after this phenomenon appeared, to aid in investigating this unsteadiness. These results are discussed next.

C. Kulite Analysis

At throat Mach numbers above the 0.79 design point, unsteady rotor blade stresses appeared while testing the approach inlet. To investigate this, wall Kulites were installed in the inlet at locations 2.8 cm (1.1 in.) and 13.0 cm (5.1 in.) ahead of the rotor face for the purpose of measuring pressure fluctuations as well as wave direction at those stations. The resulting transducer output was recorded on magnetic tape and, when played back in unfiltered form, yielded pressure fluctuations corresponding to the blade passing frequency of the fan.

In order to eliminate blade passing fluctuations and allow determination of the direction of wave travel, the tape output was filtered at 500 Hz and played back on photosensitive paper at a speed equivalent to 13 milliseconds per centimeter. Inlet throat Mach numbers ranging from 0.791 to 0.865 were examined.

Reading No. 609, corresponding to a one-dimensional throat Mach number of 0.857 gave what appeared to be the most clearly defined cyclical pressure fluctuations. A portion of the output is shown in Figure 62. On the figure are indicated disturbances with wavelengths of roughly 0.6 and 0.3 centimeters, which are the most significant ones shown with any clarity.

If the inlet were considered to be an organ pipe, the frequency of a disturbance propagating through it may be written as:

$$f = \frac{a(1-M^2)}{kL}$$

where a is the local speed of sound, L the length of the pipe (in this case from the throat to the fan), and k is either 1, 2, or 4, depending on whether the pipe is closed at both ends, open at both ends, or open at one end and closed at the other, respectively. The conditions in the inlet, particularly at the Kulite stations, are such that the equation may be reduced to:

$$f = \frac{260.6}{k}/\text{sec}$$

Since the playback speed corresponds to 13 ms/cm, the cycle frequency and wavelength may be expressed as:

$$f = \frac{3.38}{k}/\text{cm}, \quad \lambda_{cycle} = 0.30k \text{ cm}$$

The centimeters are measured directly on the photosensitive readout paper.

The two wavelengths noted on Figure 62 appear to be in the cycle wavelengths of an equivalent organ pipe. The inlet throat, normally an open end, becomes closed when the inlet chokes or a shock system develops at high throat Mach numbers below unity, which is the case here. The fan end of the inlet appears to act as a closed end.

The greatest pressure fluctuations correspond to a wavelength where k = 1. The system is closed at both ends, and a shock system has developed at the throat. The other fluctuations consist of 2nd, 3rd, 4th, and nth order harmonics of the closed organ pipe frequency. The 2nd order harmonic is indicated, but higher orders quickly become too compounded to discern.

To conclude, it appears that pressure instabilities are initiated by the unsteadiness of the shock system at the throat and resonate in the organ pipe mode of the inlet. The instability is Mach number-dependent, occurring only at throat Mach numbers above the 0.79 design point. It does not impair the performance of the approach inlet within its design range.

D. Inlet Wall Mach Numbers

Static pressure taps were installed in the inlet to provide sufficient information to draw a well-defined axial Mach number distribution. Additinally, two rings of four taps each, spaced at 90° circumferential increments, were installed at the throat and ahead of the fan face. Because this was a static test with the inlet at a zero degree angle of attack, these circumferentially distributed taps were used to indicate flow uniformity.

Figure 63 shows the variation in peak wall Mach number for the takeoff inlet. Figure 64 shows the same information plotted for the approach mode. In both cases, the peak Mach number was measured immediately forward of the throat. At the design point, the hybrid inlet peak wall Mach number was below the design estimate by 0.8% at takeoff and 1.5% at approach, possibly an effect of wall curvature in the throat region. In both takeoff and approach operating modes, the peak Mach numbers were uniformly greater for the hybrid than the accelerating inlet. This again is probably due to slight differences in curvature between the treated and untreated inlets. This would tend to be especially evident near the throat, since this is a region of high wall curvature and hence flow acceleration.

Comparing Figures 63 and 64, one can see the peak wall Mach number of the approach inlet nearing vertical much earlier than the same inlet at takeoff. This occurs as a result of differing radial velocity profiles at the throat during takeoff and approach and explains why the takeoff inlet, with its less severe radial velocity gradient, can be run to much higher throat Mach numbers.

Figures 65 and 66 show the axial wall Mach number distribution at the design point compared to a design stage Streamtube Curvature (STC) computational analysis. The STC prediction for the takeoff inlet (Figure 65) was made under inviscid conditions and without wedge blockage. Part of the reason for this is that because of the complex flowpath geometry, i.e., wedge blockage distribution, sharp curvature changes around wedges, etc., such liberties would have to be taken in modeling the inlet that the credibility of the output would be questionable. For this reason, there are differences in wall Mach numbers in the aft end of the diffuser. The higher than expected peak wall Mach number is also a curvature related effect, since the model geometry, with its surface discontinuities, cannot be modeled exactly. The prediction for the approach configured inlet (Figure 66) was corrected for boundary layer growth, and wedge blockage is very small. All points agree with the predicted distribution.

Finally, Figures 67 and 68 show several Mach number distributions for both inlet modes, all measured in an interval bounding the design point. The high Mach number plateau aft of the throat for the takeoff inlet at $M_{TH} = 0.87$ (Figure 67) is explained as an attached supersonic bubble that develops well above the design throat Mach number.

SECTION VII

EXHAUST DUCT PERFORMANCE RESULTS AND DISCUSSION

A. Effect of Wall Treatment and Splitter on Performance

The most important effect of the acoustic treatment and splitter on the fan duct performance was to approximately double the total pressure loss between the fan frame discharge and the nozzle inlet. An increase was expected since both the wetted surface area and friction factor were considerably increased as a result of the splitter and acoustic treatment. The third effect contributing to the increased losses was the turbulent wake shedding from the splitter trailing edge. This was a consequence of the expected flow separation along the splitter trailing edge closure.

The hardwall configuration was designed to preserve the same flow area distribution present in the acoustically treated splitter duct. As a result, this configuration retained essentially the same static pressure and Mach number distributions and provided a reasonable baseline for comparison of the effects on overall performance due to the splitter and treatment. Test data from both configurations were utilized to evaluate the effect of the acoustic splitter and treatment on aerodynamic performance through the comparison of this configuration with the hardwall design with no splitter.

The instrumentation used to obtain the test data is described in Section IV. The total pressure loss in the ducts was determined from the average total pressures calculated from the profile data supplied by each of the two radial traversing probes. These profile data were in analog form via X-Y plots giving total pressure, temperature, and probe yaw angle as a function of percent annular height at both locations. Typical total pressure profiles at the fan frame discharge and nozzle inlet are plotted in Figure 69. The calculation of average total pressure and temperature was determined by digitizing the data and integrating, by an area-weighted average technique, across the annulus. Calculations were corrected for yaw angle, annulus blockage area (due to structural pylons), and estimated pitch misalignment in the diffuser section. This same procedure was used for both duct configurations. The results of these calculations are summarized in Table VII.

Table VII. Average Total Pressure Loss Calculations for Treated and Hardwall Exhaust Ducts.

	$\Delta P_T/P_T$(%) Takeoff	Cutback	Approach
Splitter duct	1.35	3.24	2.05
Hardwall duct	0.79	1.28	0*

* Actually measured slightly negative

The static pressure and Mach number distributions were determined by means of 40 static pressure taps in the splitter duct and 31 in the hardwall configuration. Plots of these distributions against axial length are presented in Figures 70 through 76 for takeoff, in Figures 77 through 83 for power cutback, and in Figures 84 through 90 for approach operation. Each of these three sets of figures has several parts: Predicted and measured wall static pressure distribution with the splitter, predicted and measured wall surface Mach number distribution with the splitter, and measured wall static pressure and wall surface Mach number distributions for the hardwall configuration. Note that the Mach number distributions were based on both the upstream and downstream measured total pressures. This gives a band of Mach number limits shown by upper (solid) and lower (dotted) curves. This procedure was utilized to express the variation of total pressure with respect to axial length between the two probes.

The nozzle discharge coefficients were calculated for the three nozzles tested using the measured aft-probe average total pressure corrected for the total pressure loss from there to the nozzle exit as estimated from skin friction drag calculations. These coefficients and the losses at each condition are given in Table VIII.

Table VIII. Calculated Nozzle Discharge Coefficients and Estimated Pressure-Loss Factors.

		Takeoff	Cutback	Approach
C_f - Discharge Coefficient	Splitter duct	0.9567	0.9697	0.9830
	Hardwall duct	0.9391	0.9464	0.9535
Nozzle pressure loss, $\Delta P_T/P_T$		0.00115	0.00131	0.00087

B. Comparisons With Prediction

The aerodynamic design of the fan duct is presented in Reference 1. The reader is referred to this material for a more detailed explanation of predicted performance data given here. Predicted pressure losses were determined only for the treated splitter configuration.

The design was based on predicted fan exit profiles for the scale-model vehicle. The total pressure losses were calculated by the relationship:

$$\frac{\Delta P_T}{P_{T_1}} = \frac{DRG}{P_{S_1} A_1}$$

where, DRG was the body friction drag (from a boundary layer analysis program), A_1 was the initial flow area and P_{S_1} and P_{T_1} were the initial static and total pressures, respectively.

There were four operating conditions considered in the design: takeoff, power cutback, cruise, and approach. The test data selected for analysis were for those conditions of corrected fan speed which conformed most closely to the design points. There were no test data available for the cruise case, however, since altitude simulation was not possible in the test facility used. Table IX gives the pertinent operating parameters at these conditions.

Table IX. Test Operating Parameters.

Bypass Parameter	Takeoff		Cutback		Cruise		Approach	
	Design	Test	Design	Test	Design	Test	Design	Test
$N/\sqrt{\theta}$ (%)	92.1	92.7	89.6	92.49	100.00	-	64.7	65.43
W (kg/sec)	87.31	89.21	95.62	96.91	101.05	-	75.52	66.3
P_T (kN/m^2)	164.14	154.12	148.57	138.64	183.57	-	122.48	113.31
T_T (K)	363.07	353.70	346.17	352.26	350.68	-	320.20	315.89

Takeoff Condition

The predicted takeoff duct wall and splitter surface static pressure distributions presented in Figure 70 can be compared with test results presented in Figure 71. The average static pressure level of the test results is lower than predicted. The measured fan frame discharge total pressure and temperature were lower than design; the measured physical airflow, however, was slightly higher. A consistent probe yaw angle of around 1.3° across the profile suggests a slight flow swirl which could account for a small reduction in the effective flow area and a resultant increase in the duct Mach number from predictions as shown by Figures 72, 73, and 74. At station 266 (an axial location of 266 cm) the flow function ($\bar{m}_1$) for the design conditions was about:

$$\bar{m}_1 = 0.347$$

and for the test conditions:

$$\bar{m}_2 = 0.423$$

The design flow function at this location, corrected by the measured values of pressure, temperature, airflow, and effective area gives:

$$\bar{m}_{1k} = \bar{m}_1 \times \left(\frac{P_{T_1}}{P_{T_2}}\right) \times \left(\frac{T_{T_2}}{T_{T_1}}\right) \times \left(\frac{A_1}{A_2}\right) \times \left(\frac{W_2}{W_1}\right)$$

$$= 0.347 \times (1.065) \times (0.9874) \times (1.064) \times (1.021)$$

$$= 0.396$$

This corrected flow function corresponds to a new design Mach number of around 0.5 which represents an increase of nearly a tenth. The differences between the predicted static pressure and those which were measured are, for the most part, accountable to higher than expected duct Mach numbers. This was due mainly to differences in the fan frame discharge conditions from those used for the initial design. Other test Mach number distributions at the takeoff condition are given in Figures 73, 74, and 76.

The predicted total pressure loss at takeoff was 1.67% while the measured loss was 1.35%. The measured loss does not include the losses encountered in the flow regions upstream and downstream of the probes, as does the predicted loss, thus some of the discrepancy can be explained.

Cutback Condition

The cutback condition yielded much the same behavior as takeoff with respect to the resultant static pressure and Mach number distributions. Comparison of the predicted results and the test results in Figures 77 through 83 shows that the trends are similar to takeoff except for different magnitudes. The predicted values for static pressure are again, for the most part, uniformly larger than the measured values and vice versa for Mach number.

The measured fan frame discharge conditions again differed slightly from those used in the design. In addition, for the cutback case, the data with the closest corrected fan speed to the design point were 92.5%. This 2.9% difference in corrected fan speed from design can account for about a 2.3% increase in corrected airflow based on the fan test data.

Using the same procedure as before, the station 266 design flow function would be about:

$$\bar{m}_1 = 0.4237$$

for the test data:

$$\bar{m}_2 = 0.4936$$

correcting the $\bar{m}_1$ by the test conditions:

$$\bar{m}_{1k} = \bar{m}_1 \times \left(\frac{P_{T_1}}{P_{T_2}}\right) \times \left(\frac{P_{T_2}}{T_{T_1}}\right) \times \left(\frac{W_2}{W_1}\right) \times \left(\frac{A_1}{A_2}\right)$$

$$= 0.4237 \times (1.0717) \times (1.009) \times (1.012) \times (1.064)$$

$$= 0.4934$$

Using the corrected flow function raises the design Mach number at station 266 to 0.724 which is very close to the measured 0.726 at the same station on the test vehicle.

The predicted and measured total pressure losses were 2.33% and 3.24%, respectively. The predicted loss was based on an initial static to total pressure ratio which is different from the test results. The effect of the corrected ratio to the calculated loss is:

$$\frac{\Delta P_T}{P_{T_1}} = \frac{DRG}{P_{S_1} A_1} \times \left(\frac{P_{S_1}}{P_{S_2}}\right) \times \left(\frac{P_{T_2}}{P_{T_1}}\right)$$

$$= 0.02334 \times 1.164 \times 1.0717$$

$$= 2.91\%$$

Though the measured loss is still higher, the correction reduces the difference to 11%.

Cruise Condition

The cruise operating point total pressure loss for the splitter and hardwall ducts was estimated by applying a linear variation in the duct pressure drop with the duct entering dynamic pressure (q). For the small changes in Reynolds and Mach numbers between the takeoff and cruise conditions this approach was considered valid.

At the cruise operating point a $\Delta P_T/P_T$ loss of 1.41% for the splitter duct and 0.79% for the hardwall was estimated. The 1.41% compares favorably to the 1.6% predicted in the design analysis.

An important observation is the $\Delta P_T/P_T$ penalty the splitter duct incurs over the hardwall at the important cruise operating point (1.41% compared to 0.79%). By means of the assumed cycle influence coefficient at the cruise point, this added loss of the splitter and acoustic treatment would result in about a 0.68% increase in specific fuel consumption at constant fuel flow.

Approach Condition

The static pressure distributions determined from both the predictions and the test results are presented in Figures 84, 85, and 89. It is evident from comparison of these plots that the basic trends in static pressure are essentially the same, but that the test results generally show a somewhat lower level of static pressure (relative to ambient). At station 266, for example, (where the first total probe was located), the inner wall design static pressure ratio was about 1.02 (Figure 84), whereas the test value was 0.96 (Figure 85). The total pressure, temperature, and physical airflow were all lower than design at this location, yet the Mach number, was about the same as design [Figures 87 (compared with 86) and 88]. Since the reduced pressure, temperature, and airflow all interacted to give the same Mach number, the ratio of the static to total pressure at this location remain unchanged. Hence, the lower total pressure must be accompanied by a proportionate decrease in static pressure, as the results indicate.

The plots of Mach number distributions for approach (Figures 87 and 88) exhibit much the same trends as predicted (Figure 86), just as the static pressures do. Along the splitter the predicted Mach number varied between 0.57 and 0.31 on the inner wall and 0.44 and 0.29 on the outer wall. The splitter test results were between 0.6 and 0.32 on the inner and 0.47 and 0.43 on the outer. The original design intent was a 0.35 wall surface Mach number based on an acoustic requirement.

The procedures used to determine the total pressure losses were explained in Section VII-A. The predicted loss for the approach case between the fan frame and the nozzle inlet was 2.12%. The measured loss between the two traverse probes was 2.05%. The first probe was located about 15 cm downstream of the fan frame discharge, and the second probe about 22 cm upstream of the nozzle flange (Station 371). The actual loss therefore, between the same stations used to calculate the predicted loss, will be slightly higher. The amount by which the actual loss should be increased is very small, however, since the effects of the splitter and acoustic treatment are greatly diminished in the two flow regions neglected.

SECTION VIII

SUMMARY OF RESULTS

The following results were obtained regarding the aerodynamic performance of the single stage advanced technology fan vehicle:

1. The fan demonstrated performance levels which were somewhat below the objectives set for this design. The peak efficiency objective, however, was met at 95% speed. The adiabatic efficiency and total airflow at the design point were below the objectives by 1.8% and 2.9%, respectively. The measured stall line was within 1.5% of the goal at part speed and down by 4.5% at design speed.

2. The flow deficiency of the fan appears to be due to a limit set by the flow induction surface of the blade, rather than a throat area limitation. It would require opening the flow induction portion of the blade by about one degree to increase the flow to the design value.

3. Fan rotor-tip shock losses were magnified as a result of the low flow at design and are believed to be the largest contributing factor to the high rotor total pressure loss coefficients in the tip region. Increased trailing edge camber should also help improve the efficiency.

4. Testing with the short bellmouth inlet configuration showed an improvement in the fan aerodynamic performance. The design speed efficiency was increased from 80.6% to 82.2% at the operating-line condition. The flow at this point was increased by 0.6%. The lack of radial rakes in the inlet and bypass ducts appear to be part of the reason for the better performance. This test configuration also had tighter tip-shroud seal clearances. The tighter clearances probably accounted for most of the stall-line improvement and possibly some of the efficiency improvement.

5. Aerodynamic performance measurements with the hybrid inlet showed only minimal performance losses. At high speed in the takeoff mode, this inlet caused approximately 2 to 3% stall margin loss while the efficiency was down by about 0.5%. No appreciable flow reduction was evident. At low speed, in the approach mode, the stall margin losses were greater; however, the remaining margin above the low operating line approach point was sizeable. The measured flows were again similar to the bellmouth tests. Efficiency decrements were difficult to establish because of the lack of fixed inlet instrumentation and low temperature rise across the fan at this speed.

6. The hybrid inlet used as the suppression device for forward-quadrant noise was shown to have acceptable aerodynamic performance. Total pressure recoveries were 98.9 and 98.2% at the design takeoff and approach conditions (throat Mach number = 0.79) respectively, and distortions were less than 10%.

7. The bypass duct wall acoustic treatment and splitter system used for aft-quadrant fan noise suppression were also shown to have acceptable aerodynamic performance in that a cruise specific fuel consumption penalty of about 0.68% was estimated from the static test results.

APPENDIX A

LIST OF SYMBOLS AND NOMENCLATURE

Symbol	Description	Units
A	Area	m^2 or cm^2
a	Local speed of sound	m/sec
ASME	American Society of Mechanical Engineers	
C_f	Nozzle discharge coefficient $C = \frac{W\sqrt{T_T}}{P_T A_{18} \bar{m}_{18}}$, $\bar{m}_{18} = f(P_T/P_{amb}, \gamma)$	nondimensional
D	Diffusion factor: $D_{rotor} = 1 - \frac{V_2'}{V_1'} + \frac{r_2 V_{\Theta 2} - r_1 V_{\Theta 1}}{2\bar{r}\sigma V_1'}$ $D_{stator} = 1 - \frac{V_2}{V_1} + \frac{r_1 V_{\Theta 1} - r_2 V_{\Theta 2}}{2\bar{r}\sigma V_1}$	
D'	Inlet recovery defect, $1 - \bar{P}_T/P_{T_\infty}$	nondimensional
D_F	Fan diameter	cm
DRG	Body friction drag	N
DV	Discharge valve	
EPNdB	Effective perceived noise decibels	
f	Frequency of disturbance propagation through inlet	sec^{-1}
FAR	Federal Air Regulation	
i	Incidence angle (difference between flow angle and camber-line angle at leading edge in cascade projection)	degrees

Symbol	Description	Units
ID	Inner diameter	cm
k	Constant of value 1, 2, or 4 (depending on nature of inlet in an organ pipe analogy)	nondimensional
L	Length	m
LE	Leading edge	
M	Mach number	
$\bar{m}$	Flow function: $W\sqrt{T_T}/P\ A$	$kg\sqrt{^\circ K}/N\cdot sec$
N	Physical fan rotation speed	rpm
OD	Outer diameter	cm
OGV	Outlet guide vane	
O/L	Operating line (flow versus speed at constant throttle area)	
P	Total pressure	N/m^2
p	Static pressure	N/m^2
P/P	Pressure ratio	nondimensional
$\bar{P}_T$	Mean total pressure: $\eta_R' P_{T_{amb}}$	
q	Dynamic pressure (total pressure-static pressure)	N/m^2
R	Radial distance from vehicle centerline to define flowpath	m
r	Radius	cm
$\bar{r}$	Mean radius, average of streamline leading-trailing edge radii	cm
R_i	Radius where total pressure reaches ambient	cm
R	Inlet wall radius	cm
rpm	Revolutions per minute	

Symbol	Description	Units
sfc	Specific fuel consumption	kg/N-hr
Stall Margin (%)	$\frac{\left(\frac{P/P}{W}\right)_{stall} - \left(\frac{P/P}{W}\right)_{Operating\ line}}{\left(\frac{P/P}{W}\right)_{Operating\ line}} \times 100$	
STC	Refers to Streamline Curvature Computation analysis	
T	Temperature	° K
T/T	Temperature ratio	nondimensional
U	Rotor speed	m/sec
u	Axial velocity	m/sec
V	Velocity	m/sec
W	Weight flow	kg/sec
X	Axial distance	cm
Y or y	Distance from wall surface	cm
β	Flow angle (angle whose tangent is the ratio of tangential to axial velocity)	degrees
Δ	Change in	
δ	Pressure correction: $P_{actual}/986.0\ N/m^2$	nondimensional
δ'	Boundary layer thickness	cm
$\delta°$	Deviation angle (difference between flow angle and camber-line angle at trailing edge in cascade projection)	degrees
λ	Cycle wavelength of disturbance propagating through the inlet	cm
η	Efficiency	nondimensional

Symbol	Description	Units
η'	Inlet total pressure recovery	nondimensional
Θ	Temperature correction: $T_{actual}/288.4°$ K	nondimensional
ϕ	Slope of meridional streamline	degrees
Ψ	Stream function (percent flow from outer diameter)	nondimensional
$\bar{\omega}$	Total pressure loss coefficient:	nondimensional

$$\text{Rotor } \bar{\omega} = \frac{P'_{2_{id}} - P'_2}{P'_1 - P_1}$$

$$\text{Stator } \bar{\omega} = \frac{P_1 - P_2}{P_1 - P_1}$$

(Note: Superscript ' means "relative to rotor")

Subscripts

ad	Adiabatic
amb	Refers to ambient conditions
Def	Refers to measurement taken in velocity defect region of flowfield
k	Corrected value
id	Ideal value
m	Meridional direction
max	Maximum value of variable
min	Minimum value of variable
R	Refers to final overall recovery level
S or s	Refers to static condition
T	Total condition; or refers to recovery value determined by traverse probes
TH	Refers to measurement taken at inlet throat

Symbol	Description
wall	Refers to measurements taken at wall
Z	Axial direction
ω	Refers to measurement taken with boundary layer rake in inlet behind a wedge
0	Reference value of variable
1	Leading edge; design or initial value; entrance station
2	Trailing edge; test or final value; exit station
14.2	Station upstream of splitter (about 50 cm from rotor LE)
14.3	Station downstream of splitter (about 155 cm from rotor LE)
18	Station at nozzle discharge
∞	Refers to condition outside of boundary layer

REFERENCES

1. Sullivan, T.J., Younghans, J.L., and Little, D.R., "Single Stage, Low Noise, Advanced Technology Fan, Volume I - Aerodynamic Design," NASA CR-134801, March 1976.

2. Schoener, J.L., Black, G.R., and Roth, R.H., "Single Stage, Low Noise, Advanced Technology Fan, Volume II - Structural Design," NASA CR-134802, March 1976.

3. Kazin, S.B. and Mishler, R.B., "Single Stage, Low Noise, Advanced Technology Fan, Volume III - Acoustic Design," NASA CR-134803, March 1976.

4. Jutras, R.R., "Single Stage, Low Noise, Advanced Technology Fan, Volume V - Fan Acoustics, Section I - Results and Analysis," NASA CR-134894. Section 2 - 1/3-Octave Data Tabulations and Selected Narrow-band Traces," NASA CR-134895, May 1976.

5. Compagnon, M.A., "Propulsion System Studies for an Advanced High Subsonic Long-Range Jet Commercial Transport Aircraft," NASA CR-121016, November 1972.

6. "Studies for Determining the Optimum Propulsion System Characteristics for Use in a Long-Range Transport Aircraft - Comprehensive Data Report," NASA Contract NAS3-15544, June 1972.

7. Ware, T.C., Kobayashi, R.J., and Jackson, R.J., "High Tip Speed, Low Loading Transonic Fan Stage, Part III - Final Report," NASA CR-121263.

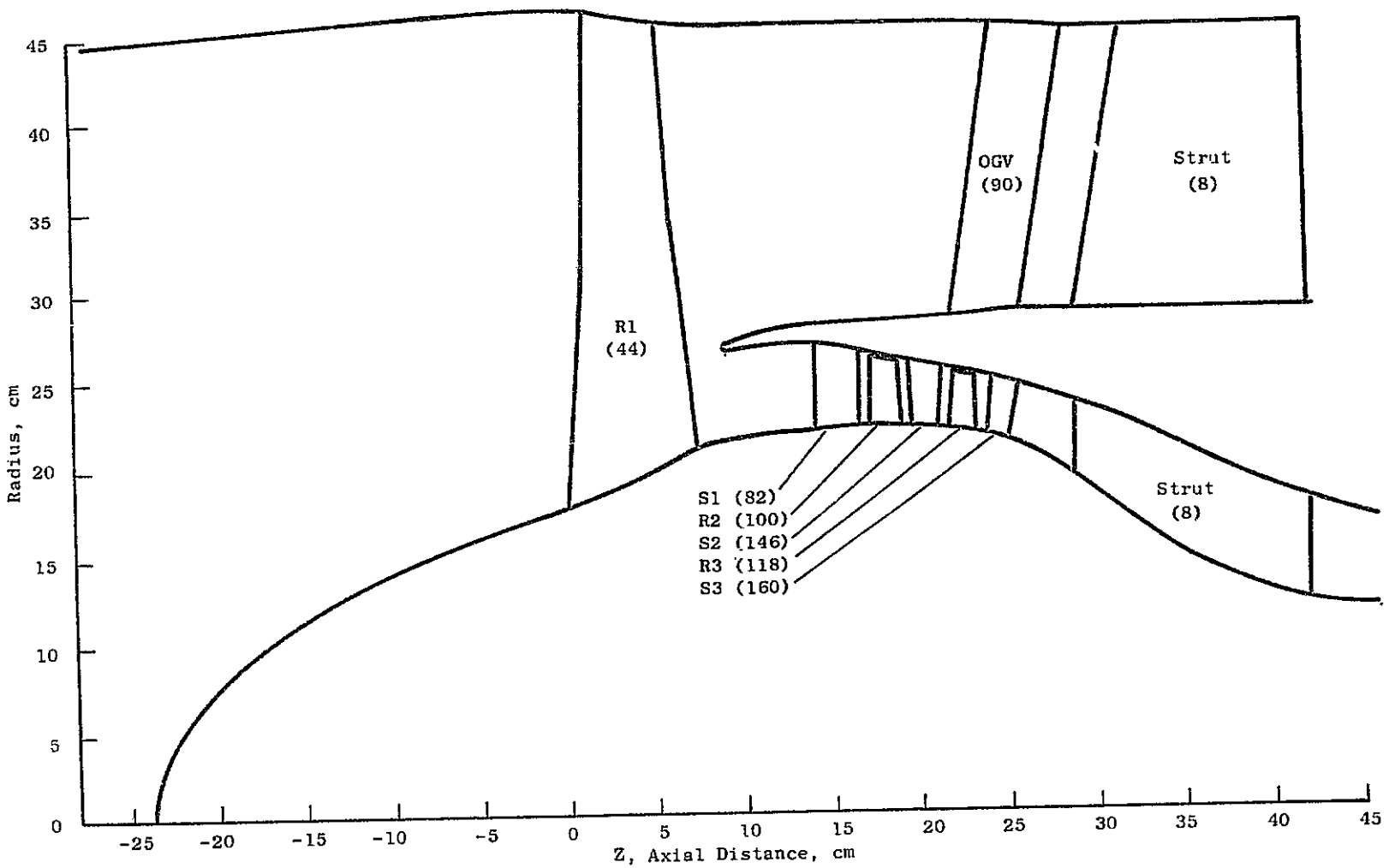

Figure 1. Advanced Technology Fan and Booster Flowpath.

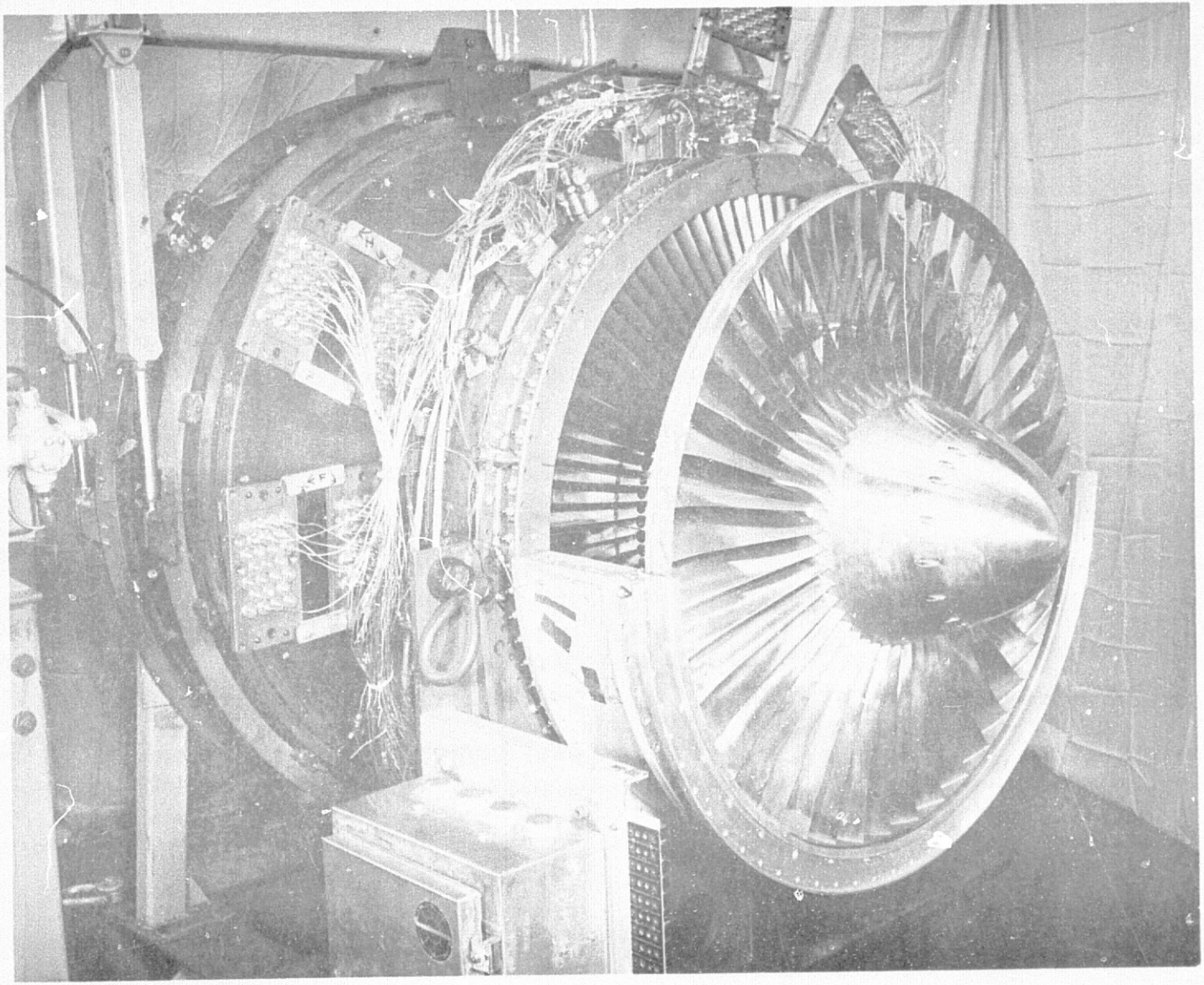

Figure 2. Advanced Technology Fan.

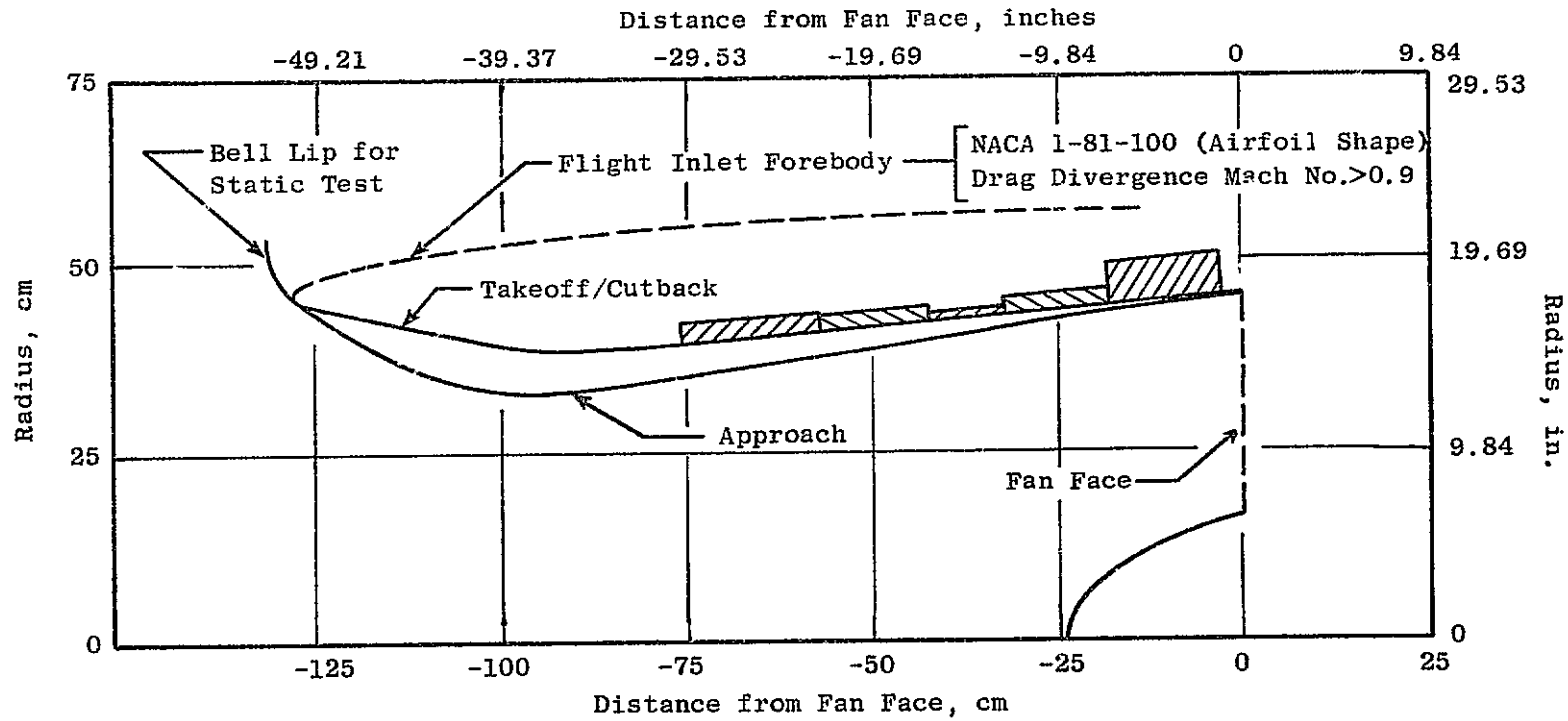

- Translating Panels and Variable Nozzle to Provide $M_{TH} = 0.79$ at All Three Operating Points
- $L/D_{Inlet} = 1.5$ (With Bell Lip), $L/D_{Treat} = 0.85$
- Treatment Located Where $M_{Wall} \leq 0.70$

Figure 3. Hybrid Inlet Aerodynamic Design.

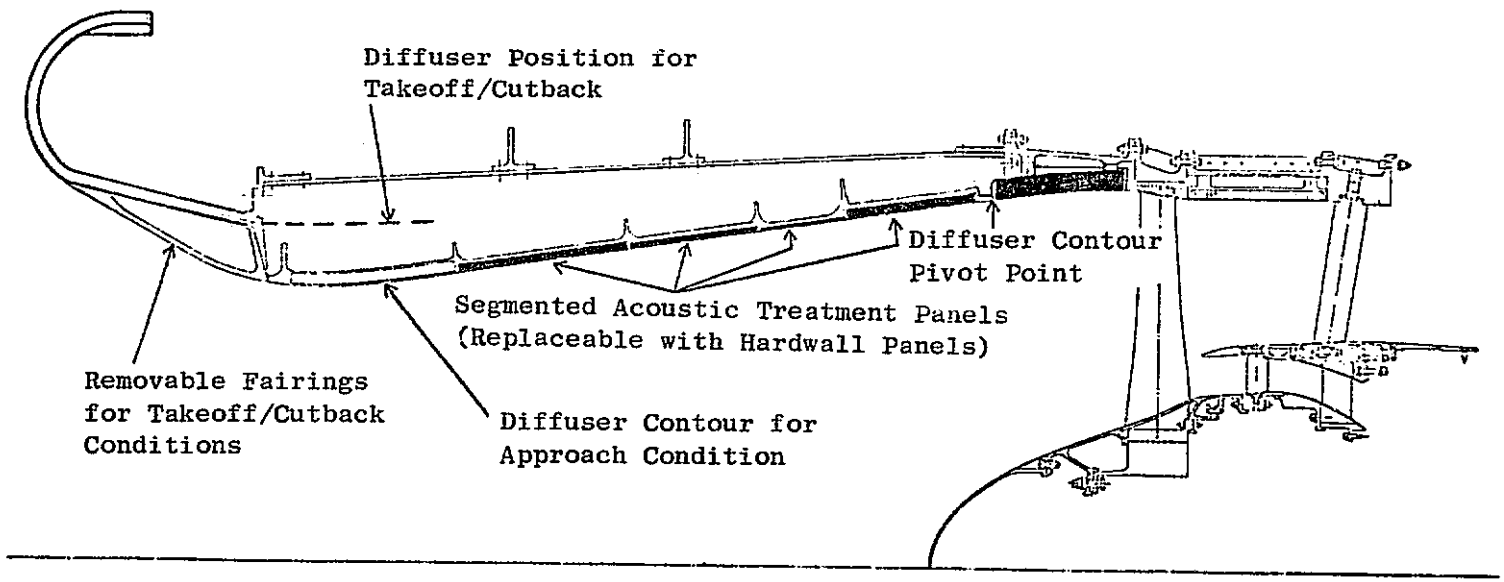

Figure 4. Cross Section of Fan Hybrid Inlet Suppressor Model.

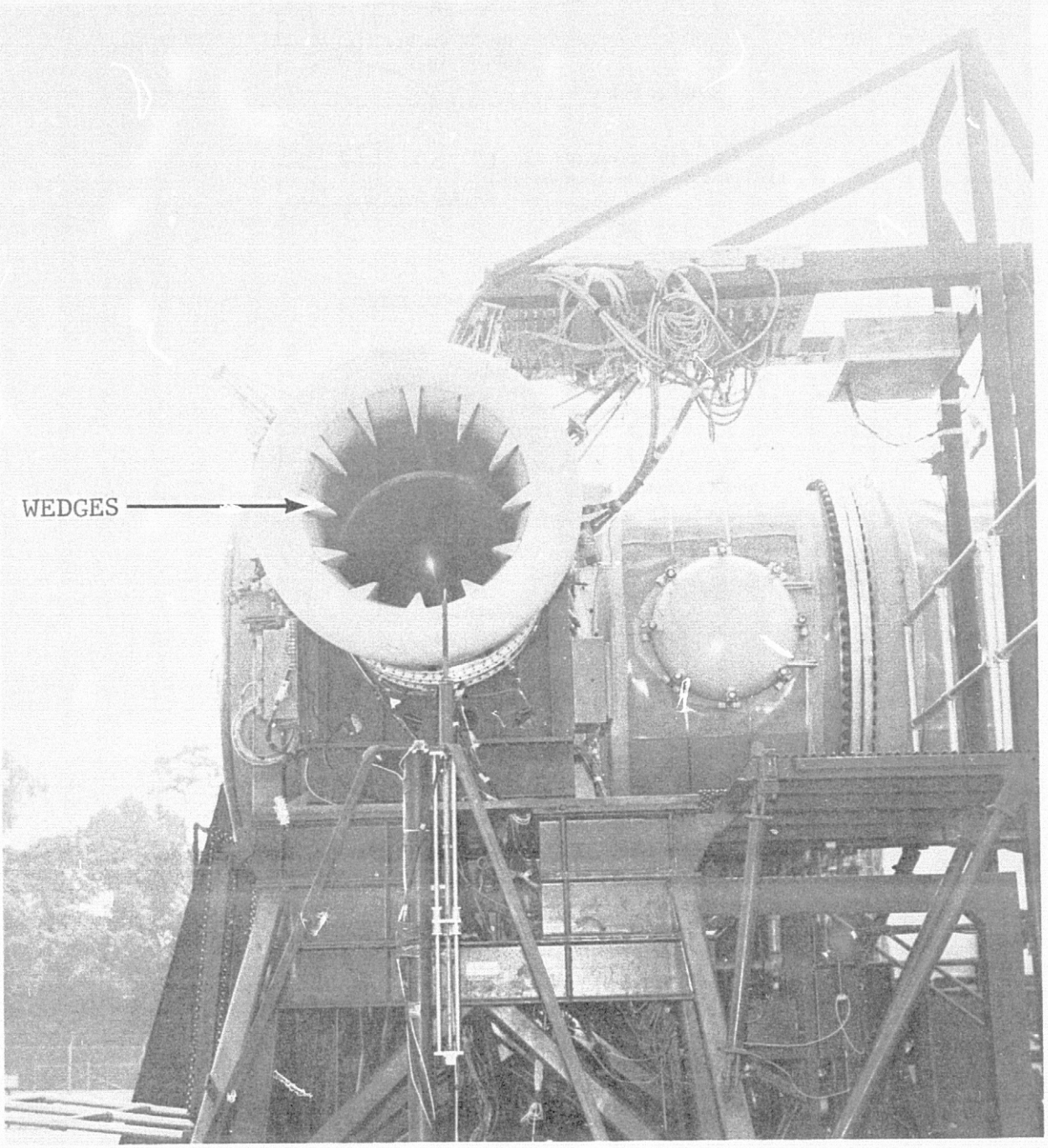

Figure 5. Hybrid Inlet in Takeoff/Cutback Configuration.

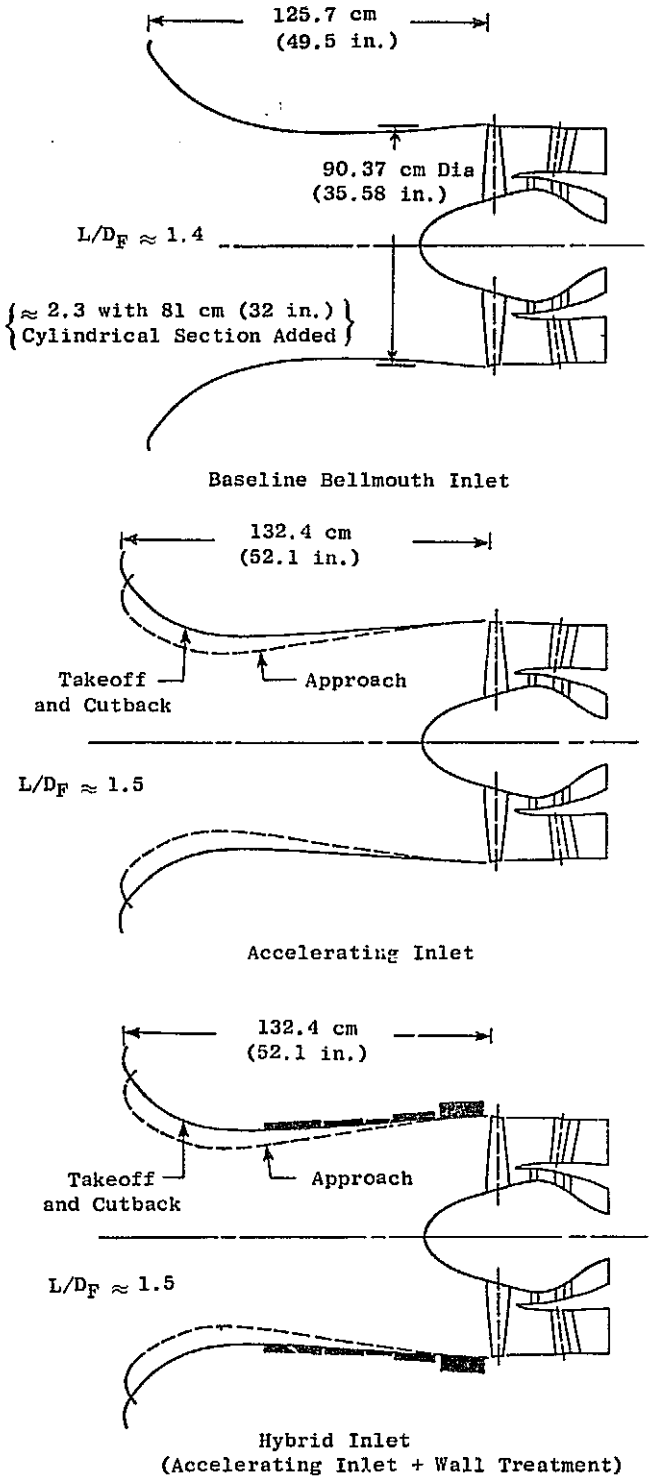

Figure 6. Fan Inlet Configurations for Rear-Drive Tests.

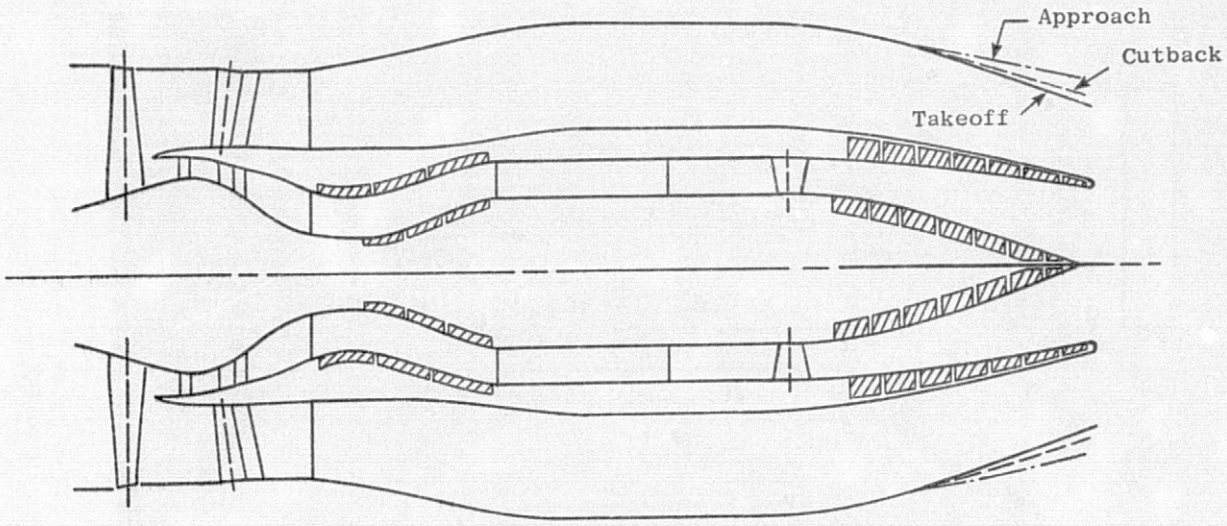

• Hardwall

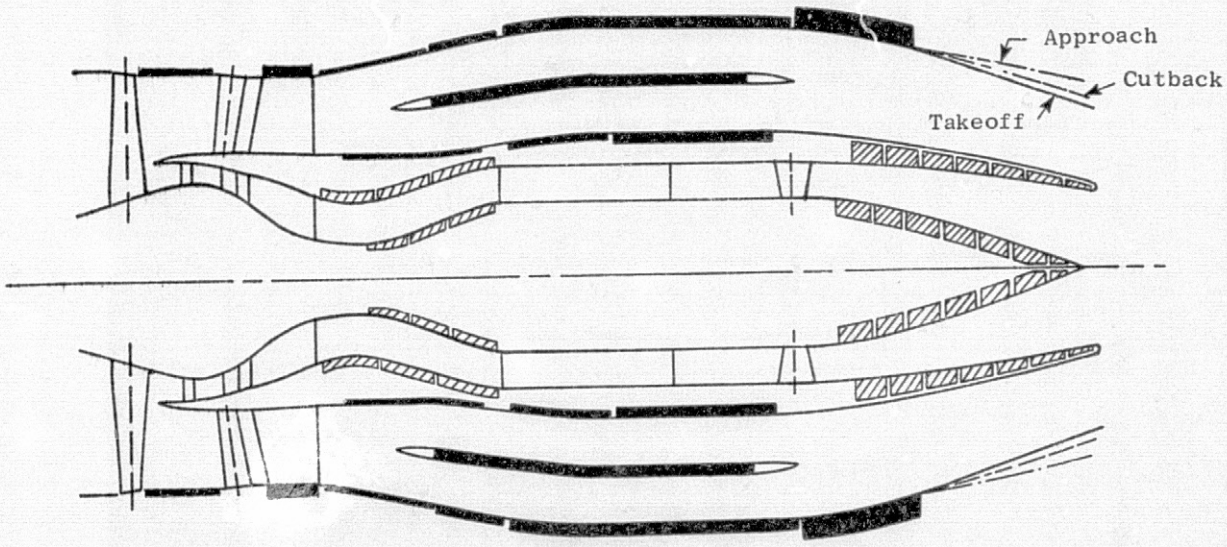

• Treated with Splitter

Figure 7. Fan Duct Configurations for Front-Drive Tests.

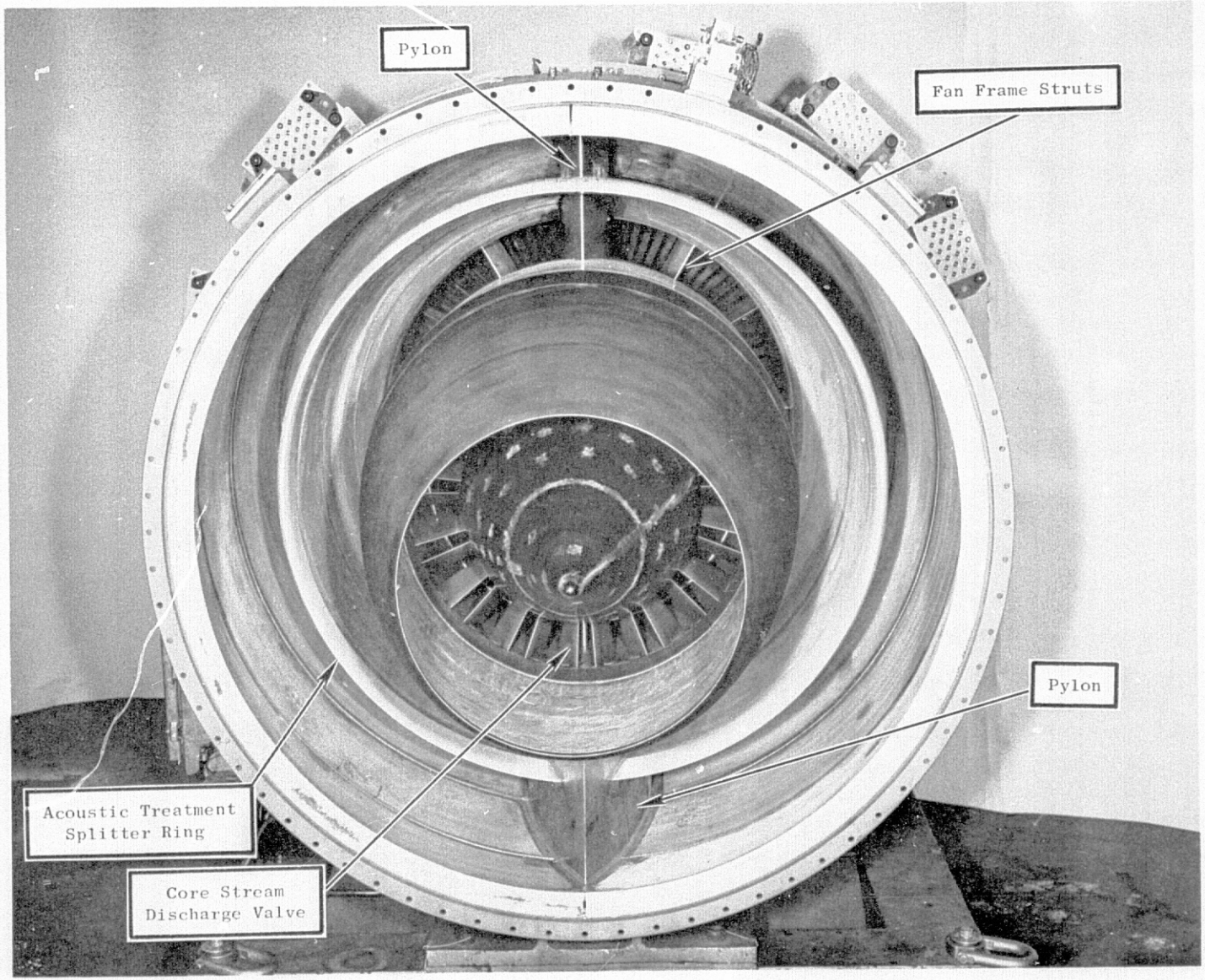

Figure 8. Exhaust Duct with Nozzles Removed.

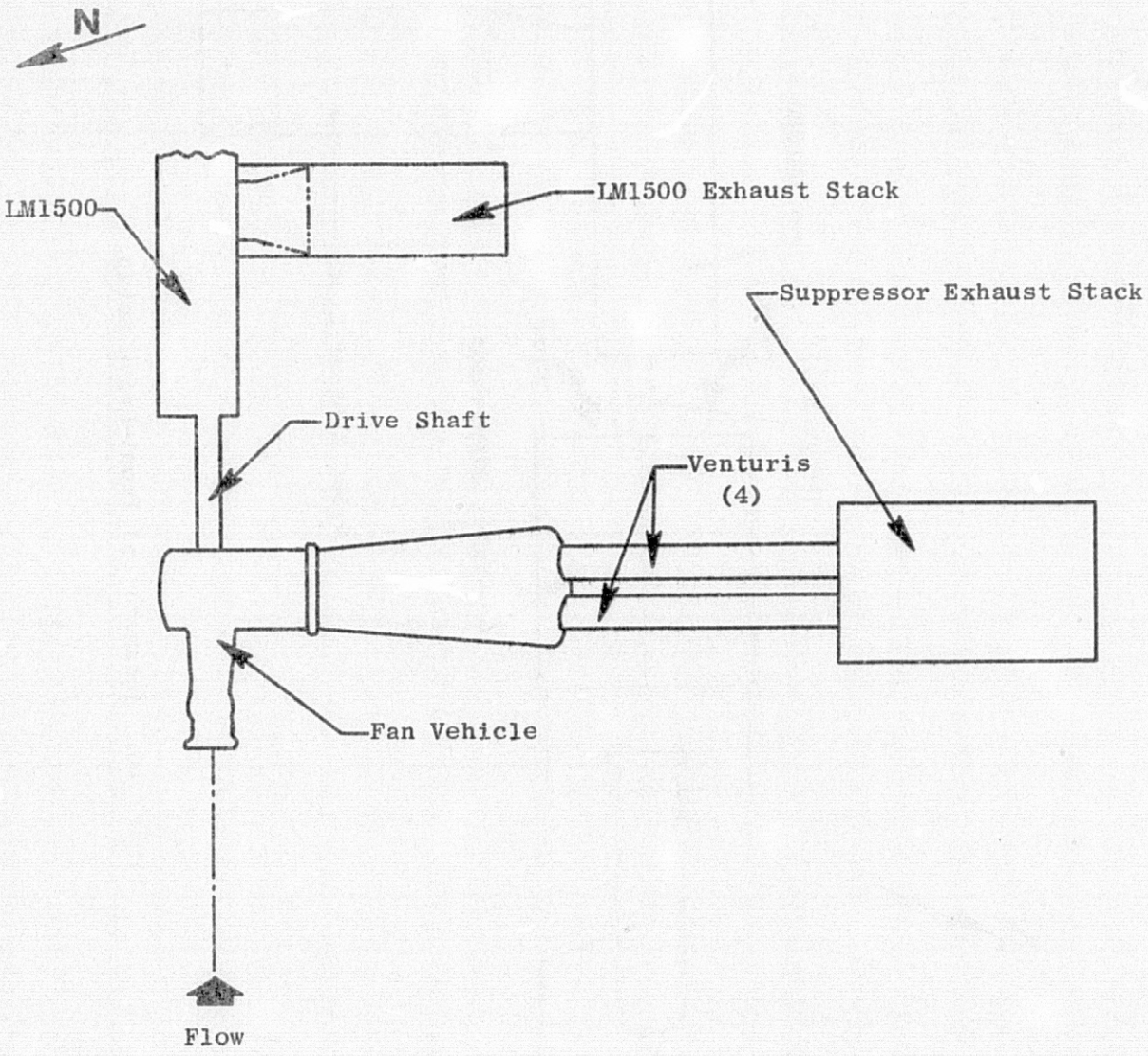

Figure 9. Schematic of Rear-Drive Setup.

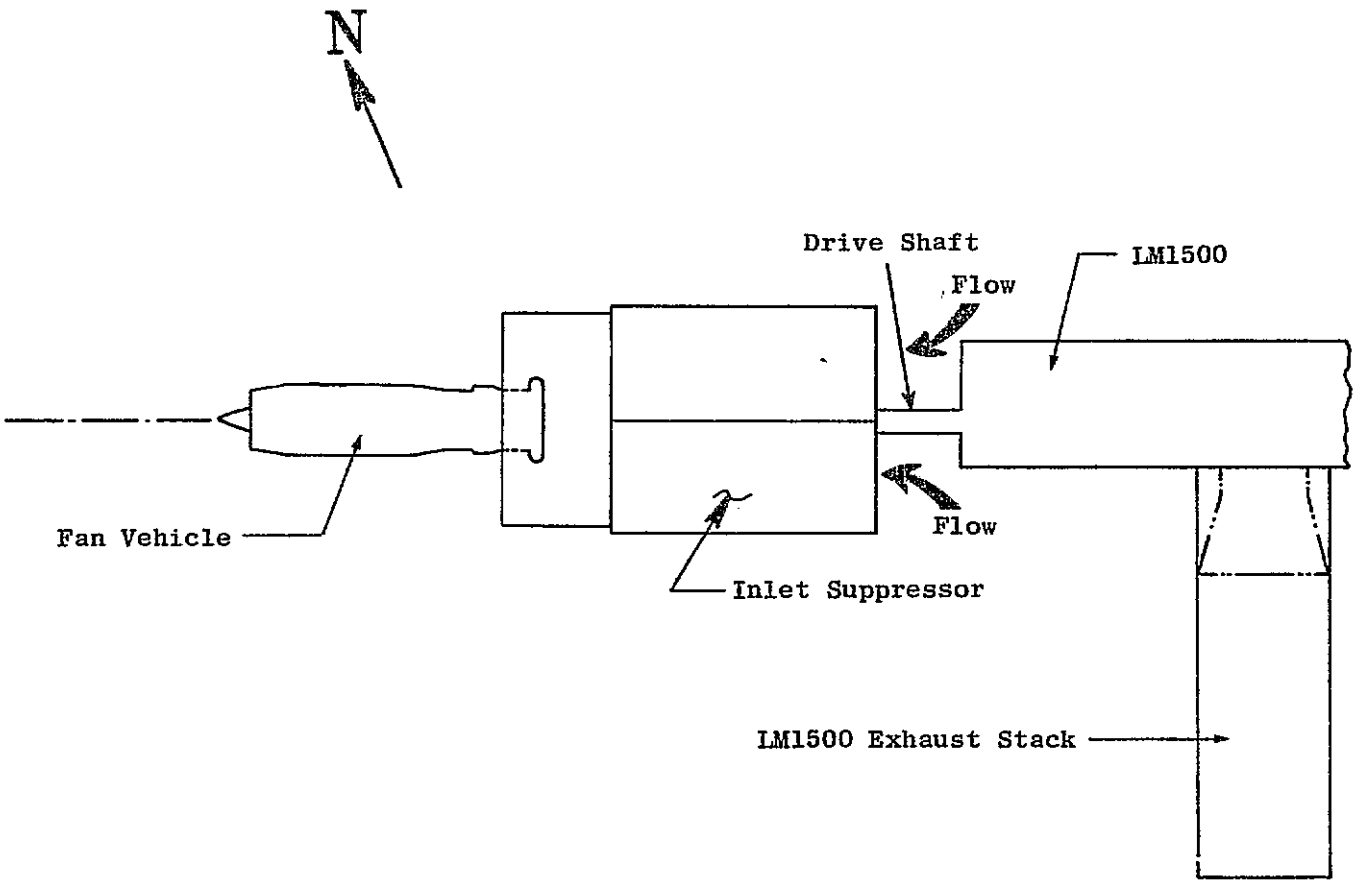

Figure 10. Schematic of Front-Drive Setup.

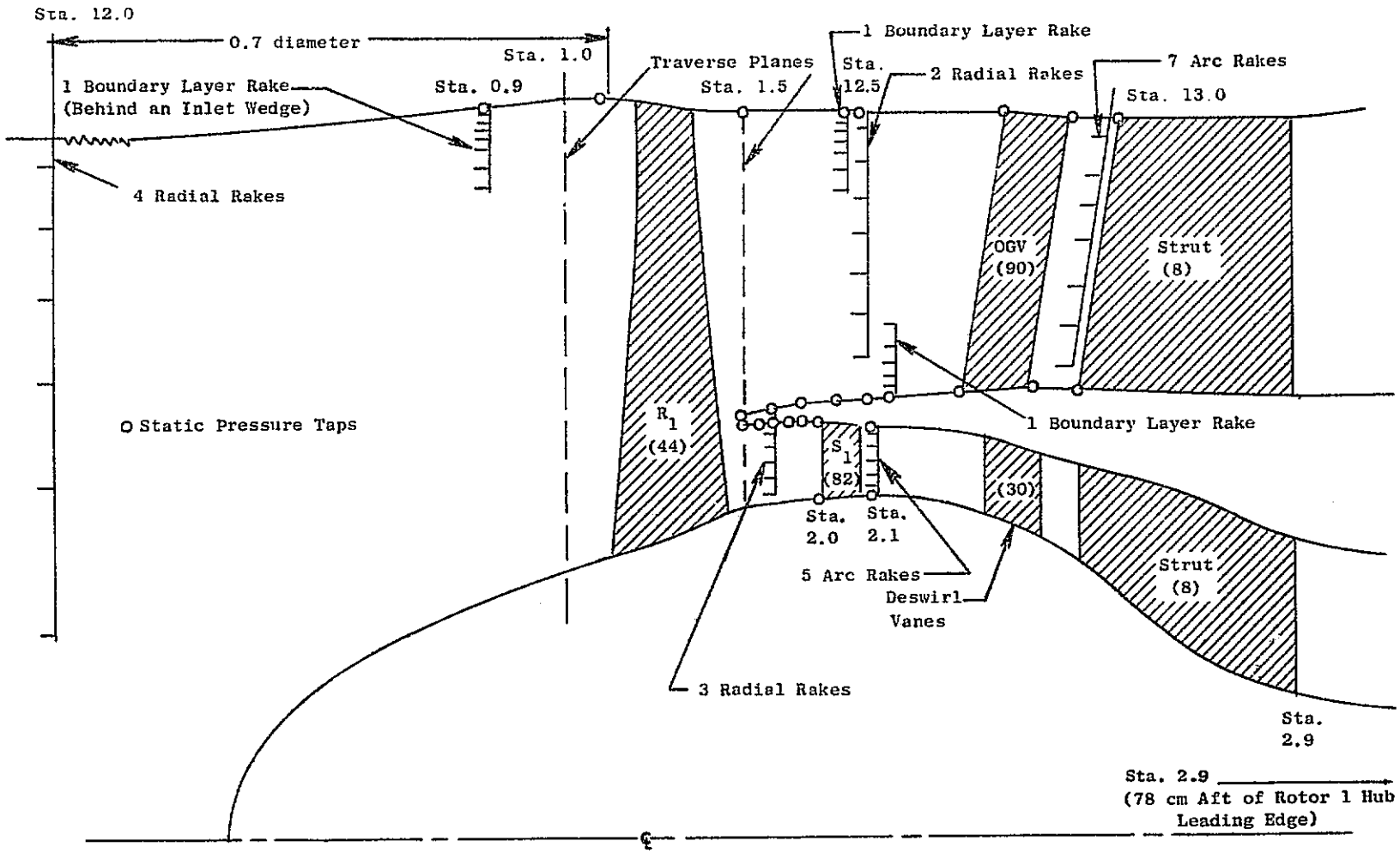

Figure 11. Schematic of Major Aerodynamic Instrumentation.

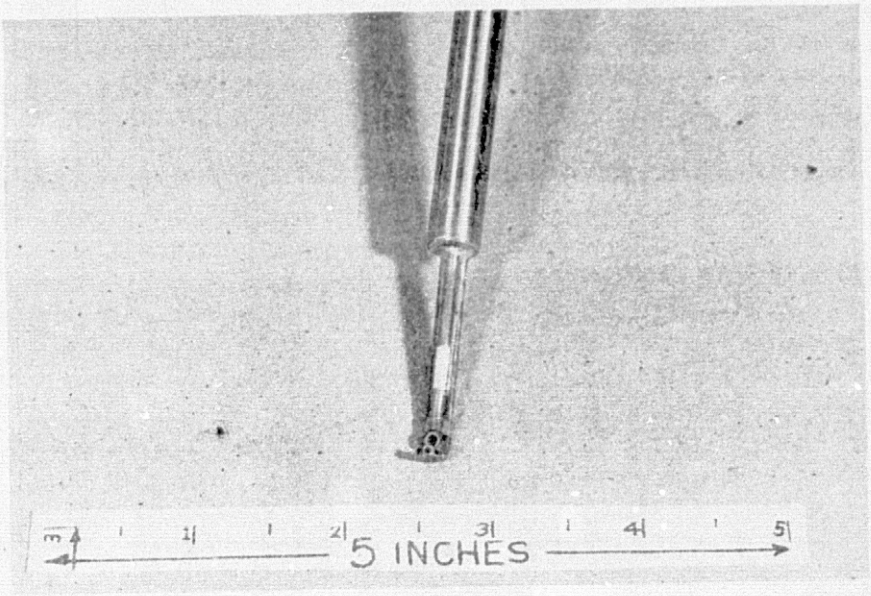

Figure 12. Cobra Traverse Probe (C7608367).

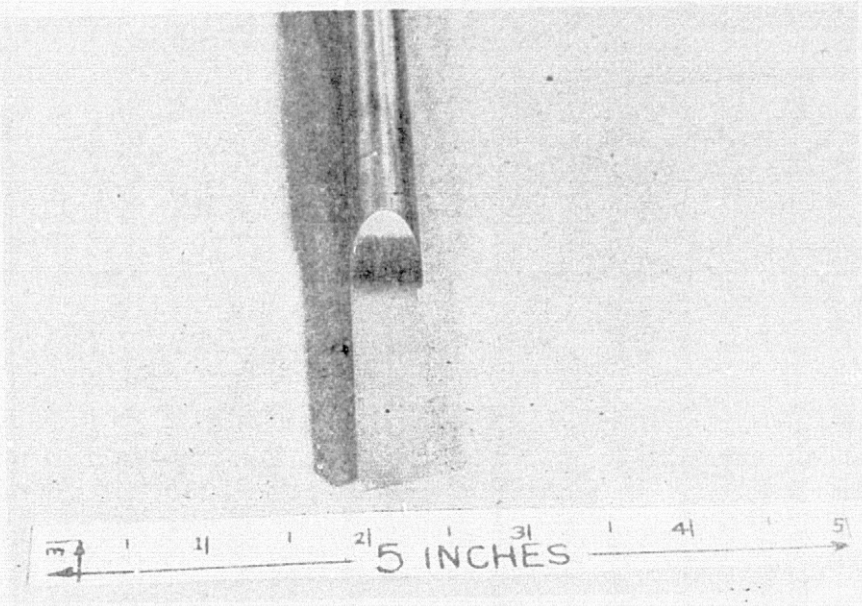

Figure 13. Wedge Traverse Probe (C7608369).

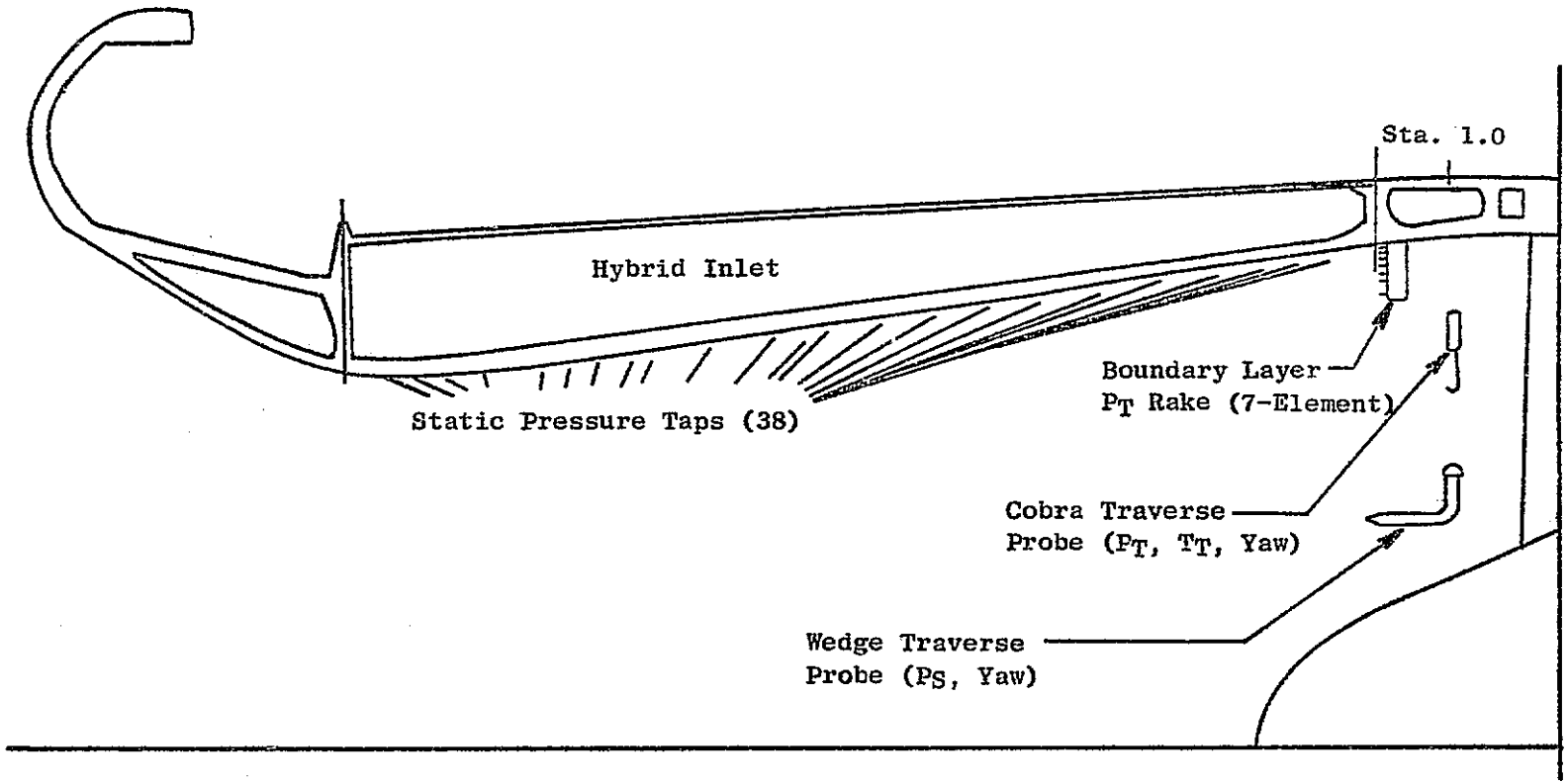

Figure 14. Schematic of Hybrid Inlet Aerodynamic Instrumentation.

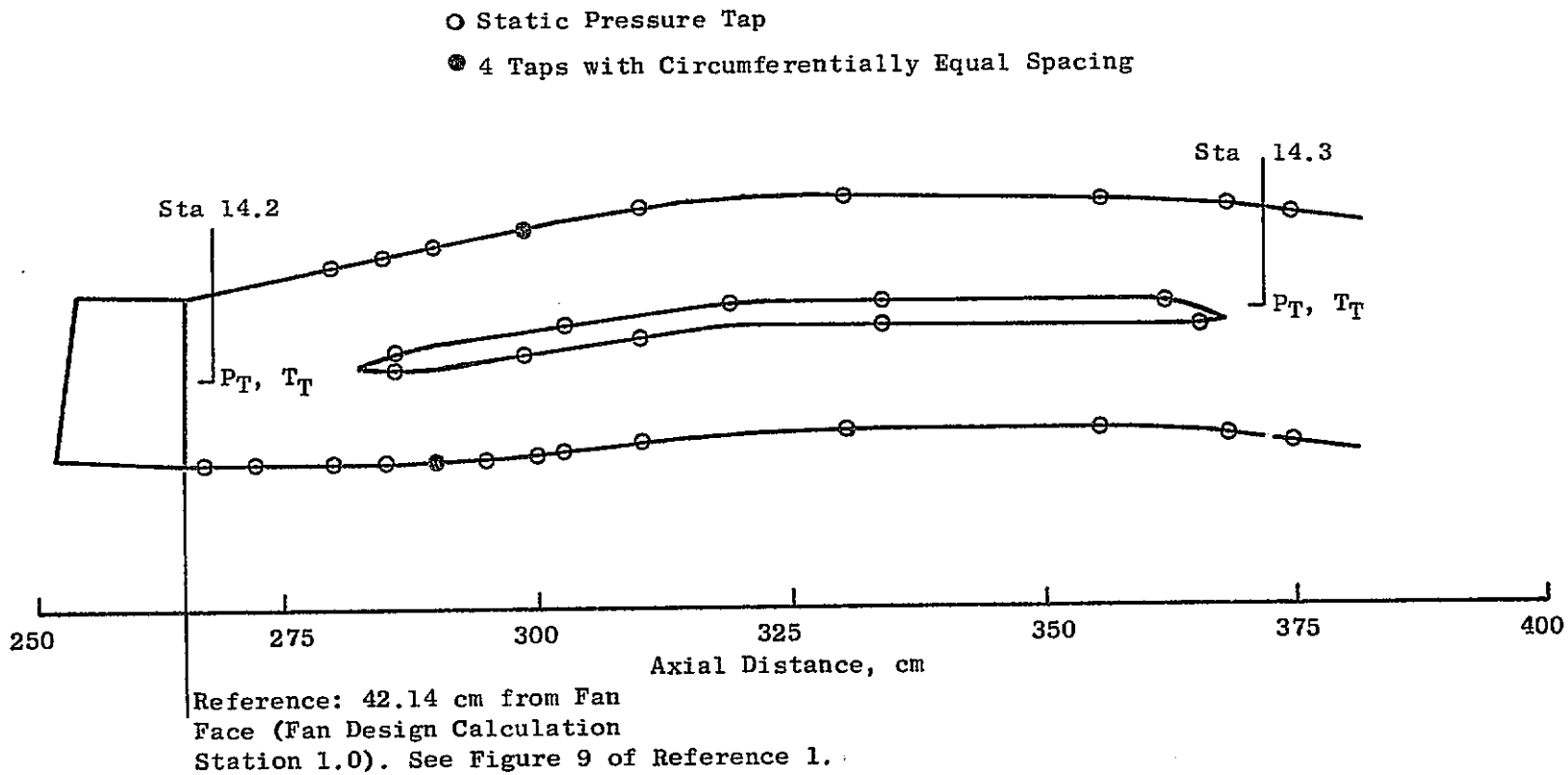

Figure 15. Fan Exit Duct Instrumentation Schematic.

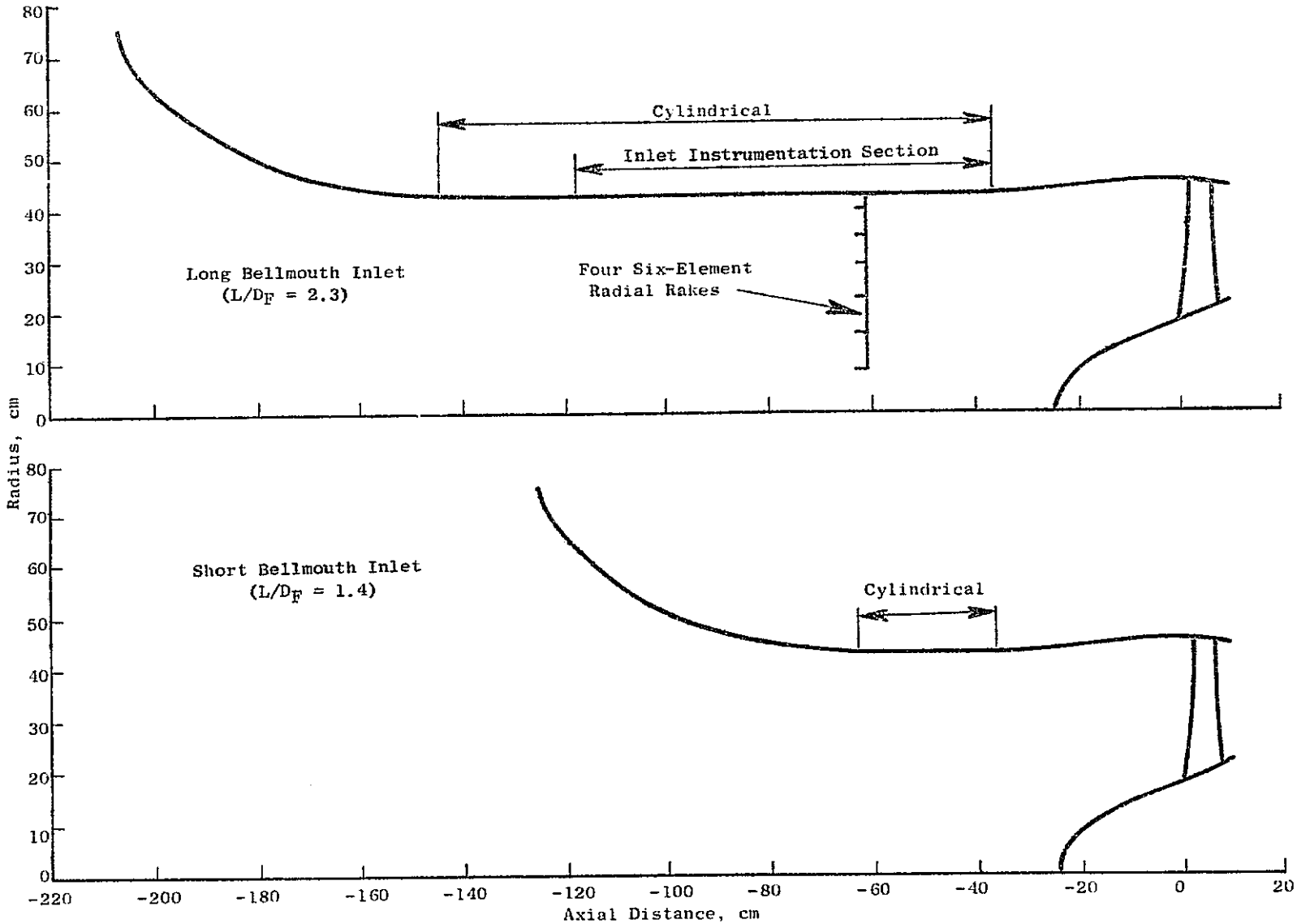

Figure 16. Fan Inlet Configurations for Aerodynamic Performance Tests.

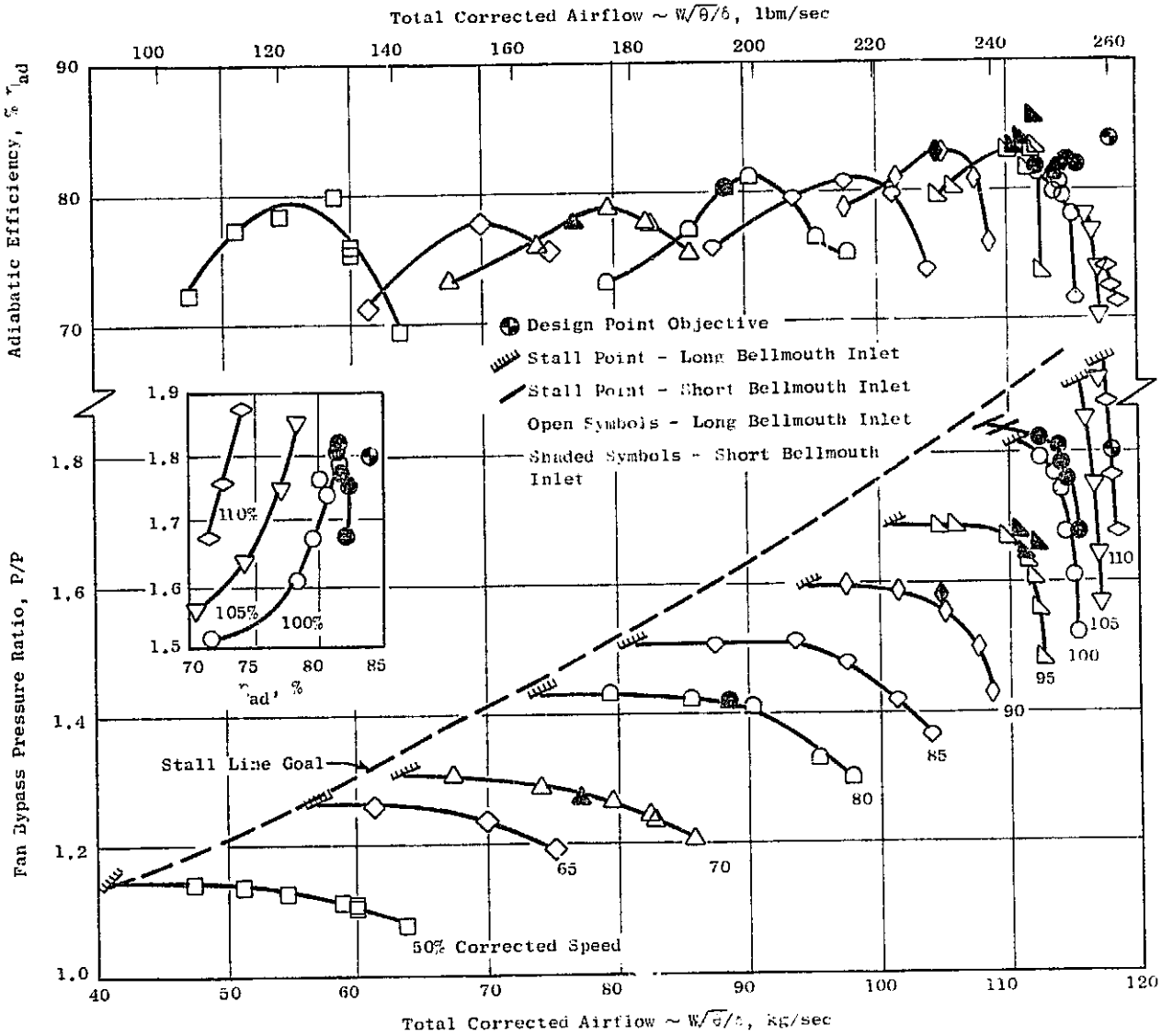

Figure 17. Overall Fan-Stage Performance Map.

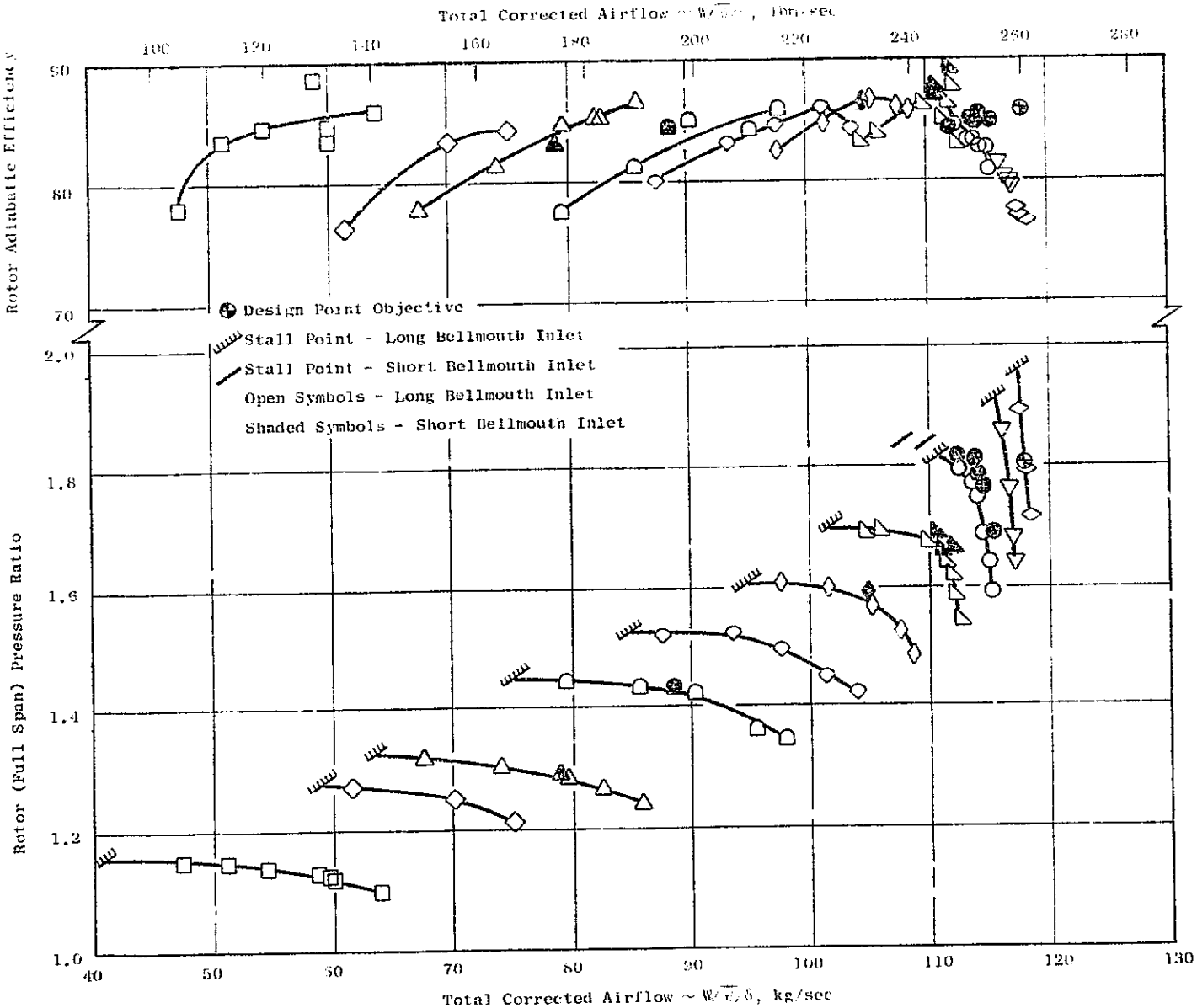

Figure 18. Fan Rotor Performance Map.

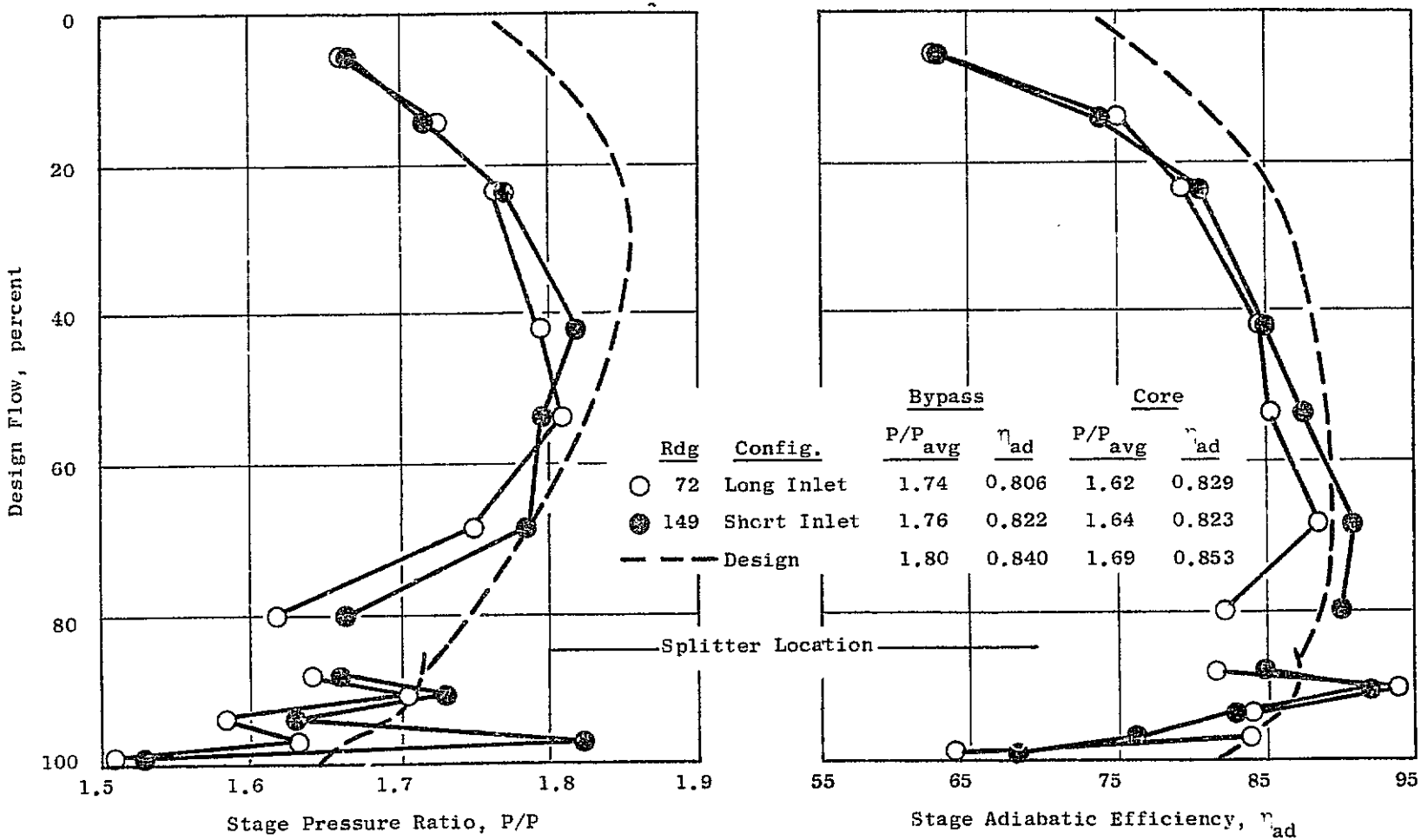

Figure 19. Nominal Operating-Line Stage Pressure Ratio and Adiabatic Efficiency, Long and Short Bellmouth Inlet Test Data, 100% Speed.

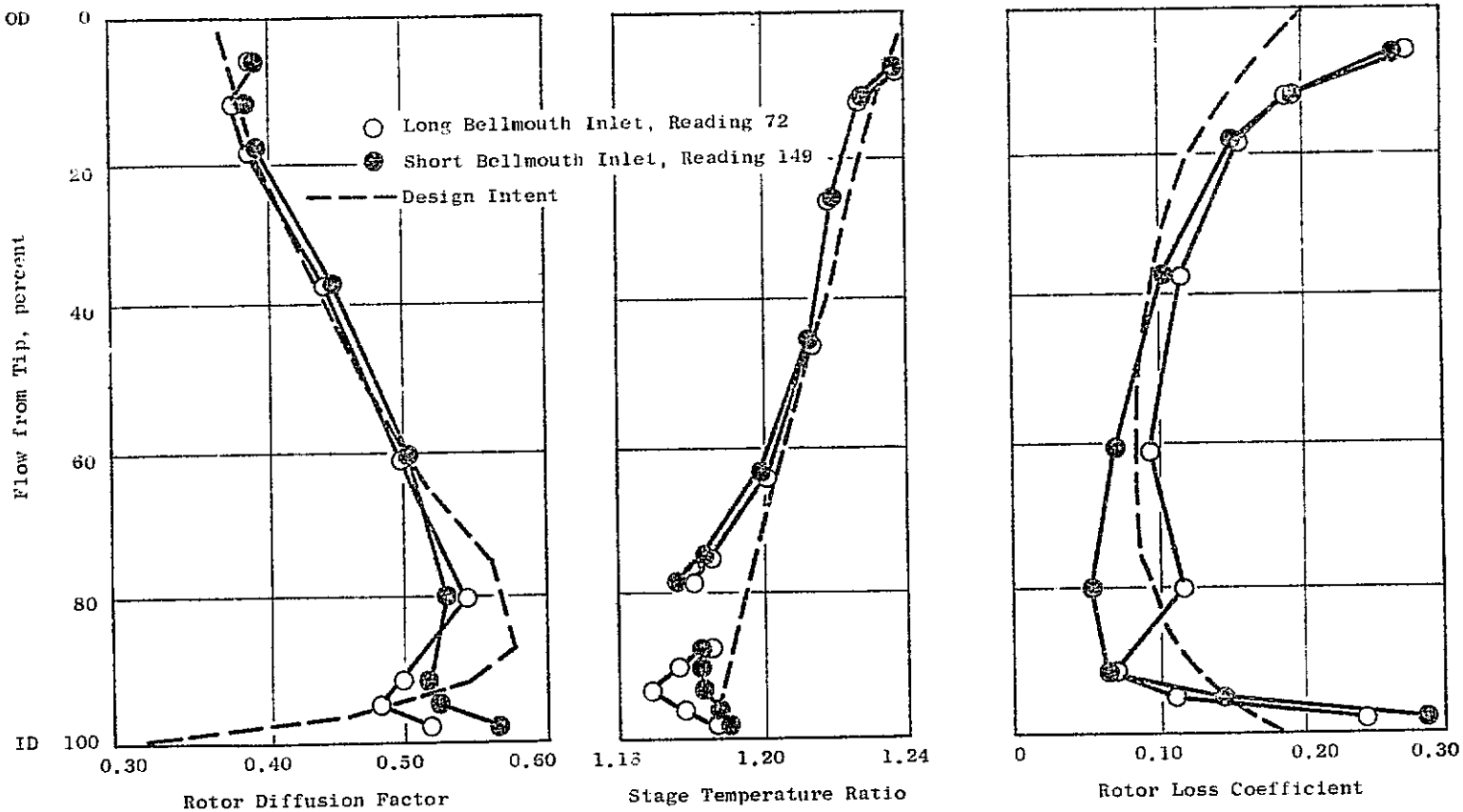

Figure 20. Nominal Operating-Line Rotor Diffusion Factor, Stage Total Temperature Ratio, and Rotor Total Pressure Loss Coefficient, Long and Short Bellmouth Inlet Test Data, 100% Speed.

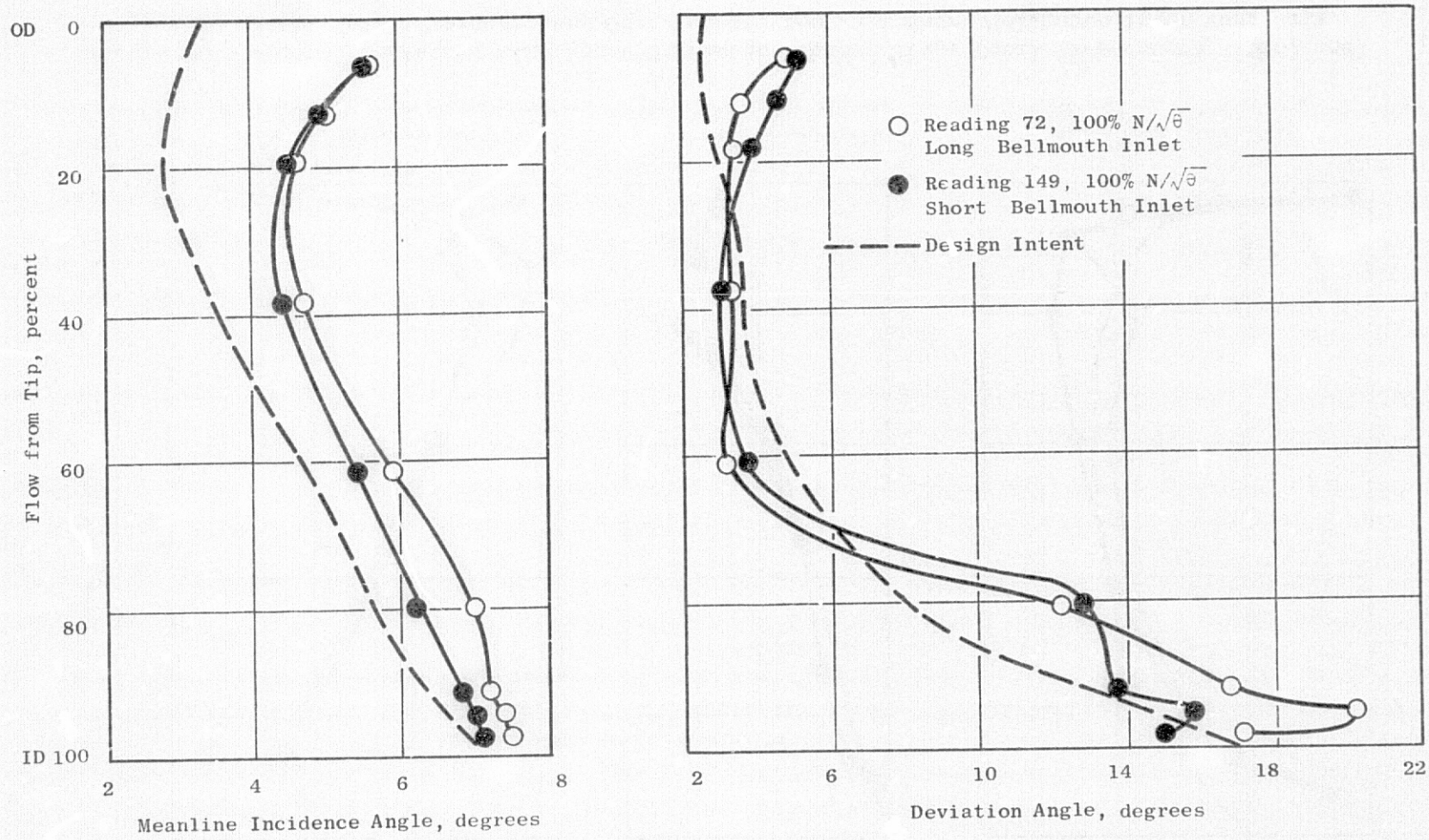

Figure 21. Fan Rotor Incidence and Deviation Angles, Design Versus Test.

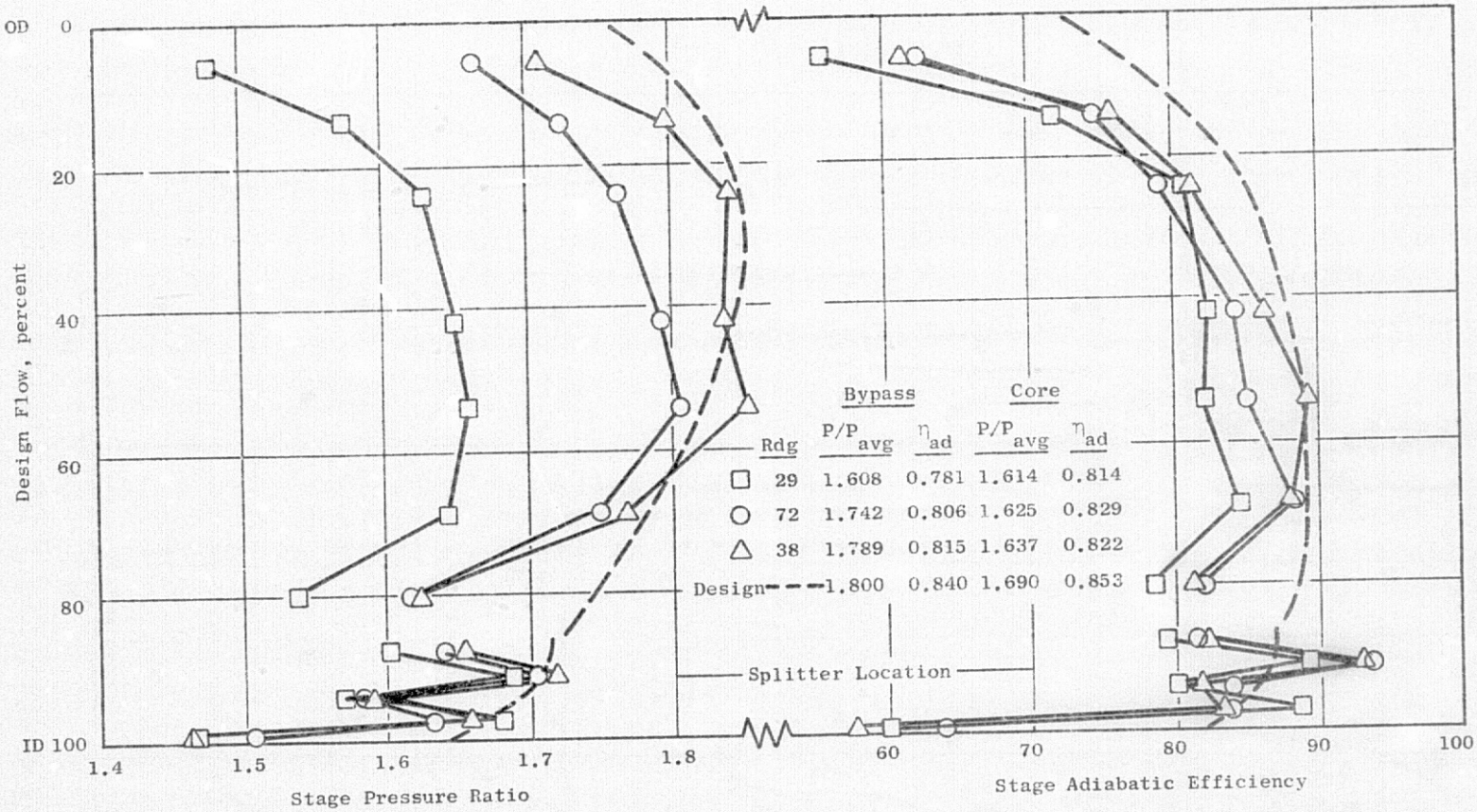

Figure 22. Long Bellmouth Inlet Stage Pressure Ratio and Efficiency, 100% Speed.

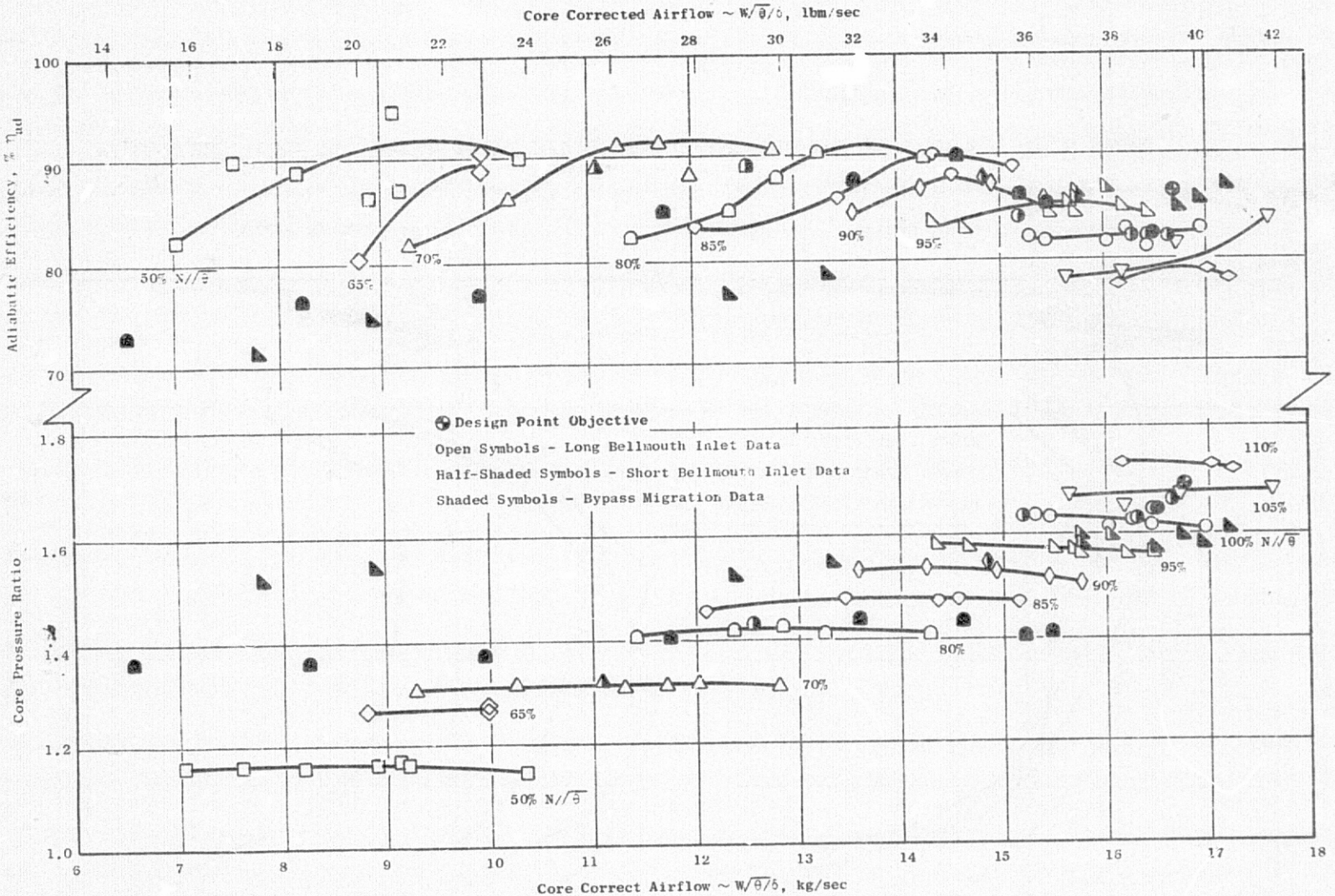

Figure 23. Overall Fan Stage Hub Performance Map.

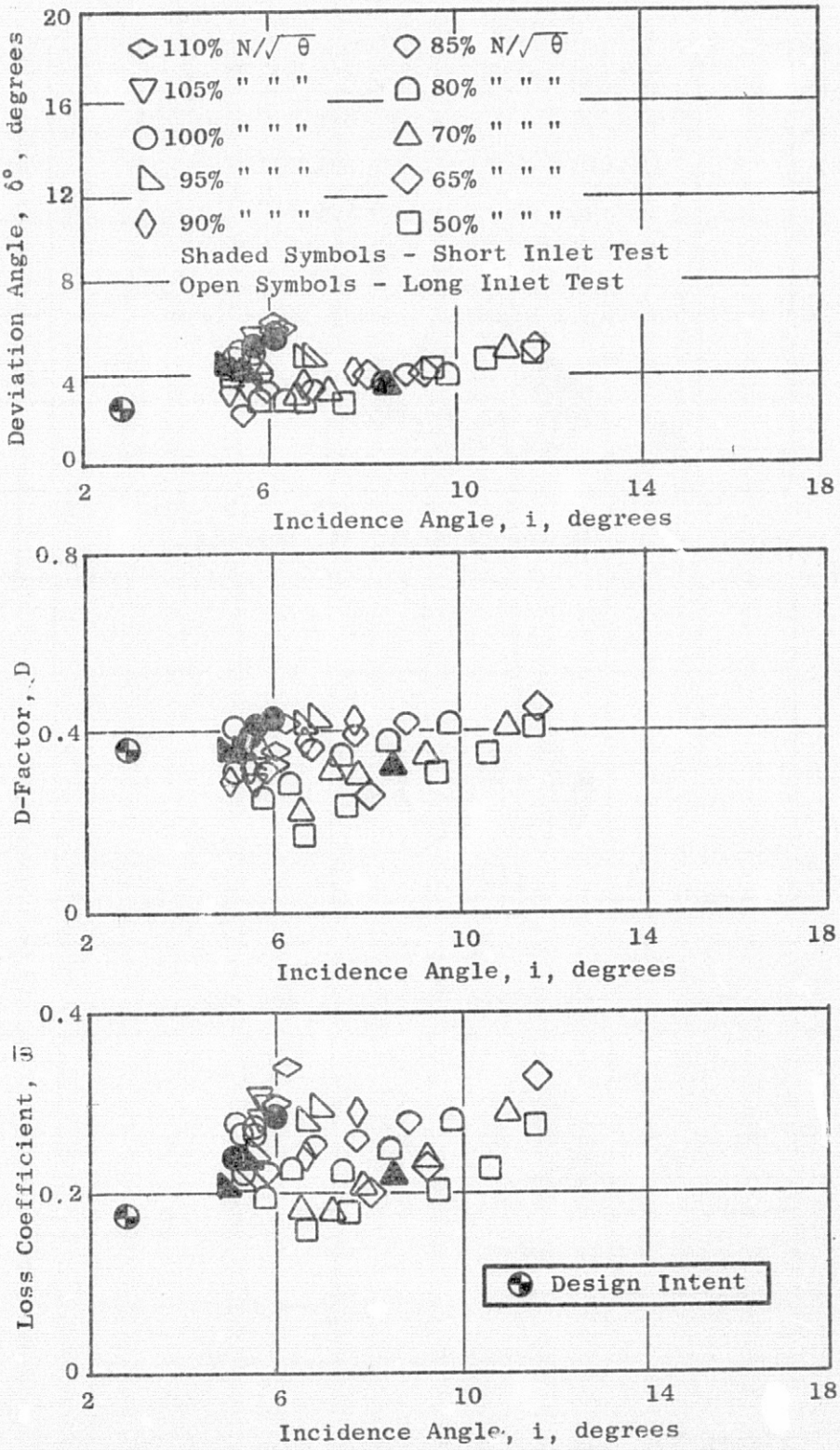

Figure 24. Rotor Blade-Element Data, 5% Immersion.

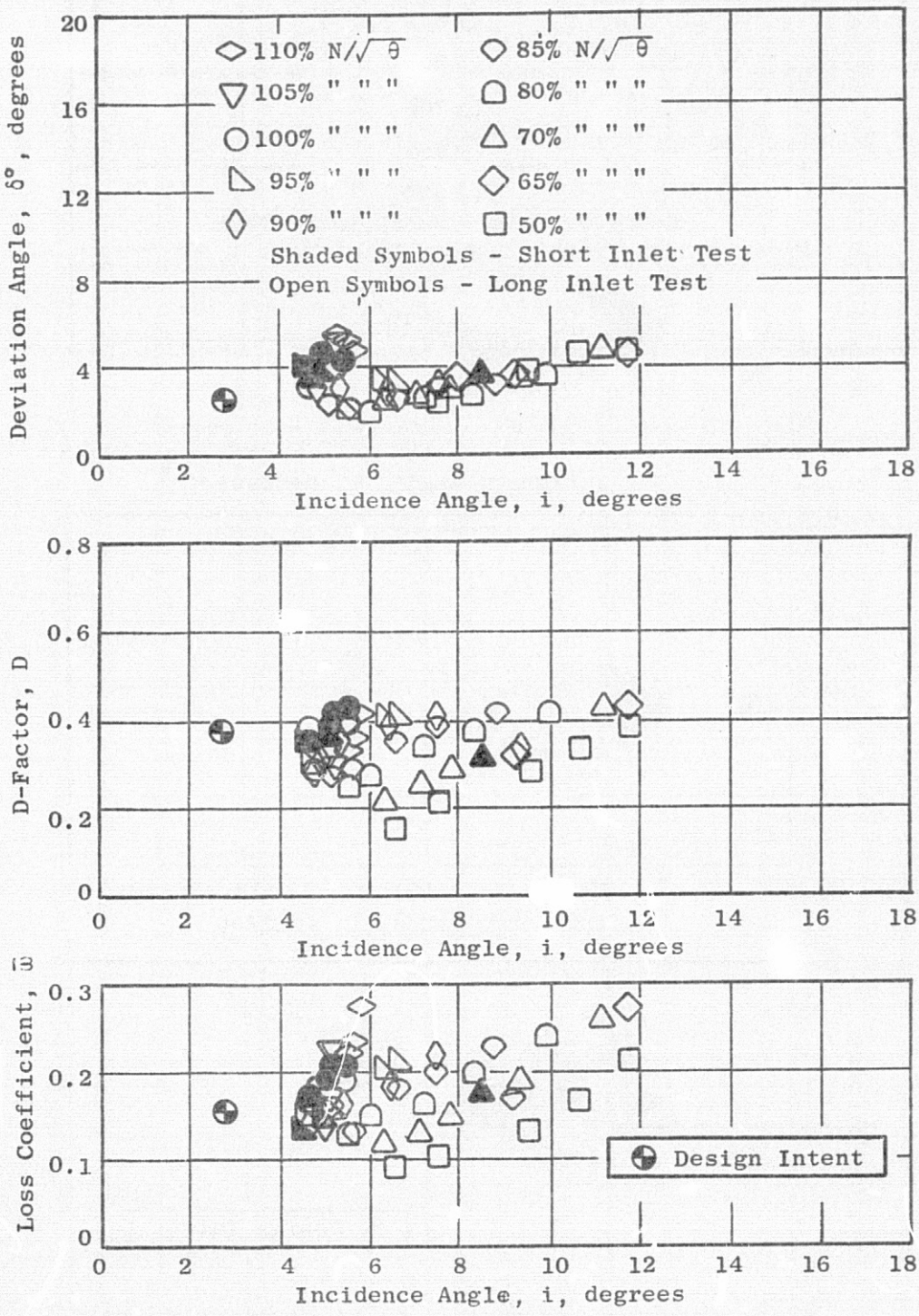

Figure 25. Rotor Blade-Element Data, 10% Immersion.

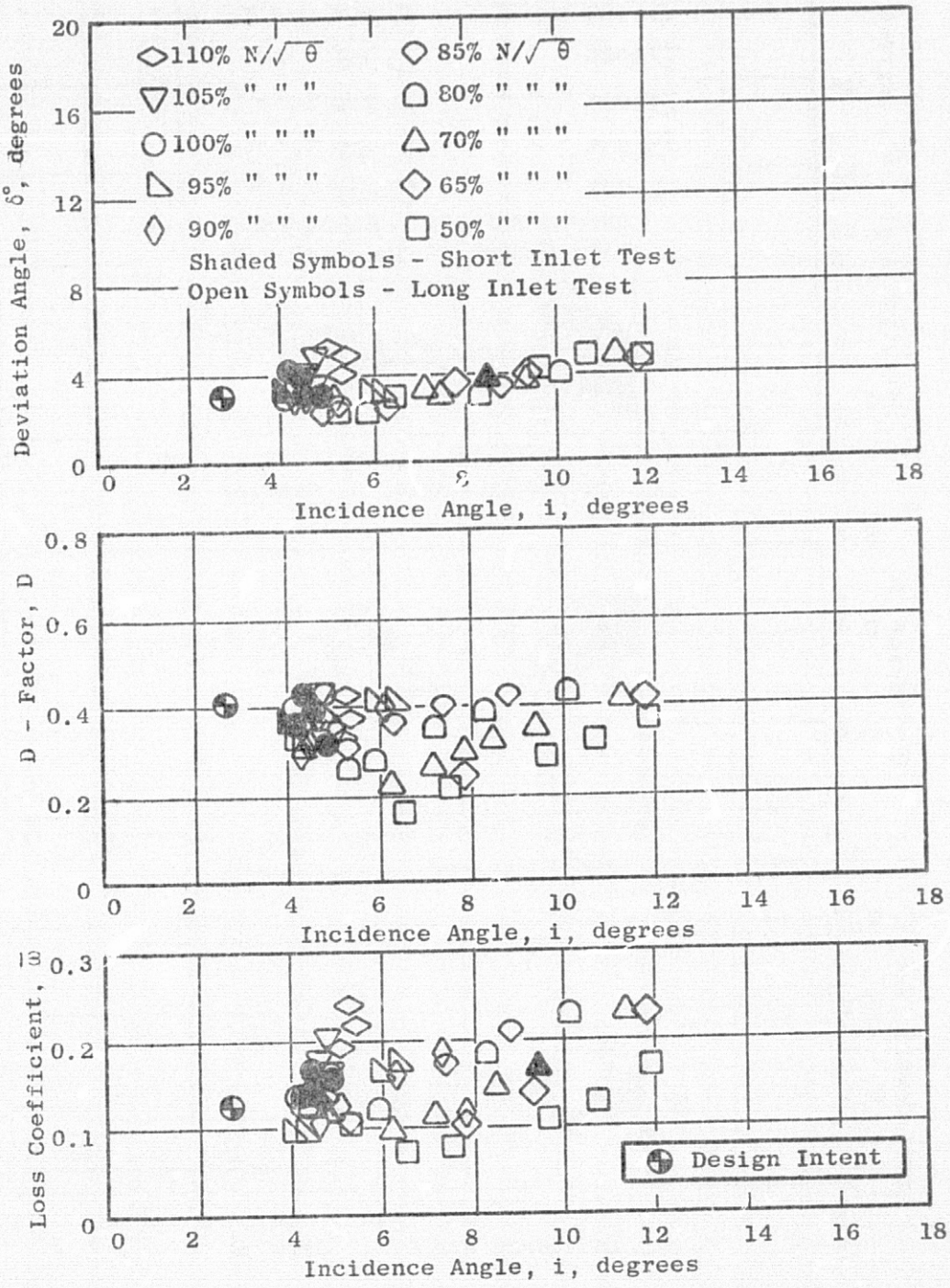

Figure 26. Rotor Blade-Element Data, 15% Immersion.

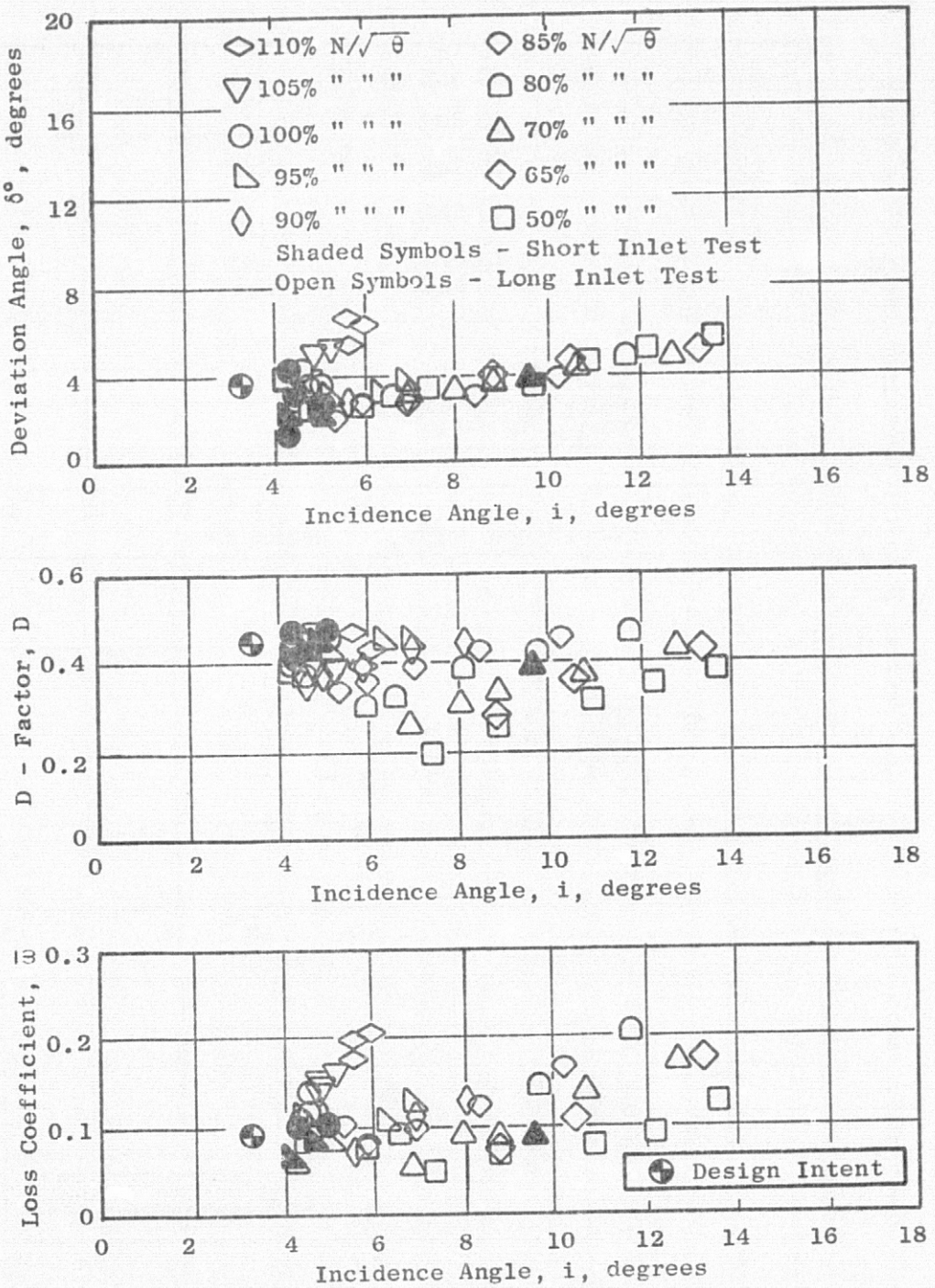

Figure 27. Rotor Blade-Element Data, 30% Immersion.

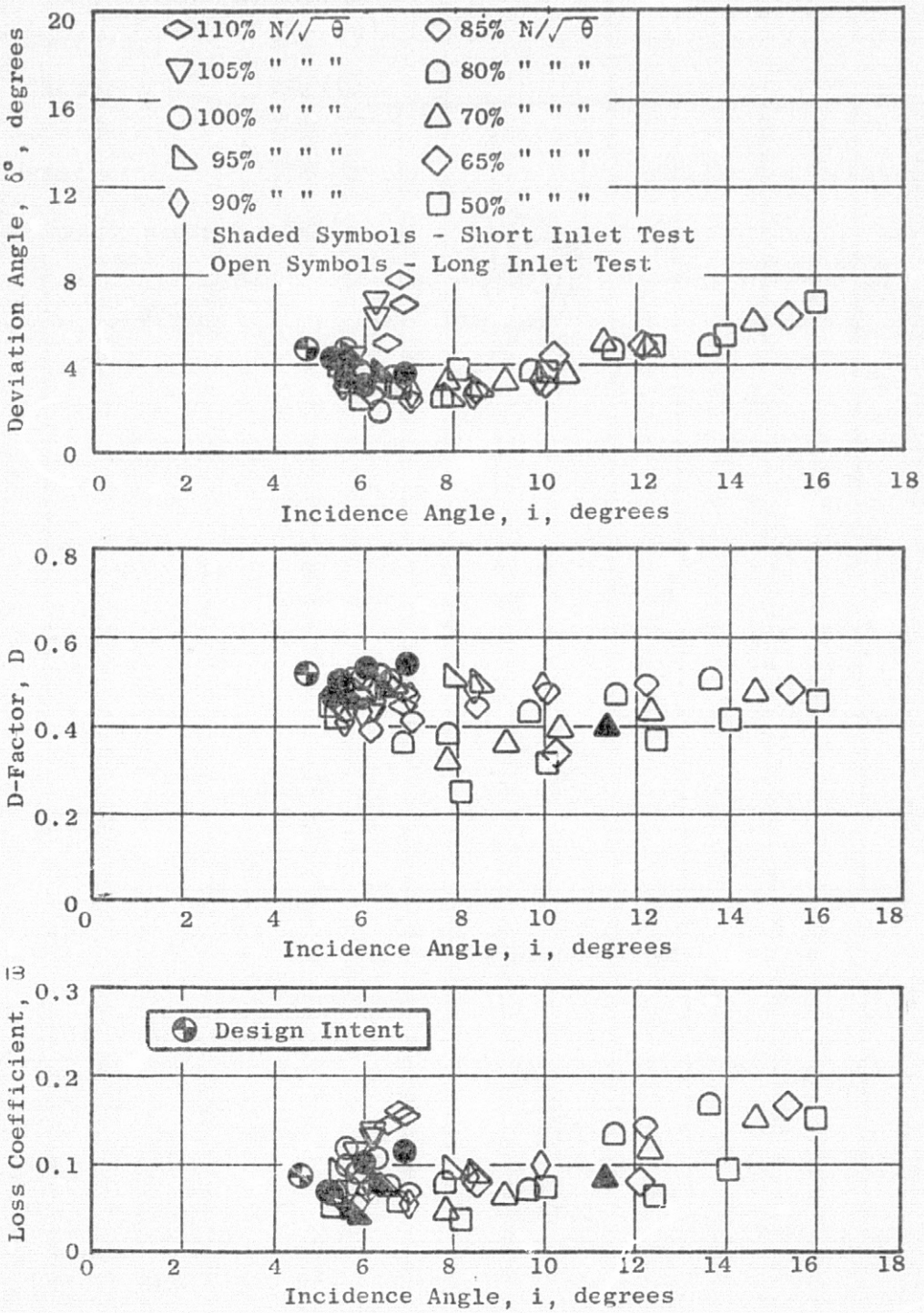

Figure 28. Rotor Blade-Element Data, 50% Immersion.

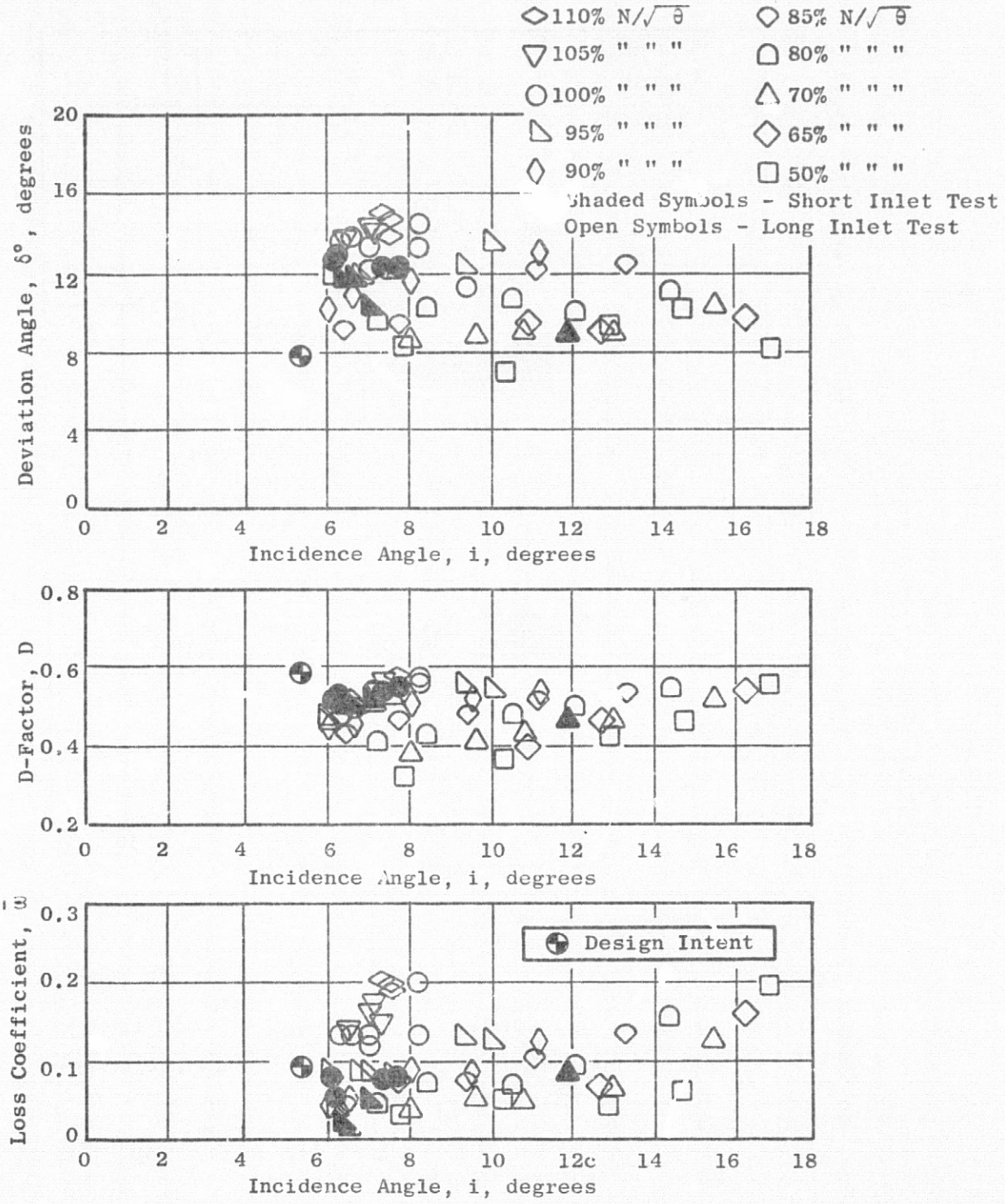

Figure 29. Rotor Blade-Element Data, 70% Immersion.

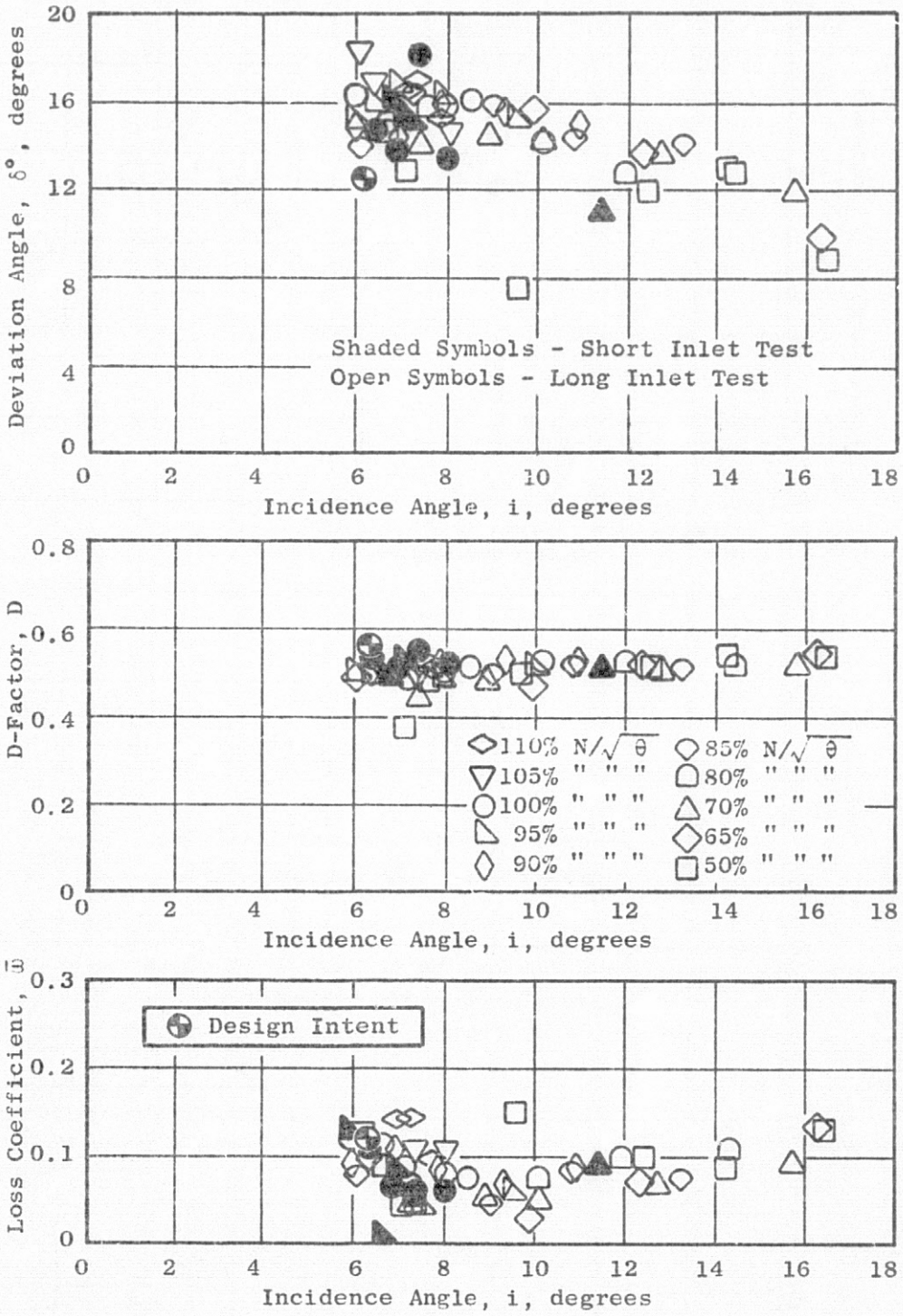

Figure 30. Rotor Blade-Element Data, 85% Immersion.

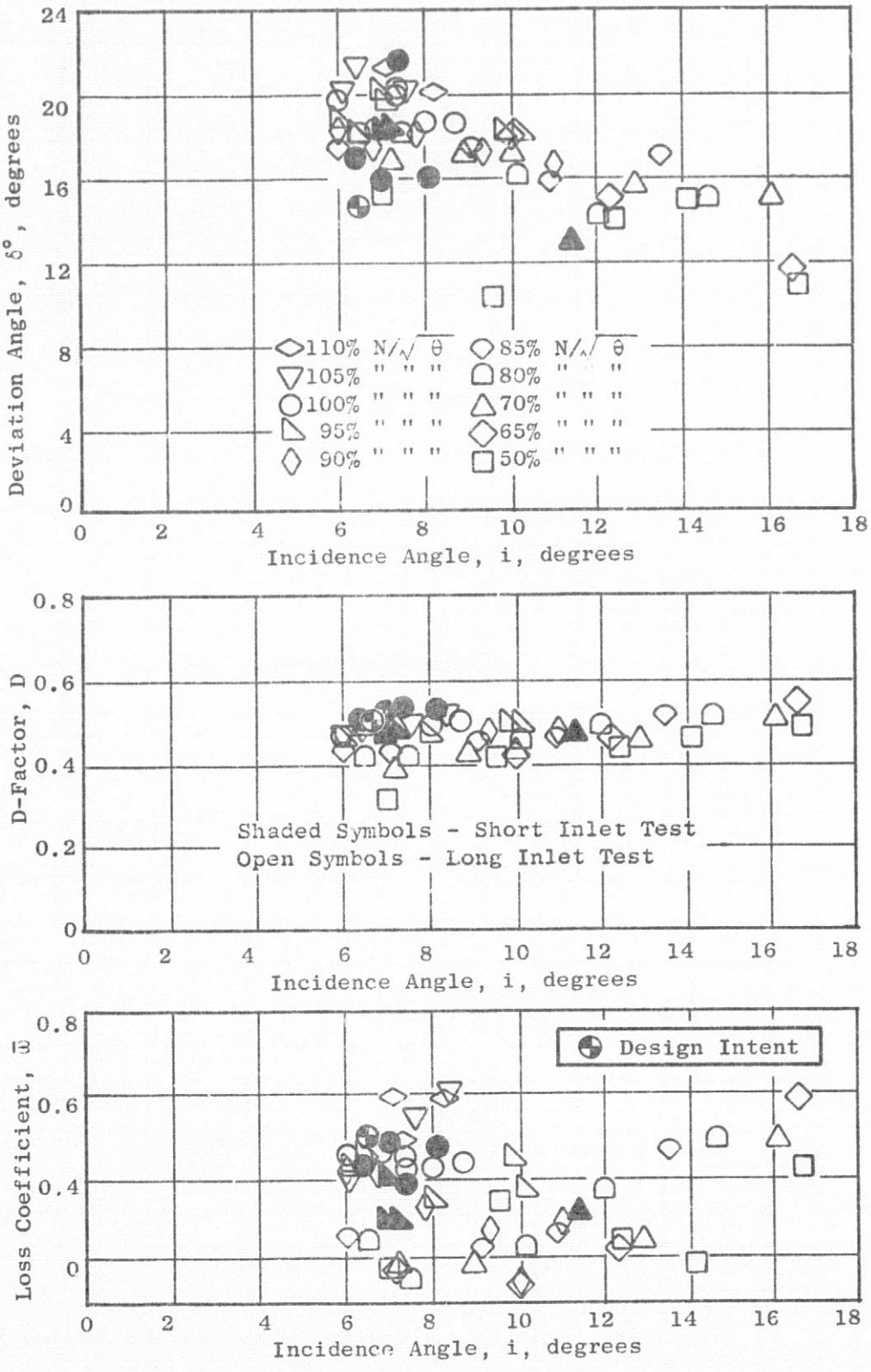

Figure 31. Rotor Blade-Element Data, 90% Immersion.

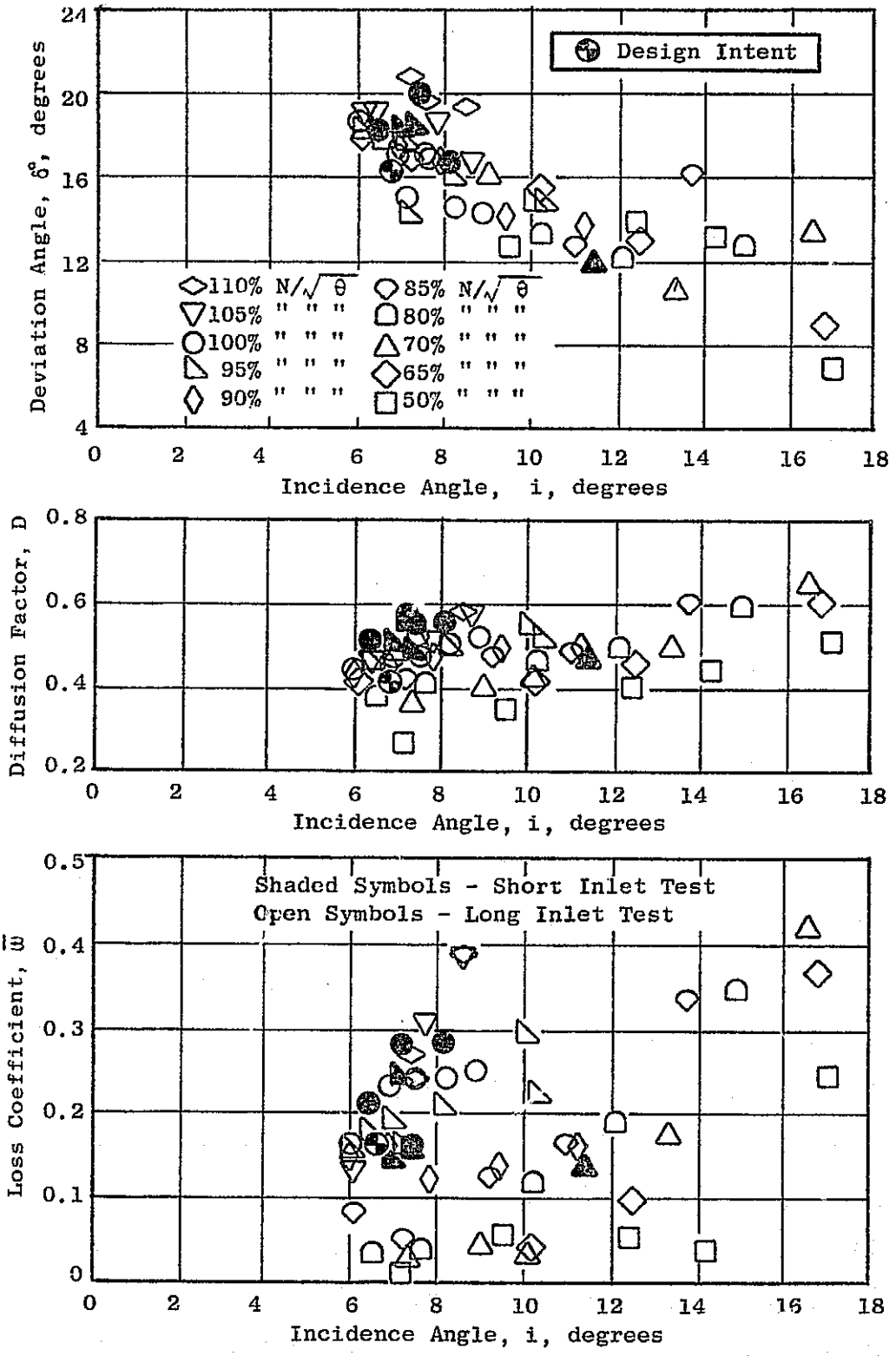

Figure 32. Rotor Blade-Element Data, 95% Immersion.

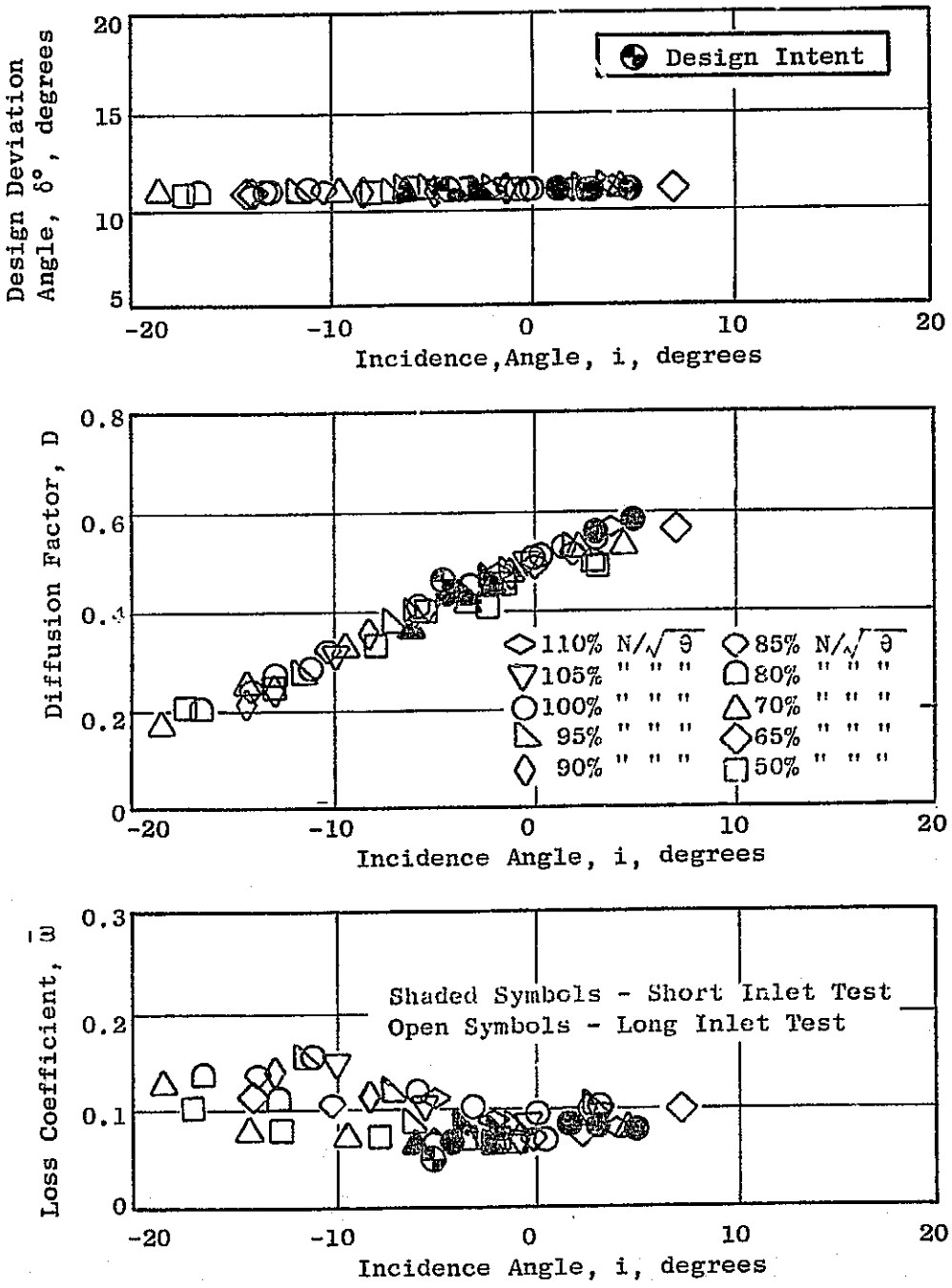

Figure 33. Bypass OGV Blade-Element Data, 10% Immersion.

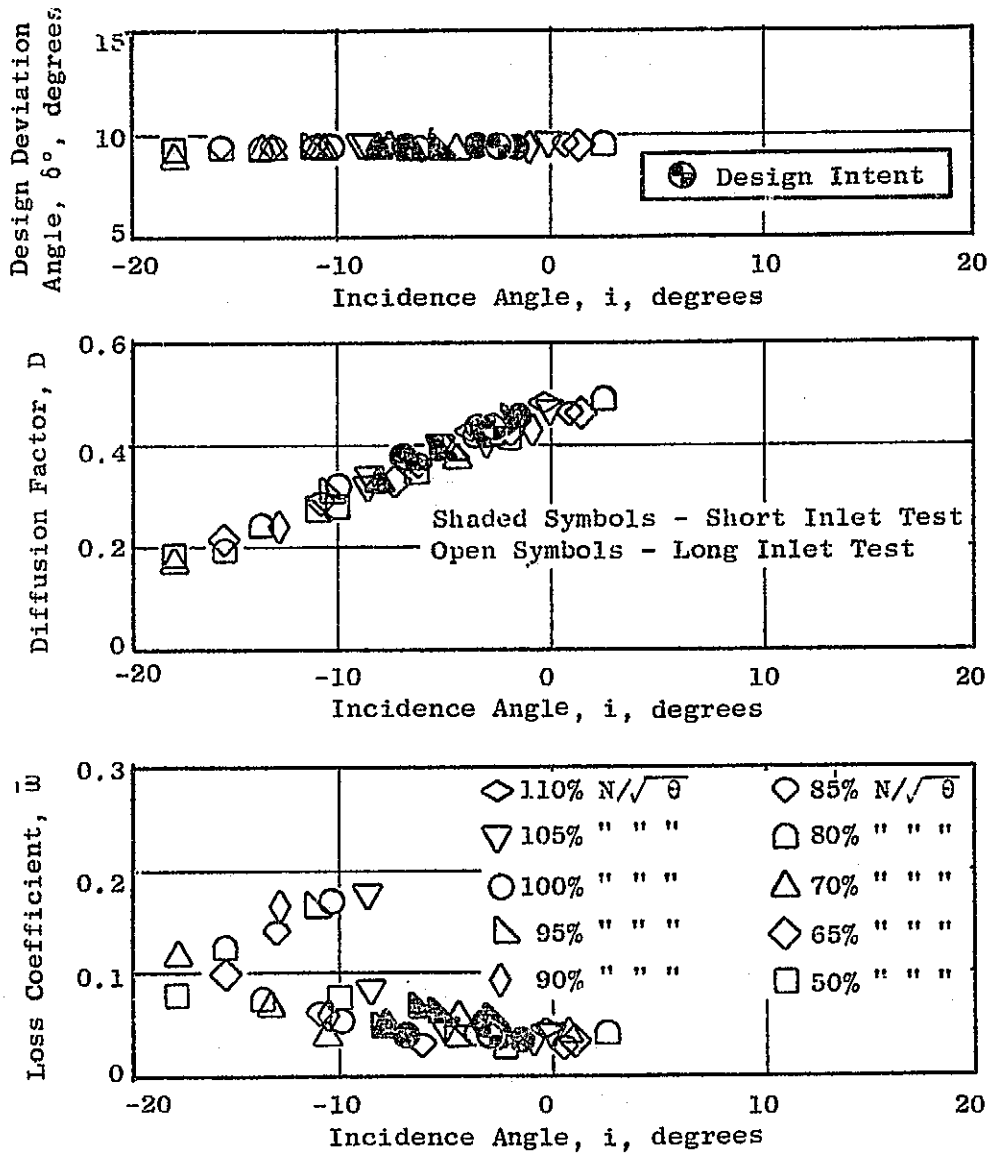

Figure 34. Bypass OGV Blade-Element Data, 30% Immersion.

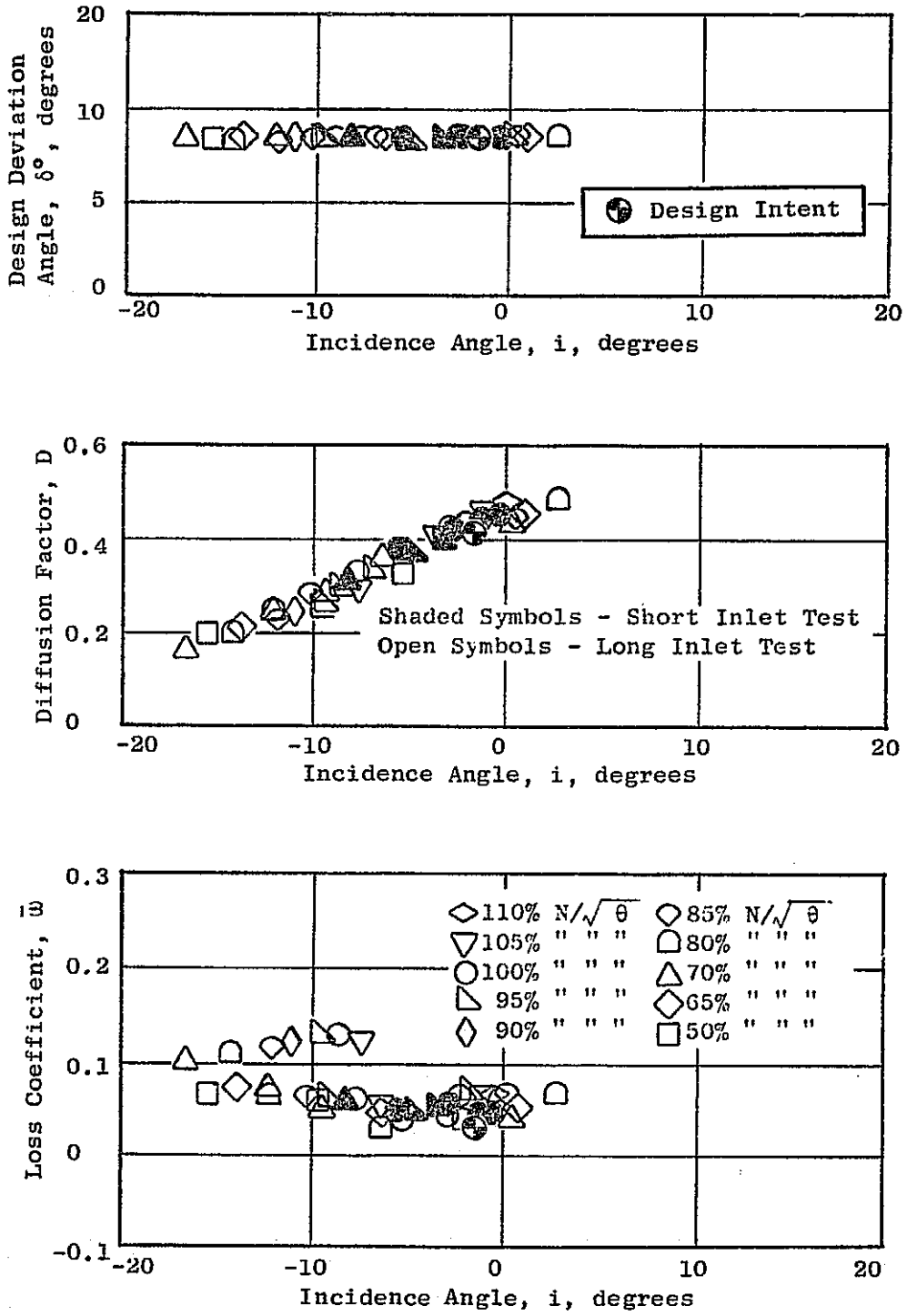

Figure 35. Bypass OGV Blade-Element Data, 50% Immersion.

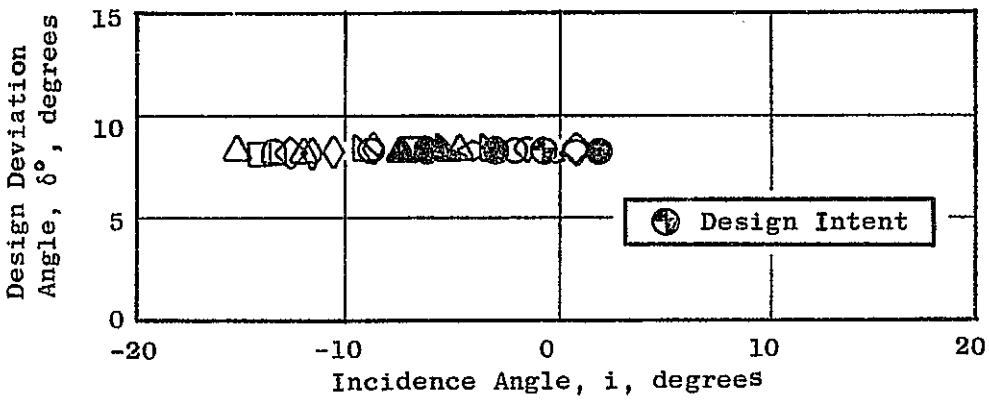

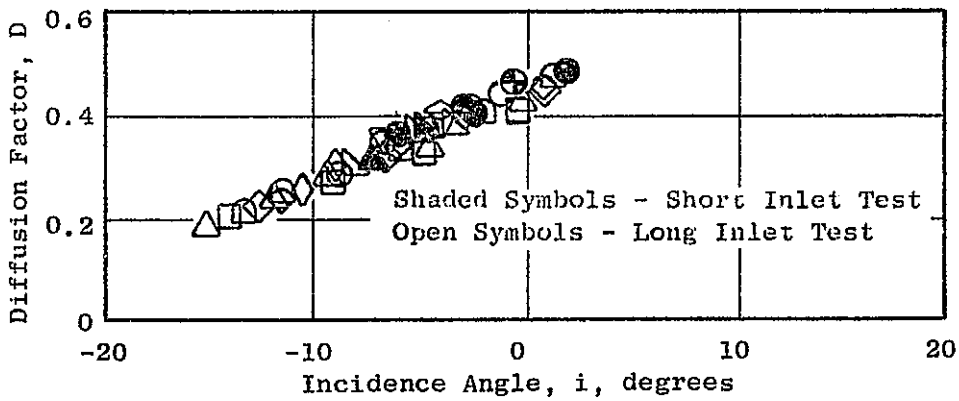

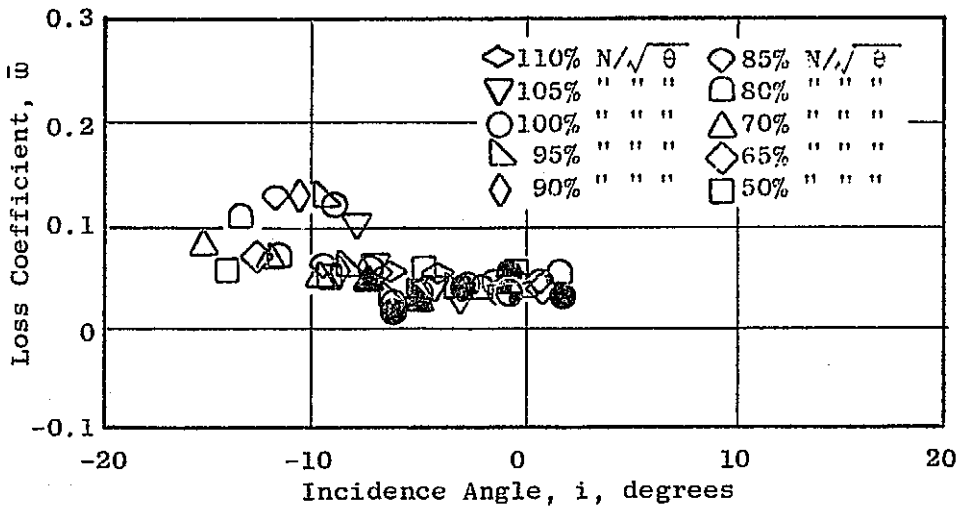

Figure 36. Bypass OGV Blade-Element Data, 70% Immersion.

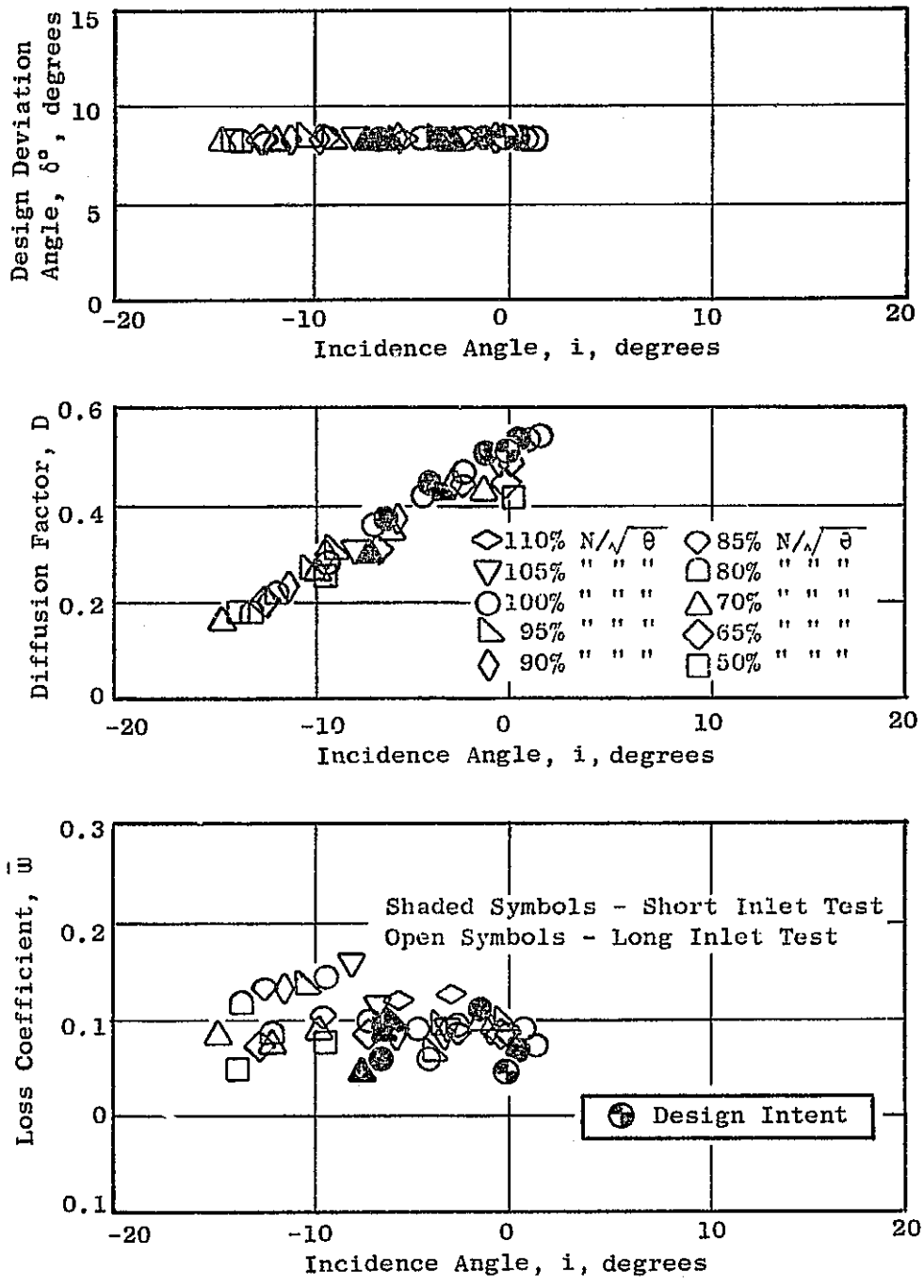

Figure 37. Bypass OGV Blade-Element Data, 90% Immersion.

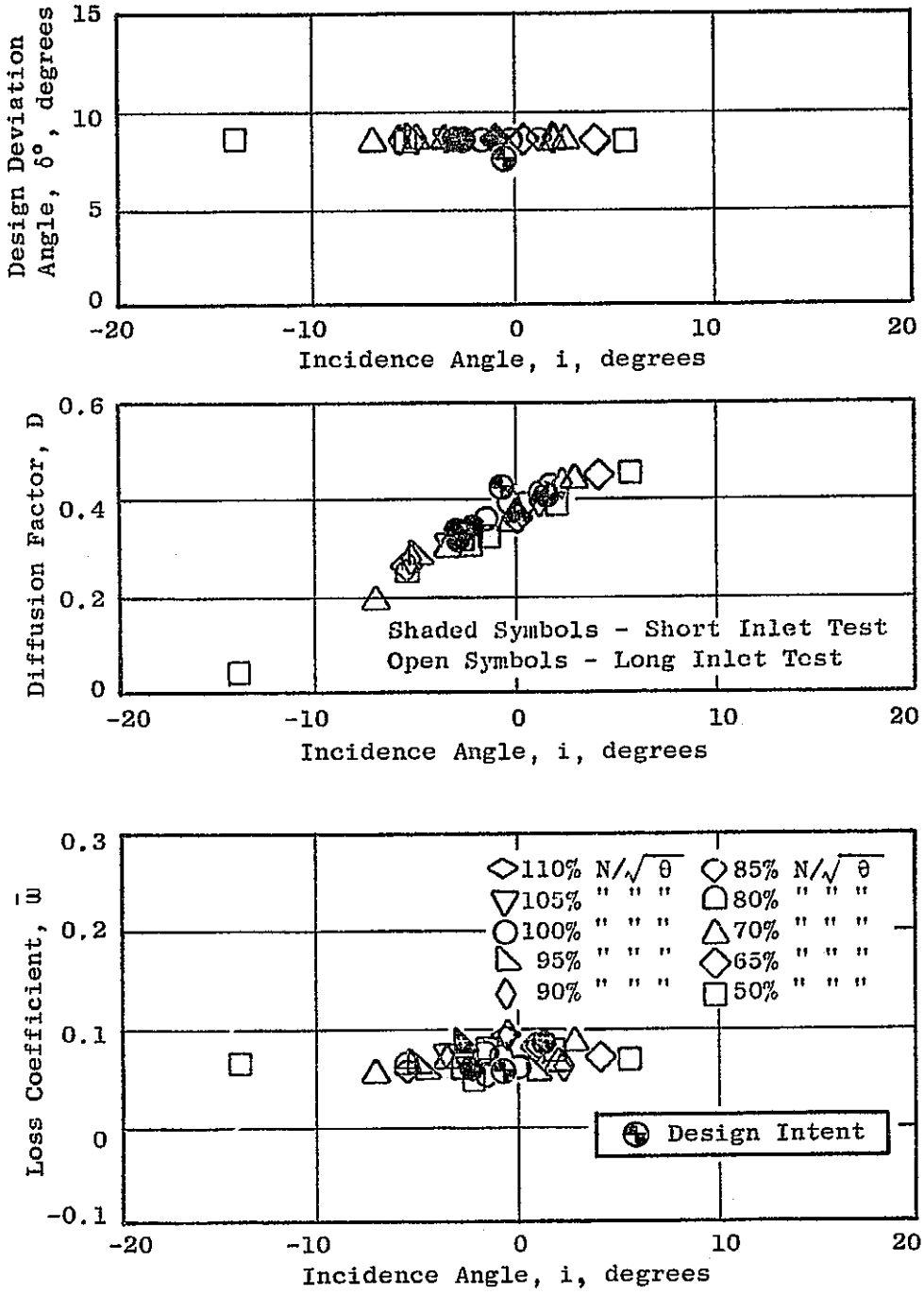

Figure 38. Core Stator Blade-Element Data, 15% Immersion.

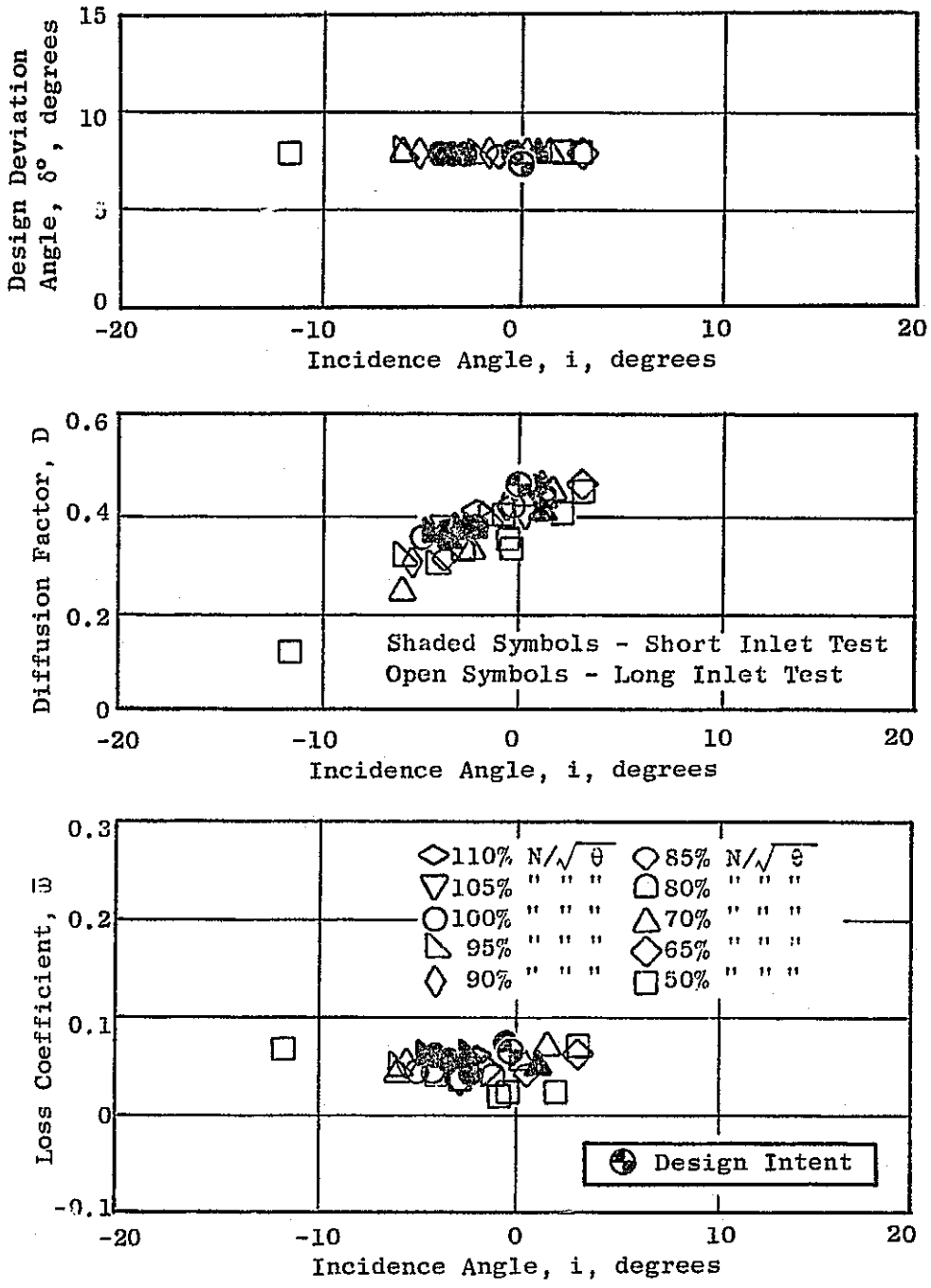

Figure 39. Core Stator Blade-Element Data, 30% Immersion.

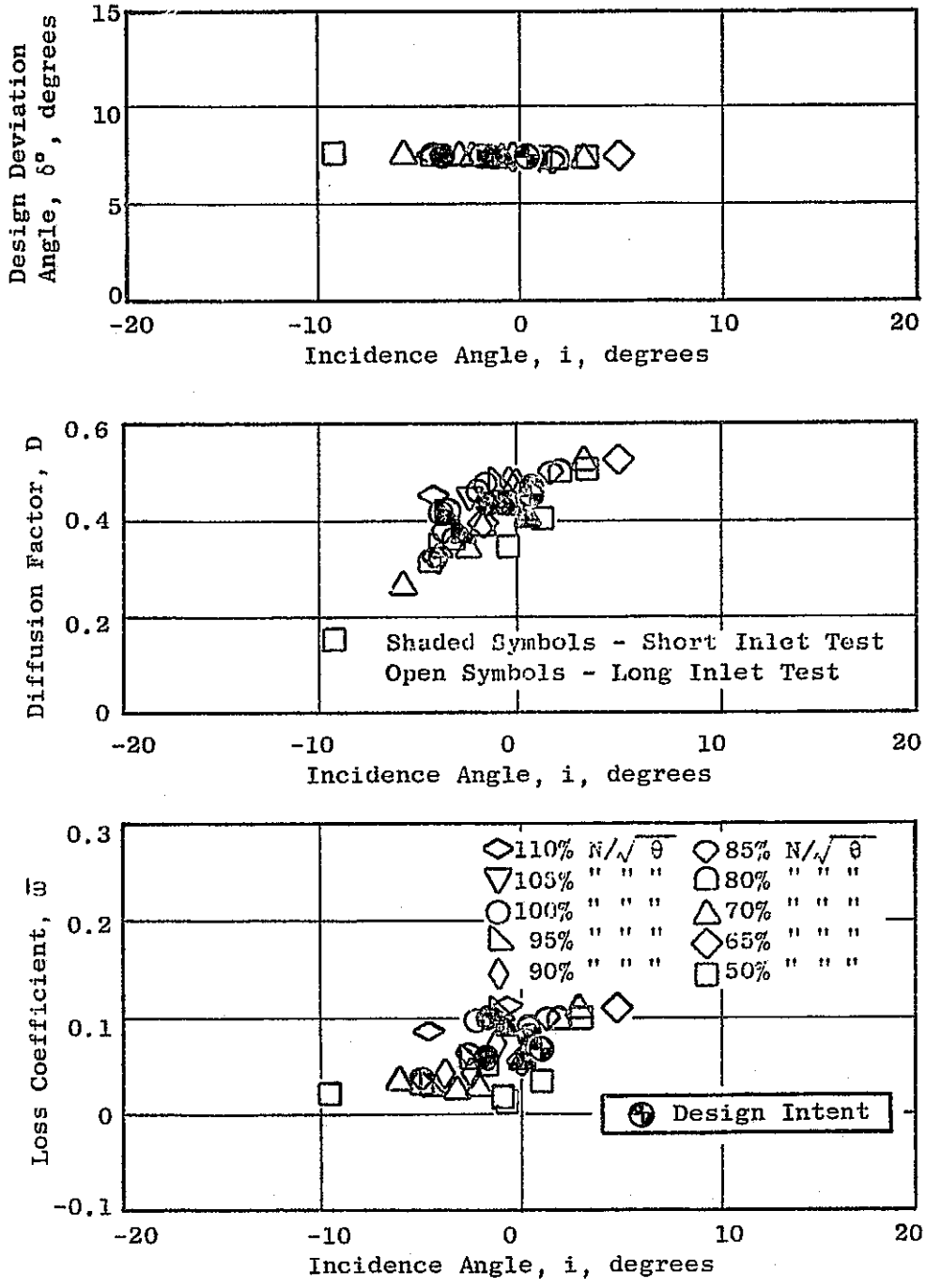

Figure 40. Core Stator Blade-Element Data, 50% Immersion.

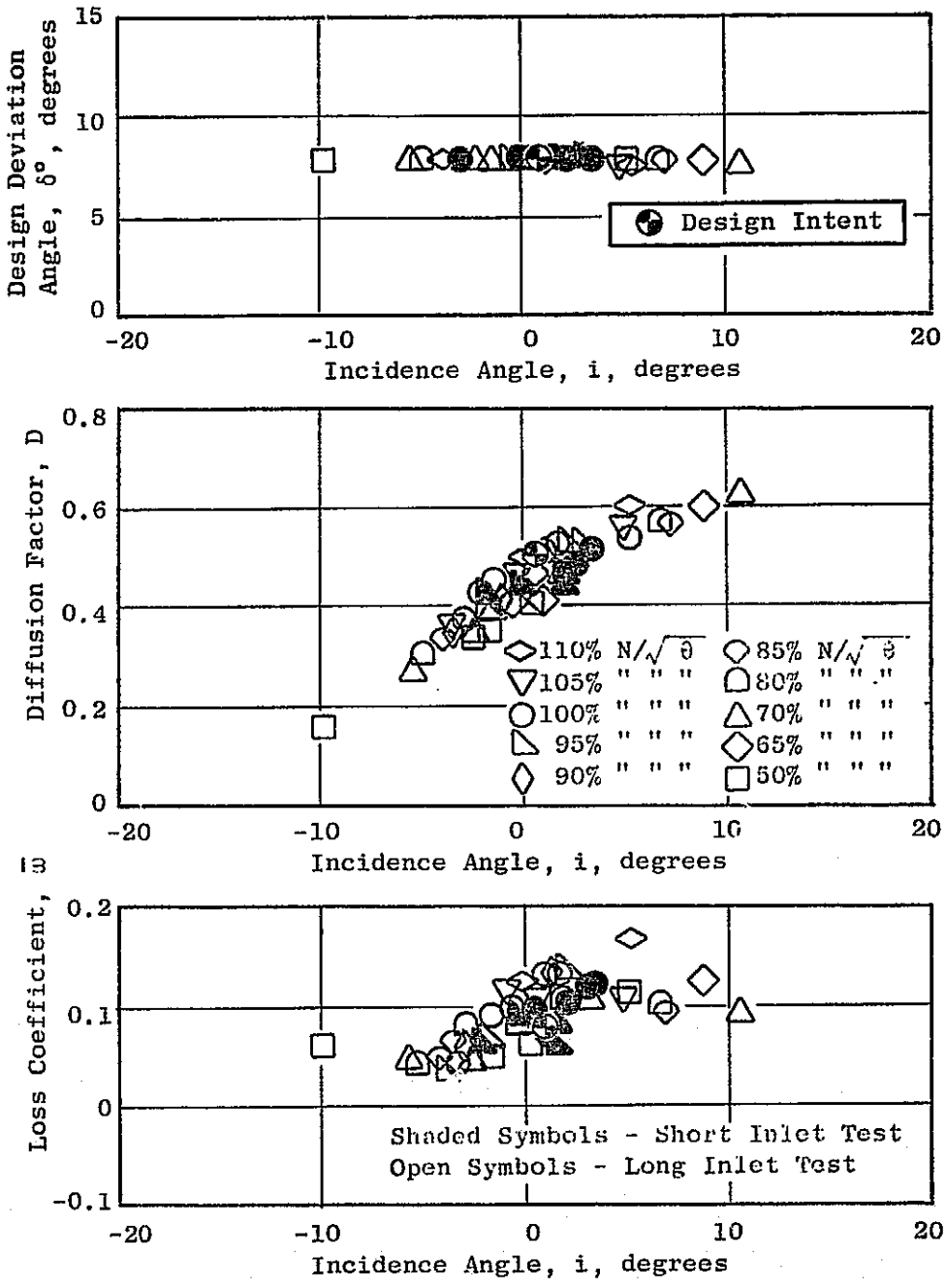

Figure 41. Core Stator Blade-Element Data, 70% Immersion.

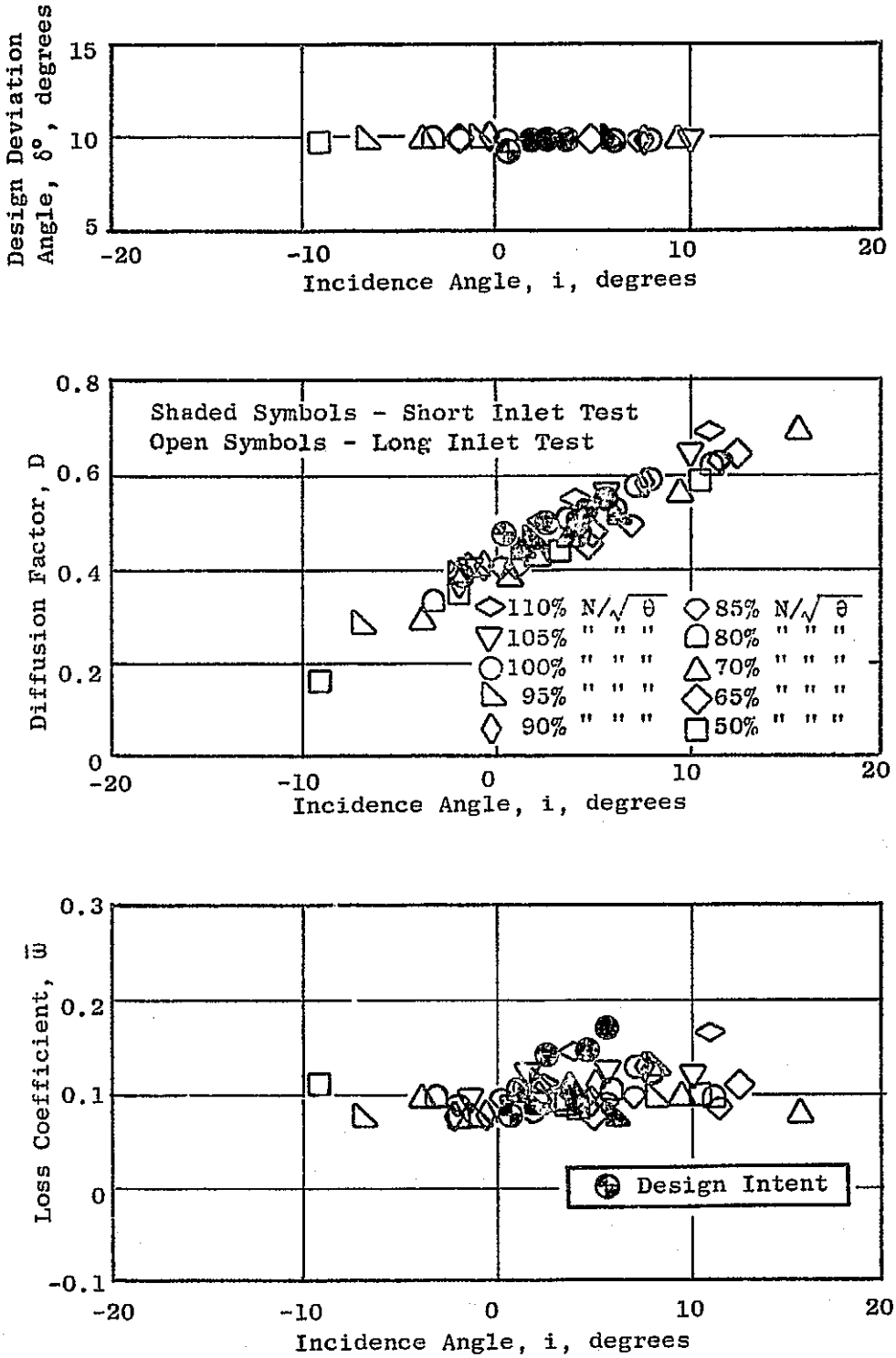

Figure 42. Core Stator Blade-Element Data, 85% Immersion.

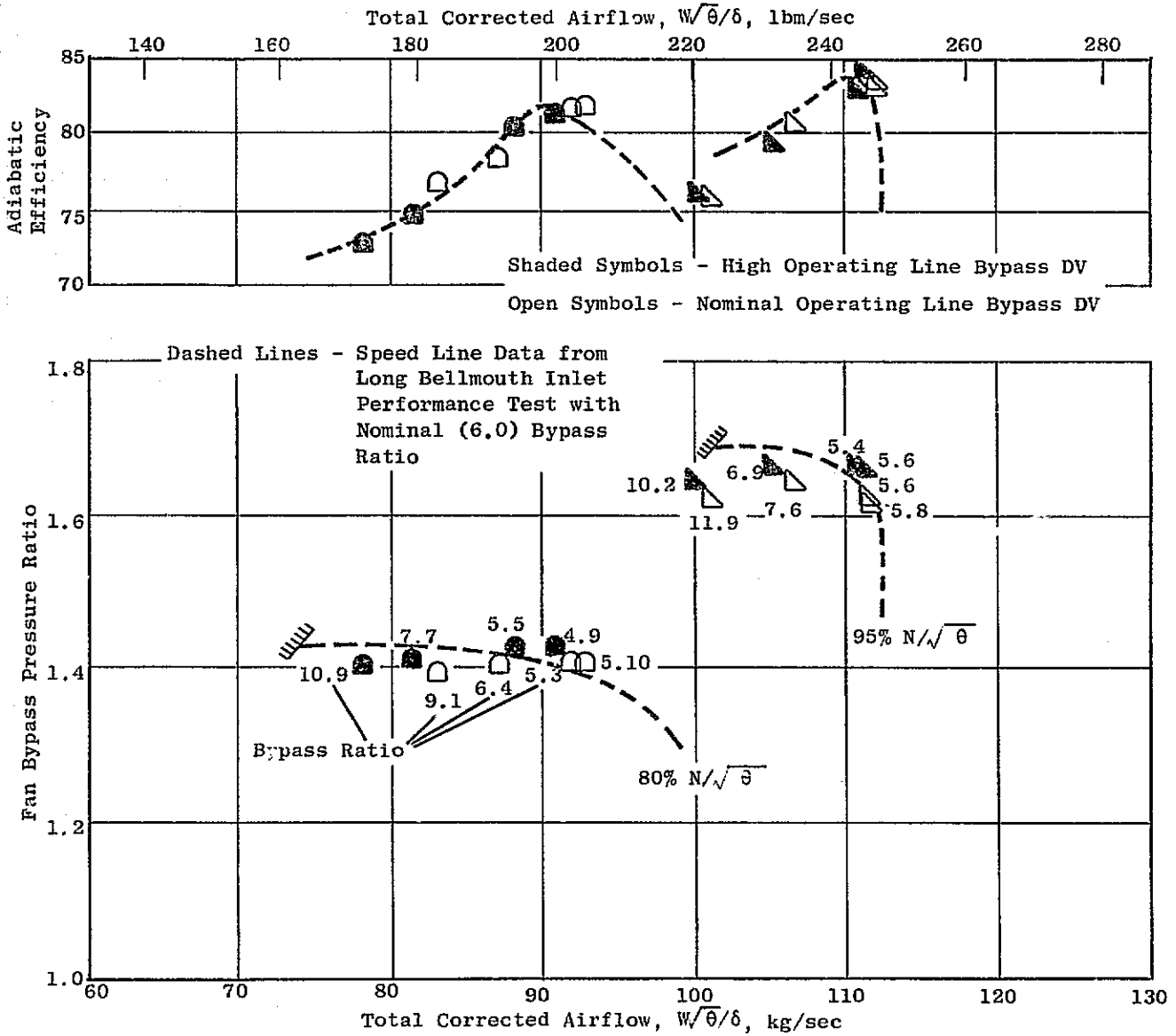

Figure 43. Bypass Migration Stage Performance.

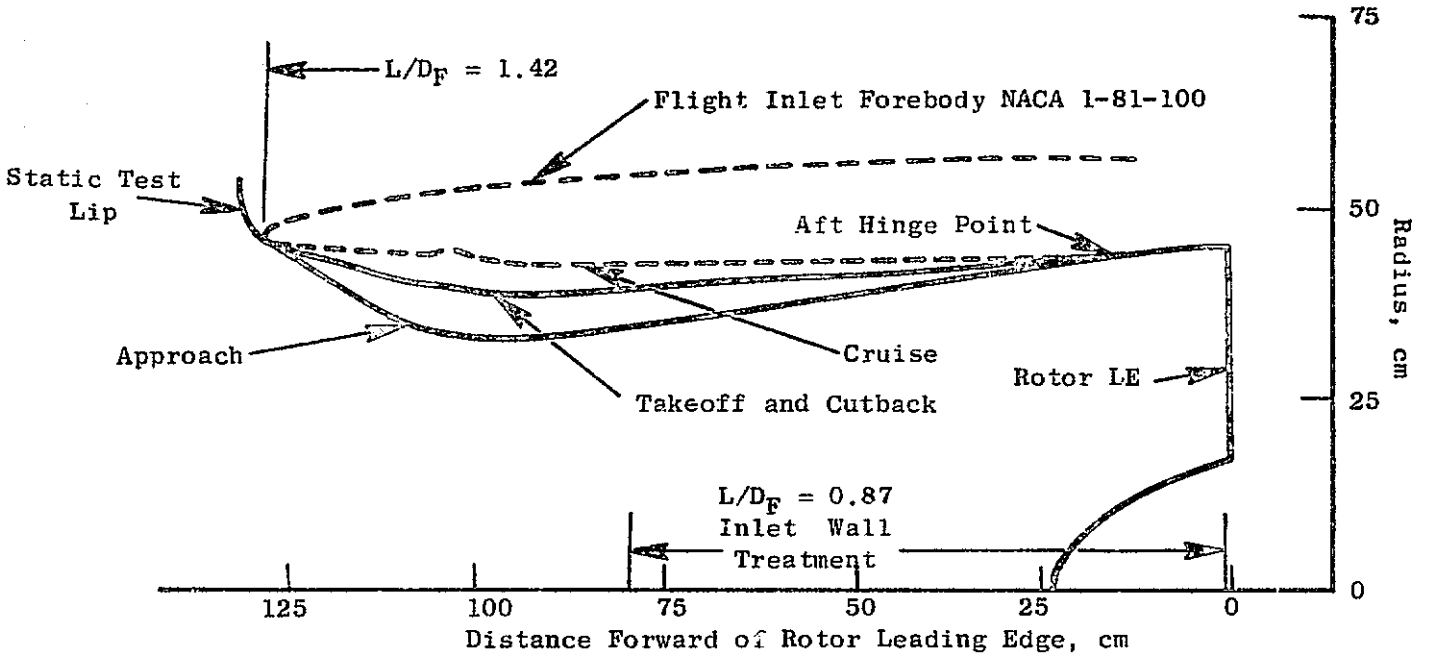

Figure 44. Hybrid Inlet Flowpath.

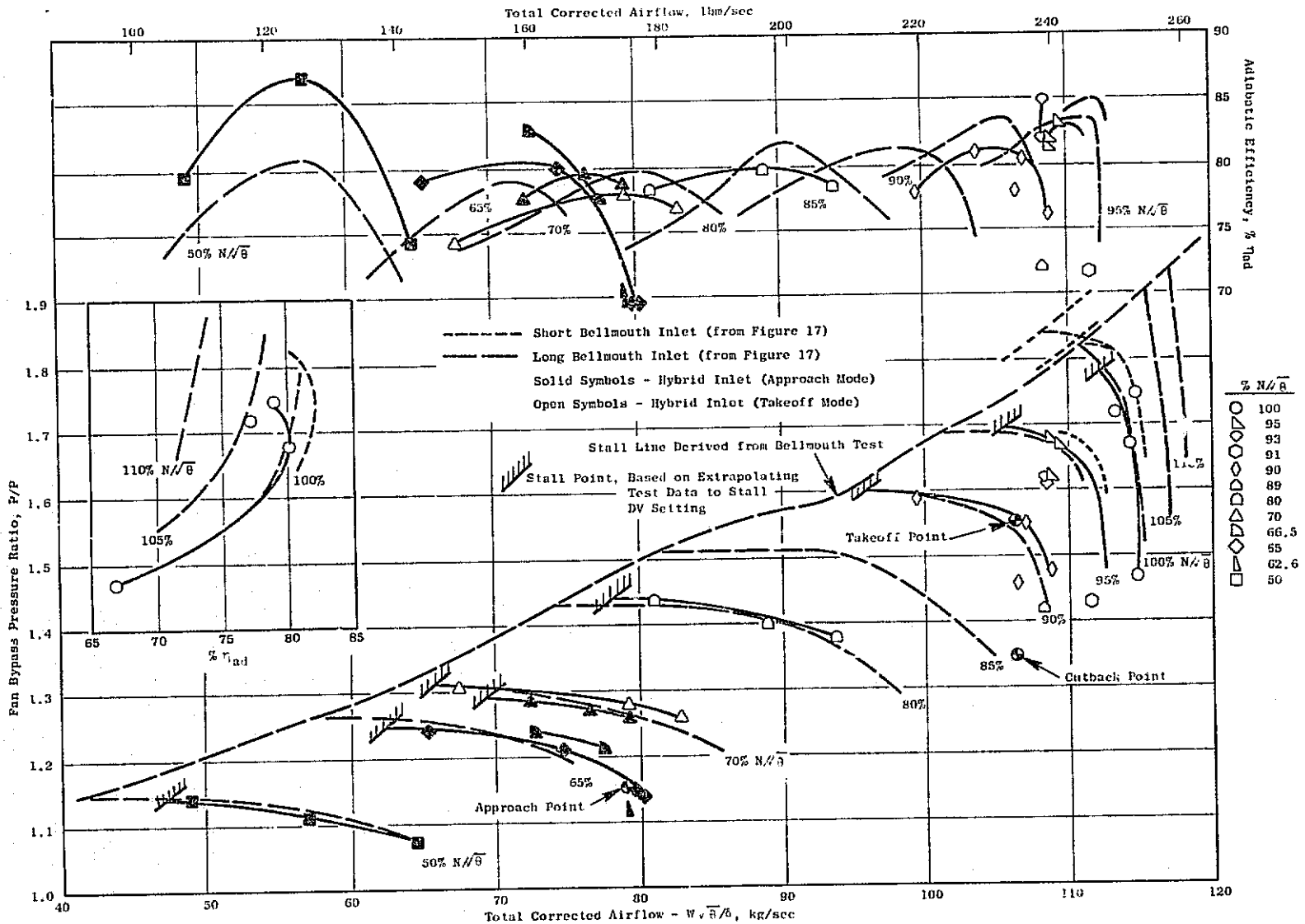

Figure 45. Overall Fan-Stage Performance Map with Hybrid Inlet.

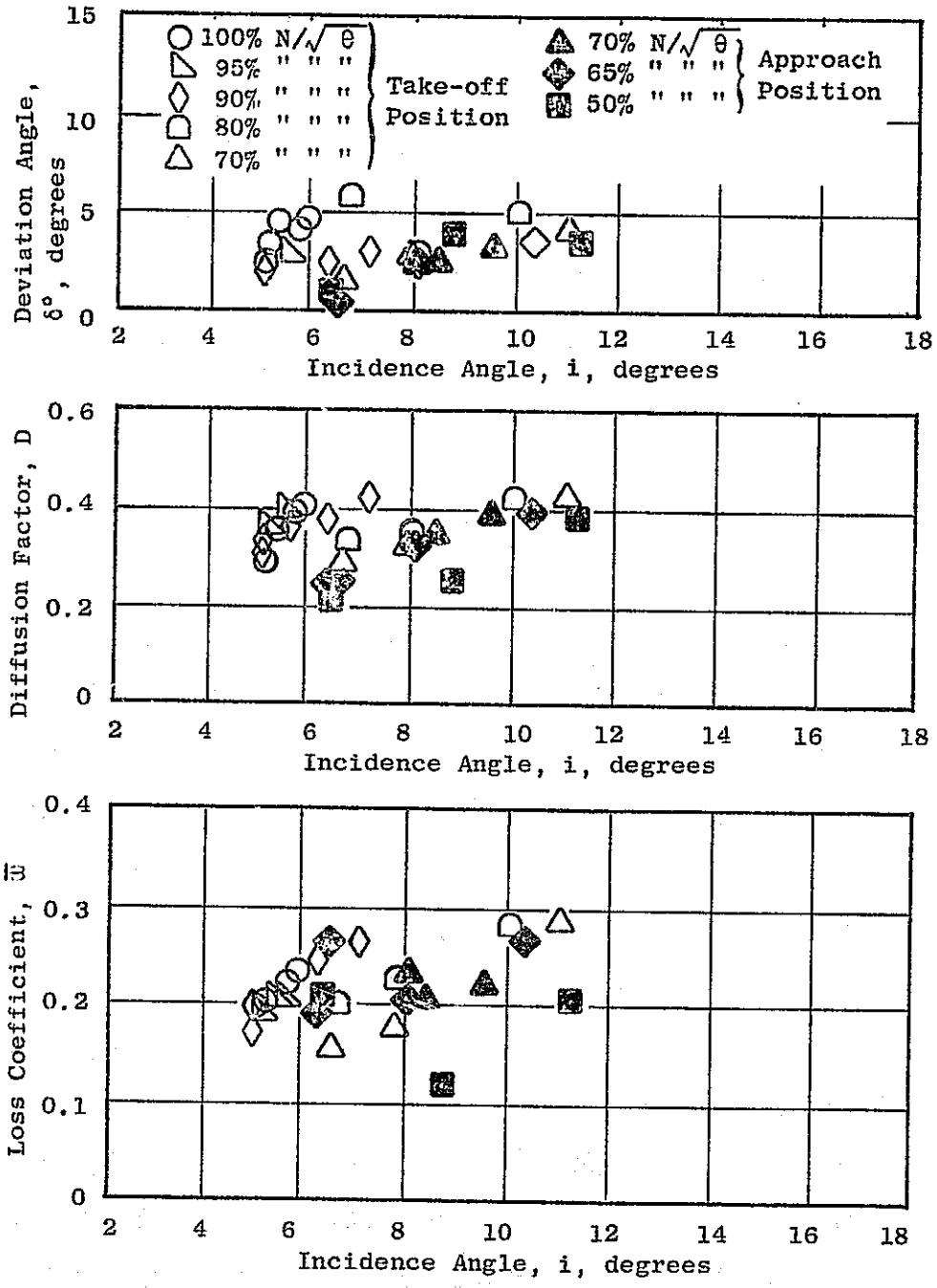

Figure 46. Rotor Blade-Element Data, Hybrid Inlet, 10% Immersion.

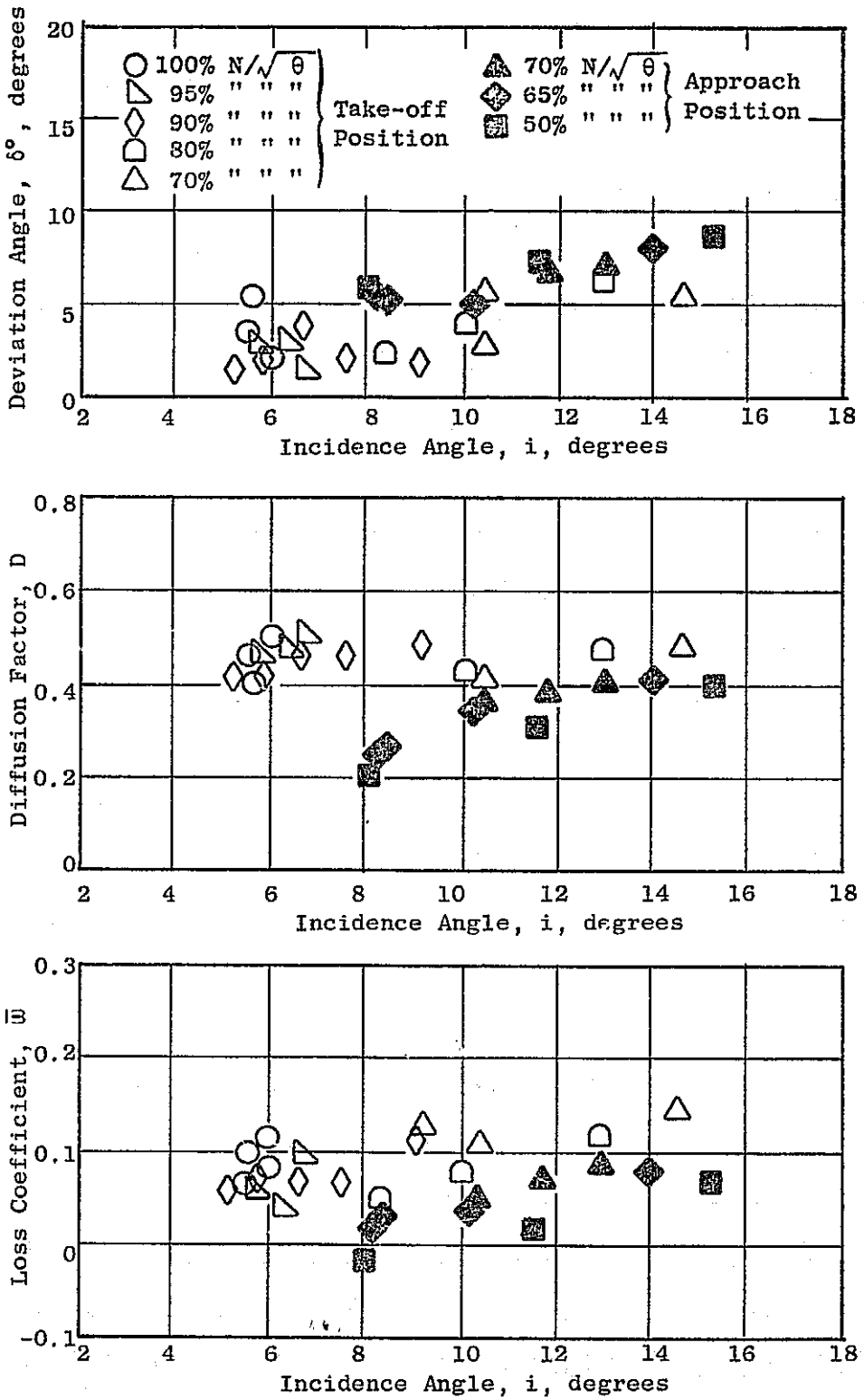

Figure 47. Rotor Blade-Element Data, Hybrid Inlet, 50% Immersion.

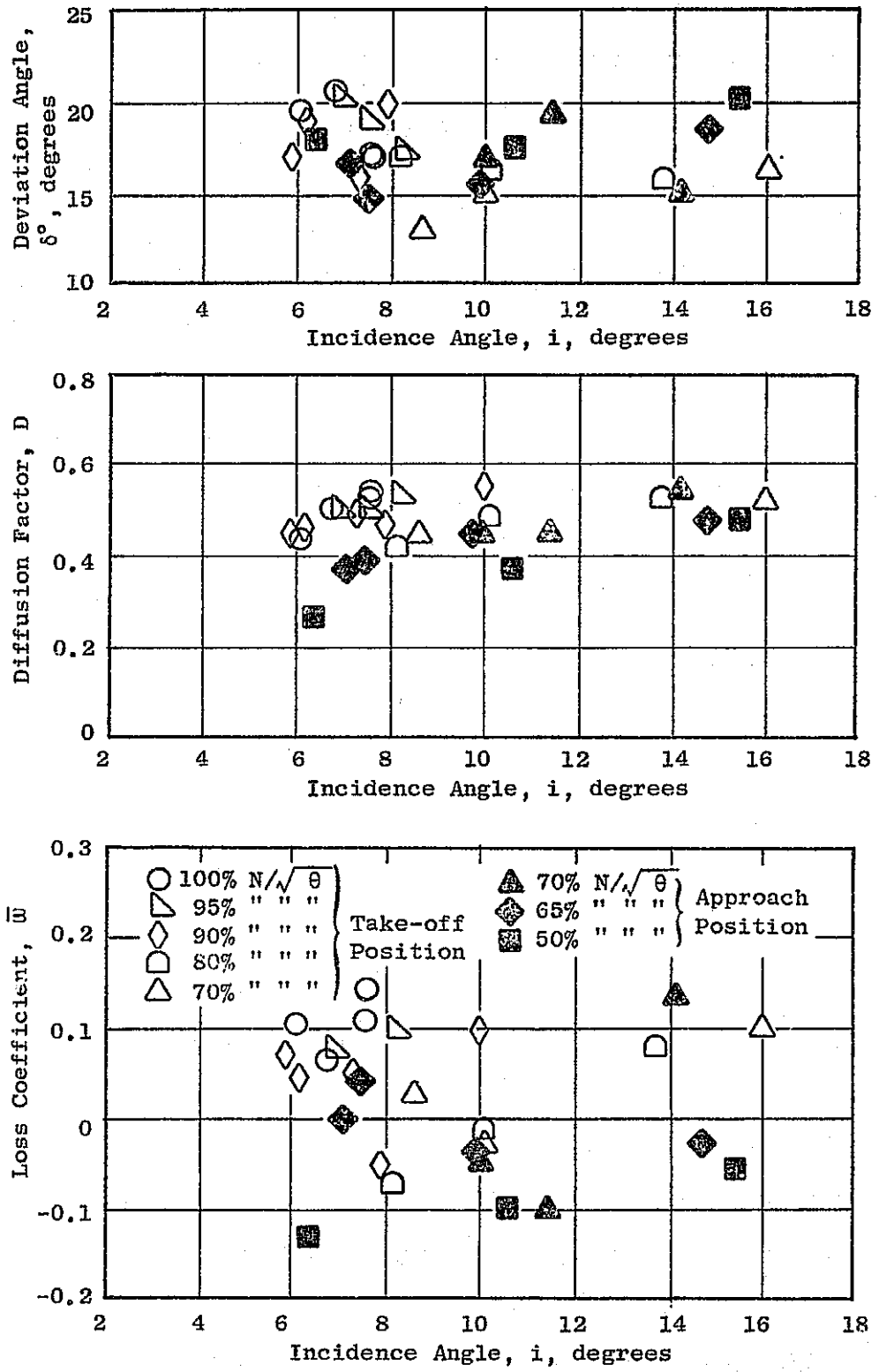

Figure 48. Rotor Blade-Element Data, Hybrid Inlet, 90% Immersion.

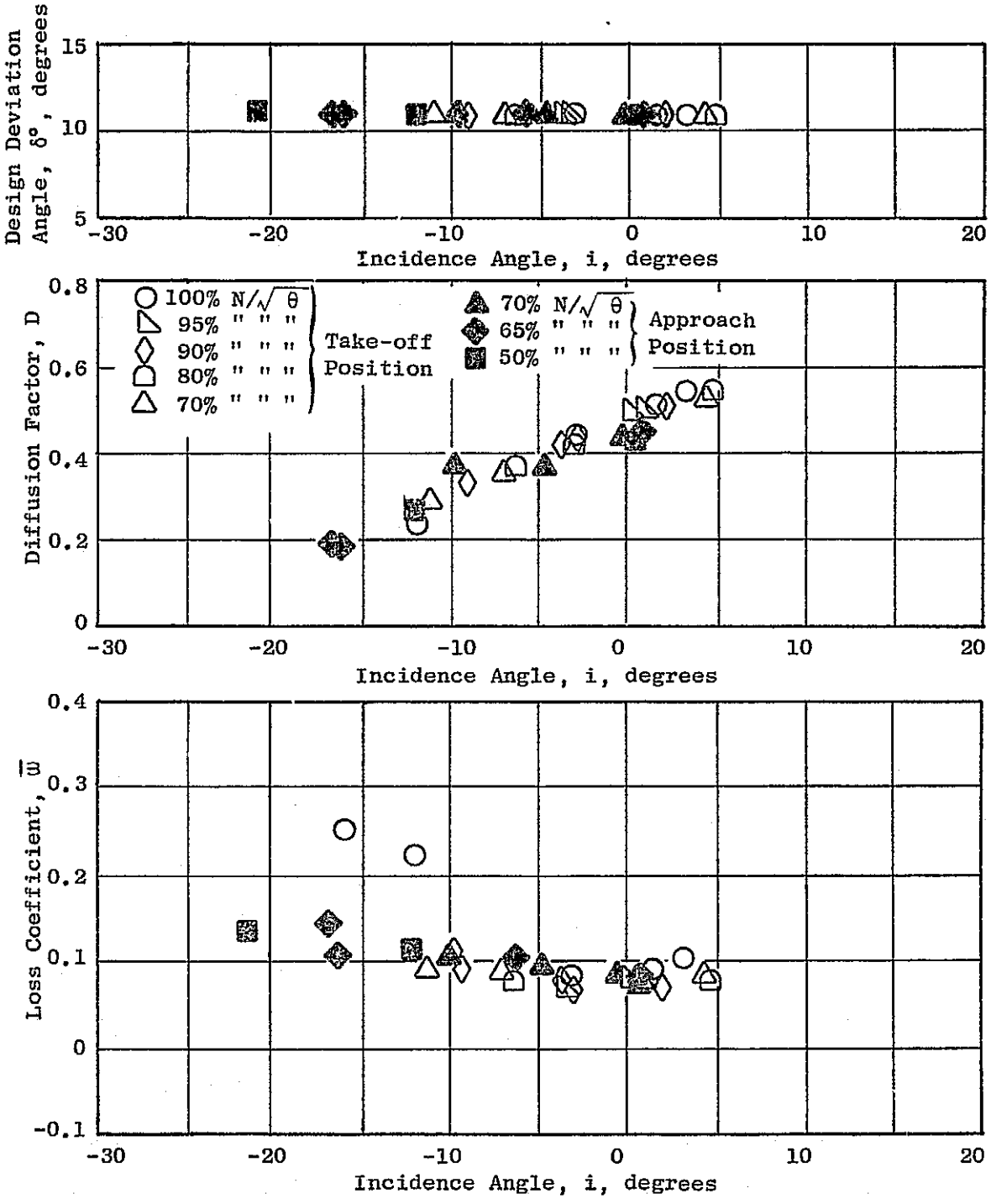

Figure 49. Bypass OGV Blade-Element Data, Hybrid Inlet, 10% Immersion.

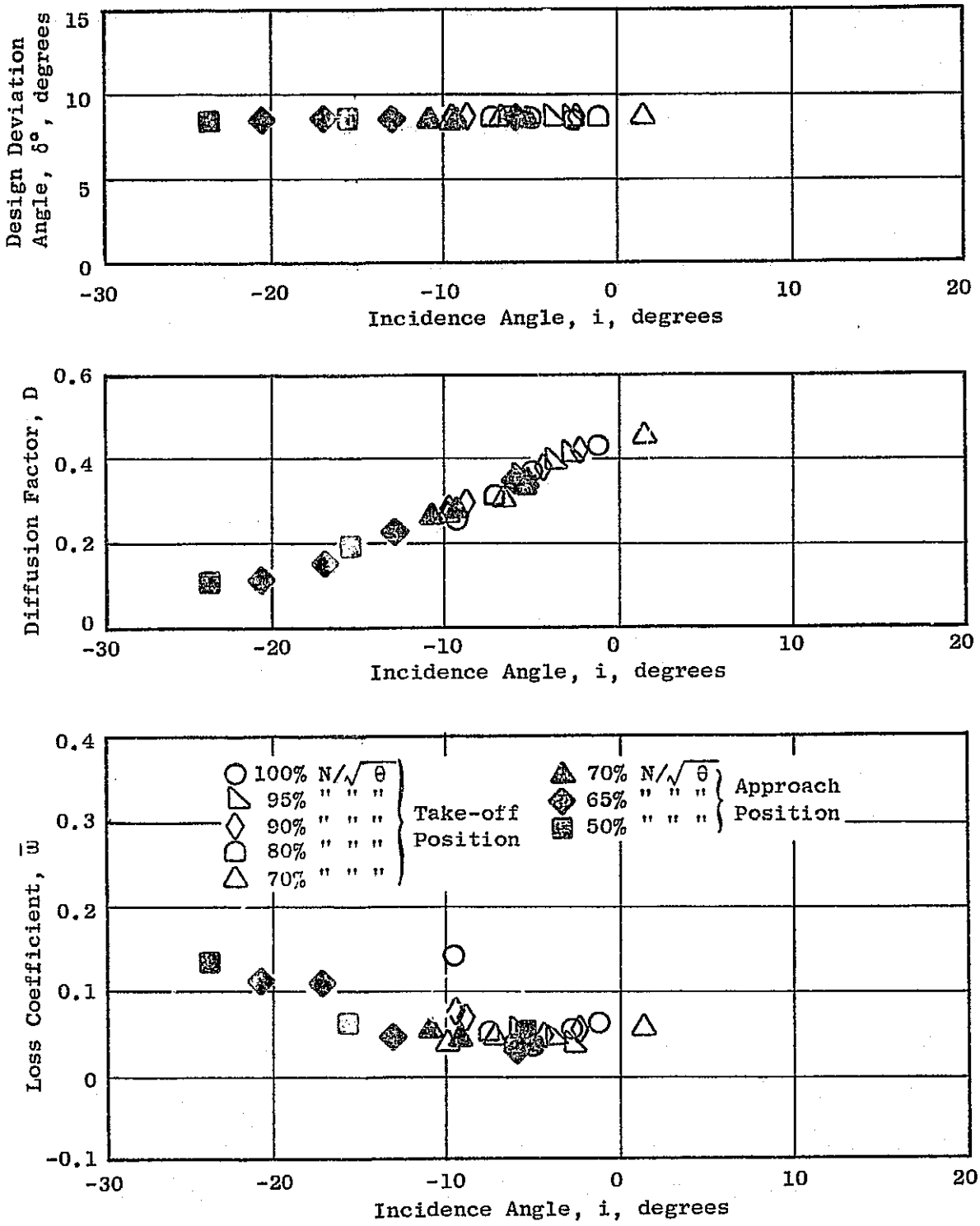

Figure 50. Bypass OGV Blade-Element Data, Hybrid Inlet, 50% Immersion.

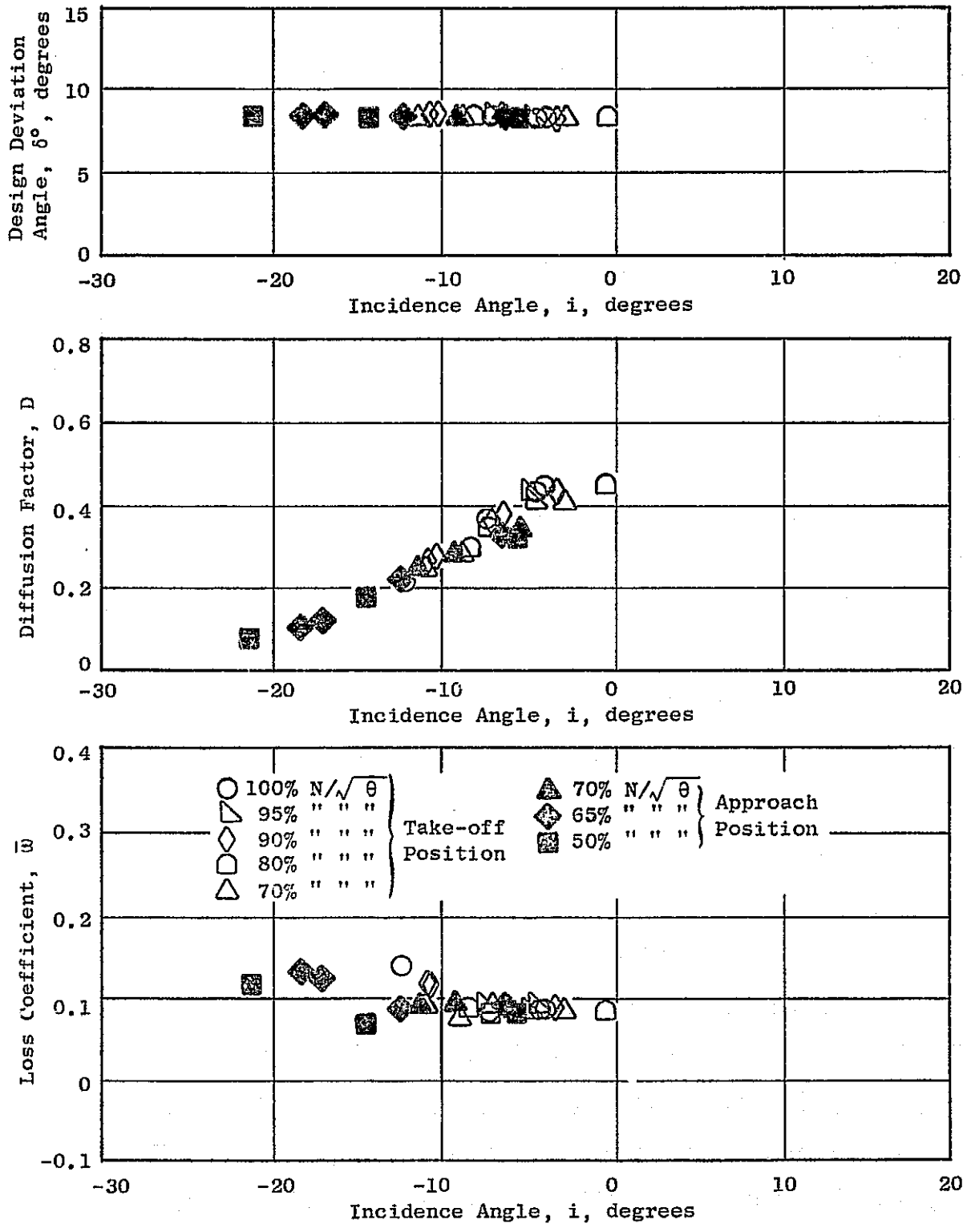

Figure 51. Bypass OGV Blade-Element Data, Hybrid Inlet, 90% Immersion.

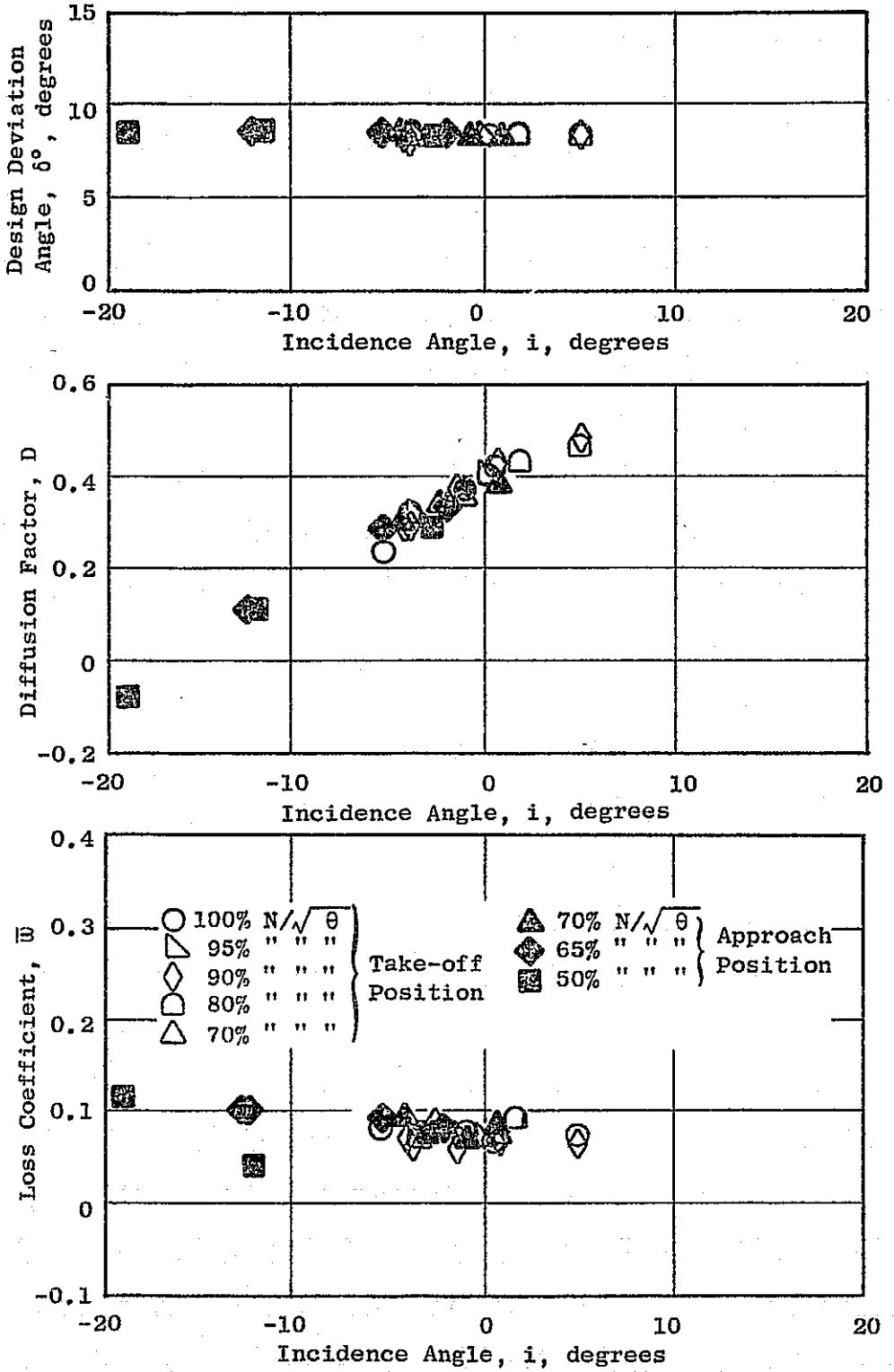

Figure 52. Core Stator Blade-Element Data, Hybrid Inlet, 15% Immersion.

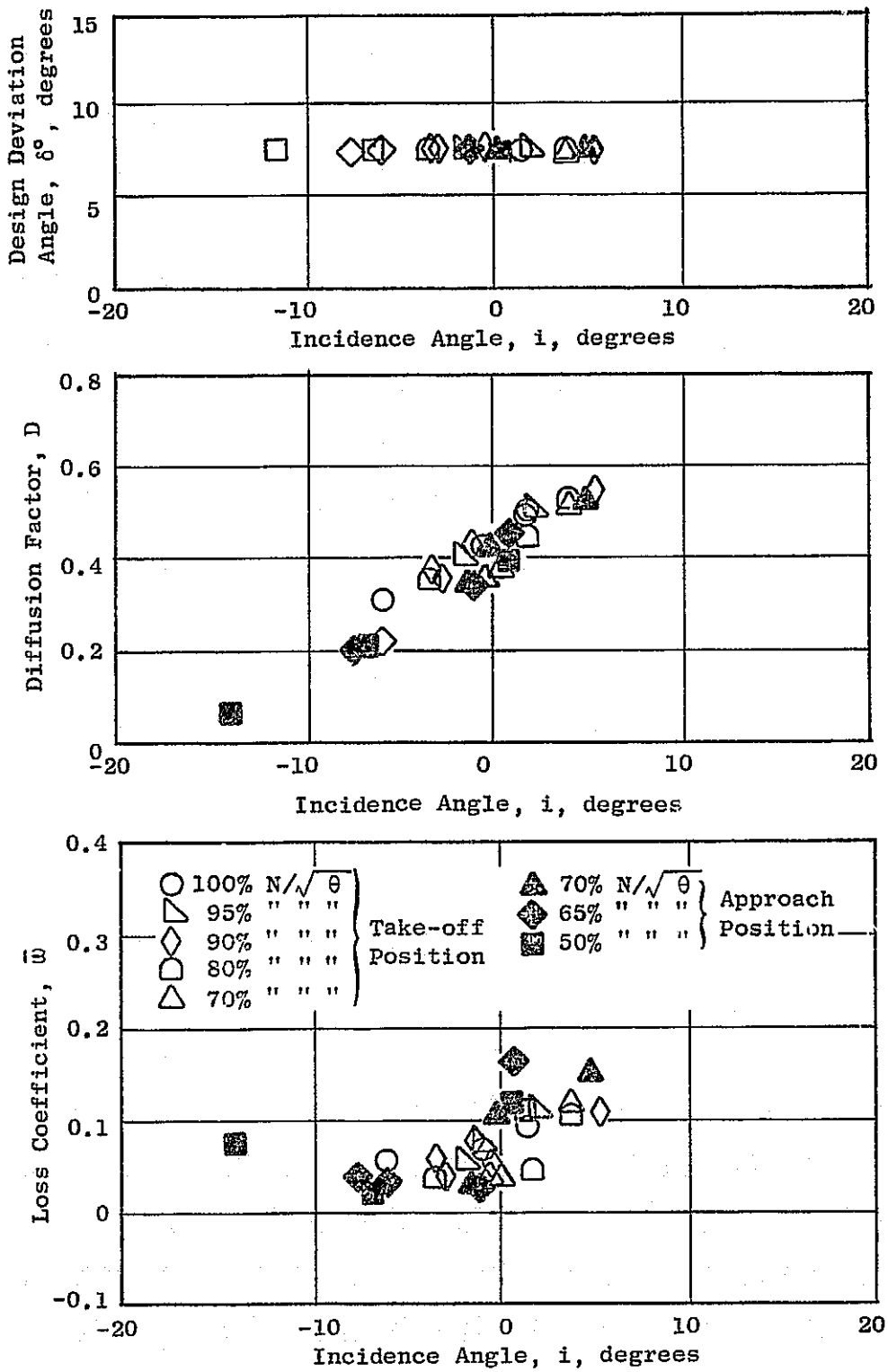

Figure 53. Core Stator Blade-Element Data, Hybrid Inlet, 50% Immersion.

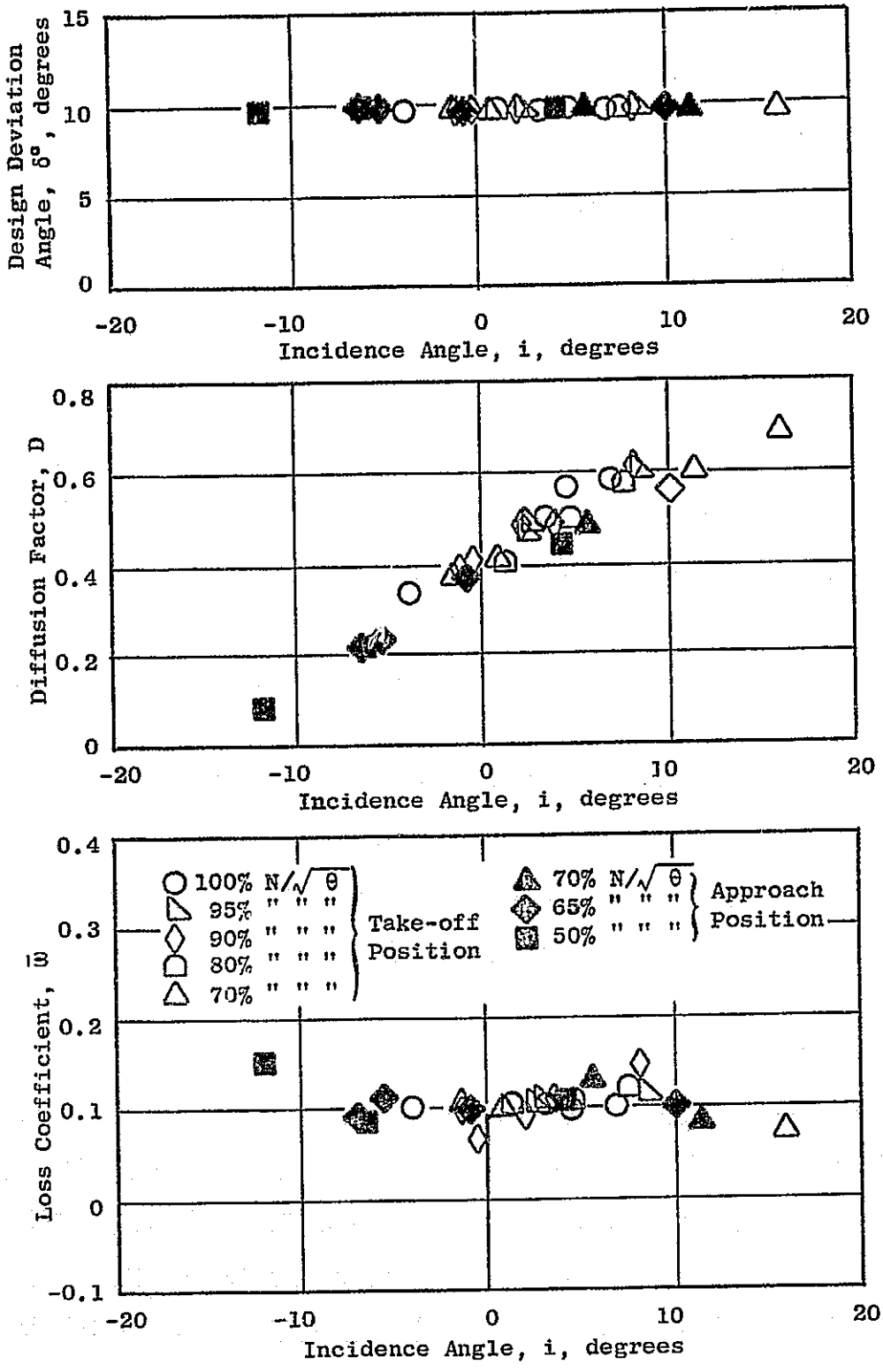

Figure 54. Core Stator Blade-Element Data, Hybrid Inlet, 85% Immersion.

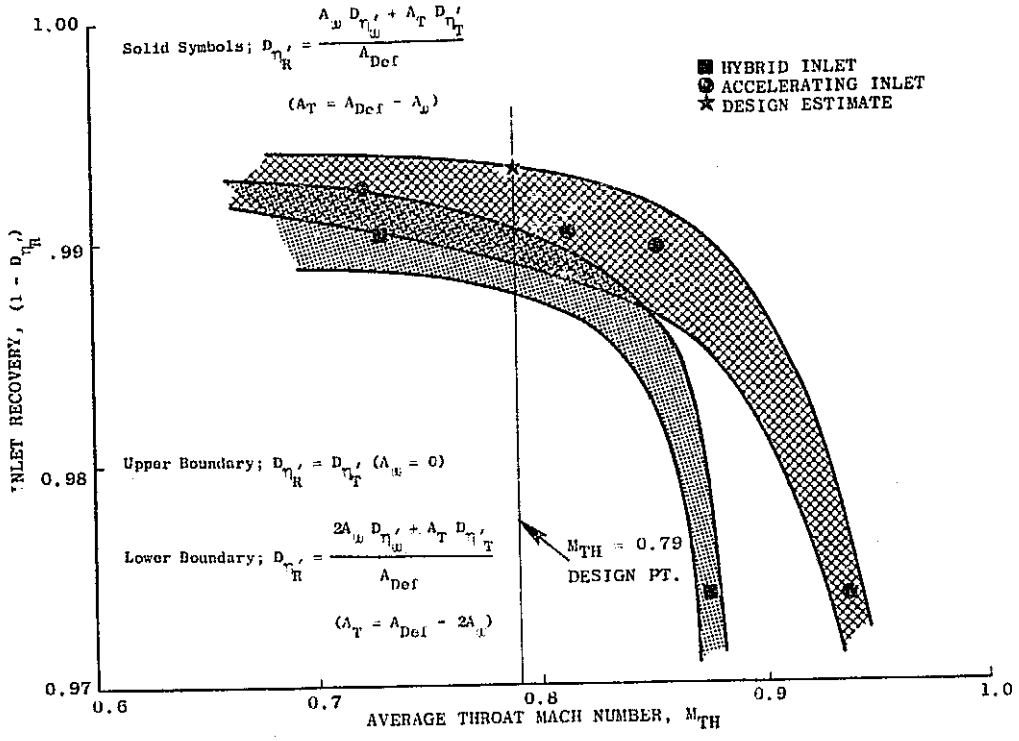

Figure 55. Takeoff Inlet Total Pressure Recovery.

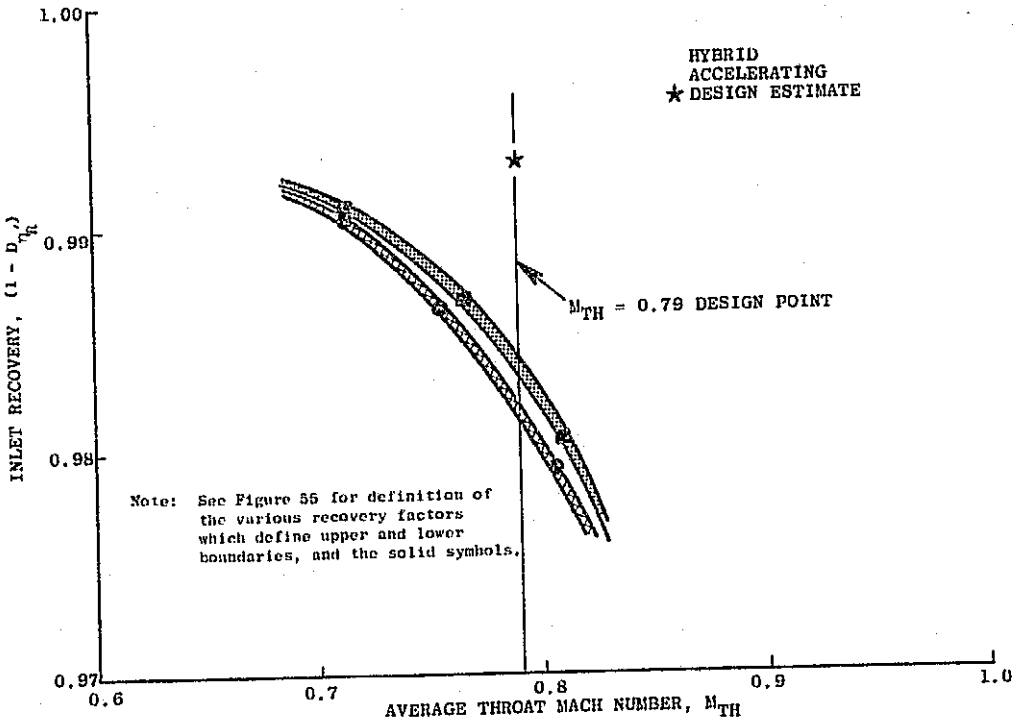

Figure 56. Approach Inlet Total Pressure Recovery.

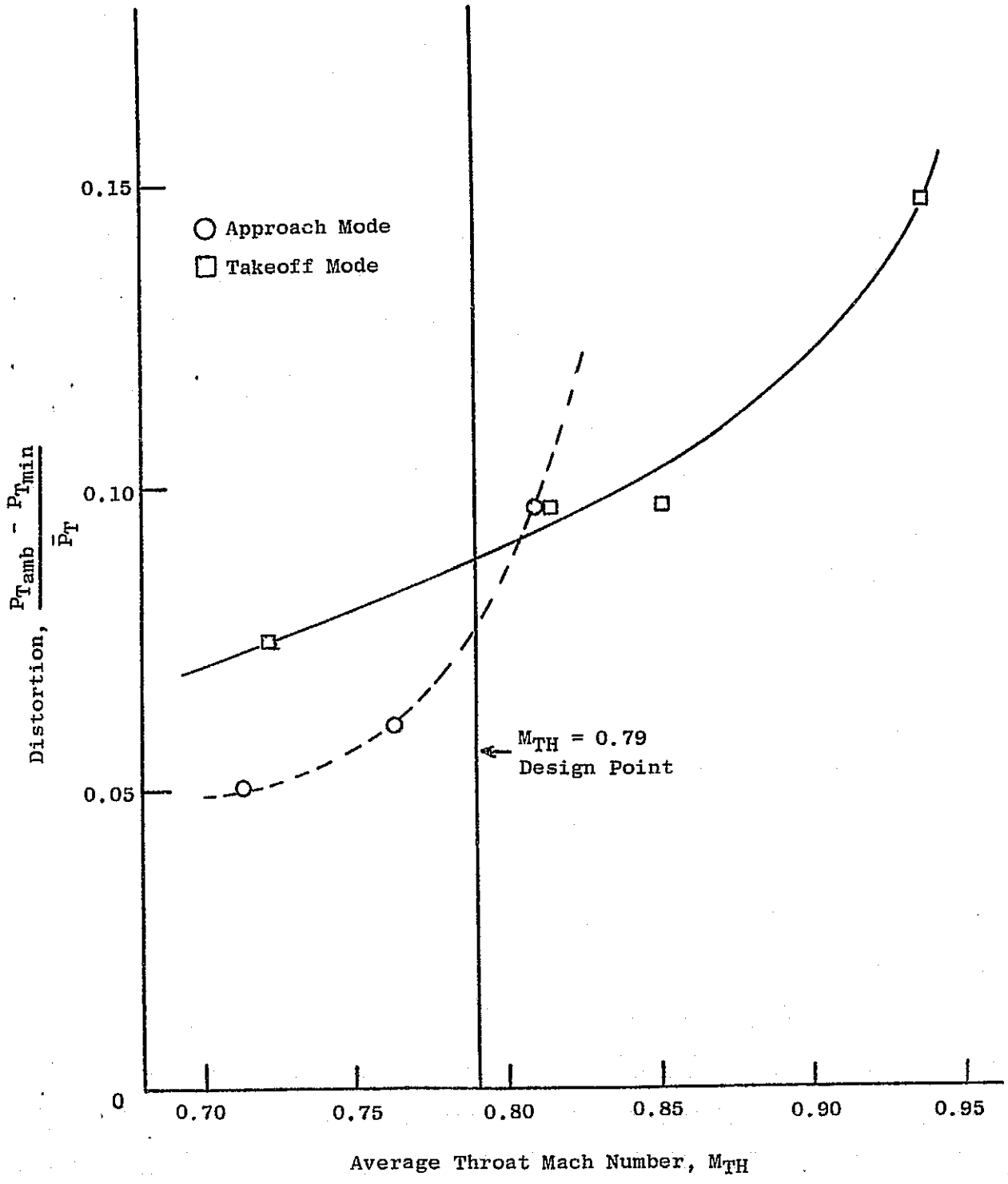

Figure 57. Inlet Distortion.

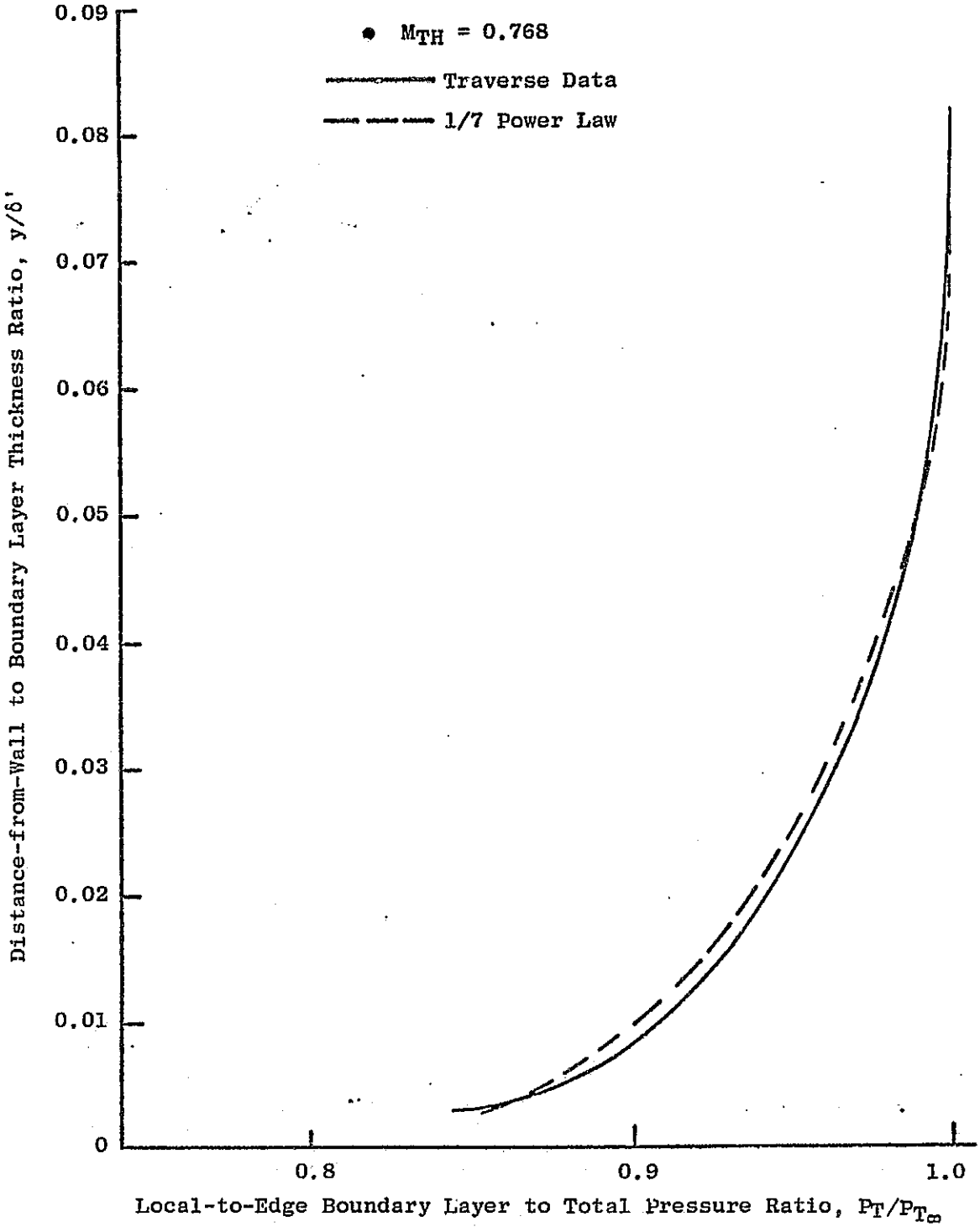

Figure 58. Hybrid Takeoff Inlet Boundary Layer Pressure Profile.

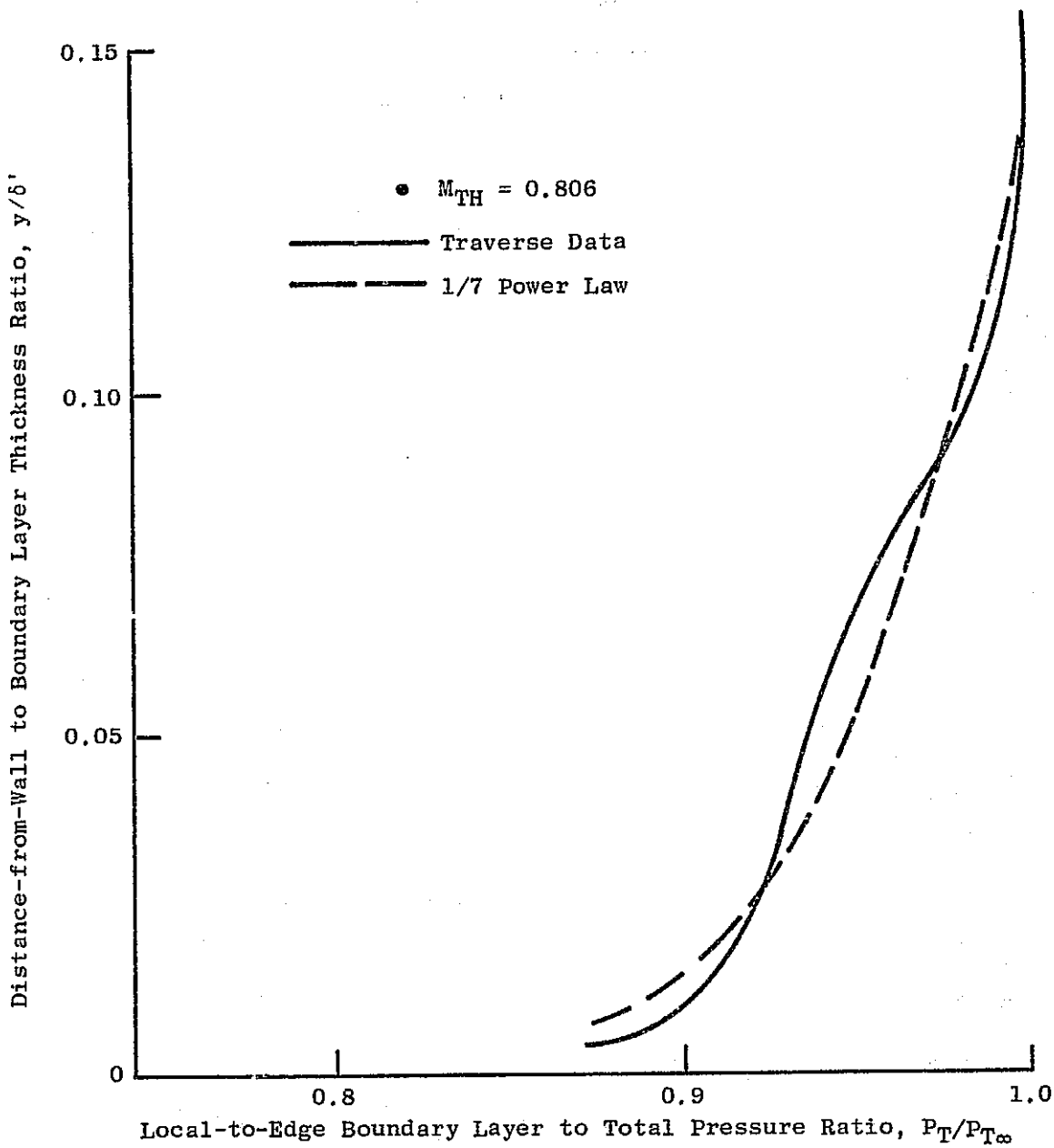

Figure 59. Hybrid Approach Inlet Boundary Layer Pressure Profile.

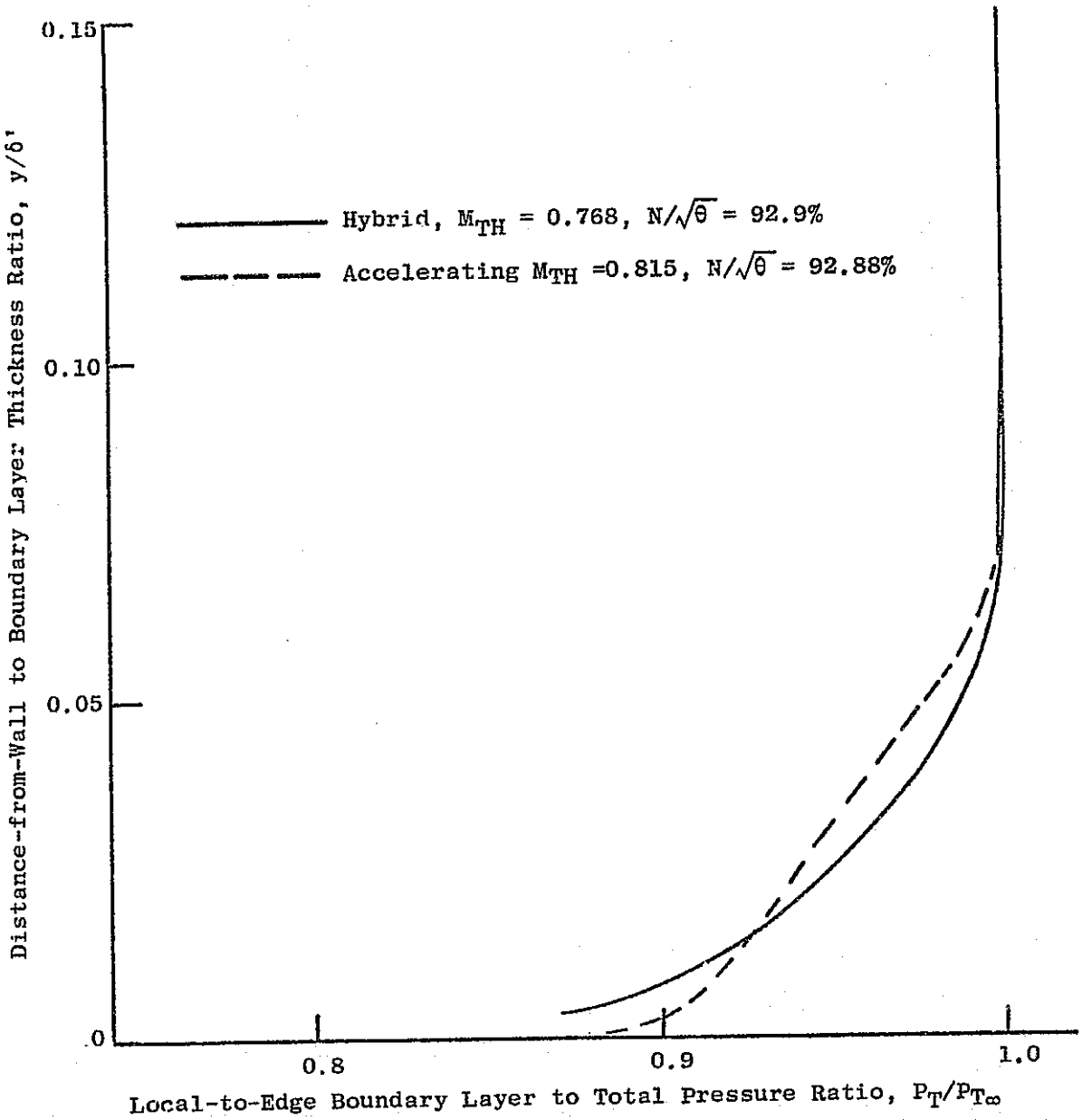

Figure 60. Takeoff Inlet Boundary Layer Pressure Profiles.

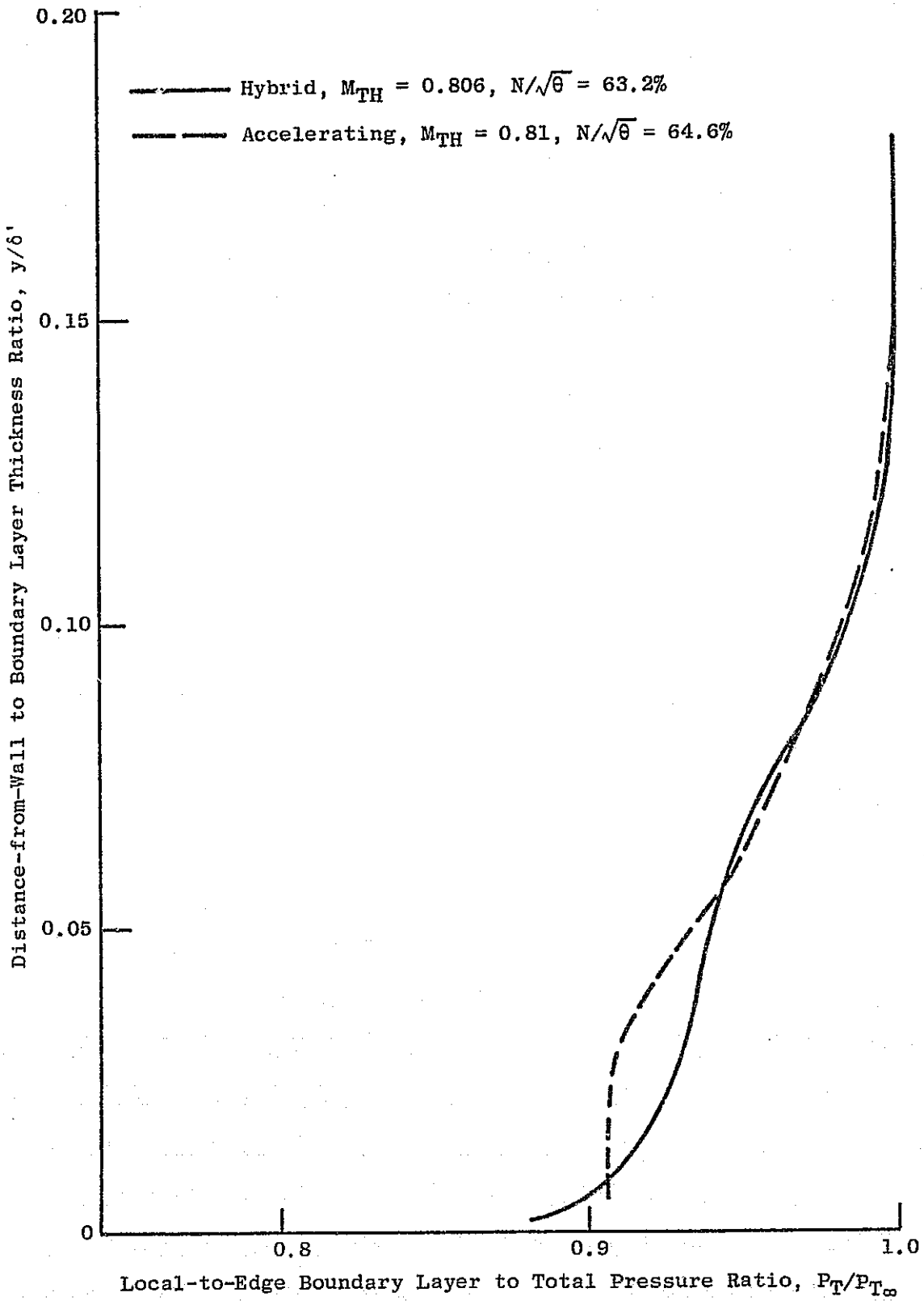

Figure 61. Approach Inlet Boundary Layer Pressure Profiles.

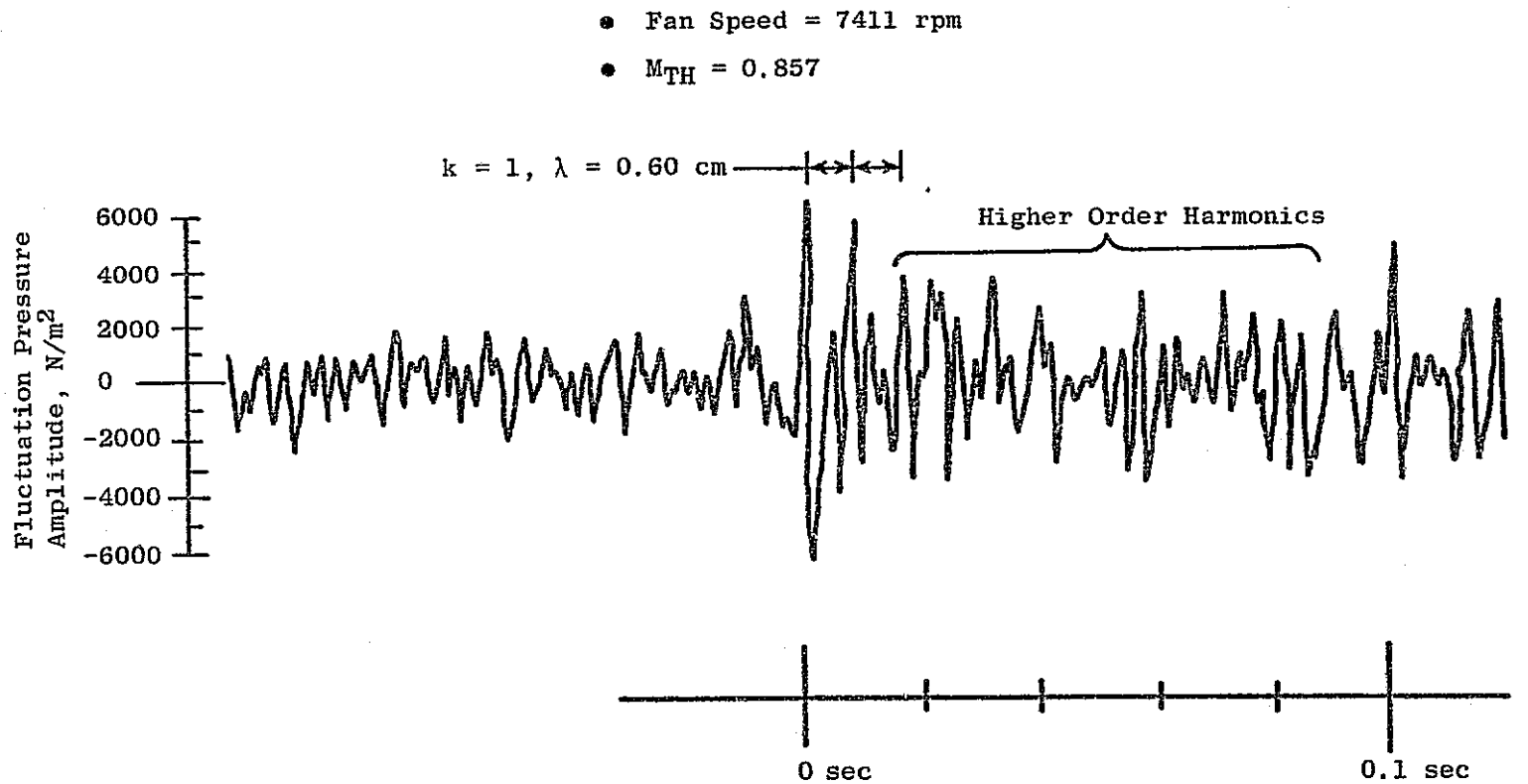

Figure 62. Approach Inlet Wall Kulite, Reading No. 609.

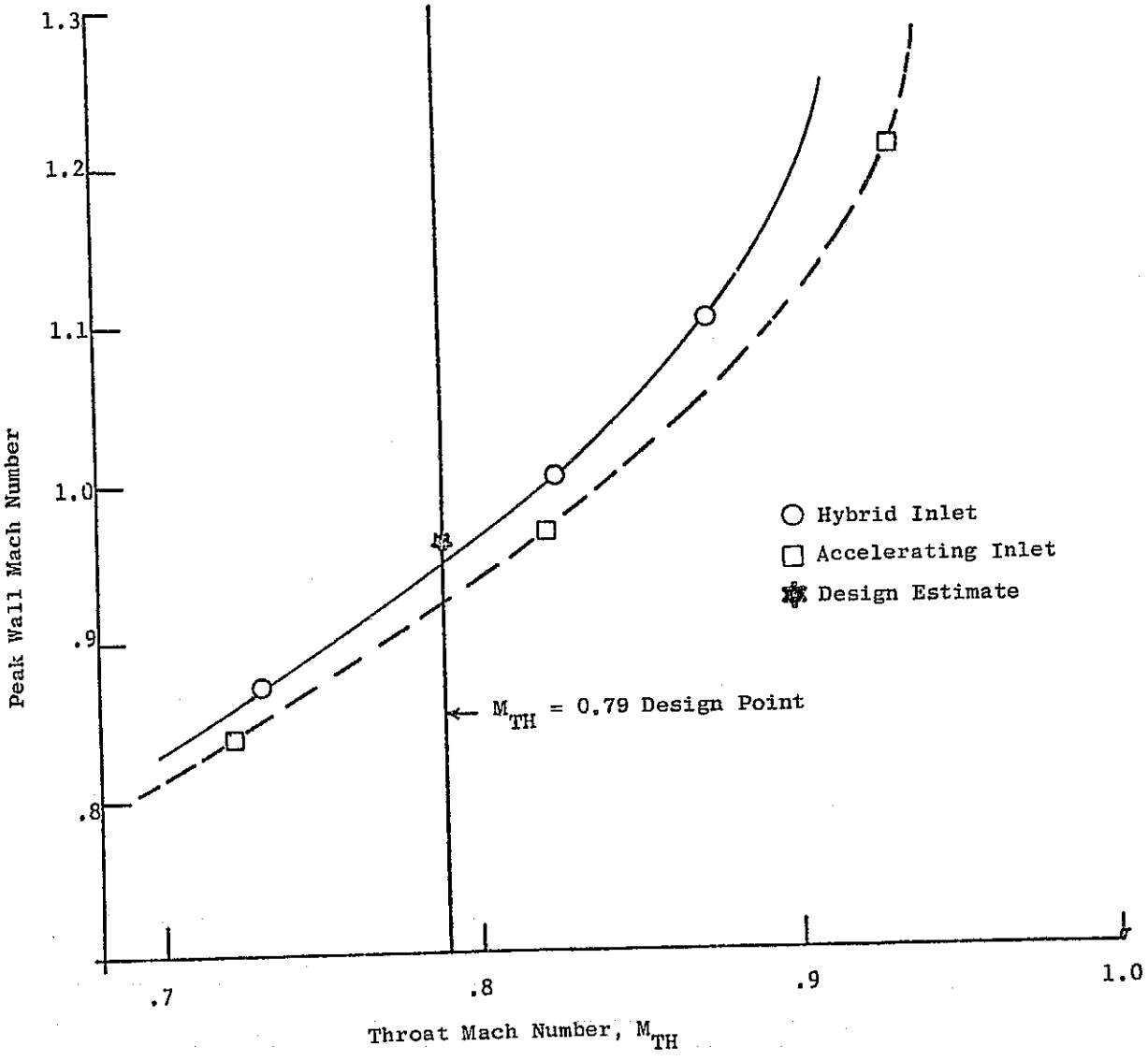

Figure 63. Takeoff Inlet Peak Wall Versus Throat Mach Number.

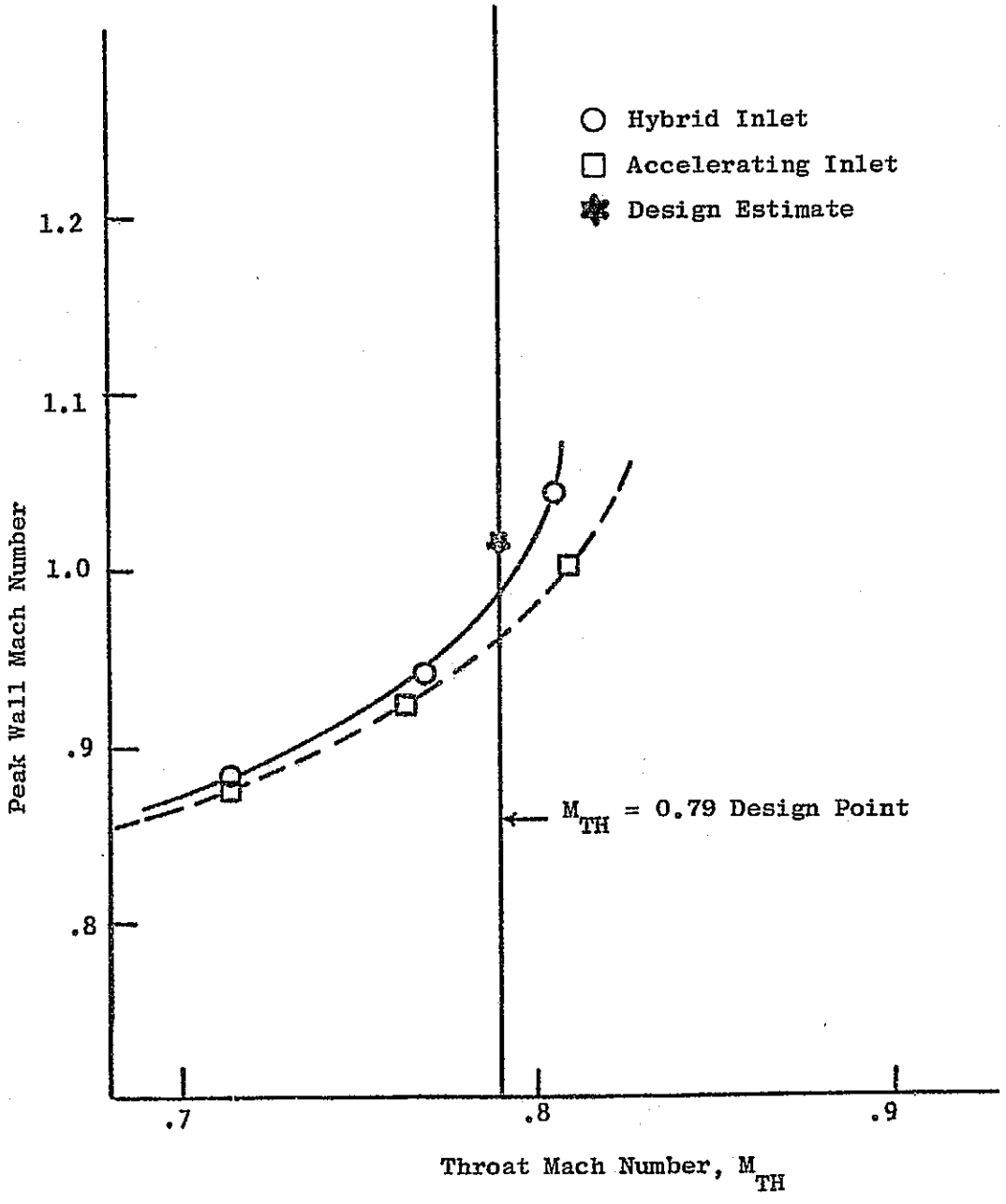

Figure 64. Approach Inlet Peak Wall Versus Throat Mach Number.

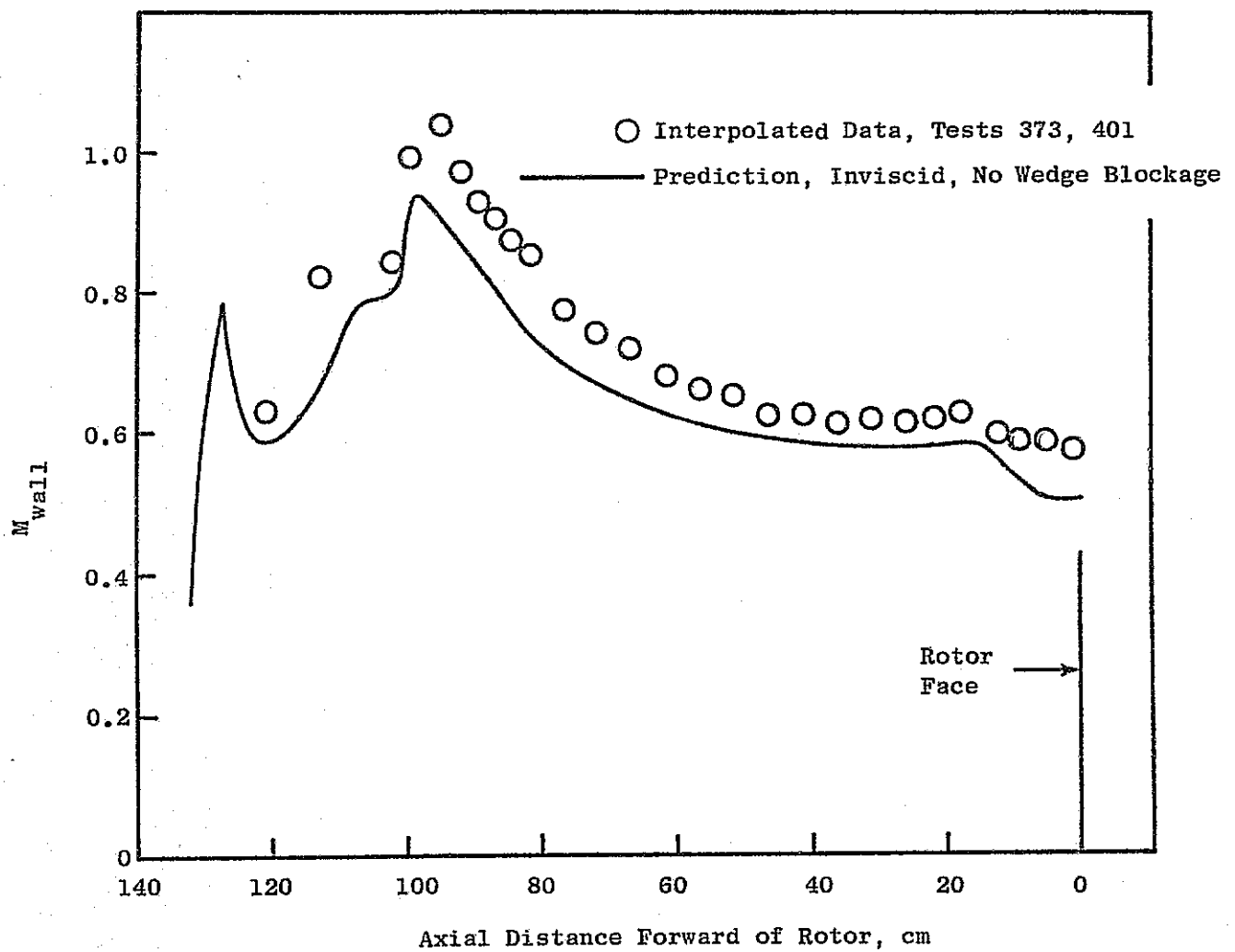

Figure 65. Hybrid Takeoff Inlet Axial Mach Number Distribution, $M_{TH} = 0.79$.

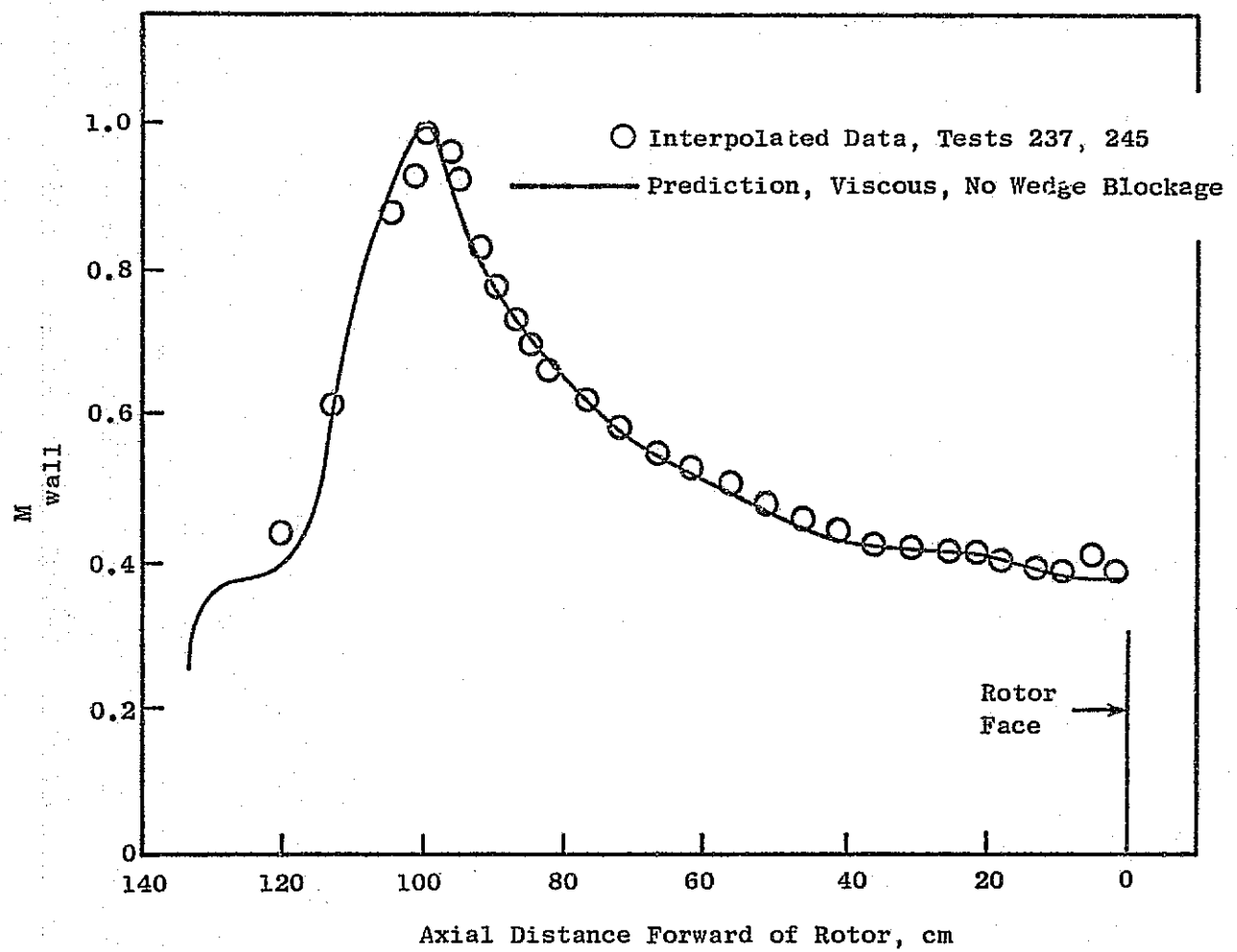

Figure 66. Hybrid Approach Inlet Axial Mach Number Distribution, $M_{TH} = 0.79$.

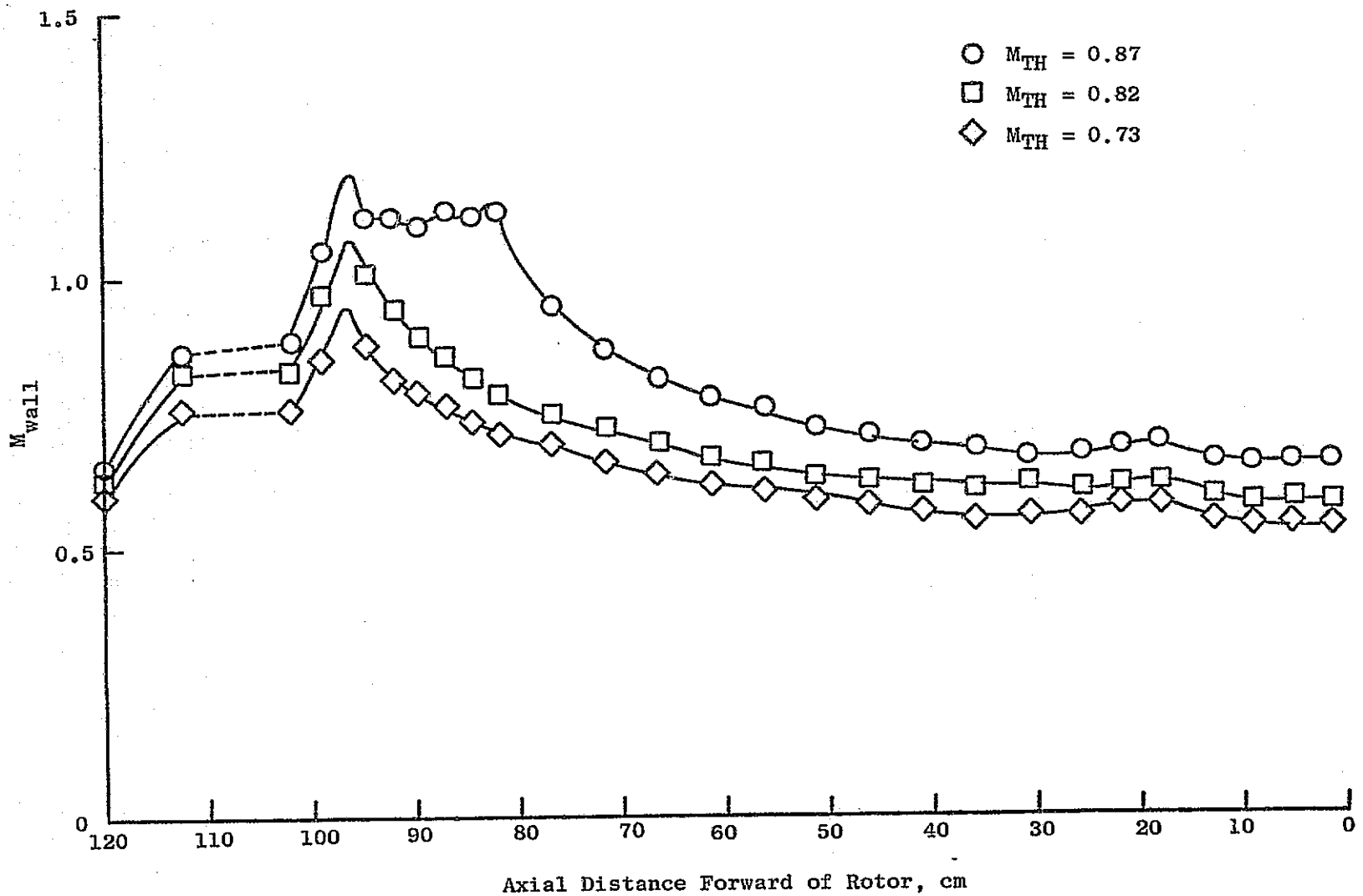

Figure 67. Hybrid Takeoff Inlet Axial Mach Number Distribution.

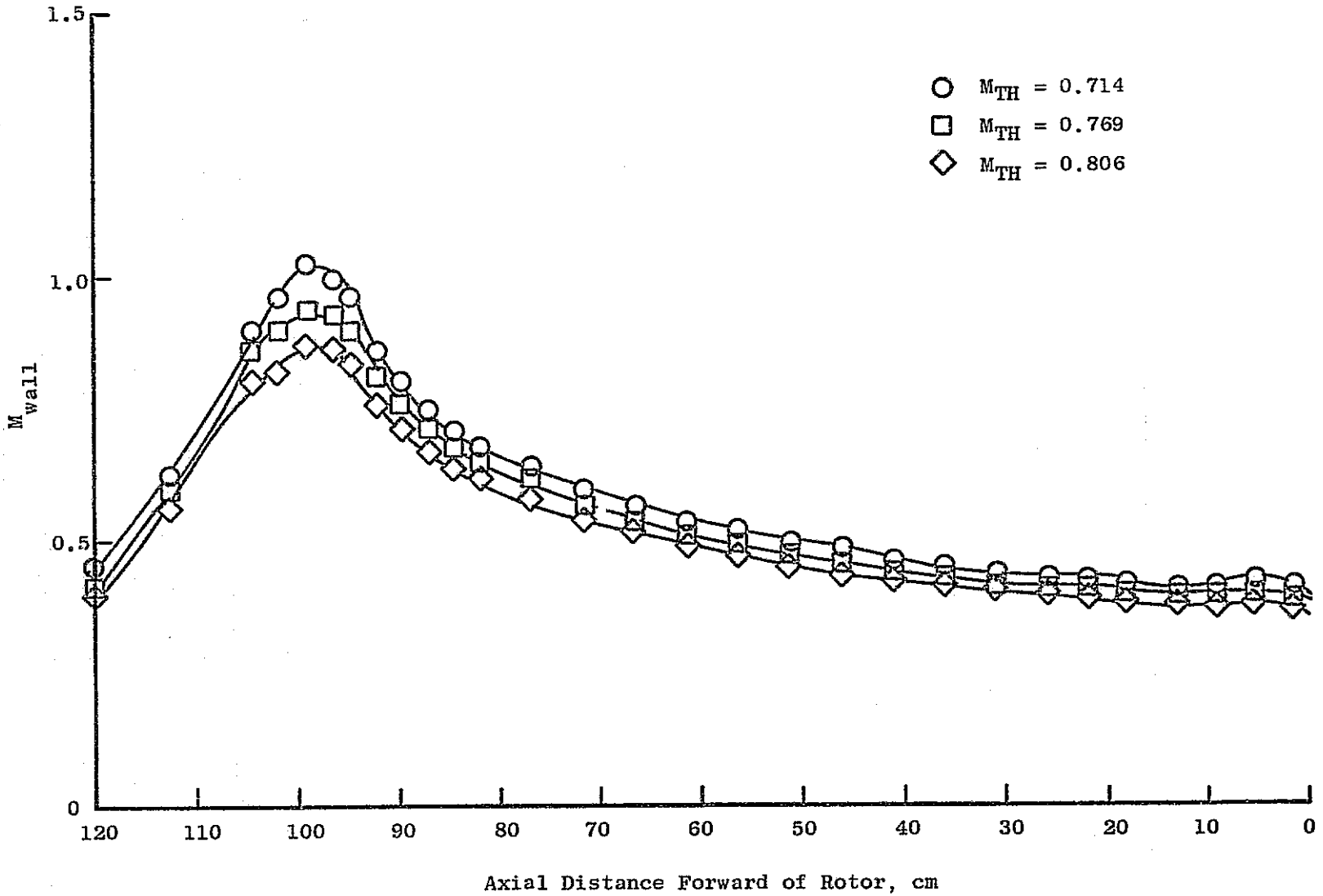

Figure 68. Hybrid Approach Inlet Axial Mach Number Distribution.

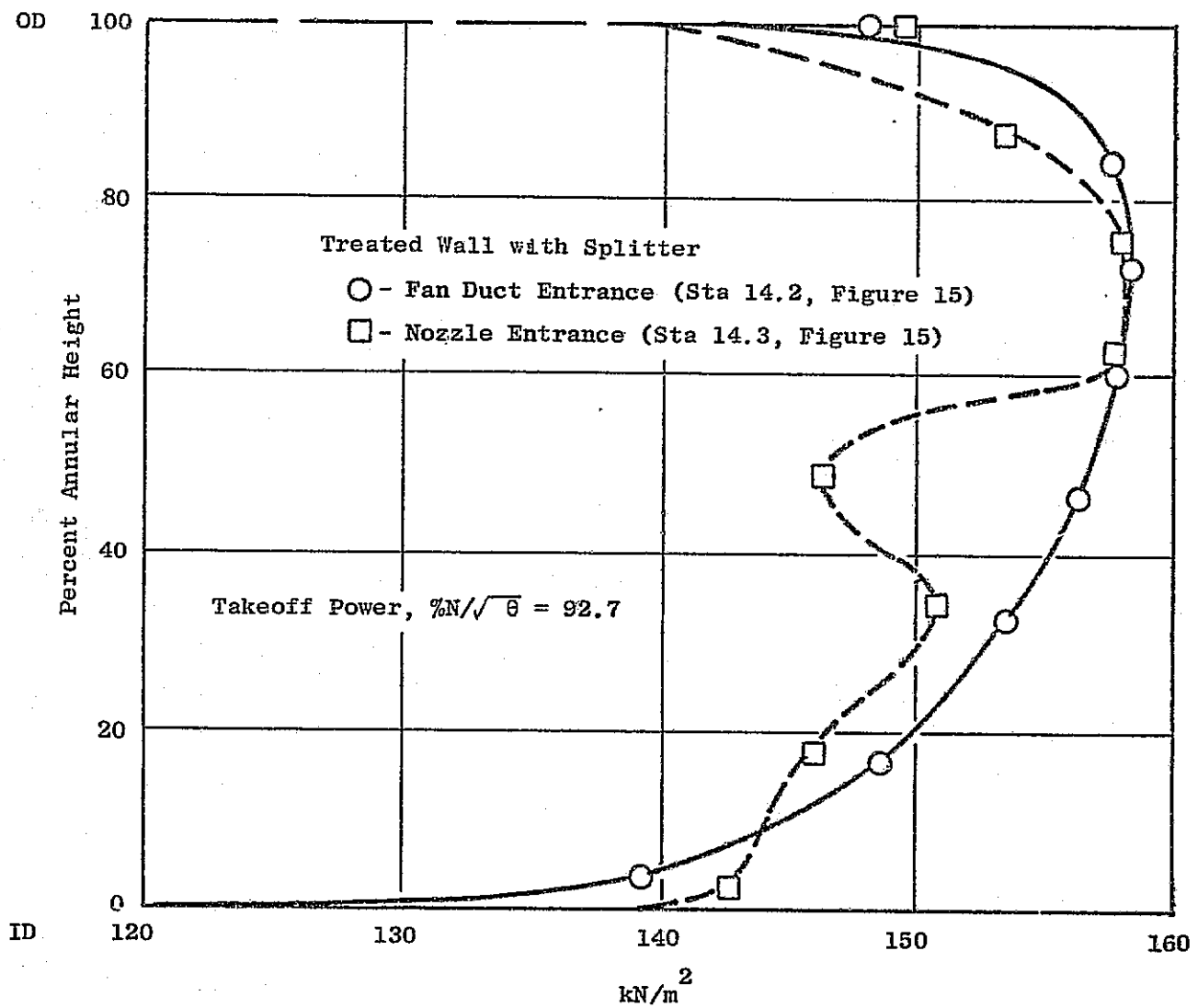

Figure 69. Fan Exit Duct Total Pressure Profiles.

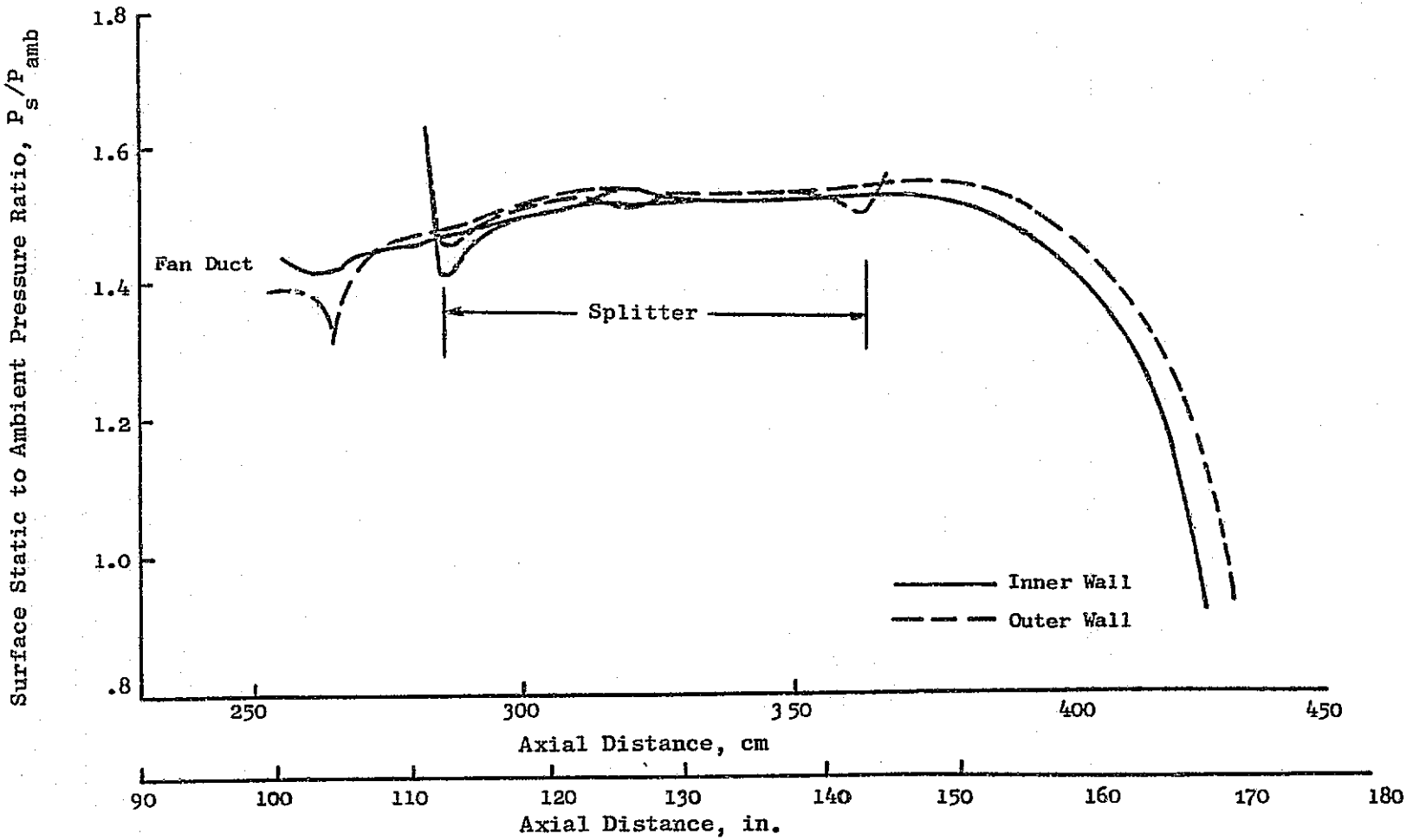

Figure 70. Fan Exit Duct (with Splitter) Predicted Static Pressure Distributions at Takeoff Point Operation.

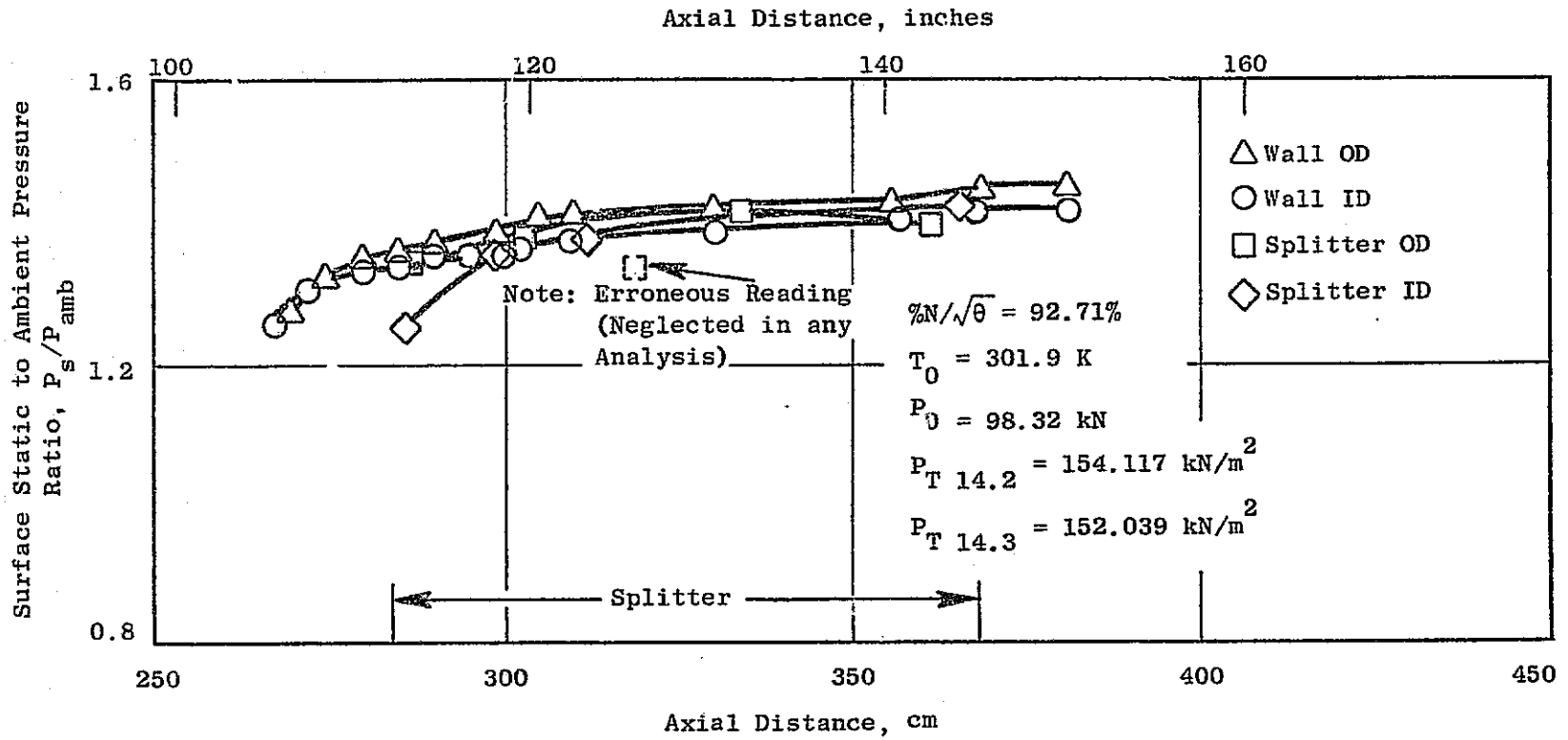

Figure 71. Fan Exit Duct (with Splitter) Measured Static Pressure Distributions at Takeoff Point Operation.

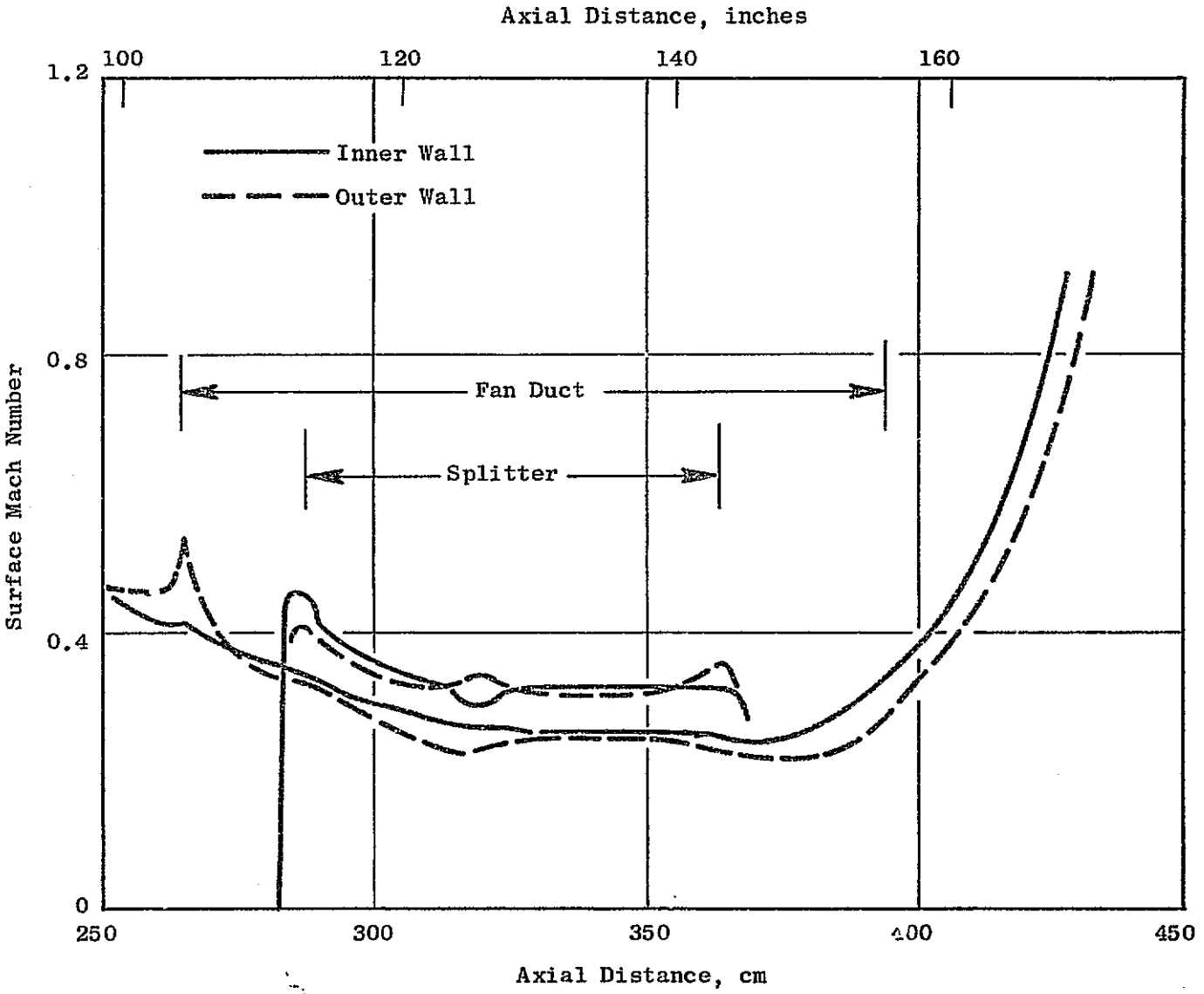

Figure 72. Fan Exit Duct (with Splitter) Predicted Mach Number Distributions at Takeoff Point Operation.

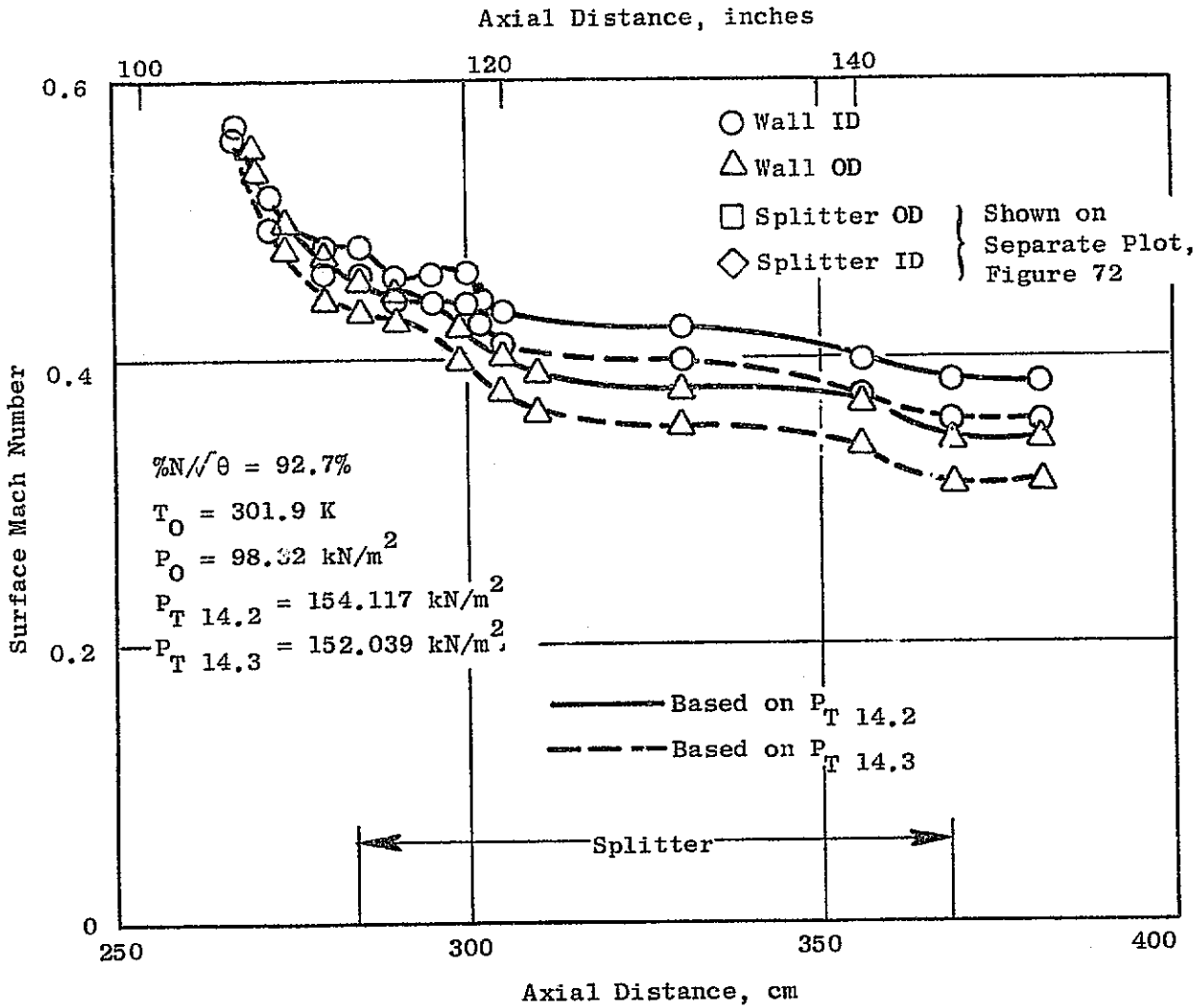

Figure 73. Fan Exit Duct (with Splitter) Test Wall Mach Number Distributions at Takeoff Point Operation.

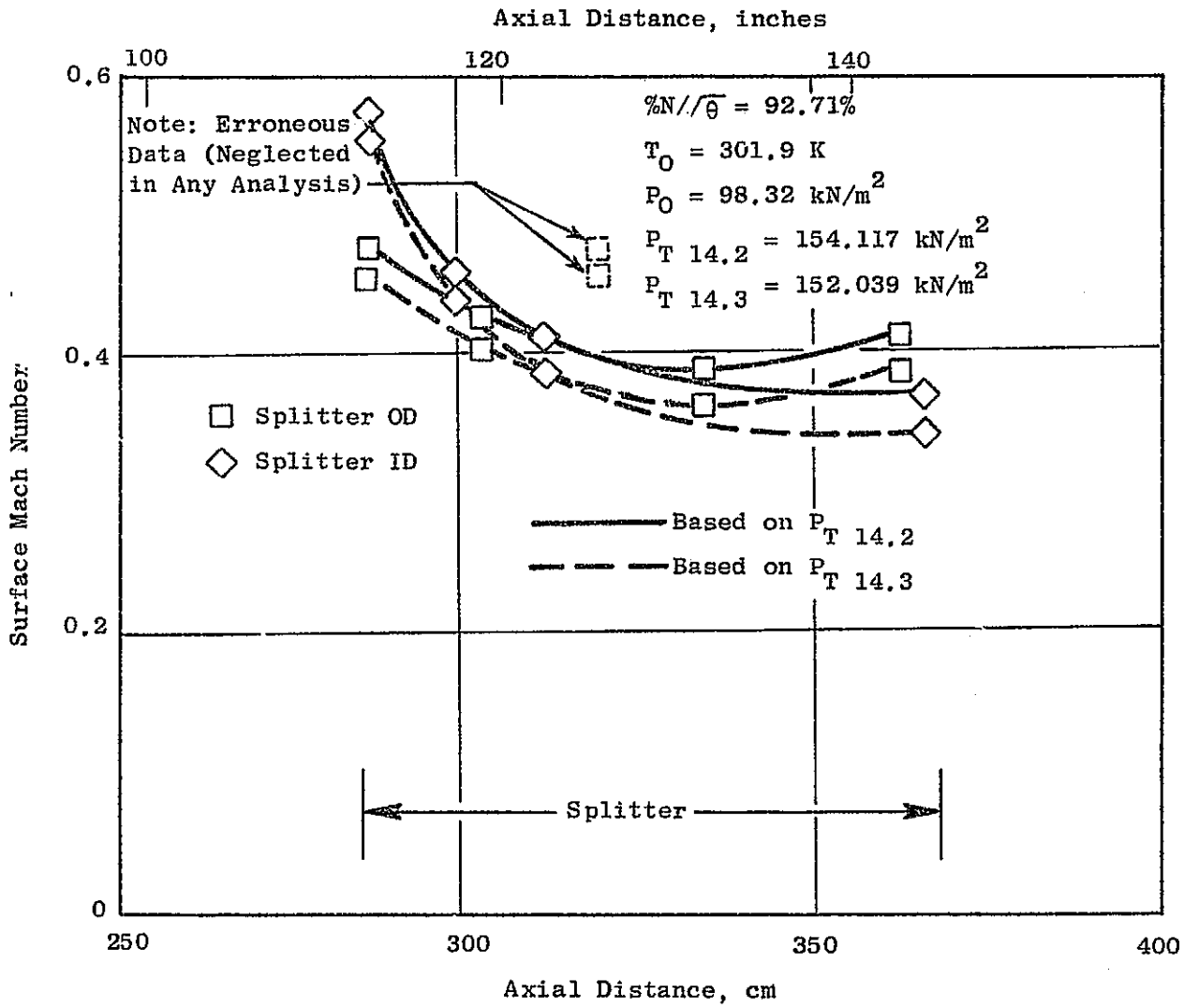

Figure 74. Fan Exit Duct (with Splitter) Test Splitter Mach Number Distributions at Takeoff Point Operation.

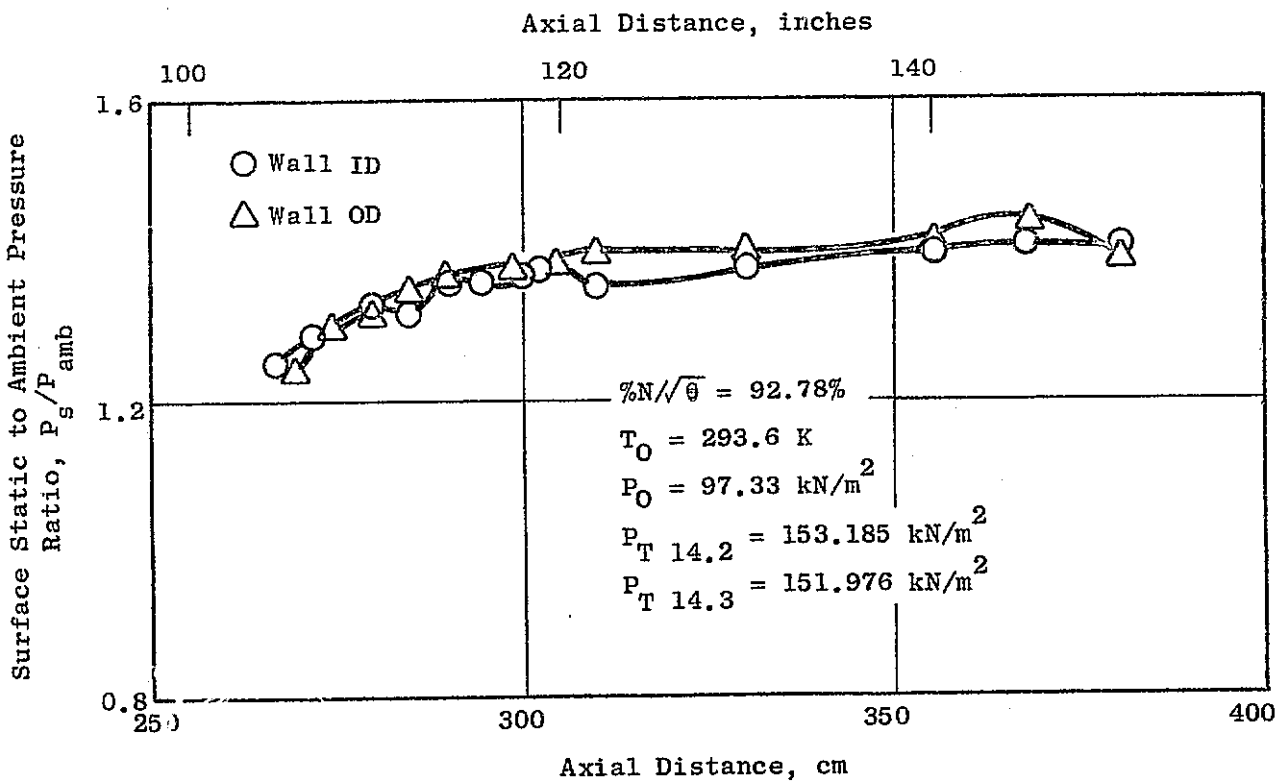

Figure 75. Fan Exit Duct (Hardwall) Measured Static Pressure Distributions at Takeoff Point Operation.

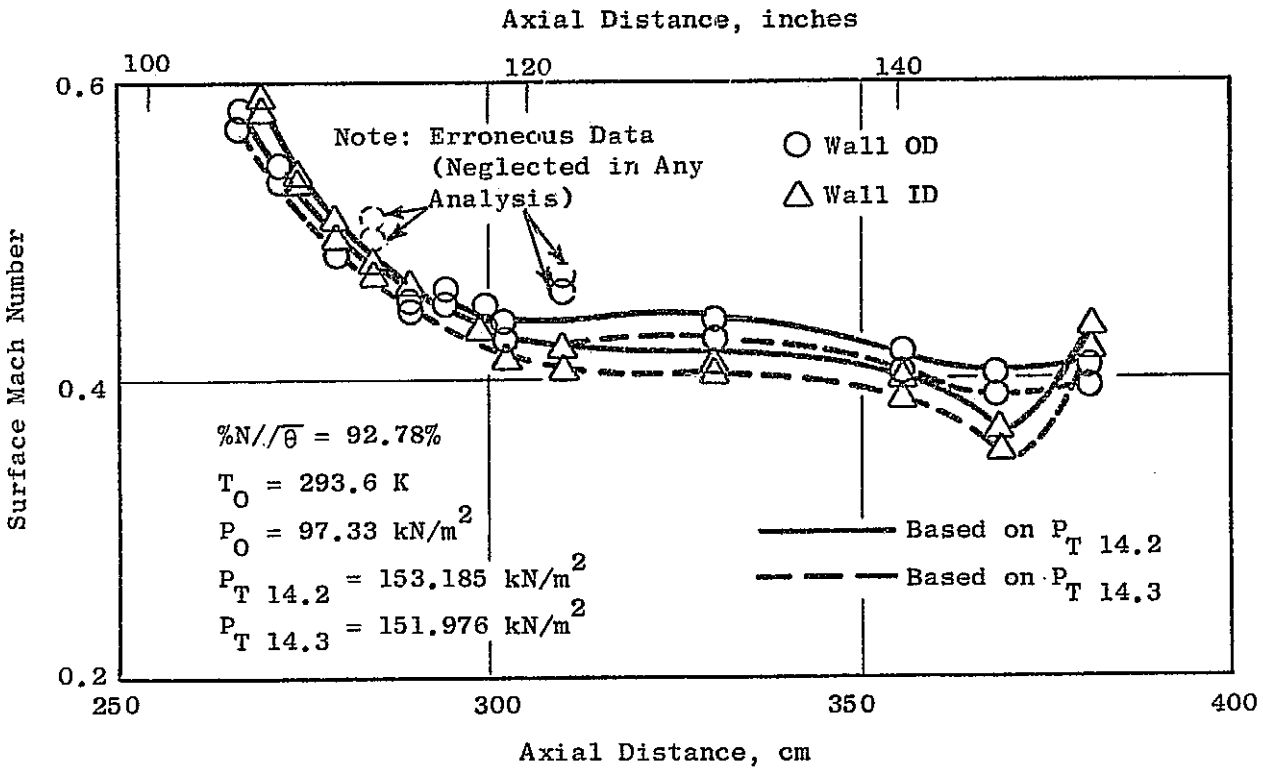

Figure 76. Fan Exit Duct (Hardwall) Test Mach Number Distributions at Takeoff Point Operation.

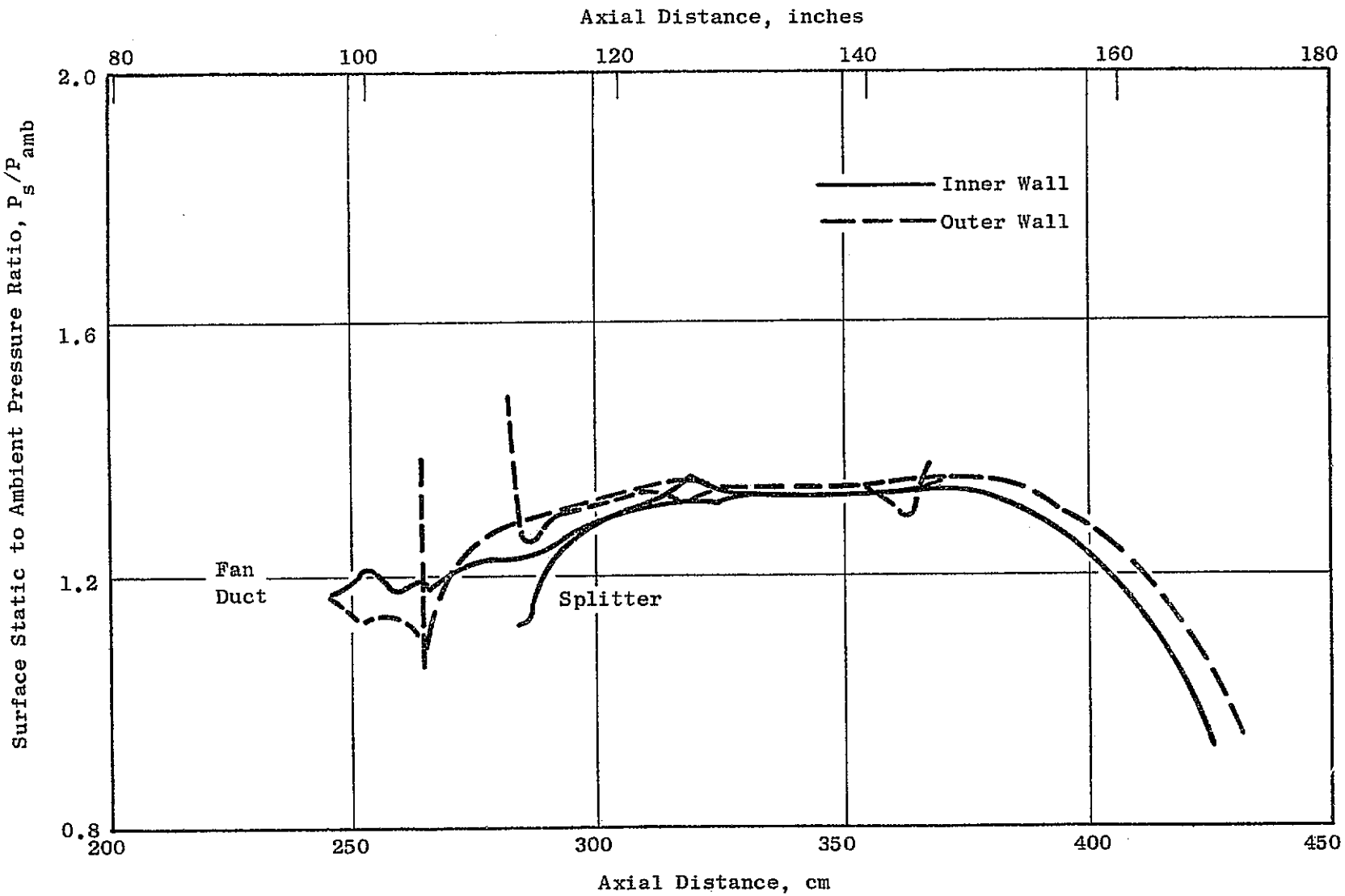

Figure 77. Fan Exit Duct (with Splitter) Predicted Static Pressure Distributions at Power Cutback Point Operation.

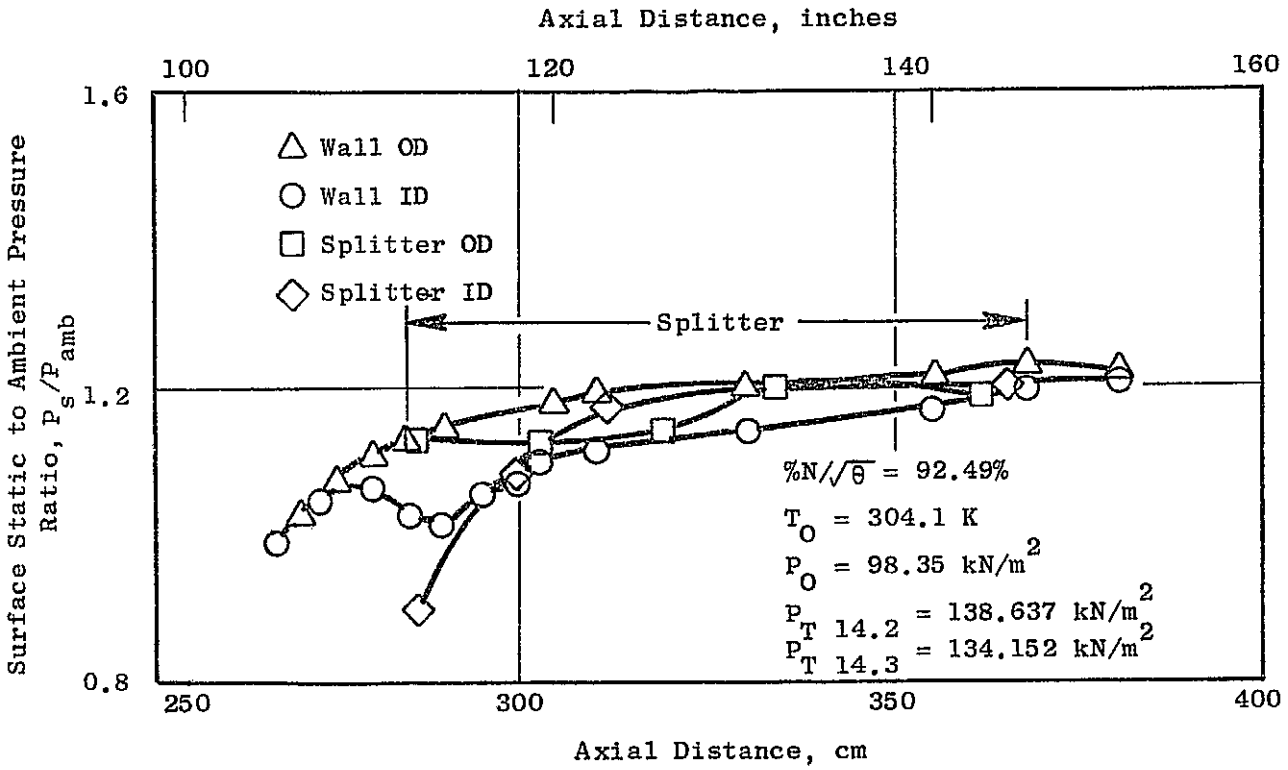

Figure 78. Fan Exit Duct (with Splitter) Measured Static Pressure Distributions at Power Cutback Point Operation.

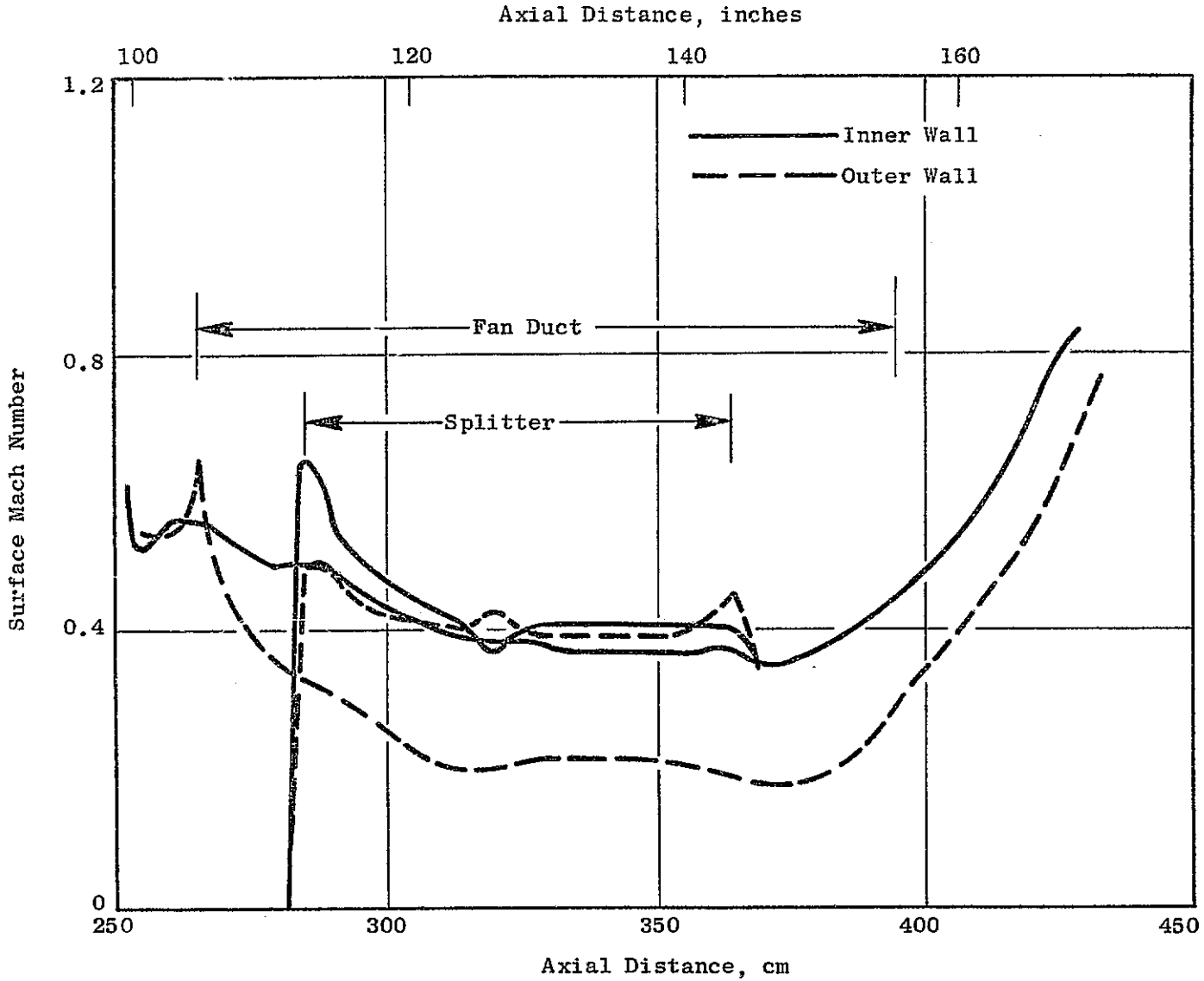

Figure 79. Fan Exit Duct (with Splitter) Predicted Mach Number Distributions at Power Cutback Point Operation.

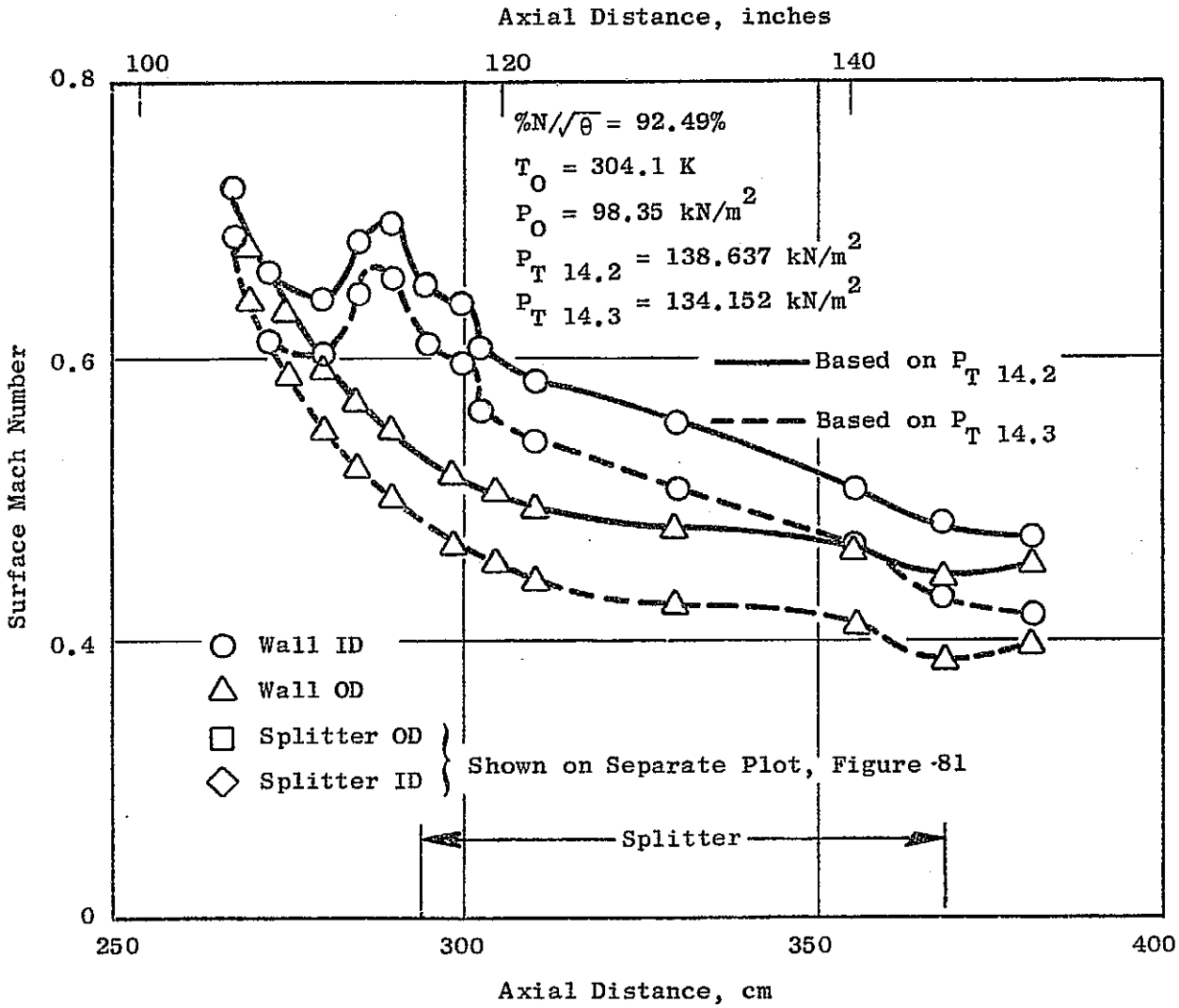

Figure 80. Fan Exit Duct (with Splitter) Test Wall Mach Number Distributions at Power Cutback Point Operation.

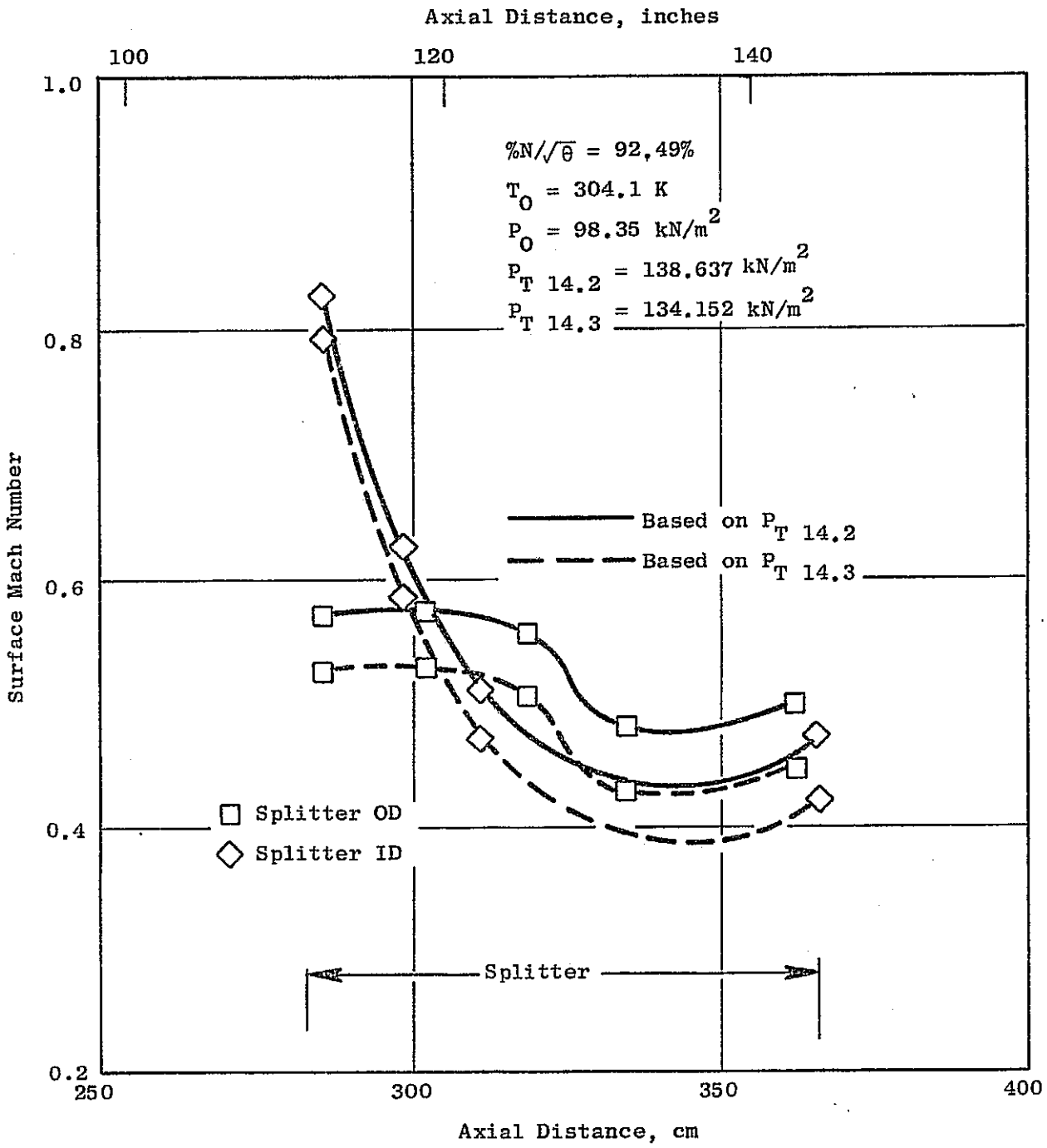

Figure 81. Fan Exit Duct (with Splitter) Test Splitter Mach Number Distributions at Power Cutback Point Operation.

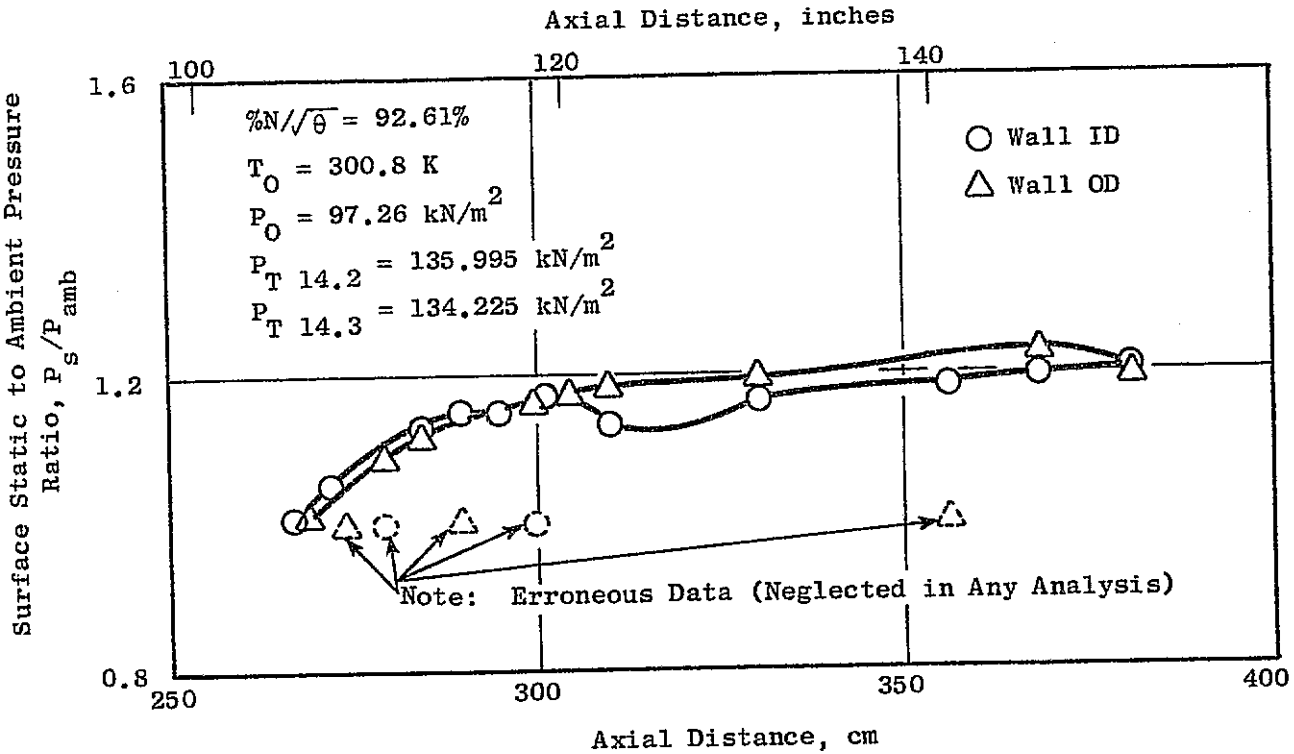

Figure 82. Fan Exit Duct (Hardwall) Measured Static Pressure Distributions at Power Cutback Point Operation.

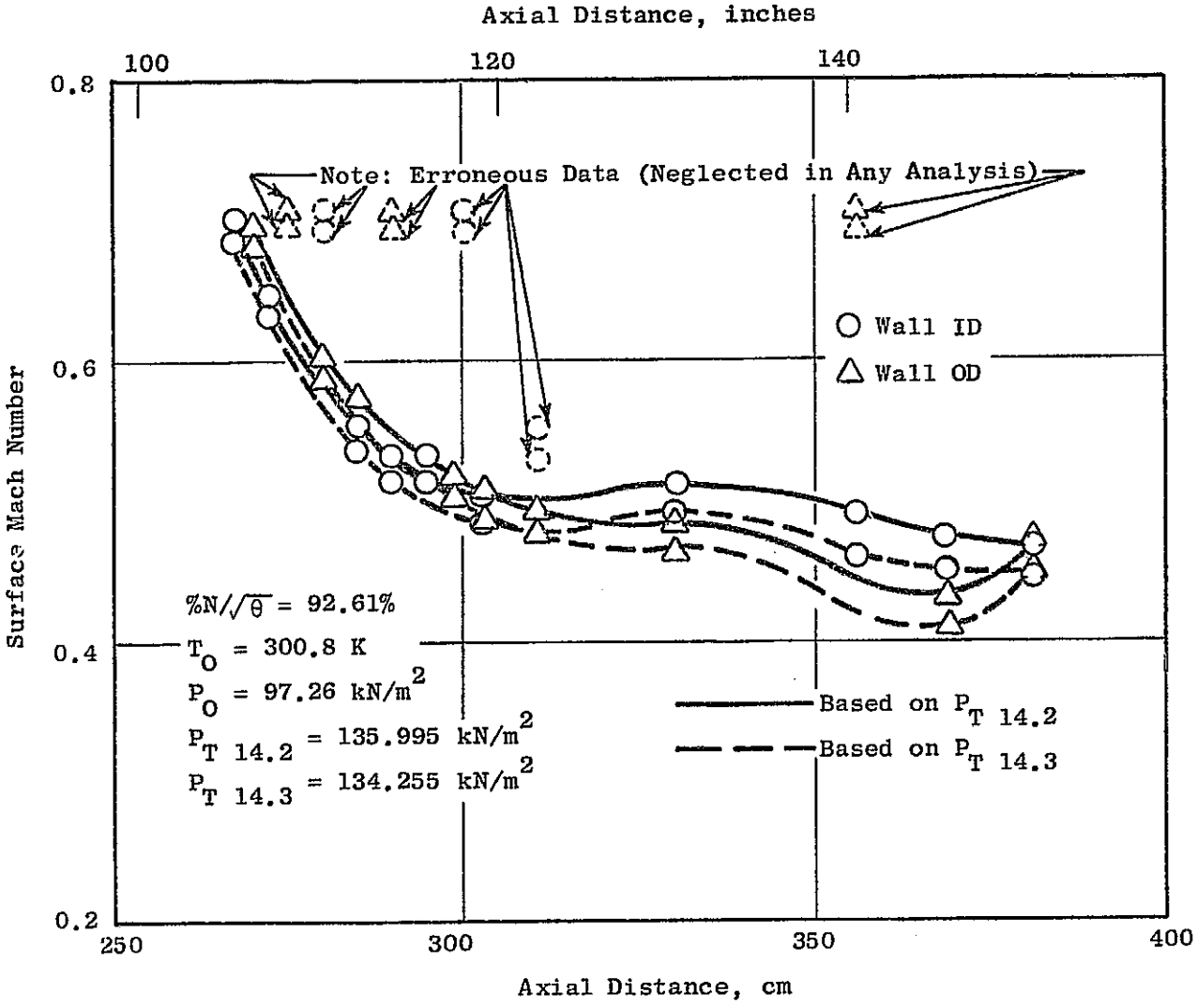

Figure 83. Fan Exit Duct (Hardwall) Test Mach Number Distributions at Power Cutback Point Operation.

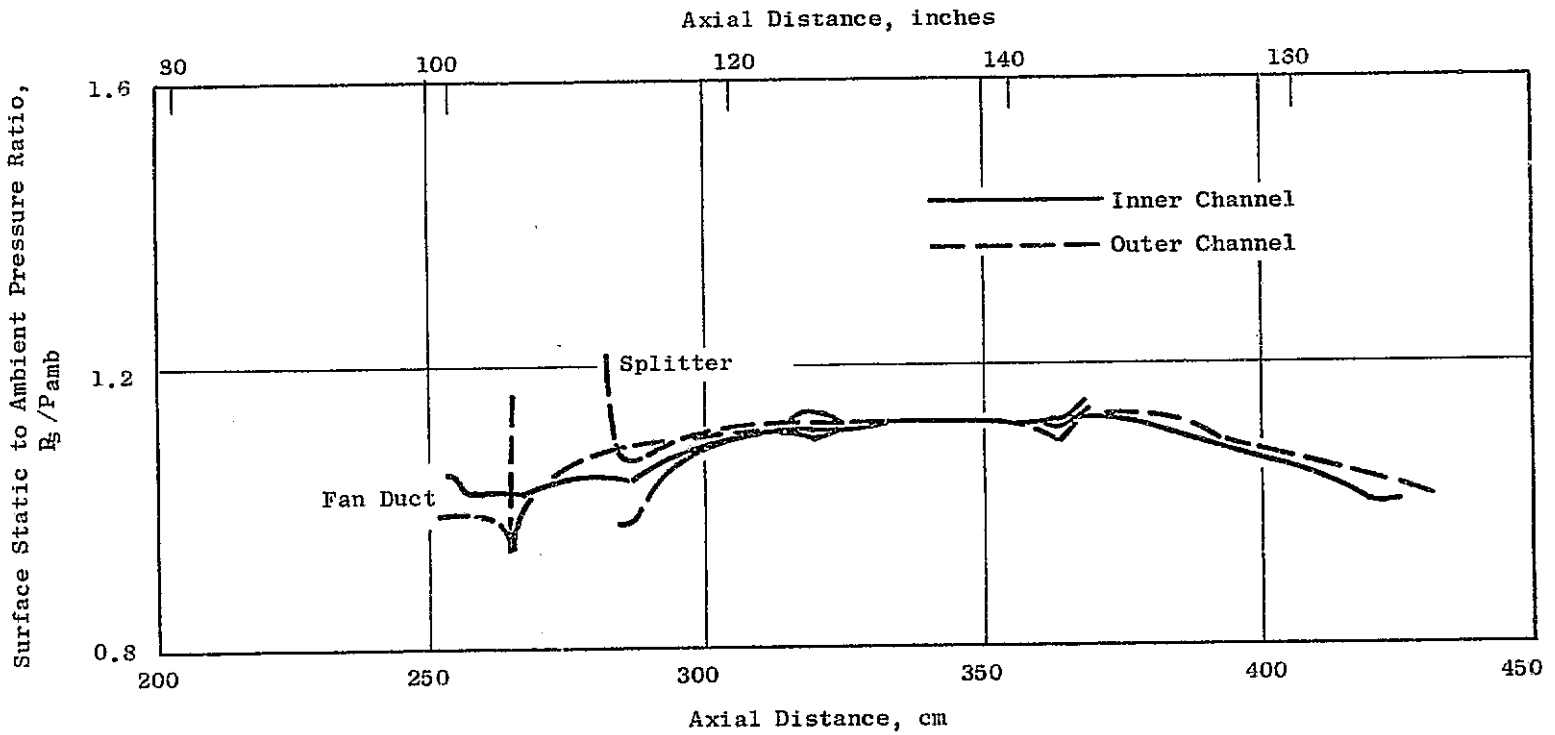

Figure 84. Fan Exit Duct (with Splitter) Predicted Static Pressure Distributions at Approach Point Operation.

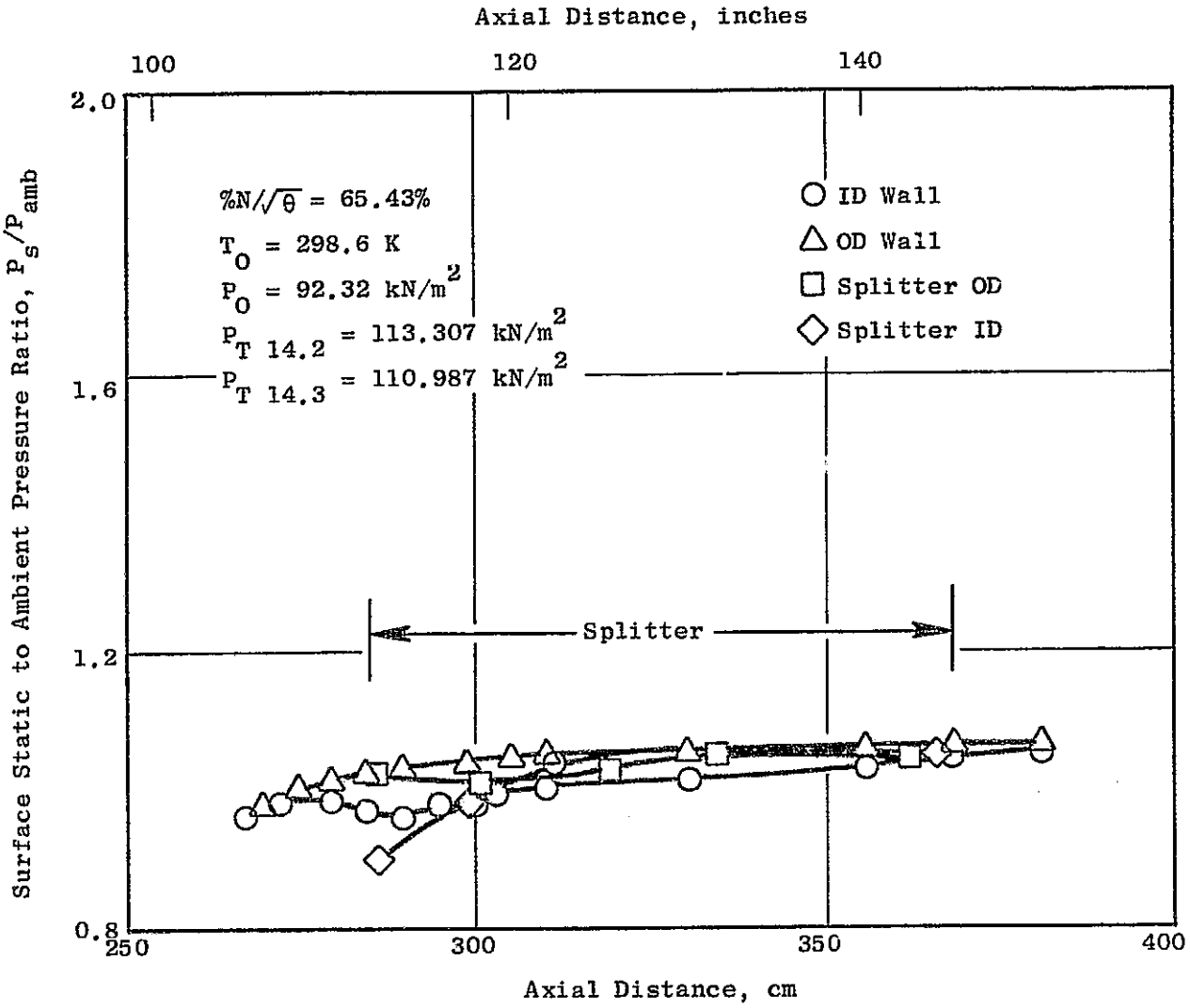

Figure 85. Fan Exit Duct (with Splitter) Measured Static Pressure Distributions at Approach Point Operation.

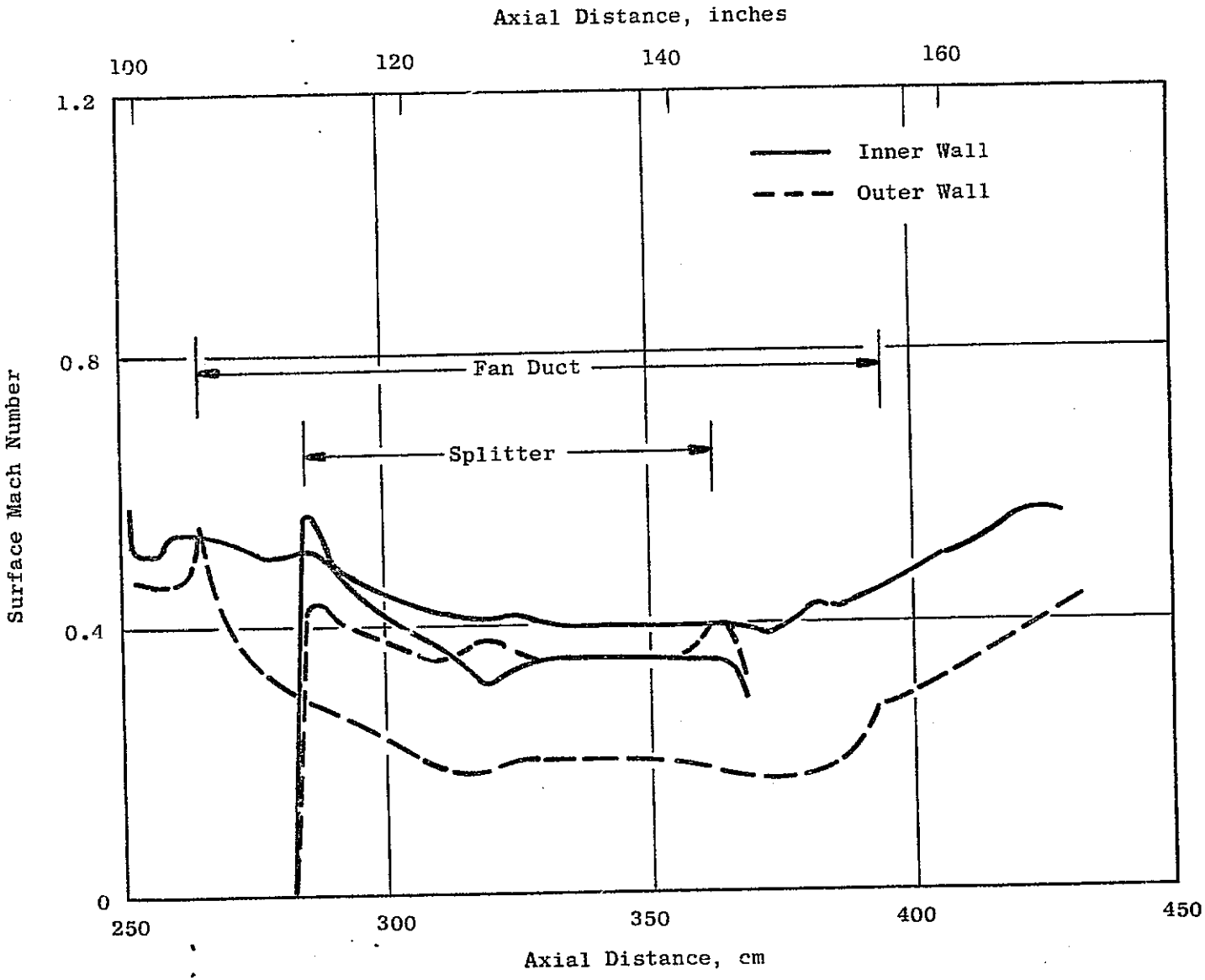

Figure 86. Fan Exit Duct (with Splitter) Predicted Mach Number Distributions at Approach Point Operation.

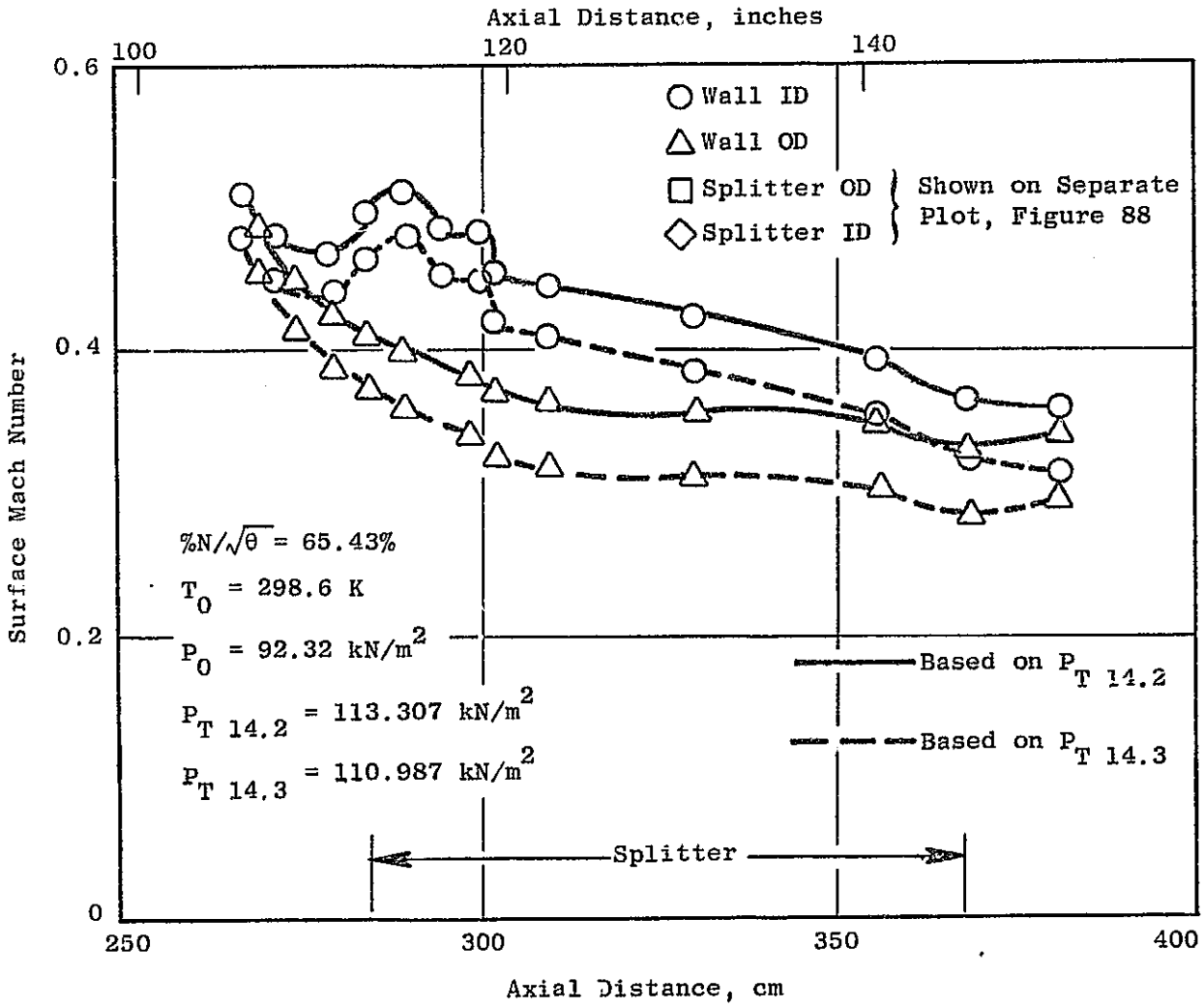

Figure 87. Fan Exit Duct (with Splitter) Test Wall Mach Number Distributions at Approach Point Operation.

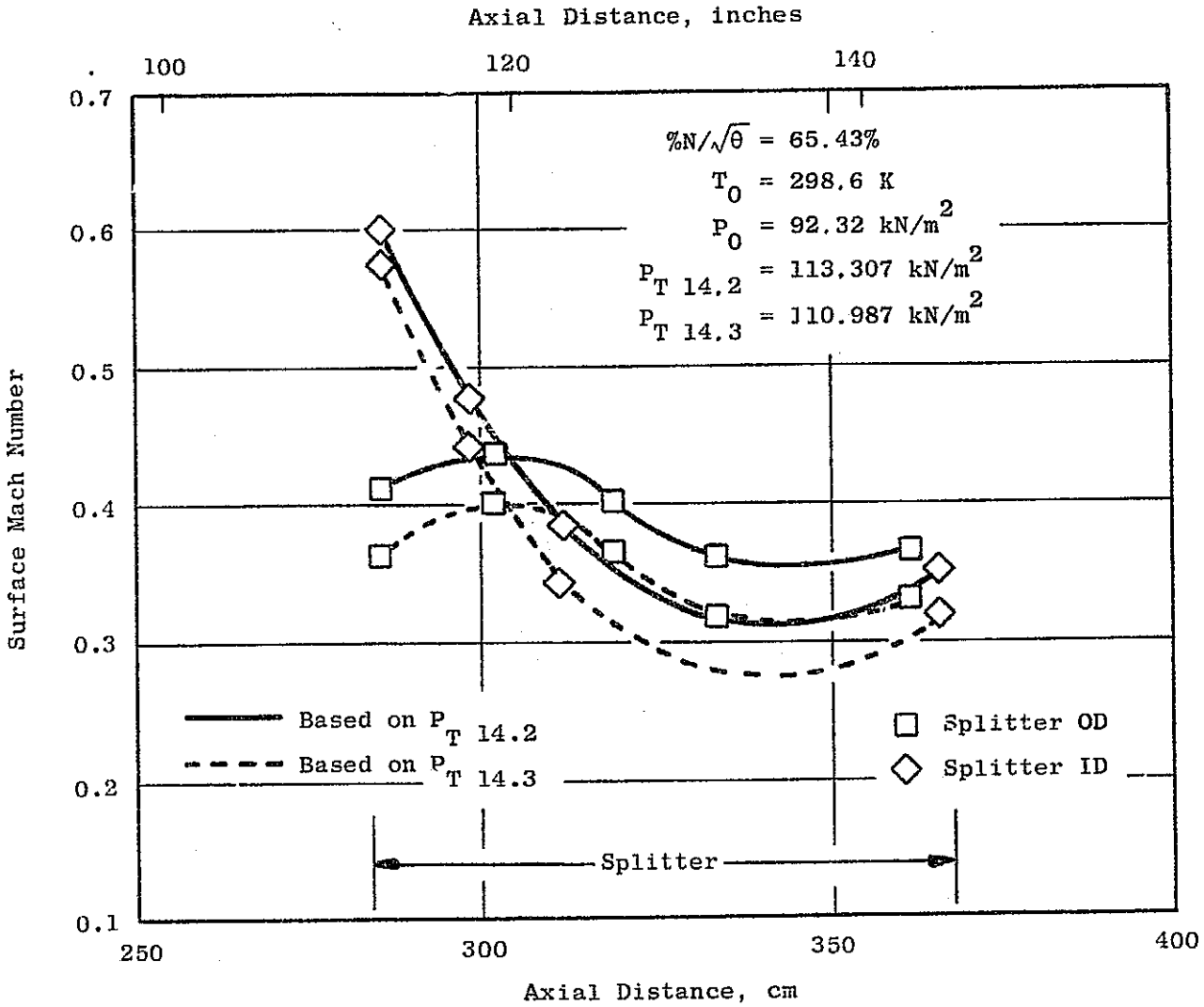

Figure 88. Fan Exit Duct (with Splitter) Test Splitter Mach Number Distributions at Approach Point Operation.

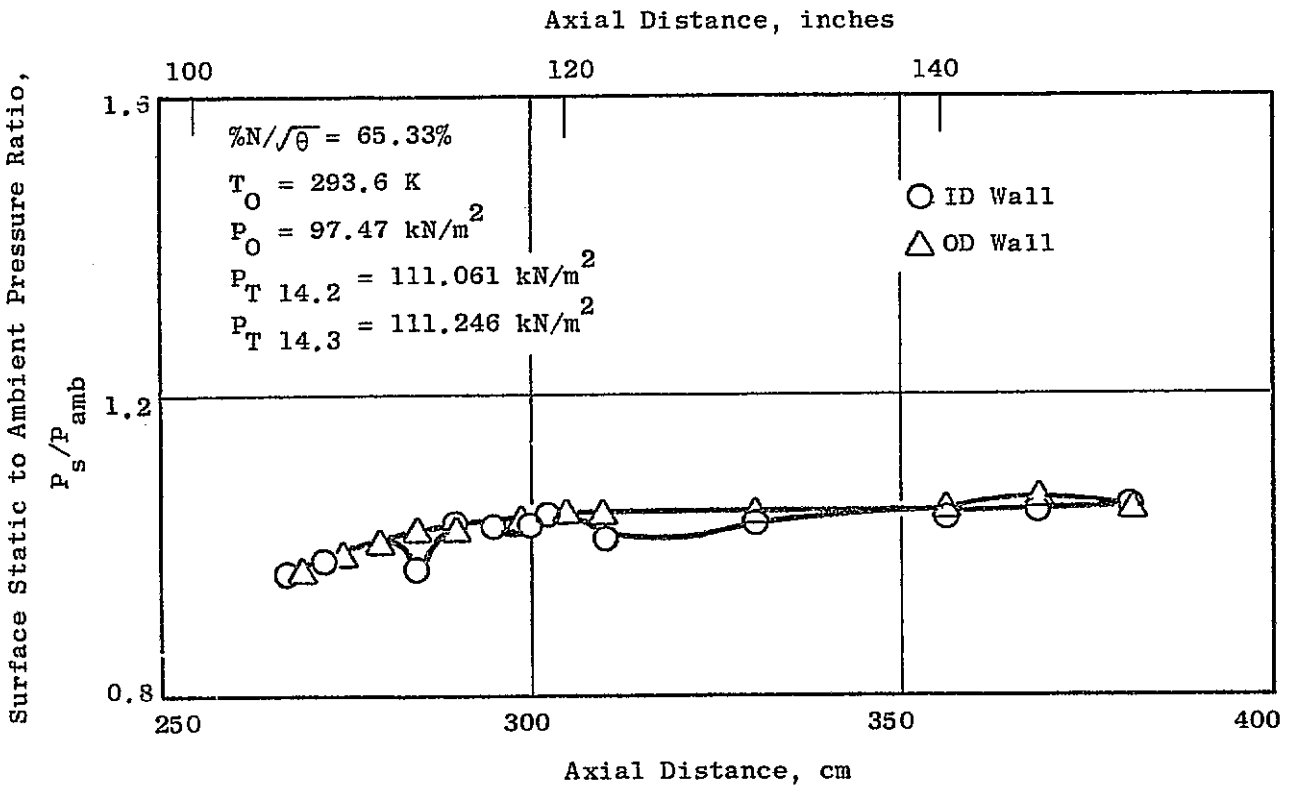

Figure 89. Fan Exit Duct (Hardwall) Measured Static Pressure Distributions at Approach Point Operation.

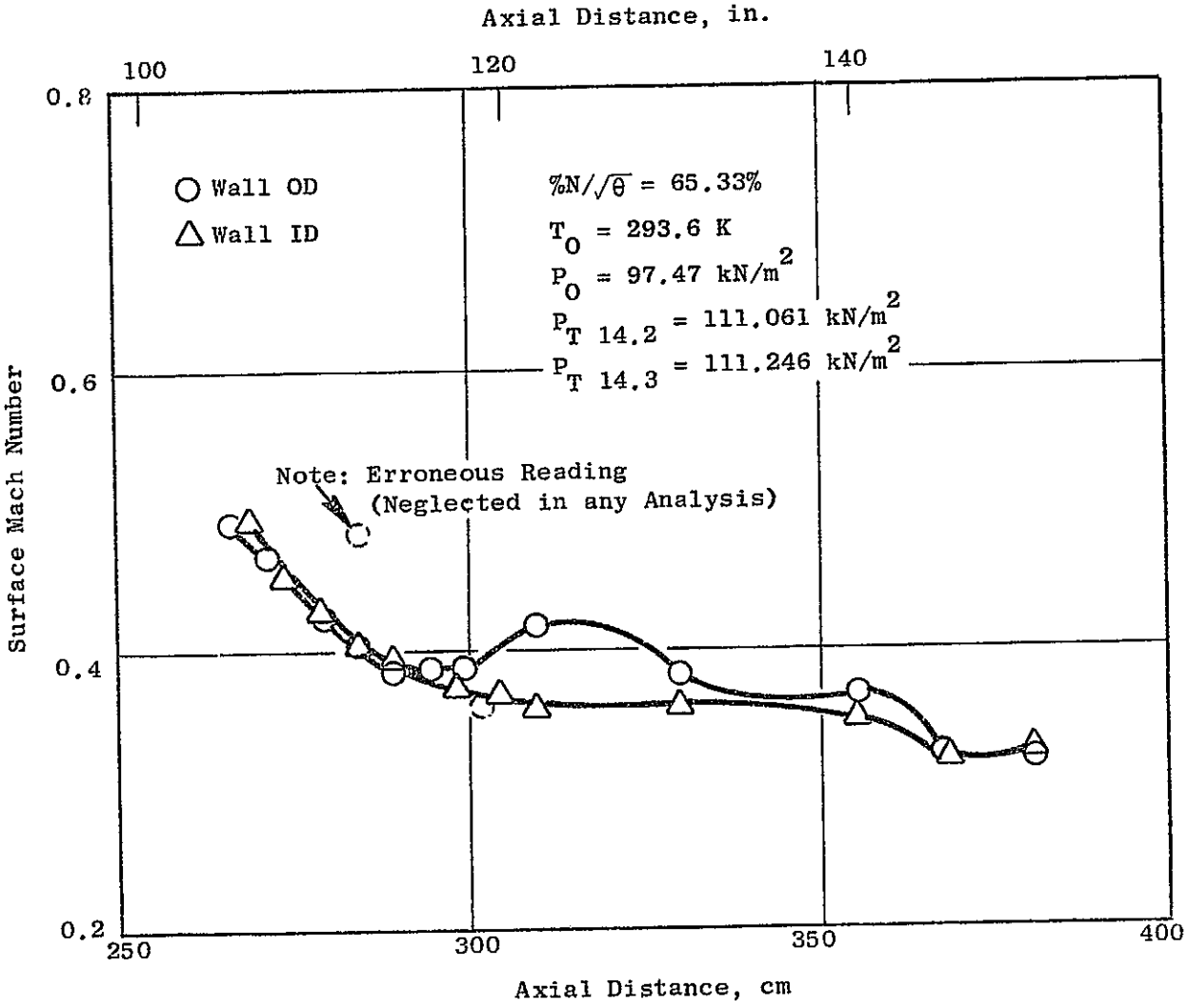

Figure 90. Fan Exit Duct (Hardwall) Test Mach Number Distributions at Approach Point Operation.